Potential Flow Model for Gaussian Plume Interaction with Simple Terrain Features

Environmental Research and Technology, Inc.
Concord, MA

Prepared for

Environmental Sciences Research Lab.
Research Triangle Park, NC

Mar 81

EPA-600/4-81-008
March 1981

PB81-171237

POTENTIAL FLOW MODEL FOR GAUSSIAN PLUME INTERACTION WITH SIMPLE TERRAIN FEATURES

by

A. Bass
D. G. Strimaitis
B. A. Egan

Environmental Research & Technology, Inc.
Concord, Massachusetts 01742

Contract No. 68-02-2759

Project Officer

John F. Clarke

Meteorology and Assessment Division
Environmental Sciences Research Laboratory
Research Triangle Park, NC 27711

ENVIRONMENTAL SCIENCES RESEARCH LABORATORY
OFFICE OF RESEARCH AND DEVELOPMENT
U.S. ENVIRONMENTAL PROTECTION AGENCY
RESEARCH TRIANGLE PARK, NC 27711

TECHNICAL REPORT DATA
(Please read Instructions on the reverse before completing)

1. REPORT NO. EPA-600/4-81-008	2.	3. RECIPIENT'S ACCESSION NO. PB81 171837
4. TITLE AND SUBTITLE POTENTIAL FLOW MODEL FOR GAUSSIAN PLUME INTERACTION WITH SIMPLE TERRAIN FEATURES		5. REPORT DATE March 1981 Issuing Date. 6. PERFORMING ORGANIZATION CODE
7. AUTHOR(S) A. Bass, D. G. Strimaitis, B. A. Egan		8. PERFORMING ORGANIZATION REPORT NO.
9. PERFORMING ORGANIZATION NAME AND ADDRESS Environmental Research and Technology, Inc. Concord, Massachusetts 01742		10. PROGRAM ELEMENT NO. CDTA1D/05-0625 (FY-81) 11. CONTRACT/GRANT NO. 68-02-2759
12. SPONSORING AGENCY NAME AND ADDRESS Environmental Sciences Research Laboratory Office of Research and Development U.S. Environmental Protection Agency Research Triangle Park, NC 27711		13. TYPE OF REPORT AND PERIOD COVERED Final 1977 - 1979 14. SPONSORING AGENCY CODE EPA/600/09
15. SUPPLEMENTARY NOTES		

16. ABSTRACT

The theory of turbulent plumes embedded within potential flow fields is discussed for flows modified by special complex terrain situations. Both two-dimensional and three-dimensional isolated terrain obstacles are considered. Concentration estimates are evaluated using a Gaussian solution to the appropriate diffusion equation; dispersion coefficients are modified to account for terrain-induced kinematic constraints, and plume centerline trajectory is obtained from a stream line of the potential flow. Specific limitations to the theory and its applicability are reviewed.

A computer algorithm is developed and documented to perform these calculations. Dispersion estimates and ground-level concentrations are given for a variety of meteorological situations. Parameters of the problem include obstacle height, effective source height, distance between source and obstacle, crosswind aspect ratio of the obstacle, and atmospheric stability. The potential flow theory, originally applicable to neutral flows, is extended by an empirical approximation to slightly stable flows. Model computations are compared to laboratory experimental results for neutral and stable flows, and to field measurements from the Tennessee Valley Authority Widow Creek Power Plant.

17. KEY WORDS AND DOCUMENT ANALYSIS

a. DESCRIPTORS	b. IDENTIFIERS/OPEN ENDED TERMS	c. COSATI Field/Group
Meteorology		04B
* Plumes		21B
* Hills		08F
* Three dimensional flow		20D
* Two dimensional flow		12A
* Mathematical models		

18. DISTRIBUTION STATEMENT RELEASE TO PUBLIC	19. SECURITY CLASS (This Report) UNCLASSIFIED	21. NO. OF PAGES 202
	20. SECURITY CLASS (This page) UNCLASSIFIED	22. PRICE

EPA Form 2220-1 (9-73)

DISCLAIMER

This report has been reviewed by the Environmental Sciences Research Laboratory, U.S. Environmental Protection Agency, and approved for publication. Approval does not signify that the contents necessarily reflect th views and policies of the U.S. Environmental Protection Agency, nor does mention of trade names or commercial products constitute endorsement or recommendation for use.

PREFACE

This report describes the results of a program to develop and evaluate a transport/diffusion model for estimating ambient ground-level concentrations from point sources in areas of complex terrain.

At the beginning of the investigation, development of two modified Gaussian-type plume models was proposed, as guided by regulatory requirements. The first model was to be a worst-case, single-point-source model to be used as a screening tool for estimating hourly-averaged ground-level air quality impact on a variety of individual terrain features; the second model was to be an extension to handle multiple terrain features. At the conclusion of a project technical review held at the Meteorology Laboratory on 20-21 July 1978 at the request of the government project officer, it was mutually agreed that implementation of the worst-case screening model would be premature. Instead, the program was directed toward further model refinements and extensions, and included detailed comparisons of model predictions with field measurements and laboratory experiments.

In the execution of this program, Environmental Research & Technology, Inc. (ERT) has:

- adapted the potential flow theory approach for neutral situations by including the effects of terrain-induced perturbations on plume trajectory, and on vertical and crosswind dispersion;
- developed empirical approximations to the potential flow theory to address both:
  - slightly stable flows; and
  - obstacles of arbitrary crosswind aspect ratio;
- implemented and documented a computer algorithm to perform these potential flow theory calculations; and investigated the variations of results with changes in effective stack height, obstacle height, distance to obstacle, stability, and aspect ratio; and
- made a preliminary assessment of the model through a comparison of model results with U.S. Environmental Protection Agency tow tank and wind tunnel experiments and with atmospheric data from TVA's Widows Creek Power Plant.

ABSTRACT

The theory of turbulent plumes embedded within potential flow fields is discussed for flows modified by special complex terrain situations. Both two-dimensional and three-dimensional isolated terrain obstacles are considered. Concentration estimates are evaluated using a Gaussian solution to the appropriate diffusion equation; dispersion coefficients are modified to account for terrain-induced kinematic constraints, and plume centerline trajectory is obtained from a stream line of the potential flow. Specific limitations to the theory and its applicability are reviewed.

A computer algorithm is developed and documented to perform these calculations. Dispersion estimates and ground-level concentrations are given for a variety of meterological situations. Parameters of the problem include obstacle height, effective source height, distance between source and obstacle crosswind aspect ratio of the obstacle, and atmospheric stability. The potential flow theory, originally applicable to neutral flows, is extended by an empirical approximation to slightly stable flows. Additionally, an interpolation scheme is proposed for objects of arbitrary crosswind aspect ratio between the limiting cases of a hemisphere and a half-circular cylinder.

For neutral and slightly stable flows over two-dimensional obstacles, predicted maximum ground level concentrations are similar to those expected over flat terrain. For flows over three-dimensional obstacles, however, the model predicts an order of magnitude increase in the ground level concentration. Model computations are compared to laboratory experimental results for neutral and stable flows over an isolated obstacle with a crosswind aspect ratio equal to that of the hemisphere, and for neutral flows over obstacles with aspect ratios that vary between those of the hemisphere and the circular cylinder. Peak concentrations at the crests of these obstacles are found to be overpredicted by no more than a factor of two. A preliminary test of the model against field measurements indicates that the model computations generally bracket the observed concentrations, with the major uncertainty being the specification of the dispersion parameters.

The performance of the potential flow model differs markedly from that of the level plume and the terrain-following plume approaches to predicting ground-level concentrations in complex terrain. The level plume predictions characteristically overpredict by one to two orders of magnitude, and the terrain-following plume predictions characteristically underpredict by several orders of magnitude at small aspect ratio. Consequently, the potential flow approach provides a real potential for simulating physical interactions of a plume with terrain features in complex terrain under conditions where the atmospheric stratification is neutral to slightly stable, and where direct plume impingement on the hill side is not expected.

Recommendations are made for extending the applicability of the modeling approach, and for providing additional data for adequate validation. Several of the areas cited for enhancement and extension include alternate turbulence

typing schemes, an algorithm for estimating concentrations in hill wakes, generalized potential flow stream functions for additional terrain shapes, and additional laboratory data for stable flow over a variety of obstacle shapes.

This report is submitted in fulfillment of Contract No. 68-02-2759 by Environmental Research & Technology, Inc. under the sponsorship of the U.S. Environmental Protection Agency.

CONTENTS

FIGURES

TABLES

LIST OF SYMBOLS AND ABBREVIATIONS

SYMBOL	
a	height of obstacle
a', b'	coefficients of boundary layer enhanced dispersion coefficient
b	half of the crosswind breadth of obstacle
C	plume path coefficient
C_0, C_1, C_2	coefficients of polynomial fit for z_{CF}
$D_{1,2}$	normal and crosswind dimensionless diffusivities
$\overline{D}_{1,2}$	normal and crosswind "effective" diffusivities
$f_{1,2}$	trial solution functions
Fr	Froude number
g	acceleration due to gravity
$g(s)$	trial solution function
G	gross boiler load
G_{CYL}, G_{SPH}	weighting functions for velocity in aspect ratio computation
H_s	effective source height
h_t	local terrain height
Δh	final plume rise
L	Monin-Obukhov length
$\dot{M}$	experimental mass flux
n_s	distance along normal from plume centerline to surface (assuming no errors)
n_s^*	distance along normal from plume centerline to surface (with errors)
Q	emission rate of pollutant
R	ratio of ground level to centerline concentration (assuming no errors)
R^*	ratio of ground level to centerline concentration (with errors)
$R(s)$	distance from axis of symmetry to plume centerline for axisymmetric obstacle

SYMBOL	
R_s	stack top radius (m)
s	along plume centerline path length
s,n,γ	curvilinear coordinates for system that follows the plume centerline
$\bar{S}$	speed-up factor
S_{CYL}, S_{SPH}	speed-up factor for cylindrical ridge and hemispherical hill
SC	atmospheric dispersion stability class
t	along plume centerline advection time
T_a	ambient average temperature
T_s	stack exhaust temperature
T(s)	crosswind line integral
T_c	terrain correction factor
u(s)	along streamline velocity
U	horizontal wind speed
U_c	velocity at crest of obstacle
U_{CYL}, U_{SPH}	velocity field component assuming potential flow over cylindrical ridge, hemispherical hill respectively
U_∞	uniform velocity upwind of source
v	velocity normal to streamline
V_s	stack exhaust velocity
W_{CYL}, W_{SPH}	weighting functions for streamline height in aspect ratio computation
x	distance along X axis from source
X_s	downwind distance from source to obstacle center
z_C	height of streamline above crest for neutral flow
z_{CF}	height of streamline above crest for stratified flow
Z_{CYL}, Z_{SPH}	height of streamline above surface for flow over cylindrical ridge, hemispherical hill
z_o	roughness length
$\alpha_{y,z}$	ratios of complex terrain to flat terrain spread statistics
$\beta(\lambda)$	aspect ratio term in speed-up equation
$\delta(x)$	streamline depression at any x due to stratification
Δ	streamline depression at crest due to stratification
ζ	stream function gradient factor

SYMBOL	
η	plume height perturbation factor
λ	obstacle crosswind aspect ratio
$\lambda_{1,2}$	limiting two-dimensional and three-dimensional aspect ratios
$\sigma_{y,z}$	crosswind and vertical dispersion coefficients
$\sigma_{yf,zf}$	crosswind and vertical dispersion coefficients in flat terrain
σ_z'	boundary layer enhanced vertical dispersion coefficient
σ_z^*	vertical dispersion coefficient with errors
$\phi(s)$	normal to streamline line integral
χ	concentration
$\chi', \hat{\chi}$	dimensionless concentration
$\psi_{2D,3D}$	stream function for two-dimensional, axisymmetric three-dimensional flows
ψ_s	stream function through source
ψ_p	streamline equation of plume centerline
θ	potential temperature

ABBREVIATIONS

cm	centimeter
EPA	U.S. Environmental Protection Agency
ERT	Environmental Research & Technology, Inc.
FMF	Fluid Modeling Facility
km	kilometer
m	meter
NAAQS	National Ambient Air Quality Standards
PGT	Pasquill-Gifford-Turner
PSD	prevention of significant deterioration
TVA	Tennessee Valley Authority
LT	local time

ACKNOWLEDGMENT

The authors wish to acknowledge helpful review and suggestions of Dr. F. Pasquill, a consultant to the project. We also acknowledge the helpful advice provided by Drs. J. C. R. Hunt, W. H. Snyder, and R. E. Britter. Special thanks are extended to John F. Clarke and to George C. Holzworth, for their overall judgment and direction on the project.

The major contributions of R. G. Isaacs and Dr. J. Calman to earlier versions of this report are gratefully acknowledged.

Laboratory data was kindly furnished by Dr. William H. Snyder, Environmental Sciences Research Laboratory, U.S. Environmental Protection Agency, and Widows Creek Power Plant data was kindly furnished by Mr. John P. Blackwell, Air Resources Program, Tennessee Valley Authority.

SECTION 1

INTRODUCTION

This study has been motivated by the requirement for a treatment of plume dispersion in complex terrain that is practical for regulatory use, yet retains much of the essential physics of the problem. For regulatory purposes, the modeling approach should emphasize cases with potential for high ground-level concentrations. These include:

- stable conditions and low wind speeds, under which direct plume impact or blocking by nearby terrain obstacles may occur, and
- neutral or slightly stable conditions and moderate or high wind speeds, under which the plume centerline trajectory passes over and close to the terrain surface.

This report addresses the development of modeling methods for neutral and slightly stable conditions. The general approach employed follows the theory of turbulent plumes embedded within potential flow fields as developed by Hunt and Mulhearn (1973) and Hunt and Snyder (1978). The theory is applied to the calculation of ground-level concentrations using a Gaussian form of solution to the diffusion equation. Streamfunctions proper to potential flow over a cylinder (aspect ratio = ∞) and to potential flow over a sphere (aspect ratio = 1) form cornerstones of the model. These are extended to describe flows over terrain features of intermediate crosswind aspect ratio by a weighting of the two limiting streamfunctions. This weighting scheme was derived in part using results from wind tunnel experiments for flows over obstacles of intermediate aspect ratio (Snyder et al. 1979).

In addition, although the model is strictly applicable only to neutral flows, an empirical approximation scheme is included to define streamline lowering caused by increased stratification. The empirical basis for this portion of the model is derived from stratified tow-tank experiments (Snyder 1977 and Snyder 1978).

Other restrictions in the use of the model have not been addressed. These limitations to the model arise from the neglect of boundary layer phenomena such as flow separation, unsteady wake effects, time-dependent effects of stability (e.g., lee wave generation), and surface heating effects. In addition, the theory is applicable in a strict mathematical sense only for thin plumes.

This report discusses the rationale for selecting particular modeling approaches, provides full technical documentation for the algorithms developed, and presents, for a number of specific test situations, the results of comparisons between model calculations and laboratory and field observations.

The report consists of twelve sections and four appendices. Section 2 presents a summary of the study and its conclusions, and Section 3 states recommendations for future laboratory and/or field experiments to further define and validate the modeling approaches. Section 4 briefly overviews the technical aspects of complex terrain modeling.

Section 5 describes the theoretical basis for applying potential flow theory to the modeling of plume transport and diffusion in complex terrain. The assumptions, applicability, and limitations of the theory developed by Hunt and coworkers are reviewed and approximations are introduced for practical application of the theory. A method is presented for calibrating model dispersion coefficients to various diffusion parameter systems. In Section 6 the theory is applied to the calculation of ground-level and centerline concentrations for a variety of cases that illustrate the model's behavior, under neutral stratification, with variations in effective stack height, obstacle size, and relative stack/obstacle position. These calculations are compared with U.S. Environmental Protection Agency (EPA) Fluid Modeling Facility (FMF) wind tunnel experiments in Section 7.

The effect of stratification has been parameterized, using data from FMF laboratory tow tank experiments, by an approximation incorporated within the potential flow model; this technique is described in Section 8. The limitations of the technique are reviewed, and recommendations are proposed for handling cases that are inappropriate to the potential flow theory approach. Comparisons of model calculations with stratified tow tank experiments are made in Section 9.

In Section 10 a technique based on theoretical arguments and wind tunnel experiments is proposed to generalize the model to objects of arbitrary crosswind aspect ratio. The technique is evaluated in Section 11, where the model is compared in detail to laboratory experiments simulating neutral atmospheric flow over obstacles of triangular cross-section with crosswind aspect ratios between 1 and infinity.

Preliminary tests of the model against field data are described in Section 12. A total of seven test cases are presented, so the analysis does not constitute a validation of the model. The comparison does, however, highlight a procedure for applying the model to the atmosphere, and illustrates the need for complete and detailed observations in any future validation programs.

Finally, a description of the computer model that has been developed to perform the computations is provided (Appendix A), including a flow chart (Appendix B), full program source listing (Appendix C), and an example of the output (Appendix D).

SECTION 2

SUMMARY AND CONCLUSIONS

In complex terrain, two classes of meteorological conditions often are associated with the likelihood of large ground-level concentrations: (1) low wind speed, stable cases, and (2) moderate or high wind speed, neutral or slightly stable cases. The first class of conditions generally leads to high concentrations through direct plume impingement or terrain blocking. The present model does not treat direct plume impingement or terrain blocking under stable conditions. Specific recommendations for treating plume dispersion under stable atmospheric conditions are presented in Section 3.

The second class of situations promotes high concentrations because, as the plume is transported over terrain features, it is forced to pass close to the terrain surface. Physical mechanisms relevant to this class of conditions include terrain-induced alteration of the plume centerline trajectory and kinematic constraints on horizontal and vertical dispersion. The dispersion process in these situations is modeled as a Gaussian plume embedded in a potential flow field. This approach falls between the two extremes found in present modeling approaches in neutral situations:

a) the terrain-following method, where the plume rises everywhere over the terrain at a local elevation equal to the height of the plume above the stack base; and

b) the level plume method, where the local terrain height is subtracted from the effective height of the plume.

In Case a, maximum ground-level concentrations are about the same as over flat terrain, while in Case b, near-plume axis concentrations are predicted at ground level for terrain elevations approximately equal to effective stack height. Neither extreme deals with terrain-induced changes in plume trajectory and plume dispersion rates.

Various model modifications have been adopted (e.g., the CRSTER model with terrain truncated at the height of the stack top) to remedy this situation. However, such treatments are ad hoc; by contrast, the potential flow theory as described here appears to offer a practical and more physically justifiable method for incorporating these effects within a Gaussian plume model.

A research computer algorithm based on the potential flow approach computes ground-level pollutant concentrations; plume centerline concentrations; height of plume trajectory above the surface; and horizontal and

vertical dispersion coefficients. In the method used, for example, the equation of the plume centerline for flow over a hemisphere provides the plume trajectory in neutral flow by:

$$z^2 \left(1 - \frac{a^3}{(x^2 + z^2)^{3/2}}\right) = H_s^2 \left(1 - \frac{a^3}{(X_s^2 + H_s^2)^{3/2}}\right) \qquad (2\text{-}1)$$

In this equation, x and z are the horizontal and vertical cartesian coordinates of a point on the streamline relative to the center of the obstacle, X_s and H_s are the position and height of the stack, and a is the height of the hill. The velocity along the plume trajectory, u(s), is determined by the gradient of the stream function, ψ^{3D}, describing the trajectory of the plume centerline, such that:

$$u(s) = \left[\left(\frac{\partial \psi^{3D}}{\partial x}\right)^2 + \left(\frac{\partial \psi^{3D}}{\partial z}\right)^2\right]^{1/2} \qquad (2\text{-}2)$$

where

$$\psi^{3D}(x,z) = 0.5\ U_\infty z^2 \left(1 - \frac{a^3}{(x^2 + z^2)^{3/2}}\right) \qquad (2\text{-}3)$$

and U_∞ is equal to the velocity far upstream of the hill. A Gaussian form of the dispersion equation using coordinates along and normal to the trajectory:

$$\chi'(s,n,\gamma) = \frac{1}{g(s)} \exp\left[-f_1(s)\, n^2 - f_2(s)\, \gamma^2\right] \qquad (2\text{-}4)$$

provides dimensionless concentration estimates, $\chi' = (\chi U_\infty a^2/Q)$, where by definition,

$$f_1(s) = [u(s)R(s)]^2/[4\phi(s)] \qquad (2\text{-}5a)$$

$$f_2(s) = 1/[4T(s)] \qquad (2\text{-}5b)$$

$$g(s) = 4\pi[\phi(s)T(s)]^{1/2} \qquad (2\text{-}6)$$

and

$$\phi(s) = \int_0^s D_1(s')\, R^2(s')\, u(s')ds' \qquad (2\text{-}7)$$

$$T(s) = \int_0^s [D_2(s')/[u(s')R^2(s')]]ds' \qquad (2\text{-}8)$$

A similar sequence of Equations (see Section 5, Equations 5-7 through 5-13) for flow over two-dimensional obstacles uses the two-dimensional stream function for flow over a half-cylinder:

$$\psi^{2D}(x,z) = U_\infty z \left(1 - \frac{a^2}{(x^2 + z^2)}\right) \qquad (2\text{-}9)$$

To account for the effects of stability, an approximation consistent with laboratory observations is adopted to lower the neutral streamline (Section 8, Equations 8-1 through 8-8). The height of the neutral streamline within two obstacle heights of the obstacle center is lowered by an amount, δ:

$$\delta(x) = \Delta\left(1 - \frac{|x|}{2a}\right), \text{ for } |x|<2a \qquad (2\text{-}10)$$

$$\delta(x) = 0, \text{ for } |x| \geq 2a$$

where

Δ is $z_C - z_{CF}$, and

z_C, z_{CF} are the streamline heights above the crest in neutral flow, and in a flow characterized by Froude number Fr, respectively.

A second approximation is derived (Section 10) to account for an obstacle with arbitrary crosswind aspect ratio, λ. In this case, two and three-dimensional streamlines are weighted to provide an intermediate plume centerline trajectory:

$$z_C = [Z_{SPH}(\psi, x) - Z_{CYL}(\psi,x)]\lambda^{-1.1} + Z_{CYL}(\psi,x) \qquad (2\text{-}11)$$

and the velocity components are weighted by the aspect ratio dependent speed-up factor, S (Equations 10-13 and 10-14):

$$U(x,z,\lambda) = 2.0[S(\lambda) - 1.5]\, U_{CYL}(x,z)$$

$$+2.0[2.0 - S(\lambda)]U_{SPH}(x,z) \qquad (2\text{-}12)$$

Model computations indicate that maximum concentrations vary significantly with obstacle size, effective stack height, and relative distance between the stack and the obstacle (Section 6). Comparisons of model predictions with available observations test the model performance for a limited number of possible combinations of these and other factors. Table 1 summarizes the range of model parameters involved in the comparisons. Note

that λ is the crosswind aspect ratio of the obstacle (Section 10), Fr is the Froude number characterizing the importance of density stratification in defining the flow (Section 8), X_s/a is the distance between the stack and the obstacle normalized by the obstacle height, and H_s/a is the effective stack height normalized by the obstacle height.

TABLE 1. RANGE OF MODEL PARAMETERS EVALUATED IN LABORATORY AND FIELD TESTS OF THE POTENTIAL FLOW MODEL

Comparison Study	λ	Fr	X_s/a	H_s/a
Smooth Tunnel (Section 7)	1, ..., ∞	999	3.7	0.4,0.6
Tow Tank (Section 9)	1	0.97	3.7	0.4
Rough Tunnel (Section 11)	1,2,3,∞	999	3.7	0.5,1.0
Widows Creek (Section 12)	4	1.3-1.7	32	>1
	∞	0.4-1.0	12	>1

The "smooth tunnel" comparisons (Section 7) and the "tow tank" comparisons (Section 9) test the model under conditions that minimize the influence of processes not contained in the model. They show that the model is able to predict the observed maximum surface concentration within a factor of two (generally, overpredicting), depending on the interpretation of the observed plume properties in the absence of the obstacle.

The "rough tunnel" comparisons (Section 11) include the effects of a strong boundary layer on flow over obstacles with a triangular cross section. Model predictions of maximum surface concentrations are again within a factor of two (overprediction) for obstacles of aspect ratio 1. However, as the crosswind aspect ratio increases, the concentration predictions fall below the observations. The data indicate that the plume size is significantly enhanced upstream and over hills with the larger aspect ratios. The deformations included in the potential flow field approximation are only partly responsible. A better understanding of plume dispersion in a deforming boundary layer flow is likely to be needed to describe these experiments more accurately.

The "Widows Creek" full-scale comparisons (Section 12) also show the importance of accurately describing plume dispersion in the atmosphere. In most cases, predicted surface concentrations are extremely sensitive to the dispersion parameters assumed. The limited comparisons of the model with field data show that most of the observations fall between model predictions when the two most appropriate dispersion parameter classes are used. But, much more field data will be required to adequately evaluate the model for full-scale applications in the atmosphere.

The comparisons with laboratory data are put into perspective by comparing the observed peak concentrations with predictions of a level plume approach and a terrain-following approach. For the level plume approach, the predicted concentrations in the cases studied equal the centerline concentrations (in the absence of reflection), which range from a factor of 5 to two orders of magnitude greater than the observed surface concentrations. In the case of the terrain-following approach, predicted concentrations are essentially zero. In terms of a "partial height correction" approach, which is an intermediate approach between the level plume and the terrain-following plume approaches (Section 7), the observations as well as the potential flow model indicate that a plume path coefficient of 0.35 is needed to simulate unstratified flow over the symmetric hill (not a ridge) in the smooth tunnel, and a plume path coefficient of 0.15 to 0.18 may be an approximate choice for a moderately stratified flow (Froude number nearly 1.0) over a symmetric hill in the tow tank. In the rough tunnel, plume path coefficients based on the observations and the potential flow model predictions vary between 0.46 and 0.76.

These preliminary assessments suggest that with verification and refinement, the approach may be applicable to the following situations:

- isolated, single terrain obstacles of arbitrary height, of cross-section approximately circular in a plane parallel to the wind direction, and of arbitrary aspect ratio in the crosswind direction; and
- neutral to slightly stable stratification (depending on effective stack height).

A number of limitations arise mainly from physical effects that are not described by the potential flow model. The model should not be applied to the following situations:

- stable flow cases in which the plume may directly impact the hill;
- dispersion cases dominated by surface boundary layer effects;
- unstable cases (e.g., strongly convective situations) for which potential theory is unsuitable; and
- cases dominated by wake effects.

The range of suitable applications of the model is also limited by the theoretical approximations made, and by the limited configurations studied experimentally. These limitations include:

- the "thin plume" approximation ($\sigma_z/n_s << 1.0$ where n_s is the height of the plume centerline above the hill crest);
- the surface boundary layer effects not considered in the model;
- the Gaussian behavior assumed in the model in contrast to non-Gaussian behavior seen in some of the experimental results;

- restriction of the available experiments to a small number of stack heights, and to fixed configuration of obstacle relative to stack; and
- the hill shapes used in the laboratory experiments, as compared to the spherical hill shape assumed in the theoretical calculations.

However, from the preliminary comparisons of the model with laboratory data, it is noted that the "thin plume" approximation may effectively be relaxed to $\sigma_z/n_s \leq 0.3$. Indeed, the errors introduced by such a relaxation are not as serious as those introduced with either the level plume or the terrain-following plume approaches.

SECTION 3

RECOMMENDATIONS

The following recommendations are proposed for extending the applicability of the model and for its verification.

- The complex terrain model uses the PGT diffusion coefficients derived from observations made in flat terrain to predict what will happen in complex terrain. The accuracy of the model might be improved by using updated dispersion curves. These updated curves would include, for example, changes with roughness length or intensity of the wind direction fluctuations.
- The changes in the properties of the boundary layer over a hill are not well understood theoretically. Further laboratory studies of the behavior of the boundary layer could lead to better engineering approximations to some of the effects.
- Developing an approximate treatment for computation of ground-level concentrations in the wake of a hill would extent the applicability of the present model.
- The applicability of the model could also be extended by incorporating known solutions to the potential flows around bodies of different shapes, e.g., a bluff, or an elliptical ridge. The problem of very stable flow around an ellipsoidal hill, or of a stack positioned away from the plane of symmetry, might also be addressed. Specific laboratory experiments of these flows would be important in testing the generalized model.
- The present model does not treat a situation in which the wind direction is oriented at some arbitrary (not perpendicular) angle to an elongated terrain obstacle. Experiments should be made to gather the data to model the effect of nonnormal wind incidence.
- The effects of varying aspect ratio and of varying stratification have been independently incorporated into the model and are assumed to be additive. This superposition of effects seems reasonable in the absence of any data to the contrary. Experiments including stratification and varying aspect ratio would provide useful data from which the approximation could be refined.

- Although not discussed in the present work, it is recommended that the modeling technique used for stable cases should incorporate recent suggestions to include (1) effects of enhanced crosswind plume meander, (2) buoyancy effects, (3) modified turbulence typing schemes, and (4) physically realistic treatment of surface reflection. A complementary set of simple modeling algorithms should be linked to the present model to handle those cases not appropriate for the potential flow approach. Field verification of such modifications would enhance the credibility of the approaches substantially.

- Routine application of the model in the atmosphere requires the determination of the Froude number for the flow at the terrain elevation. Where only limited data are available at this height, it may be necessary to infer the Froude number from surface observations. Observational data should be analyzed to reveal the uncertainties in correspondence among Froude numbers obtained from data at terrain elevation and those inferred from standard airport observations; and model sensitivity to these uncertainties should be evaluated.

SECTION 4

COMPLEX TERRAIN MODELING: TECHNICAL ISSUES AND CURRENT STATUS

The current Guideline on Air Quality Models (EPA 1978) lists no model as being generally applicable to complex terrain situations, leaving the matter to the discretion of the EPA Regional Administrator and to "expert advice." Because modeling is used to ascertain whether a proposed pollutant source will meet ambient air quality standards [e.g., National Ambient Air Quality Standards (NAAQS) and prevention of significant deterioration (PSD) increments], the decision to permit new or expanded industrial and energy production facilities in complex terrain areas may be highly sensitive to differences in complex terrain modeling techniques.

As background to the modeling approach adopted, this section provides a brief overview of the present state-of-the-art for complex terrain modeling, including key technical areas of interest, recent advances and current research, and recent field and laboratory experiments.

Physical processes of interest in complex terrain include:

- terrain-induced perturbations on wind speed and direction and plume trajectories for different stability conditions;
- terrain-induced perturbations on the kinematics of plume shape, spread, and growth for different stability conditions;
- augmented atmospheric turbulence levels and increased plume dispersion coefficients;
- effects on plume rise owing to buoyant entrainment and vertical shear; and, therefore, on estimates of maximum ground-level impact in complex terrain; and
- special aerodynamic effects, such as plume stagnation on the windward side of terrain features under stable flow conditions, and wake effects on the leeward side of terrain features.

4.1 Terrain-Induced Kinematic Constraints on Dispersion and Plume Trajectories

As a result of distortion due to air flow around terrain obstacles, a plume will pass through phases of acceleration and deceleration along its trajectory. To first order, these effects are independent of the effects of turbulent diffusion. In particular, for an incompressible fluid, mass continuity requires that an increase in velocity along a streamtube will result in a decrease in streamtube cross-sectional area, and vice versa. Thus, for example, a plume passing up and over an elevated ridge is expected to increase velocity over the crest; correspondingly, the plume vertical spread

will decrease. Hunt and Mulhearn (1973) applied two-dimensional potential flow theory to quantitatively describe the resulting ground-level concentration distribution. Their method involved superimposing diffusion effects into streamline trajectories defined by the potential flow theory. The methods used included both simple gradient-transfer (K-theory) assumptions and the statistical theory of turbulent diffusion extended to deforming flows. The results for flow over a cylindrical hill showed that for a source a few hill heights upwind, the ground-level concentrations approached those expected in the absence of the hill. Egan (1975) used potential flow assumptions to describe the closeness of approach of a plume to ground level, and the plume spread due to kinematic deformation effects, for two cases: flow normal to a half-cylinder, and flow normal to a hemisphere.

For two-dimensional flow normal to a half-cylinder, an elevated plume that follows a streamline is constrained to pass nearest to the ground just above the crest of the cylinder. However, above the crest the streamline spacing is narrower than elsewhere, which tends to decrease σ_z over the crest. These two effects tend to compensate, such that the ground-level concentrations may not be markedly larger than those expected in the absence of the hill. This result should apply qualitatively to flow normal to ridge-type terrain features.

For three-dimensional neutral flow normal to a hemisphere, the streamlines approach the surface more closely, and converge more than in the flow over a half cylinder. Axial symmetry results in distortion of a streamtube element as it passes over the crest. The flow kinematics cause a marked local increase of σ_y and a marked local decrease of σ_z over the crest, and the effects combine to increase ground-level concentrations significantly in the vicinity of the hill top.

Hunt and Mulhearn (1973) could not extend their statistical theory approach to predict the concentrations at the surface; rather, they developed an asymptotic thin plume solution to the advection-diffusion equation. This solution forms the basis of the method adopted for this analysis.

In more recent work, Britter et al. (1976) generalized the Hunt and Mulhearn model to calculate dispersion in inhomogeneous turbulent flows around hills and other obstacles. They showed that wakes downwind of terrain can produce a 30% increase in ground-level concentrations at downwind distances as great as 30 hill heights. They investigated dispersion over low hills and compared theoretical results with experimental laboratory measurements to show that hills with small slopes may have a large effect on surface concentrations. In general, they concluded, terrain-induced convergence and divergence in the flow field will dominate small-scale turbulent diffusion in controlling plume spread. Hunt and Snyder(1978) provided further evidence of the increase of ground-level concentrations for three-dimensional flows over obstacles.

4.2 Enhanced Dispersion in Complex Terrain

Field studies (e.g., Miller 1978) suggest that the routine use of the PGT dispersion estimates in complex terrain situations can lead to erroneous estimates of ground-level concentrations. Systematic errors are noted both in near-field and far-field regimes. It appears that dispersion coefficients should often be modified toward less stable values. A number of investigators

have suggested that, in complex terrain settings, a shift of one stability classification toward unstable is appropriate (Hinds 1970, Leahey et al. 1973, Leahey 1974, MacCready et al. 1974, Cramer 1975, Start et al. 1975, Start et al. 1976, and Shearer et al. 1977).

During stable conditions the effect of terrain upwind of an elevated source is primarily to increase the crosswind spread or meander of the plume, perhaps because of eddies created in the horizontal plane. Airborne measurements of plume growth under differing wind direction-terrain configurations (Schiermeier and Niemeyer 1970) show that upwind terrain is important in increasing the crosswind spread, but has lesser effect in enhancing vertical dispersion rates. For settings in which the upwind fetch does not include high terrain capable of creating eddy flows, one does not expect to observe large crosswind meander at high elevations. Crosswind meander is observed to be largest, other things be equal, for low horizontal wind speeds.

4.3 Buoyant Entrainment Effects on Peak Plume Impact in Complex Terrain

Convective activity may cause buoyant plumes to grow rapidly by entrainment of ambient air. This buoyancy-induced growth becomes less important as the plume travels downwind; and ultimately, the effects of ambient turbulence dominate the plume growth.

Over level terrain, the maximum ground-level concentration occurs at downwind distances where the vertical spread of the plume is a large fraction of the final plume elevation. At such distances the dimensions of the plume are largely the result of ambient turbulence and are largely independent of the initial buoyancy-induced entrainment. For this reason, buoyancy effects on the plume growth rates are often ignored in air quality impact analyses; rather, use is made of dispersion coefficients based on experiments with passive, nonbuoyant plumes [e.g., the PGT or American Society of Mechanical Engineers (ASME 1968) coefficients].

For a plume traveling toward complex terrain the location of maximum ground-level impact may not be far downwind, and plume dimensions in the region of maximum impact may be dominated by buoyancy effects rather than by ambient turbulence levels.

The growth caused by buoyancy can be estimated on the basis of assumptions in the Briggs plume rise formulae (Briggs 1969). Specifically, Briggs noted from observations of rising plumes that the radius, r, is about one-half the plume centerline rise. This implies that plume growth is proportional to plume rise. Cramer (1975) incorporated this observation into estimates of plume expansion by defining a virtual source distance using an initial plume dimension of $\Delta H/4.3$. Pasquill (1978) suggested that the growth is about $\Delta H/\sqrt{10}$ and that it can be incorporated by summing the squares of buoyant growth and ambient turbulent growth.

Egan et al. (1976) present examples of the difference between σ_z, the passive (nonbuoyant) PGT vertical dispersion coefficient, and $(\sigma_z)_e$, the buoyancy-enhanced dispersion coefficient, for a typical 1,000 megawatt fossil-fuel fired power plant under various atmospheric stability conditions. The largest differences occur for stable atmospheric conditions and low wind speeds; at a downwind distance of about 1,900 m (about the location of final

plume rise), significant differences in ground level concentration estimates would be expected on high terrain.

The potential flow model results with and without buoyancy enhancement are compared with the Widows Creek Power Plant data. But the FMP laboratory experiments used only neutrally buoyant plumes, so for those comparisons only the no-enhancement calculations are appropriate.

4.4 Plume Dispersion and Transport Under Stable Flow Conditions

Stably stratified flow experiments in the laboratory demonstrate that the flow properties determining the trajectory of the plume around an obstacle are sensitive to the ratio of inertial and buoyancy forces. Flow normal to a two-dimensional ridge under stable atmospheric conditions may pass over the ridge--if stratification is weak and wind speed is sufficiently high. If the temperature inversion is strong and winds light, the flow may "block" upwind of the terrain; that is, a plume may not have sufficient kinetic energy to flow over the ridge. These situations require special treatment of crosswind dispersion and reflection from the ground surface. Different modeling approaches have been taken to characterize enhanced horizontal dispersion by plume meander during light wind conditions. These include: (a) explicit sector averaging with a variable stability-dependent sector width (e.g., EPA VALLEY model); (b) multiple sector averaging (e.g., ERT ERTAQ model); and (c) statistical sector averaging using randomized wind fields (e.g., EPA CRSTER model).

In flat terrain, the zero surface flux boundary condition leads to the image source argument (Csanady 1973), implying a doubling of ground-level concentrations at large downwind distances. This doubling factor may be incorrect in many complex terrain situations. A number of investigators (Briggs 1973, Cabe 1977, and Williams 1977) have suggested that in abruptly rising terrain Gaussian models should be used without doubling the surface concentrations (the 'reflection effect'). Britter, Hunt and Puttock (1976) and Hunt, Puttock and Snyder (1979) report, on the basis of physical model studies of terrain objects, that the peak surface concentration is close to the peak plume centerline value upwind of the obstacle; doubling of concentrations is not observed. Egan et al. (1979) have recently developed an algorithm for quantitative estimates of the reflection coefficient as a function of terrain slope, plume height, and downwind distance. This algorithm gives a reflection coefficient of one for flat terrain, and zero for the limit of direct incidence on a vertical bluff. The algorithm has not yet been tested with field or physical model experiments.

The potential flow theory described in Section 5 does not address these stable flow incidence situations.

SECTION 5

APPLICATION OF POTENTIAL FLOW THEORY

5.1 Modeling Criteria and Rationale

As a practical matter, it is neither feasible nor necessary to model all possible combinations of topography and meteorological flow. For regulatory purposes, the required modeling approach should emphasize those cases with a demonstrated potential for high ground-level concentrations.

The modeling approach described in this report addresses the development of methods for neutral and slightly stable conditions. For neutral atmospheric stability conditions, potential flow theory predicts that flow close to the surface and perpendicular to an infinite, semicircular ridge (a two-dimensional terrain obstacle) will accelerate and will lift over the ridge. A typical streamline is only about one-half as high above the ridge crest as it is above the surface upwind of the obstacle. (Streamlines for potential flow over a cylinder are shown in Figure 18b in Section 8).

Because the flow accelerates, streamline spacing decreases and the vertical dimensions of a non-diffusing plume decrease by approximately a factor of two. Thus, the ratio of plume centerline height to vertical dispersion coefficient σ_z remains approximately the same as the ratio over flat terrain.

But when the flow approaches a sphere under neutral flow conditions, the comparable streamline approaches the surface much more closely, and (it can be shown) this ratio is much smaller. This results in much larger ground-level concentrations.

5.2 Gaussian Formulations in Complex Terrain

Many of the characteristics of flow fields in flat terrain are significantly altered by the presence of terrain obstacles. Flow field assumptions explicit to the application of Gaussian diffusion models include:

- uniform (non-accelerating) velocity fields,
- constant plume centerline height (equal to stack height plus plume rise) above a flat surface, and
- dispersion coefficients (σ_y, σ_z) determined by ambient turbulence levels independent of the mean flow.

Because these assumptions are not generally valid in complex terrain, use of a Gaussian plume model requires thought as to how to include these features in a terrain-influenced situation. This section discusses the modifications made in order to keep a Gaussian description of plume dispersion.

Table 2 illustrates the form of the vertical distribution of concentration, $\chi(x,z)$, and the scale of the vertical spread (proportional to σ_z) implied by solutions of the parabolic diffusion equation for a continuous crosswind line source. In Case 1 (flat terrain), both the diffusivity, K, and the wind speed, U, are assumed constant in the downwind direction, x. The solution is the familiar Gaussian form with $\sigma_z^2 = 2Kx/U$. If it is assumed that the diffusivity varies with downwind distance (again for flat terrain), the solutions have the form shown for Case 2 in Table 2, with factors expressed as line integrals along the plume trajectory. Finally, consider flow over a terrain obstacle (Case 3, Table 2) with the wind speed undergoing regions of deceleration and acceleration. Here, the downwind distance, s, is along the plume trajectory. Although the forms of the solution and scale of the vertical spread are not immediately familiar, it can be seen that they reduce to the constant wind speed and diffusivity situation (Case 1) in the limit of flat terrain. Such solutions will become more familiar in Section 5.4 (Equations 5-11 and 5-23).

Strictly, the Gaussian form of the solution to the diffusion equation does not require that the wind speed be constant along the trajectory of the plume. A non-uniform velocity field can be accommodated within the Gaussian framework by evaluating a simple integral if U(s) is known.

Plume deformation and variable trajectory height can also be accommodated. Assume, for example, that the Gaussian dispersion equation for a complex situation is written as:

$$\chi = \frac{2Q}{(2\pi\sigma_y\sigma_z U)_f\,(\alpha_y\alpha_z)} \exp\left(\frac{-\eta^2 z^2}{2(\sigma_z^2)_f \alpha_z^2}\right) \qquad (5\text{-}1)$$

where

χ is ambient pollutant concentration,

Q is emission rate of pollutant,

f denotes "flat" terrain values,

α_y, α_z is $\sigma_{y,z}/(\sigma_{y,z})_f$ the ratios of complex terrain to flat terrain dispersion coefficients (the coefficients differing because of plume deformation in the presence of terrain obstacles),

z is height of plume centerline in flat terrain, and

η is ratio of height of plume centerline above surface of terrain obstacle to the height of plume centerline above the surface in the flat terrain case.

TABLE 2. FORM OF VERTICAL DISTRIBUTION AND VERTICAL SPREAD IMPLIED BY SOLUTIONS OF THE CLASSICAL PARABOLIC EQUATION OF DIFFUSION*

Case	Diffusivity	Wind Speed U	Form of B in $\chi(x,z) = \chi(x,0)\exp(-B)$	Scale of Vertical Spread
(1) flat	K (constant)	U (constant)	$Uz^2/\left[4Kx\right]$	$2(Kx/U)^{1/2}$
(2) flat	K(x)	U (constant)	$Uz^2/\left[4\int_0^x K(x')dx'\right]$	$2\left(\frac{1}{U}\int_0^x K(x')dx'\right)^{1/2}$
(3) terrain	K(s)†	U(s)	$[U(s)]^2z^2(s)/\left[4\int_0^s K(s')U(s')\,ds'\right]$	$\frac{2}{U(s)}\left(\int_0^s K(s')U(s')\,ds'\right)^{1/}$

* $\overline{U}\frac{\partial\overline{\chi}}{\partial x} = \frac{\partial}{\partial z}\left(K\frac{\partial\overline{\chi}}{\partial z}\right)$

†s = distance along plume centerline trajectory.

Adapted from Pasquill (1978), p. 4.

This is an assumed form, not a derivation; note that the choices $\eta = \alpha_y = \alpha_z = 1.0$ reduce Equation 5-1 to the flat terrain Gaussian model. This formula conceptually distinguishes: (a) plume spread (increase in σ_y) or shrinkage (decrease in σ_z) by flow deformation and (b) change of the plume centerline trajectory owing to the presence of a terrain obstacle.

Changes in the concentration due to the accompanying changes to the velocity field are not explicitly accounted for in Equation 5-1 because these only enter into the concentration scaling factor. Small changes in the transport velocity will result in small, inverse changes to the scaling factor or centerline concentration.

The plume centerline concentrations will also depend on the product of the parameters σ_y and σ_z. The ground-level concentration, on the other hand, will vary with the ratio $(\eta/\alpha_z)^2$ in the exponential term. Egan (1975) has argued that for neutral flow over two-dimensional obstacles--where $\eta/\alpha_z \approx 1.0$--flow deformation has little or no effect on ground-level values; for flows approaching a three-dimensional obstacle, however, $\eta/\alpha_z < 1.0$, leading to ground-level concentrations larger that those in analogous flat terrain situations.

In the discussion in Section 5.4, the quantity ηz, the height of the plume centerline above the terrain, is evaluated by a particular two- or three-dimensional stream function (see Section 5.4.3) and the values of α_y, α_z in Equation 5-1 are defined (see Equations 5-56, 5-57; Section 5.5) in terms of particular line integrals. Thus, the method adopted is essentially a modified Gaussian dispersion model.

5-1/8

5.3 Modeling Approach, Applicability, and Limitations

This technique applies potential flow theory to a Gaussian point source model. It permits explicit evaluation of the terrain-induced kinematic constraints and trajectory variations. In adopting the present technique, an attempt has been made to broaden its applicability. Approximations have been developed to extend the neutral formulation to slightly stable cases and to allow for terrain obstacles with crosswind shapes intermediate between those of a cylinder and a sphere. These approximations are based both on theoretical and semi-empirical grounds. As presented in the following sections, the approach may be suitable for the following topographic and meteorological situations:

- isolated, single terrain obstacles of arbitrary height, with approximately circular cross-section in the downwind direction and arbitrary aspect ratio in the crosswind direction; and
- neutral to slightly stable stratifications.

At the outset, the limitations of the present model should be clearly stressed. These limitations arise mainly from physical effects that are not described by the potential flow model. The following cases are excluded:

- stable flow cases, where plumes are constrained to flow around rather than over the obstacle;
- cases dominated by surface boundary layer effects;

- unstable cases (e.g., convective situations); and
- cases dominated by wake effects.

Specific recommendations based on these limitations were presented in Section 3

5.4 Theoretical Basis of Potential Flow Algorithms--Neutral Flows

The potential flow complex terrain model incorporates the theory developed by Hunt and Mulhearn (1973) and Hunt and Snyder (1978) for turbulent plumes embedded within potential flow fields. They developed solutions to the diffusion equations describing flow fields over two-dimensional and three-dimensional axisymmetric terrain obstacles. Qualitatively, these solutions are of Gaussian form, with crosswind and vertical dispersion coefficients evaluated as line integrals of the velocity field along the plume centerline trajectory. Because the mathematics used are not immediately familiar, some details of the derivation are presented; the reader is urged to consult the original references.

5.4.1 Two-Dimensional Obstacles

The starting point for the calculation is the two-dimensional advection diffusion equation in the streamline coordinate system (s,n,y):

9-1/8"

$$u(s)\frac{\partial \chi'}{\partial s} + n\frac{\partial v}{\partial n}\frac{\partial \chi'}{\partial n} = D_1(s)\frac{\partial^2 \chi'}{\partial n^2} + D_2(s)\frac{\partial^2 \chi'}{\partial y^2} \qquad (5\text{-}3)$$

Here, s, n, and y are dimensionless directional coordinates in the along plume, normal, and crosswind directions relative to the plume trajectory. When the terrain is flat and the trajectory is level, the s and n directions correspond to the downwind distance, x, and the vertical distance from plume centerline, z. In Equation 5-3, u and v are velocities along and normal to the trajectory, and $D_1(s)$ and $D_2(s)$ are diffusivities in the n and y directions that vary along the trajectory. χ' is the dimensionless concentration. The variables in Equation 5-3 are nondimensionalized by the height of the obstacle, a, and the uniform velocity upwind of the source, U_∞, such that:

$$\chi' = \chi U_\infty a^2/Q \qquad (5\text{-}4a)$$

$$u(s) = U(s)/U_\infty \qquad (5\text{-}4b)$$

$$v(s) = V(s)/U_\infty \qquad (5\text{-}4c)$$

$$D_1(s) = K_1(s)/[aU_\infty] \qquad (5\text{-}4d)$$

$$D_2(s) = K_2(s)/[aU_\infty] \qquad (5\text{-}4e)$$

where Q is the source strength (mass/unit time), U(s) and V(s) are the dimensional velocities (length/unit time), and $K_1(s)$ and $K_2(s)$ are the

dimensional diffusivities (length squared/unit time). The relationship between these diffusivities and the PGT dispersion coefficients (Turner 1970) is explored in Section 5.5.

Substituting the continuity equation:

$$\frac{\partial v}{\partial n} + \frac{\partial u}{\partial s} = 0 \qquad (5\text{-}5)$$

into Equation 5-3 yields:

$$u(s)\,\frac{\partial \chi'}{\partial s} + n\,\frac{\partial u}{\partial s}\,\frac{\partial \chi'}{\partial n} = D_1(s)\,\frac{\partial^2 \chi'}{\partial n^2} + D_2(s)\,\frac{\partial^2 \chi'}{\partial y^2} \qquad (5\text{-}6)$$

Solutions to Equation 5-6 are sought that are Gaussian in form:

$$\chi'(s,n,y) = \frac{1}{g(s)}\,\exp\left[-f_1(s)\,n^2 - f_2(s)\,y^2\right] \qquad (5\text{-}7)$$

and also satisfy the additional constraint that the mass flux across the plume is constant, i.e.:

$$\int_{-\infty}^{+\infty}\int_{-\infty}^{+\infty} u(s)\,\chi'\,dn\,dy = 1.0 \qquad (5\text{-}8)$$

9-1/8"

This constraint requires that:

$$g(s) = \pi\,u(s) \,/\, \left[f_1(s)\,f_2(s)\right]^{1/2} \qquad (5\text{-}9)$$

Substituting Equation 5-7 into 5-6 yields:

$$f_1(s) = [u(s)]^2 / [4\,\phi(s)] \qquad (5\text{-}10a)$$

$$f_2(s) = 1/[4T(s)] \qquad (5\text{-}10b)$$

where:

$$\phi(s) = \int_0^s D_1(s')\,u(s')\,ds' \qquad (5\text{-}11)$$

and

$$T(s) = \int_0^s [D_2(s')/u(s')]\,ds' \qquad (5\text{-}12)$$

By Equation 5-9

$$g(s) = 4\pi[\phi(s)\ T(s)\ ]^{1/2} \tag{5-13}$$

In more familiar terms, the dispersion coefficients in the Gaussian form of the diffusion equation solution, σ_n and σ_y, are given by:

$$f_1(s) = 1/[2\sigma_n^2] \tag{5-14a}$$

$$f_2(s) = 1/[2\sigma_y^2] \tag{5-14b}$$

or

$$\sigma_n^2 = 1/[2\ f_1(s)] = 2\phi\ (s)/[u(s)]^2 \tag{5-15}$$

$$\sigma_y^2 = 1/[2\ f_2(s)] = 2T(s) \tag{5-16}$$

5.4.2 Three-Dimensional Axisymmetric Obstacles

The arguments for three dimensions proceed much the same as in the previous section. The appropriate non-dimensional diffusion equation is:

$$u(s)\ \frac{\partial \chi'}{\partial s} + n\ \frac{\partial v}{\partial n}\ \frac{\partial \chi'}{\partial n} = D_1(s)\ \frac{\partial^2 \chi'}{\partial n^2} + D_2(s)\ \frac{\partial^2 \chi'}{\partial \gamma^2} \tag{5-17}$$

where the coordinate system is now with respect to (s,n,γ). Here, γ is the angular, azimuthal coordinate from the axis of symmetry along the flow with:

$$y = \gamma R(s) \tag{5-18}$$

where R(s) is the distance from the axis of symmetry of the obstacle to the plume centerline, and y is the cross-wind distance from the plume centerline. The continuity equation in this coordinate system becomes:

$$\frac{\partial v}{\partial n} + \frac{1}{R(s)}\ \frac{d}{ds}\ [u(s)R(s)] = 0 \tag{5-19}$$

The trial solution sought is of the form:

$$\chi'(s,n,\gamma) = \frac{1}{g(s)}\ \exp[-f_1(s)\ n^2 - f_2(s)\gamma^2] \tag{5-20}$$

subject to the constraint:

$$\int_0^{2\pi} \int_{-\infty}^{+\infty} u(s)\ \chi'(s,n,\gamma)R(s)\ dnd\gamma = 1.0 \tag{5-21}$$

Substitution of Equation 5-20 into 5-17 yields:

$$f_1(s) = [u(s)R(s)]^2 / [4\phi(s)] \quad (5\text{-}22a)$$

$$f_2(s) = 1/[4T(s)] \quad (5\text{-}22b)$$

where

$$\phi(s) = \int_0^s D_1(s') [R(s')]^2 u(s') \, ds' \quad (5\text{-}23)$$

$$T(s) = \int_0^s [D_2(s')/[u(s') R^2(s')]] ds' \quad (5\text{-}24)$$

and substitution of Equations 5-20 and 5-22 into 5-21 gives:

$$\xi(s) = 4\pi [\phi(s) T(s)]^{1/2} \quad (5\text{-}25)$$

The forms of the familiar Gaussian dispersion coefficients are obtained by substituting Equation 5-22 into Equation 5-14a and b:

$$\sigma_n^2 = 2\phi(s) / [u(s) R(s)]^2 \quad (5\text{-}26)$$

$$\sigma_y^2 = 2 [R(s)]^2 T(s) \quad (5\text{-}27)$$

5.4.3 Role of Potential Flow Theory

Values of the dispersion coefficients (Equations 5-15, 5-16, 5-26, and 5-27) are determined at a particular distance, s, along the plume centerline by line integrals (such as Equations 5-23 and 5-24) which are functions of the velocity along the plume centerline streamline, u(s), and (in the three-dimensional case) by the distance, R(s), from the axis of symmetry. In the potential flow approach adopted, s, u(s), and R(s) are determined for a particular terrain shape by a stream function, ψ. That is, the variation of velocity along the plume centerline and the distance of the plume centerline from the surface (defining the plume trajectory) are evaluated analytically using the streamline equation.

It is assumed that the plume centerline follows the streamline through the point source at the effective source height, H_s. Along a streamline, the value of the stream function is constant, and the particular value of the plume centerline stream function is denoted by ψ_s. The value of ψ_s is determined by three parameters: (1) effective source height H_s; (2) height of the obstacle, a; and (3) distance along the x-axis from the base of the source to the center of the obstacle, X_s. The streamline associated with a

particular stream function, ψ, is determined by the shape and dimension of the terrain obstacle. The streamline taken to be the plume centerline is:

$$\psi(x,z) = \psi_s(X_s, H_s) \tag{5-28}$$

This gives the height of the plume centerline above the surface at any downwind distance, x. The velocity field, too, is determined by the stream function, ψ, such that the along-streamline velocity, u(s), is:

$$u(s) = \left[\left(\frac{\partial\psi}{\partial x}\right)^2 + \left(\frac{\partial\psi}{\partial z}\right)^2 \right]^{1/2} \tag{5-29}$$

The cases examined in subsequent sections include flow over a two-dimensional ridge and over a three-dimensional axisymmetric hill. In the two-dimensional case, the stream function (Milne-Thomson 1960, p. 156) is:

$$\psi^{2D}(x,z) = U_\infty z\left(1 - \frac{a^2}{x^2 + z^2}\right) \tag{5-30}$$

where U_∞ is the magnitude of the uniform wind velocity far upstream of the source. The value of the stream function through the source is then:

$$\psi_s^{2D}(X_s, H_s) = U_\infty H_s\left(1 - \frac{a^2}{X_s^2 + H_s^2}\right) \tag{5-31}$$

and the equation of the plume centerline is:

$$u_\infty z\left(1 - \frac{a^2}{x^2 + z^2}\right) = \psi_s^{2D}(X_s, H_s) \tag{5-32}$$

For example, the height of the plume centerline, z_c, at x = 0 (over the crest of the ridge) is given by solving the quadratic equation:

$$u_\infty z_c\left(1 - \frac{a^2}{z_c^2}\right) = \psi_s^{2D}(X_s, H_s) \tag{5-33}$$

Analogous equations are valid in three-dimensions for flow over a hemispherical hill. The stream function in this case (Milne-Thomson 1960, p. 464) is:

$$\psi^{3D}(x,z) = 0.5\, U_\infty z^2\left(1 - \frac{a^3}{(x^2 + z^2)^{3/2}}\right) \tag{5-34}$$

The value of the stream function through a source at (X_s, H_s) is:

$$\psi_s^{3D}(X_s, H_s) = 0.5\, U_\infty\, H_s^2 \left[1 - \frac{a^3}{(X_s^2 + H_s^2)^{3/2}}\right] \qquad (5\text{-}35)$$

and the equation of the plume centerline is:

$$z^2\left[1 - \frac{a^3}{(x^2 + z^2)^{3/2}}\right] = H_s^2\left[1 - \frac{a^3}{(X_s^2 + H_s^2)^{3/2}}\right] \qquad (5\text{-}36)$$

5.4.4 Reduction of Solution to Flat Terrain Case

To clarify the discussion in the previous sections, consider the situation of uniform flow with velocity U_∞ over flat terrain. The equations developed in Sections 5.4.1, 5.4.2, and 5.4.3 are applicable, and the solution reduces to a recognizable form.

The starting point is the appropriate stream function, ψ, which in this case (Milne-Thomson 1960) is:

$$\psi(z) = U_\infty\, z \qquad (5\text{-}37)$$

Note that there is no dependence on x, and streamlines are thus parallel to the x-axis. The value of the stream function through the source, ψ_s, is

$$\psi_s(H_s) = U_\infty\, H_s \qquad (5\text{-}38)$$

and, therefore, the equation of the plume centerline is:

$$\psi(z) = \psi_s(H_s) \qquad (5\text{-}39a)$$

or

$$z = H_s \qquad (5\text{-}39b)$$

This is also equal to the distance from the x-axis to the plume centerline, so that $R(s) = H_s$.

Substituting Equation 5-37 into Equation 5-29, the velocity along the plume trajectory is constant and equal to:

$$u(s) = \text{const} = U_\infty \qquad (5\text{-}40)$$

A solution in the form of Equation 5-20 can now be evaluated. In flat terrain the along-streamline coordinate, s, is just the downwind distance from the source, x, and the normal to the streamline, n, is just the vertical distance from the plume centerline, z. The line integrals ϕ, T, (Equations 5-23 and 5-24) reduce to:

$$\phi(x) = D_1(x)\, H_s^2\, U_\infty\, x \tag{5-41}$$

$$T(x) = D_2(x)\, x/[U_\infty\, H_s^2] \tag{5-42}$$

and f_1, f_2, and g are by substitution:

$$f_1(x) = U_\infty/[4D_1(x)x] \tag{5-43}$$

$$f_2(x) = U_\infty H_s^2/[4D_2(x)x] \tag{5-44}$$

$$g(x) = 4\pi x \left[D_1(x)\, D_2(x)\right]^{1/2} \tag{5-45}$$

Noting that the crosswind distance from plume centerline, y, is given by:

$$y = H_s\, Y \tag{5-46}$$

and substituting Equations 5-43 through 5-46 into Equation 5-20:

$$\chi'(x,z,y) = \frac{1}{4\pi\, x(D_1D_2)^{1/2}} \exp\left\{-\frac{U_\infty}{4x}\left[\frac{z^2}{D_1} + \frac{y^2}{D_2}\right]\right\} \tag{5-47}$$

This is the solution given by Sutton (1953) for a continuous point source. The familiar Gaussian dispersion coefficients σ_y,σ_z (see Equations 5-26 and 5-27) become:

$$\sigma_y^2 = 2D_2(x)\, x/U_\infty \tag{5-48}$$

$$\sigma_z^2 = 2D_1(x)\, x/U_\infty \tag{5-49}$$

5.4.5 Limitations

Although important features of the terrain-influenced flow field are reproduced by the potential flow theory approach, inherent limitations remain:

- the presence of a realistic surface boundary layer is ignored;
- relevant physical phenomenon such as velocity shear, radiative heating, and flow separation are omitted; and
- the theoretical model requires that the plume remain "thin" compared to its height above the terrain. For short stacks this criterion is often violated near the hill crest.

[Strictly speaking, the first two of these limitations also restrict the theoretical validity of a conventional Gaussian solution in flat terrain situations (Pasquill 1978), unless the set of dispersion coefficients assumed specifically account for these effects.] It is prudent to apply the potential flow theory approach only to the windward side of obstacles and not to situations dominated by lee wake or separation effects not treated in the model. In many of the results to be presented, the computed plume dimension will violate the restriction to "thin plumes", but it is not unreasonable to 'push' the theoretical formulation in these cases (Hunt, Puttock, and Snyder 1979).

5.5 PGT Scaling of Dispersion Coefficients

Evaluating the terrain-influenced dispersion coefficients (Equations 5-25 and 5-27) with this formulation requires specifying the crosswind and the normal diffusivities, D_2 and D_1. To compare model calculations with analogous flat terrain situations, an approximation scheme was implemented, using the PGT dispersion coefficients (Turner 1970) as a calibrating scale. Qualitatively, the diffusivity at a given distance from the source along the plume centerline streamline is taken as that for the same transit time in flat terrain. The consequence of this assumption is that model calculations of dispersion coefficients reduce to flat terrain values in the limits of large downwind distances or small obstacles.

Newer and possibly superior formulations of dispersion coefficients have been suggested (e.g., Pasquill 1978 and Irwin 1979), but have not yet been adopted in EPA regulatory models. Therefore, for ease of comparison, the familiar PGT values have been used in the calculations discussed in this report. Other dispersion coefficient systems can be easily incorporated within the basic methodology used here.

Substituting Equations 5-23 and 5-24 into Equations 5-26 and 5-27 gives explicit expressions for σ_z and σ_y. (From here on, the dispersion coefficient in the normal direction is denoted as σ_z.) At a distance, s, from the source along the streamline, the dispersion coefficients are given by:

$$\sigma_z^2(s) = \frac{2\,\bar{D}_1(s)}{u^2(s)\,R^2(s)} \int_o^s R^2(s')\,u(s')\,ds' \qquad (5\text{-}50)$$

$$\sigma_y^2(s) = 2R^2(s)\,\bar{D}_2(s)\int_0^s ds'/[R^2(s')\,u(s')] \qquad (5\text{-}51)$$

where $\bar{D}_1$, $\bar{D}_2$ are typical mean diffusivity values at distance s.
These values are assumed to be given by the PGT values (σ_{zf}, σ_{yf}):

$$\bar{D}_1(s) = \sigma_{zf}^2(s)/2t \qquad (5\text{-}52)$$

$$\bar{D}_2(s) = \sigma_{yf}^2(s)/2t \qquad (5\text{-}53)$$

where s is the integrated path length along the plume trajectory and t is the advection time:

$$s = \int_0^s ds' \qquad (5\text{-}54)$$

$$t = \int_0^s \frac{ds'}{u(s')} \qquad (5\text{-}55)$$

Substituting Equations 5-52 through 5-55 into Equation 5-50 and 5-51 yields the final form of the dispersion coefficients:

$$\sigma_z^2 = \sigma_{zf}^2 \left[\frac{\int_0^s R^2(s')\,u(s')ds'}{t\,u^2(s)\,R^2(s)}\right] \qquad (5\text{-}56)$$

$$\sigma_y^2 = \sigma_{yf}^2 \left[\frac{R^2(s)}{t}\int_0^s \frac{ds'}{R^2(s')\,u(s')}\right] \qquad (5\text{-}57)$$

The bracketed quantities approach 1 as streamline deformation becomes negligible, and σ_z,σ_y reduce to their flat terrain values.

Figures 1 and 2 illustrate the plume spread statistics σ_y and σ_z, respectively, for neutral flow over a circular ridge. The ridge is 1.0 km high; the point source, 200 m high, is 4.5 km from the ridge center. Calculations are shown for diffusivities scaled to reproduce the PGT neutral stability class values for σ_y and σ_z in the flat case. This illustrates that only the vertical dimensions of the plume (as characterized by σ_z) differ from flat terrain values in flow over two-dimensional obstacles. (In each of Figures 1 through 4, the center of the ridge is indicated by a short vertical bar at the downwind distance 4.5 km; the horizontal bar extending from 3.5 km to 5.5 km denotes the windward-leeward extent of the ridge.)

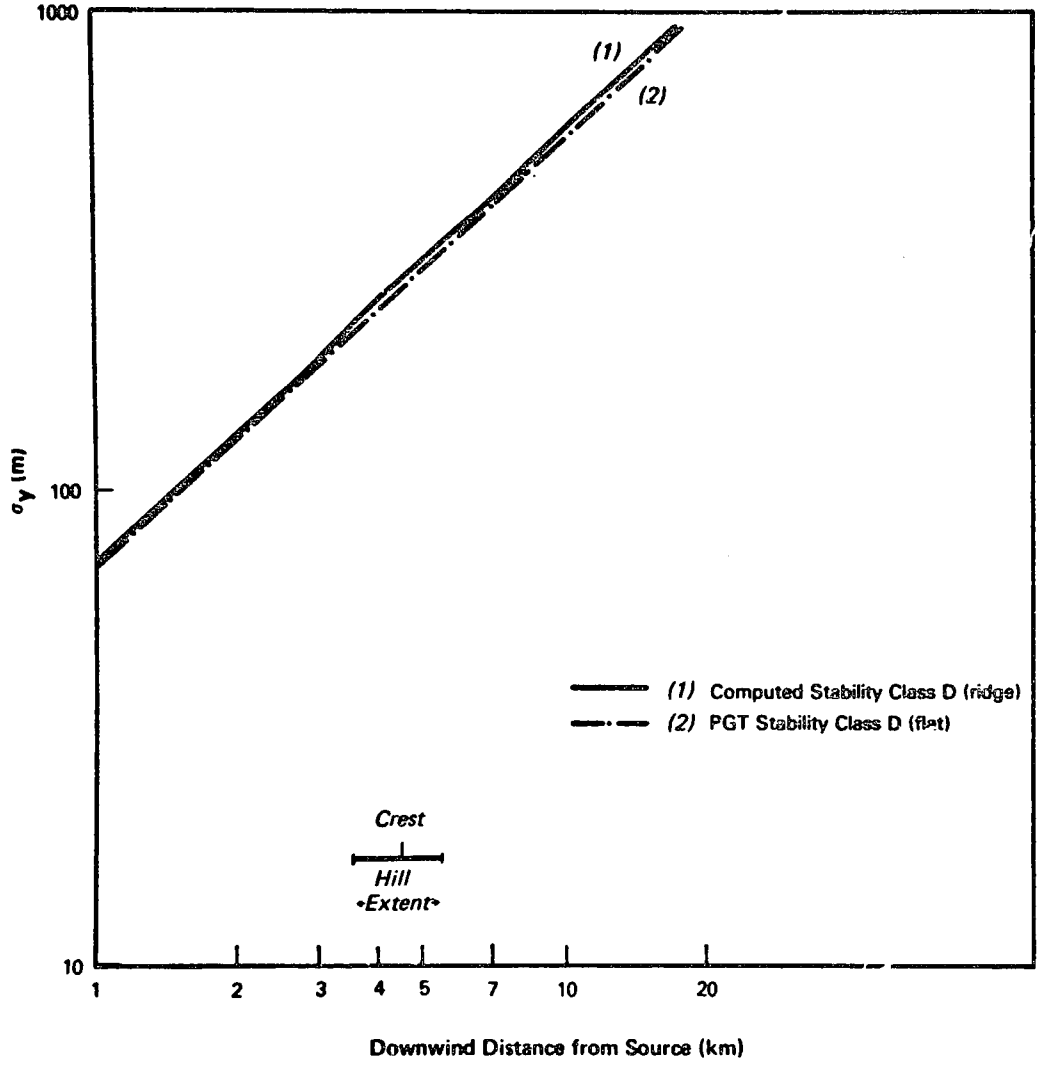

Figure 1. Horizontal dispersion coefficients for neutral flow over a circular ridge.

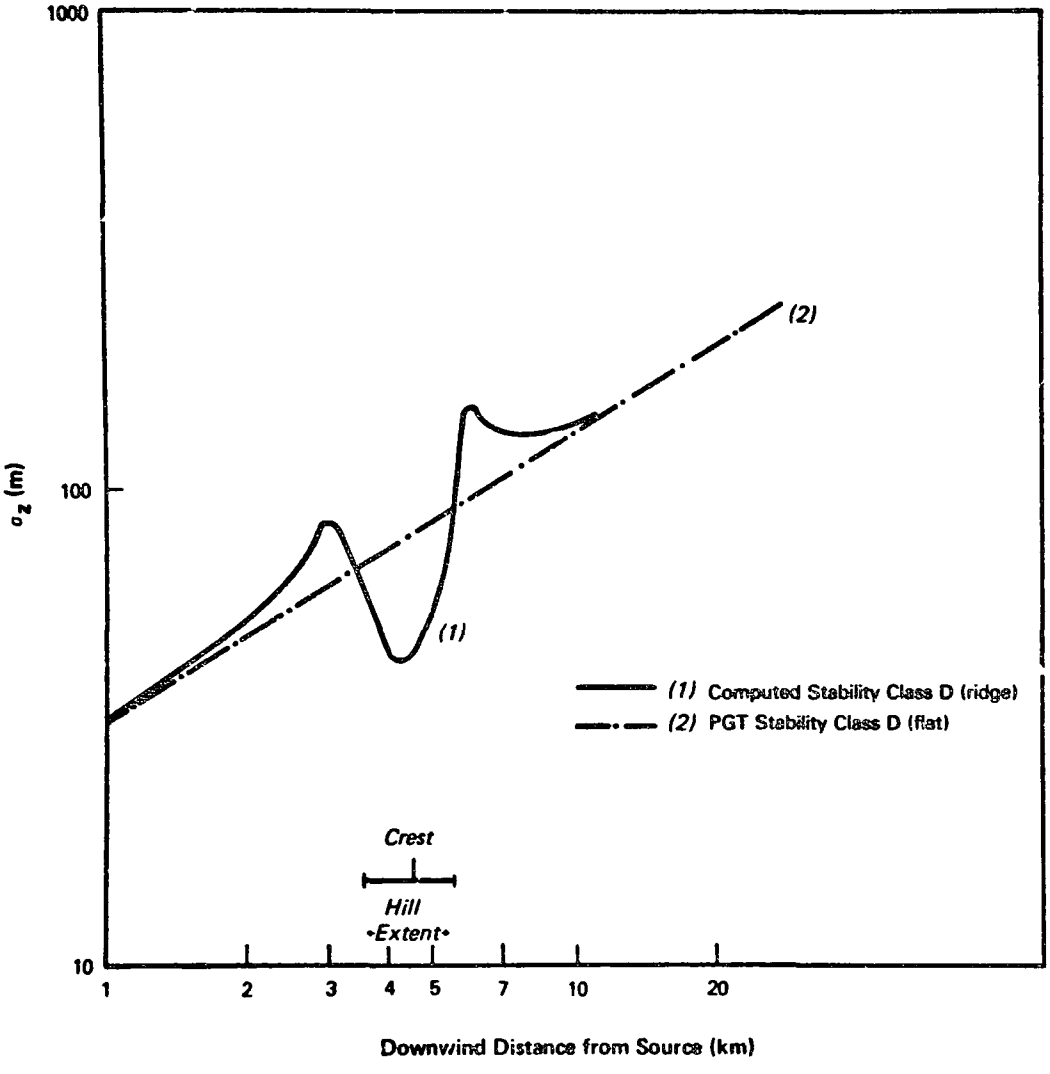

Figure 2. Vertical dispersion coefficients for neutral flow over a circular ridge.

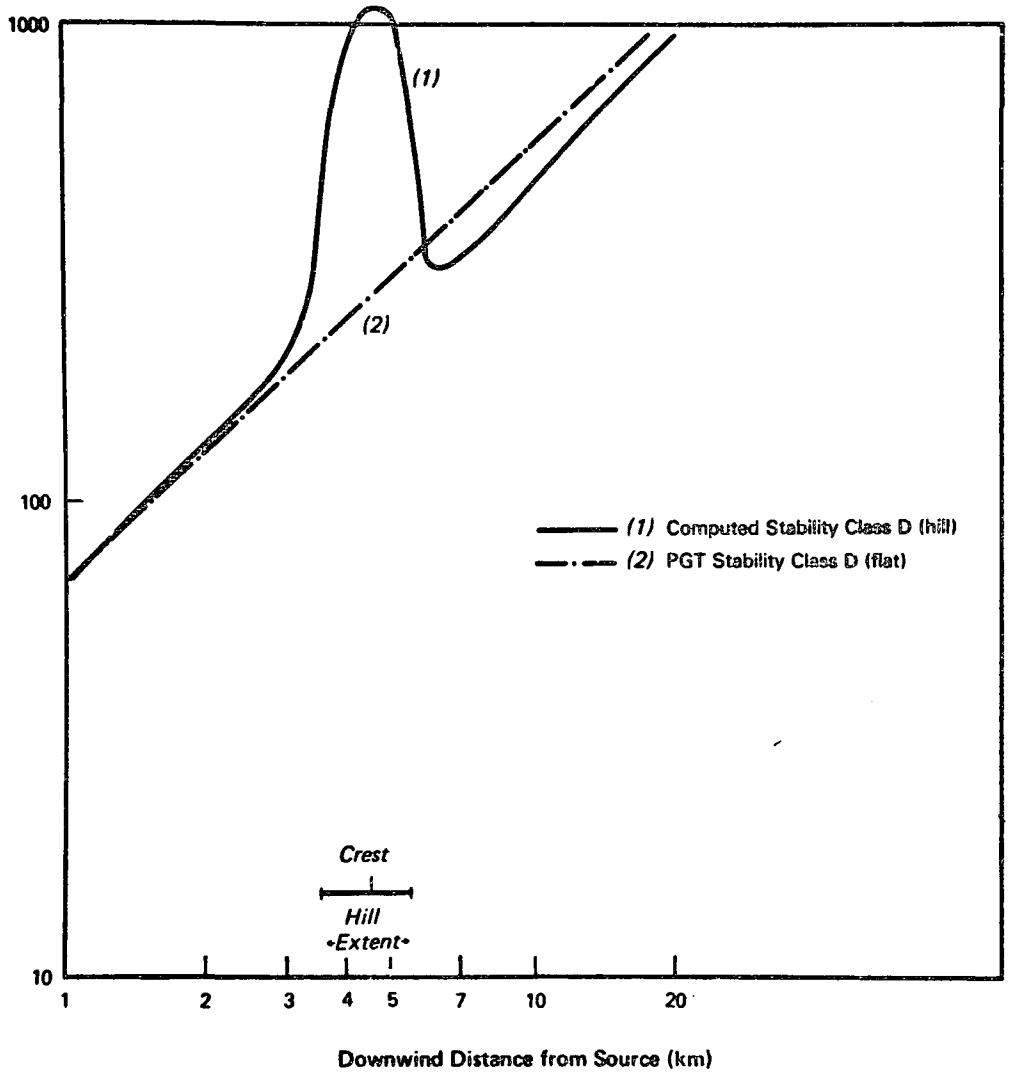

Figure 3. Horizontal dispersion coefficients for neutral flow over a hemispherical hill.

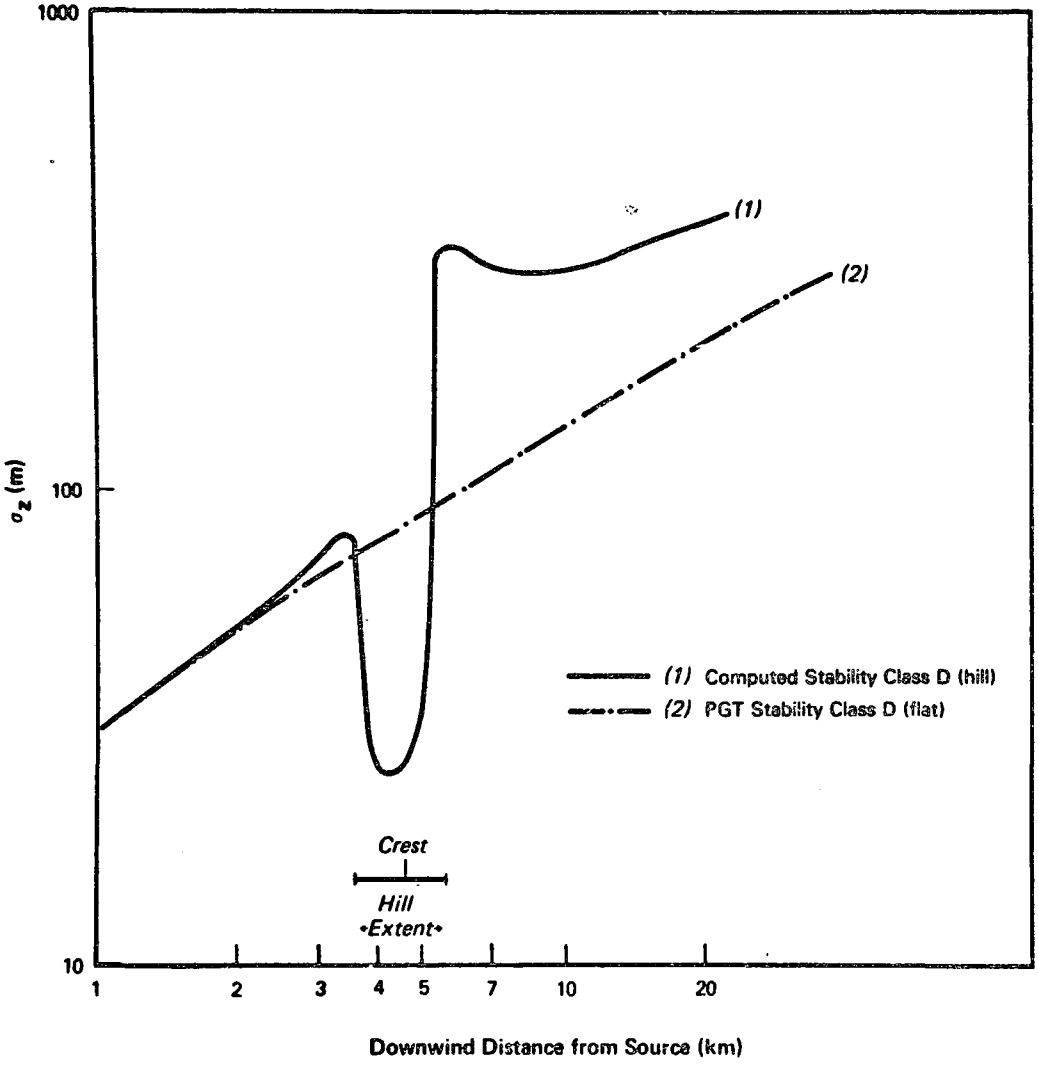

Figure 4. Vertical dispersion coefficients for neutral flow over a hemispherical hill.

As streamlines diverge to the leeward and windward side of the hill, σ_z increases. Over the ridge, vertical compression of the streamlines leads to a drastic decrease in σ_z. Over the ridge crest the vertical plume thickness is about equal to the height of the plume centerline above the surface, n_s. This marginally obeys the thin plume approximation.

Retaining the same source-obstacle geometry, but changing the terrain obstacle type from a circular ridge to a hemispherical hill, Figures 3 and 4 display the three-dimensional neutral flow results developed from Equations 5-26 and 5-27. In this case, both σ_y and σ_z are affected by the potential flow field, as evidenced by a marked increase in σ_y over the hill top. Comparing σ_z values in Figures 2 and 4 at x = 4.5 km reveals that the vertical thickness of the plume is more severely restricted in three-dimensional flow than two-dimensional flow. In fact, as indicated in Figure 4, downwind of the hill σ_z never recovers from the deformation over the hill top. At the crest, the quantity σ_z/n_s is approximately 2, clearly violating the thin plume criterion. The potential flow theory would not, strictly, be applicable in this situation; however, at least to the hill crest, useful estimates should be obtained. Downwind of the crest, σ_z is affected by two factors that tend to increase its value over that predicted by potential flow calculations alone. These are: (1) increased diffusion across streamlines because of smaller streamline spacing, and (2) terrain separation phenomena, which enhance turbulent mixing over that given by ambient turbulence rates. Because of these effects, the model should only be applied to the upwind side of terrain obstacles.

Figure 5 shows the evolution of the velocity speed up factor (the ratio of the source streamline velocity in the presence of the hill to that in the absence of the hill) for potential flows over the circular ridge and over the hemispherical hill. Both streamline patterns upwind and downwind of the obstacle crests are symmetric, so the speed-up factor has been plotted only from source to crest. The theoretical speed up value at the surface of each of the crests is 2.0 for the cylindrical ridge, and 1.5 for the hemispherical hill. Because the source streamline does not touch the surface at the crest, the surface speed up values are approached, but not attained, in Figure 5. Note that the influence of the cylindrical ridge extends farther upstream (and downstream) than does the influence of the hemispherical hill.

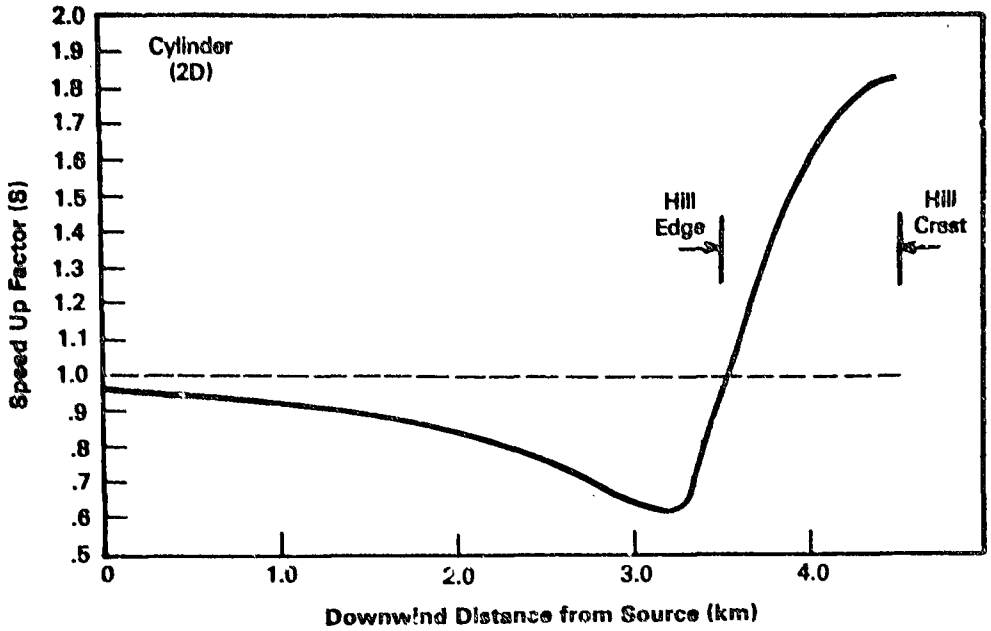

Figure 5a. Velocity speed up factors for neutral flow over a circular ridge.

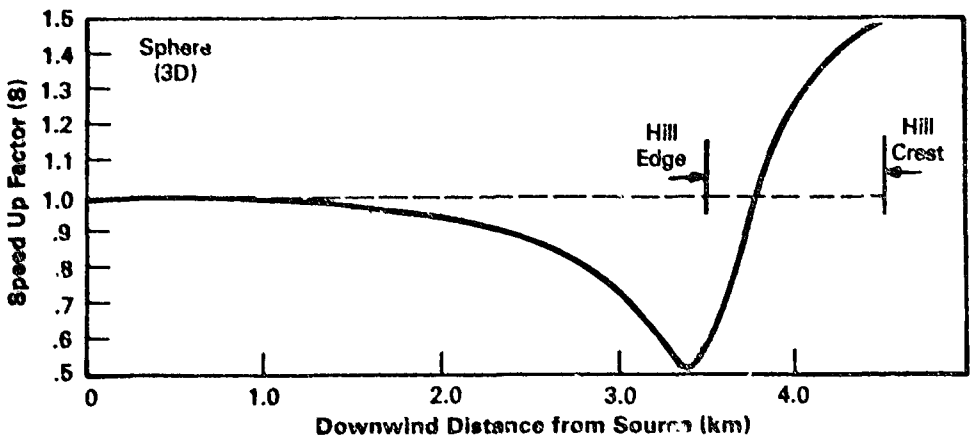

Figure 5b. Velocity speed up factors for neutral flow over a hemispherical hill.

SECTION 6

NEUTRAL FLOW

6.1 Ground-Level and Centerline Concentrations for Neutral Flow

The terrain-influenced dispersion estimates developed for neutral two- and three-dimensional flow cases were used to compute the plume centerline and ground-level concentrations shown in Figure 6. For the two-dimensional cases, concentrations are computed by substituting Equations 5-11 and 5-12 into Equations 5-10a and 5-10b and Equation 5-13 followed by Equation 5-7. The two-dimensional streamline equation for a given source-obstacle geometry is calculated from Equation 5-32. For the three-dimensional cases, concentrations follow from substitution of Equations 5-23 and 5-24 into Equations 5-22a, 5-22b and 5-25, followed by Equation 5-20. The three-dimensional streamline equation is given by Equation 5-36. For the flat terrain case, Equation 5-47 was used. In Figure 6, curve 1 is the plume centerline concentration in the flat-terrain case, and curve 2 is the centerline concentration in the three-dimensional hemispherical hill case.

In this figure and subsequent figures, results are presented in dimensionless form (see Section 5.4.1) with downwind distance from the source, $\hat{x}$, normalized by the obstacle height, a, and concentration, $\hat{\chi}$, normalized by $U_\infty a^2/Q$ (Equation 5-4a). Note that results are not independent of obstacle height a. Introduction of the PGT calibration of diffusivities (Section 5.5) which are not linear in the length scale, require that all results are specific for the particular obstacle height cited.

At plume centerline, the concentrations for the three-dimensional case, as well as for the two-dimensional case (not shown) are not appreciably different from the flat-terrain case. But they are strikingly different at ground level; compare curve 3, the ground-level concentration in the flat-terrain case, with curves 4 and 5, the ground-level concentrations in the three-dimensional and two-dimensional cases.

For the two-dimensional ridge the magnitude of the maximum ground-level concentration is about equal to the maximum in flat terrain, but the maximum occurs at about ridge top (4.5 km downwind from the source), whereas in the flat terrain case the maximum occurs about 9 km downwind.

For the three-dimensional case the maximum ground-level concentration is roughly 10 times larger than in the flat terrain case, and occurs at the leading edge of the hemispherical hill; the concentrations remain very high as the plume passes over the hill.

The ground-level concentrations for the two-dimensional flow are similar to those for the flat case because of flow acceleration effects: the reduction of σ_z in the vicinity of the two-dimensional ridge crest is largely compensated by a reduction of about equal magnitude in the closeness of

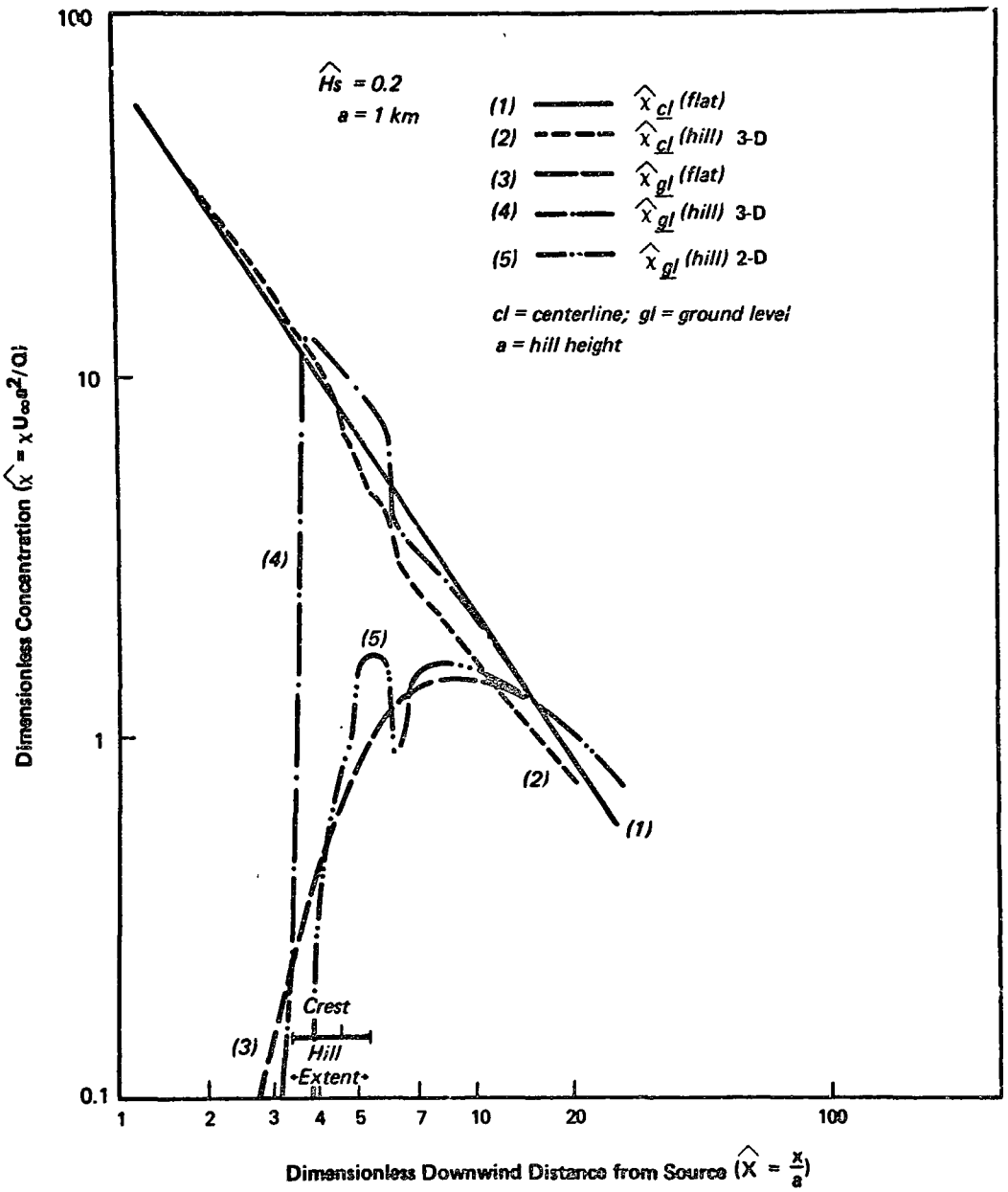

Figure 6. Centerline and ground-level concentrations for cases shown in Figures 1 through 4 (neutral flow).

approach of the plume to the ridge. In three-dimensional flow over the hemispherical hill, however, the plume approaches much closer to the hill top and maximum ground-level concentrations can substantially increase.

6.2 Dependence on Stack Height and Position

The ground-level concentrations, shown in Figure 6 as a function of downwind distance for the hemispherical hill and the cylindrical ridge, were computed for a particular geometry; that is, hill (or ridge) height of 1 km, stack height = 0.2 [hill (ridge) height], and stack located 4.5 km upwind of the hill (ridge). For each choice of geometry, the maximum ground-level concentration occurs at a unique location downwind. Calculations of maximum ground-level concentration, as well as the position of the maximum, were made for various combinations of stack height, $\hat{H}_s$, and distance between stack and hill center $\hat{X}_s$, both normalized by hill height a. Figures 7 and 8 illustrate the regions in parameter space in which calculations were performed for the two- and three-dimensional cases, respectively. For example, in the case of the hemispherical hill (Figure 8), assuming a hill height of 0.5 km and a dimensionless effective stack height of $\hat{H}_s = 0.6$, calculations were done varying the dimensionless distance between stack and hill center, $\hat{X}_s$, from values of 10 to 100. Results of this series of model calculations are shown in Figures 9 and 10 for the cylindrical ridge and in Figures 11 and 12 for the spherical hill, respectively.

Figure 9 shows that the maximum ground-level concentrations are not affected very much by the cylindrical ridge, especially for stack heights smaller than 0.8 times the ridge height. (In each instance, the dashed line is the value of the concentration for flat terrain.) For a nondimensional stack height of 0.8, and for stacks positioned between about 20 and 100 times the ridge height upwind of the ridge, the maximum ground-level concentration increases somewhat above the value corresponding to flat terrain. The position of the maximum shifts from leewards of the ridge crest to the crest, as shown in Figure 10, as $\hat{X}_s$ goes from 20 to 100.

A spherical hill exerts a much stronger influence on ground-level concentrations than does a cylindrical ridge. For short stacks not far from the hill, the maximum occurs on the crest of the hill and can be considerably greater than in the flat terrain case (see Figures 11 and 12). Farther from the hill, the maximum ground-level concentration occurs before the plume reaches the hill. This limiting behavior is shown in Figure 11, where, for the smaller stack heights, all the maximum ground-level concentrations are constant for large $\hat{X}_s$. The hill exerts negligible effect on the maximum ground-level concentration when the stack is a distance of approximately 10 hill heights or more away from the hill center.

For the higher stacks, the behavior is considerably different. Figure 11 shows that when the taller stacks are fairly close to the hill, the maximum ground-level concentration is insensitive to stack position. When the stack is positioned farther from the hill, however, the concentration increases by as much as an order of magnitude before decreasing to its value for flat terrain. This behavior can be understood by looking at the variation in position of the ground-level maximum, as shown in Figure 12. For tall stacks relatively close to the hill, the maximum occurs far downwind of the hill. However, when the stack is farther from the hill, the maximum shifts to the

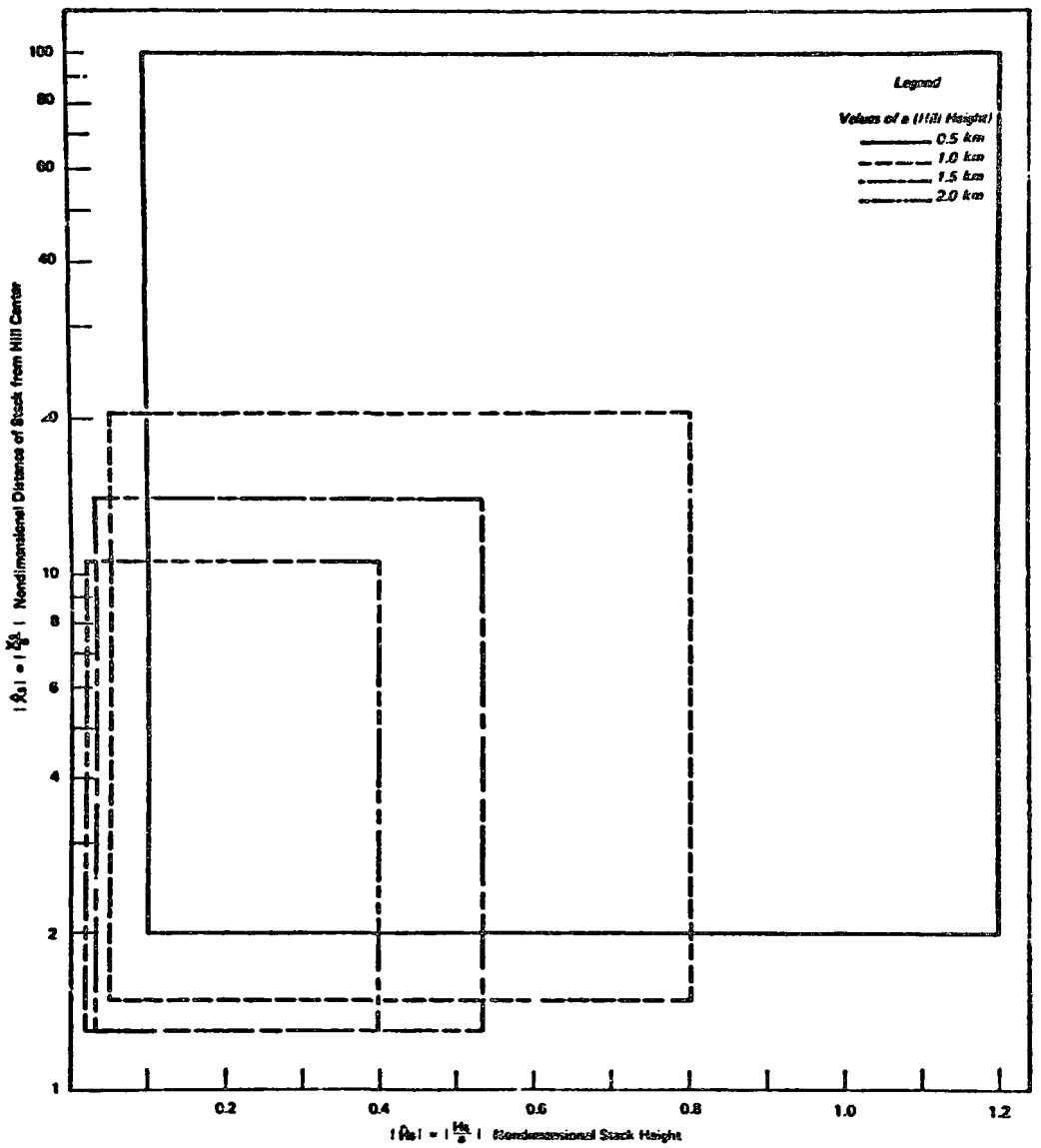

Figure 7. Domain of calculations performed for a two-dimensional cylindrical ridge and neutral flow.

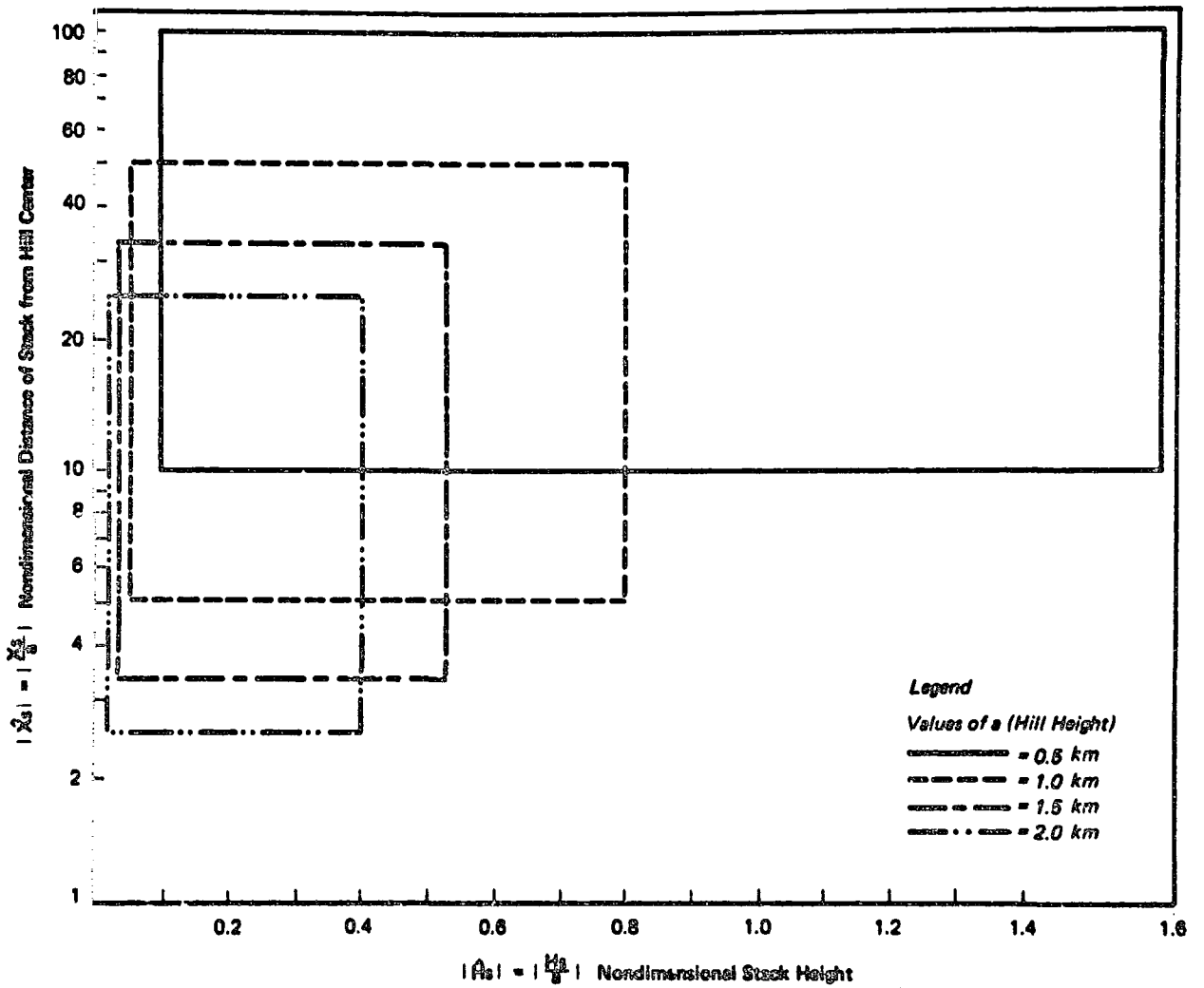

Figure 8. Domain of calculations performed for a three-dimensional hemispherical hill and neutral flow.

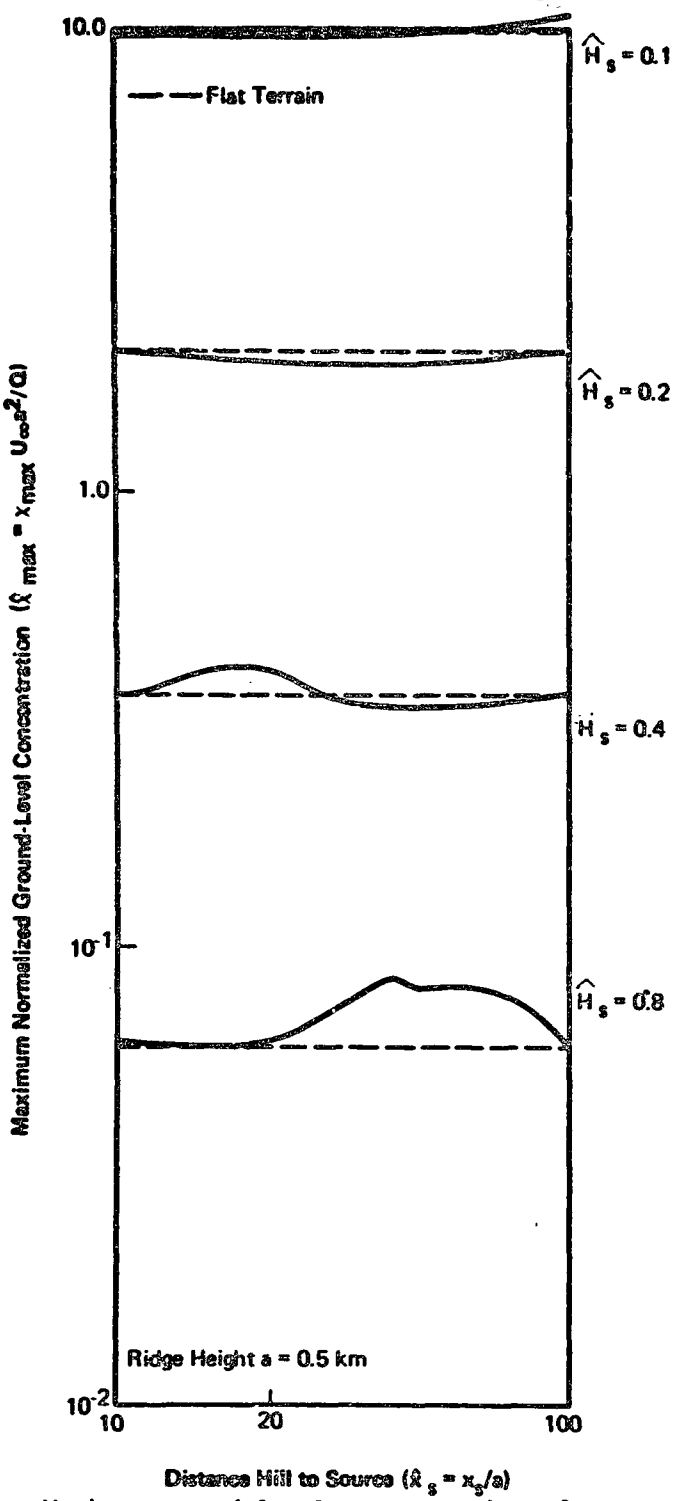

Figure 9. Maximum ground-level concentrations for a cylindrical ridge and various combinations of stack height and position.

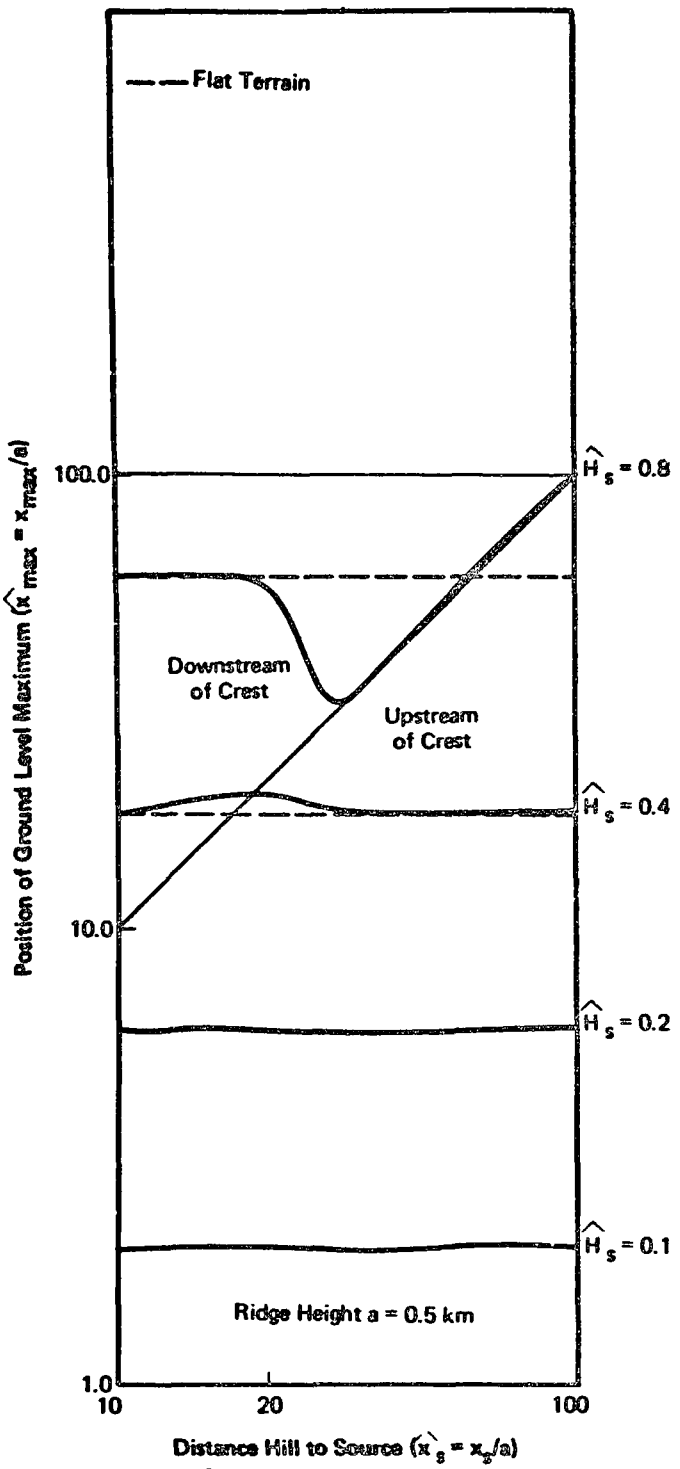

Figure 10. Position of maximum ground-level concentration for a cylindrical ridge and various combinations of stack height and position.

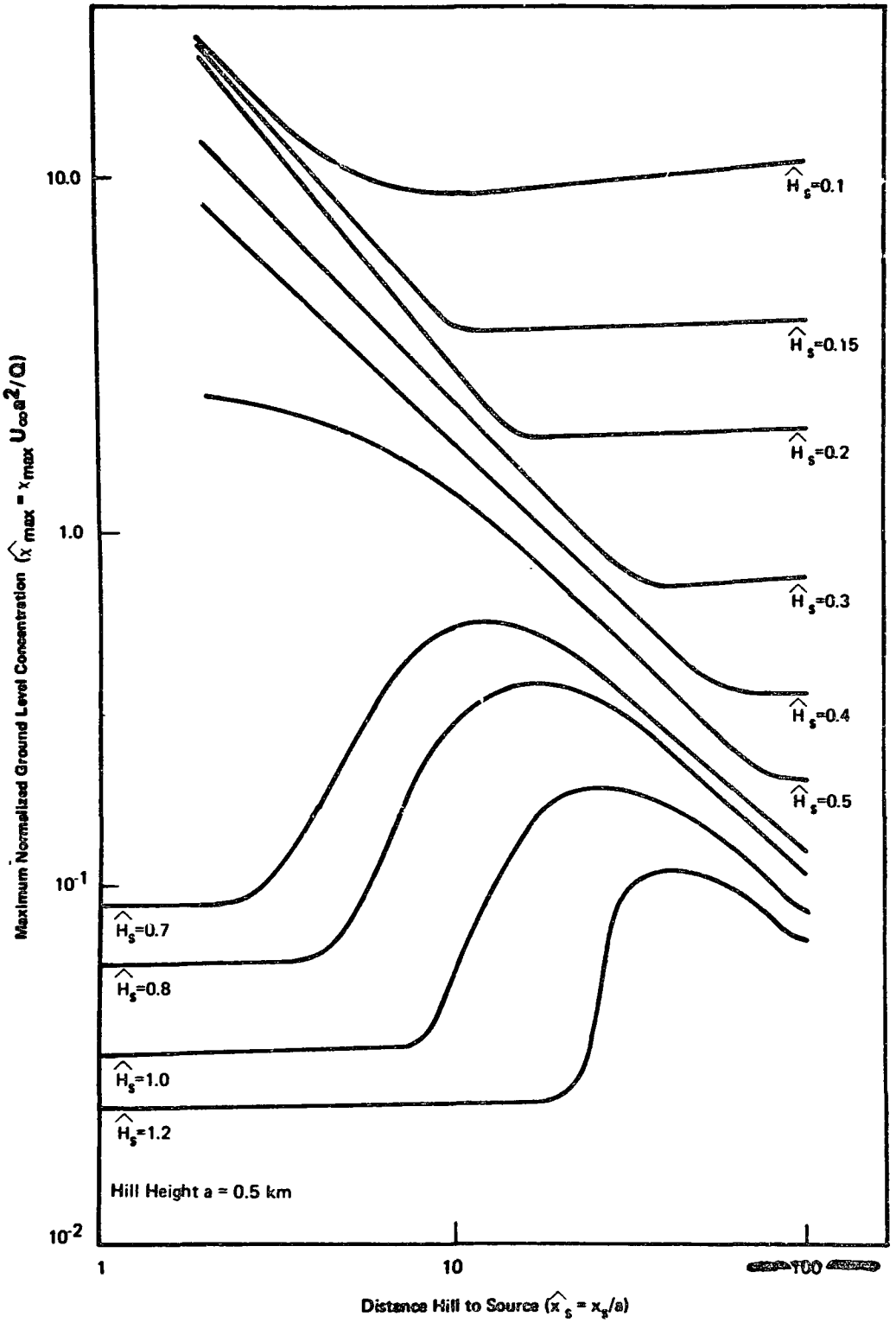

Figure 11. Maximum ground-level concentrations for a spherical hill and various combinations of stack height and position.

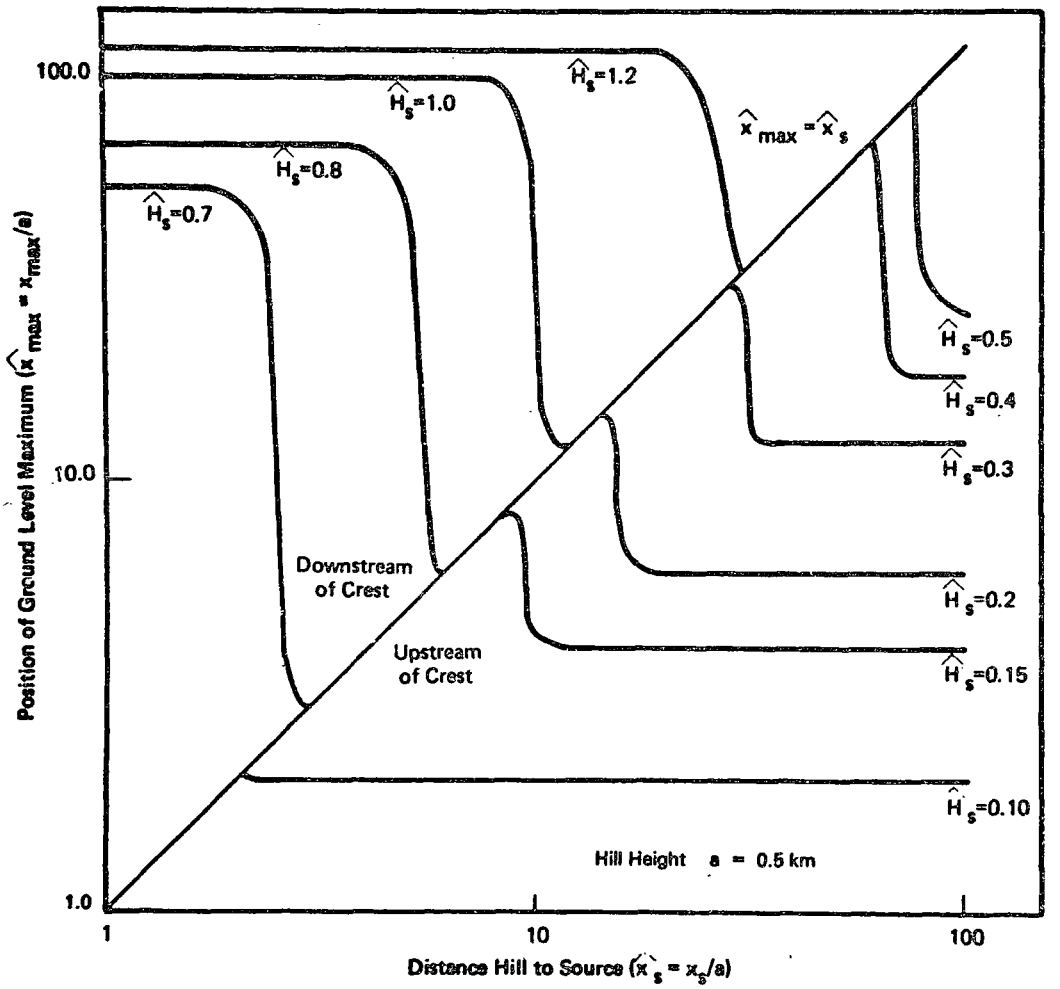

Figure 12. Position of maximum ground-level concentration for a spherical hill and various combinations of stack height and position.

crest of the hill. A notable feature of the taller stacks is that the maximum concentration occurs at the hill crest, even for stacks as far away as 100 hill heights from the hill center.

4.3 Effect of Obstacle Size

In one set of calculations the obstacle size was changed with all other variables held constant. The 400 m stack was held at a fixed distance (4.5 km) upwind of the spherical hill, and computations were made for hills varying between 500 m and 2,000 m in height. Variations of maximum ground-level concentration are shown in Figure 13. For these hill heights greater than the stack height, the maximum ground-level concentration increases rapidly. The position at which this maximum ground-level concentration occurs is shown in Figure 14.

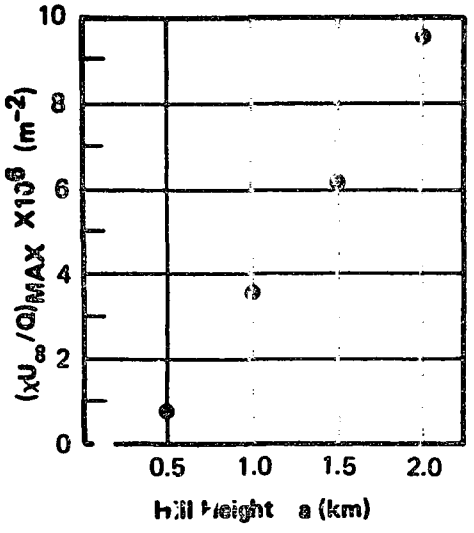

Figure 13. Maximum ground-level concentration as a function of hill height.

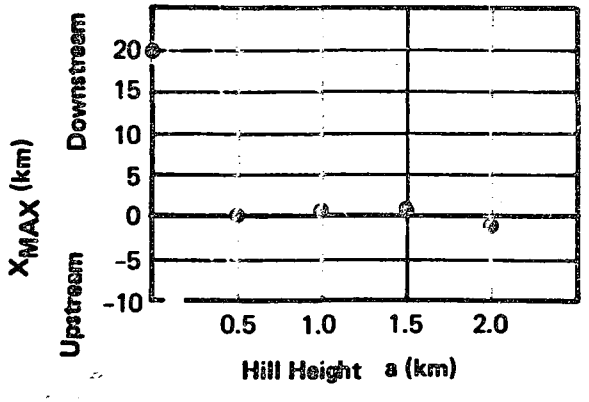

Figure 14. Position (distance from hill crest) of maximum ground-level concentration as a function of hill height.

SECTION 7

COMPARISON WITH LABORATORY EXPERIMENTS--NEUTRAL FLOW OVER A SINGLE MOUND

7.1 Background

Model computations were compared with experiments conducted at the EPA Fluid Modeling Facility (FMF) (Hunt et al. 1978) to study the flow and diffusion of pollutants in idealized complex terrain under neutral conditions (and also stably stratified conditions--see Section 9). The primary purpose of these neutral and stably stratified flow experiments was to understand the effects of stability on the flow structure over a bell-shaped hill. The hill was placed near the entrance to the wind tunnel where the flow was essentially uniform and non-turbulent except for a thin boundary layer small compared with the hill height. (The thickness of this boundary layer in the wind tunnel matched that observed over the baseplate in the towing tank, so that the approach flow structures in both the tank and the tunnel were essentially identical except for the stability--see Section 9.) In later experiments (Snyder and Britter 1979) the hill was placed in a simulated atmospheric boundary layer, but the earlier experiments are more suitable for the model comparisons because (a) the potential flow model is expected to more accurately predict the behavior of a uniform, non-turbulent air stream and (b) the "thin plume" assumptions are more closely met. Calculations were performed using the complex terrain model for the characteristic dimensions used in the EPA experiments (on the centimeter scale). Therefore, it was first necessary to determine the appropriate dispersion estimates on the laboratory scale in the absence of terrain features, so that the line integrals $\phi(s)$ and $T(s)$ could be evaluated. Details of these calculations and the results are presented in this section.

7.2 Dispersion Coefficients, Flat Terrain

The wind tunnel experiments for neutral flow in flat terrain (no obstacle present) were used to derive the dispersion parameters σ_y, σ_z, as functions of downwind distance. These experiments were performed with stack heights of 3.0 cm and 12.5 cm. But the potential flow model is not suitable for stacks immersed in the boundary layer (about 3 cm deep in the experiments), so only the experiments using the 12.5 cm stack (well above the boundary layer) were used to specify the plume spread.

The concentration profile (horizontal and vertical) was measured at three downwind distances. At each distance, a Gaussian profile of the form

$$\chi(y, z) = \frac{Q}{2\pi\sigma_y\sigma_z U} e^{-\frac{1}{2}\left(\frac{y}{\sigma_y}\right)^2} \cdot \left[e^{-\frac{1}{2}\left(\frac{z-H}{\sigma_z}\right)^2} + e^{-\frac{1}{2}\left(\frac{z+H}{\sigma_z}\right)^2} \right] \quad (7\text{-}1)$$

was fitted to the data. The measured data are catalogued by Snyder and Marsh (1977) as experiments HHSWTN.398, .401, and .403 for the vertical profiles at the three downwind distances 39.2, 84.7, and 130.2 cm. These data points are shown in Figures 15a, 15b and 15c, along with the curves given explicitly by Snyder and Marsh as best Gaussian fits to the data points. Using these sigmas, a linear functional form, $\sigma = a + bx$, was fitted to the three points and used in the model.

According to the Gaussian plume equation, at the plume centerline ($y = 0$, $z = H$) the normalized mass flux parameter $\dot{M}$ defined by:

$$\dot{M} \equiv \frac{2\pi\sigma_y\sigma_z U \chi_{CL}}{Q} \qquad (7\text{-}2)$$

is equal to unity. According to the data, $\dot{M}$ varied from 0.88 to 0.93. In other experiments, $\dot{M}$ varied from as much as 1.3 to as little as 0.74; departures from the Gaussian form are therefore apparent.

7.3 Boundary Layer Enhanced Dispersion

The vertical and horizontal dispersion coefficients used were derived by fitting a Gaussian profile to all the data points. Examination of Figures 15a, 15b, and 15c shows, however, that the measured concentration profiles deviate systematically from the best-fit Gaussian curves [as given by Snyder and Marsh (1977)] as the terrain surface is approached. The reason for the difference is probably associated with the presence of the boundary layer near the surface where the dispersion is enhanced. Also, the best-fit curves are dominated by the few points closest to the centerline, so the measured values closest to the surface carry little weight. As a first approximation in dealing with the enhanced dispersion near the surface, a second Gaussian profile was fitted through the centerline concentration and the measured concentration nearest to or at the surface level, at the three downwind distances shown in Figures 15a, 15b, and 15c. Again, a linear fit was made, $\sigma_z' = a' + b'x$, and these alternative boundary layer-enhanced dispersion estimates were used in the model along with the best-fit dispersion estimates σ_z.

7.4 Comparison with Flat Terrain Results

The results of computations using the originally derived sigmas fitted to all the data points, and using the boundary layer-enhanced sigmas, are compared in Figures 15a, 15b, and 15c. The figures show, as expected, that the predicted centerline values fall within the scatter of the observations when either set of sigma values is used. Had the actual values of σ_y and σ_z been used at each of the three downwind distances, instead of the average linear trend, the predicted centerline values would have been closer to the best-fit curve in all cases. Using the best-fit sigmas, the model reproduces the Gaussian fit away from the centerline. Using the alternative σ' dispersion curves, the model does better in reproducing the actual measurements closer to ground.

The agreement shown in these figures, when using either the σ or σ' dispersion parameters, suggests only that the model calculations are being performed in a consistent manner, and that the algorithm is functioning as

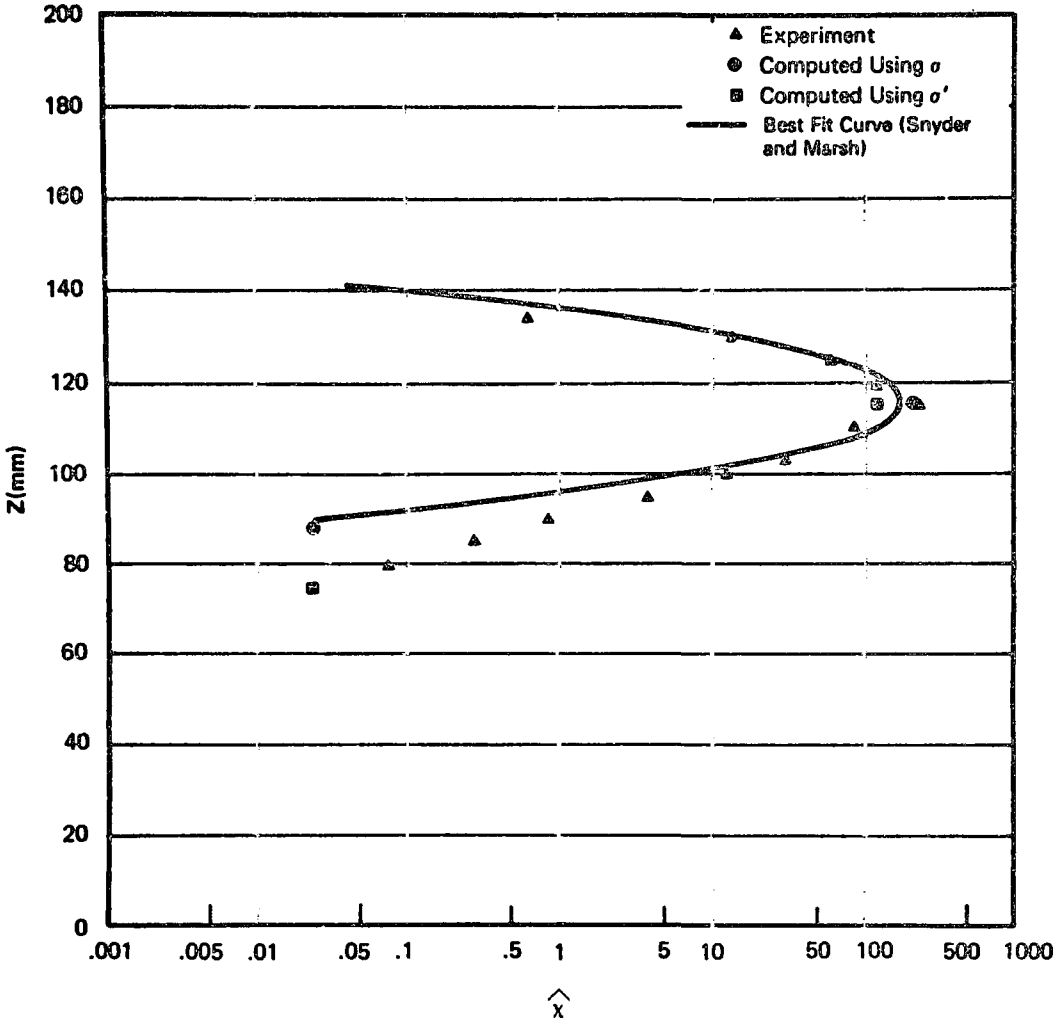

Source: Snyder and Marsh 1977

Figure 15a. Vertical concentration profile 39.2 cm downwind of a 12.5 cm stack in flat terrain.

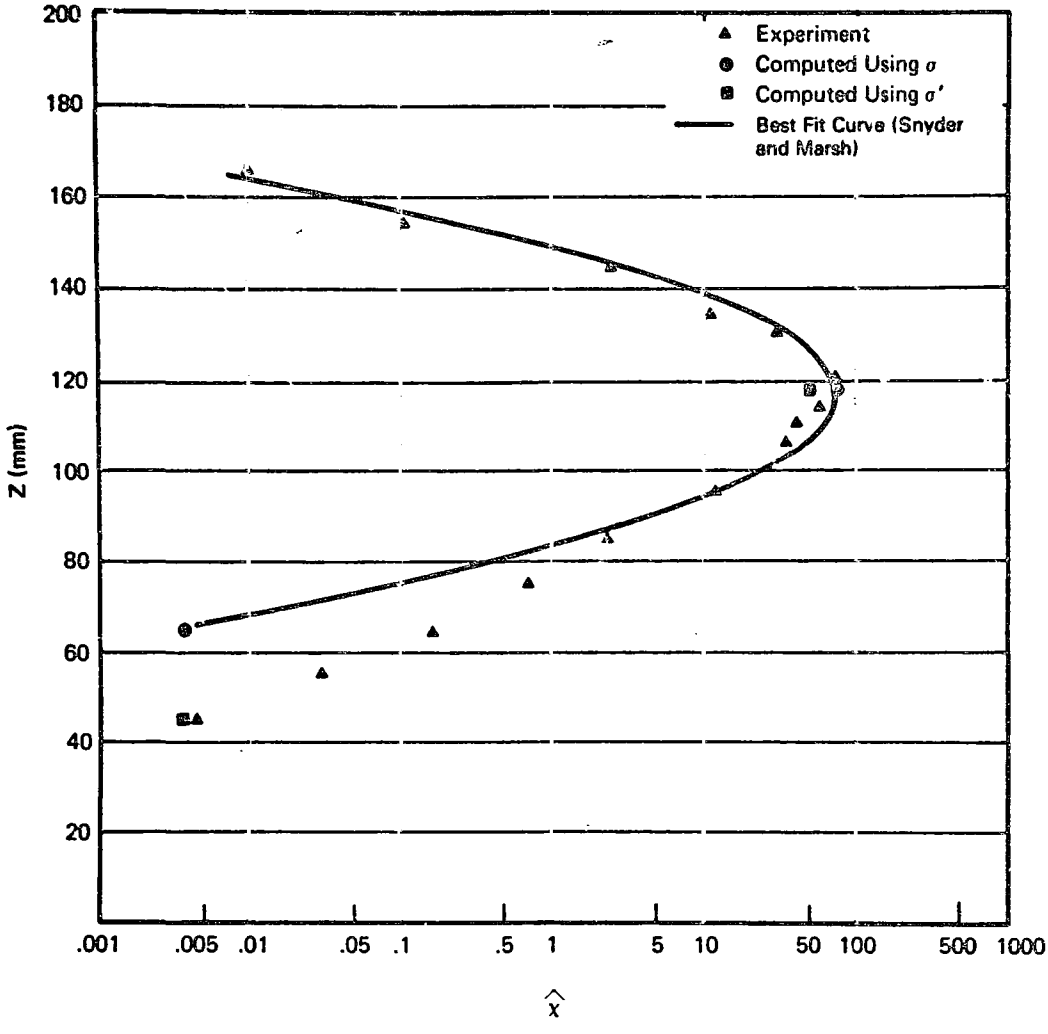

Source: Snyder and Marsh 1977

Figure 15b. Vertical concentration profile 84.7 cm downwind of a 12.5 cm stack in flat terrain.

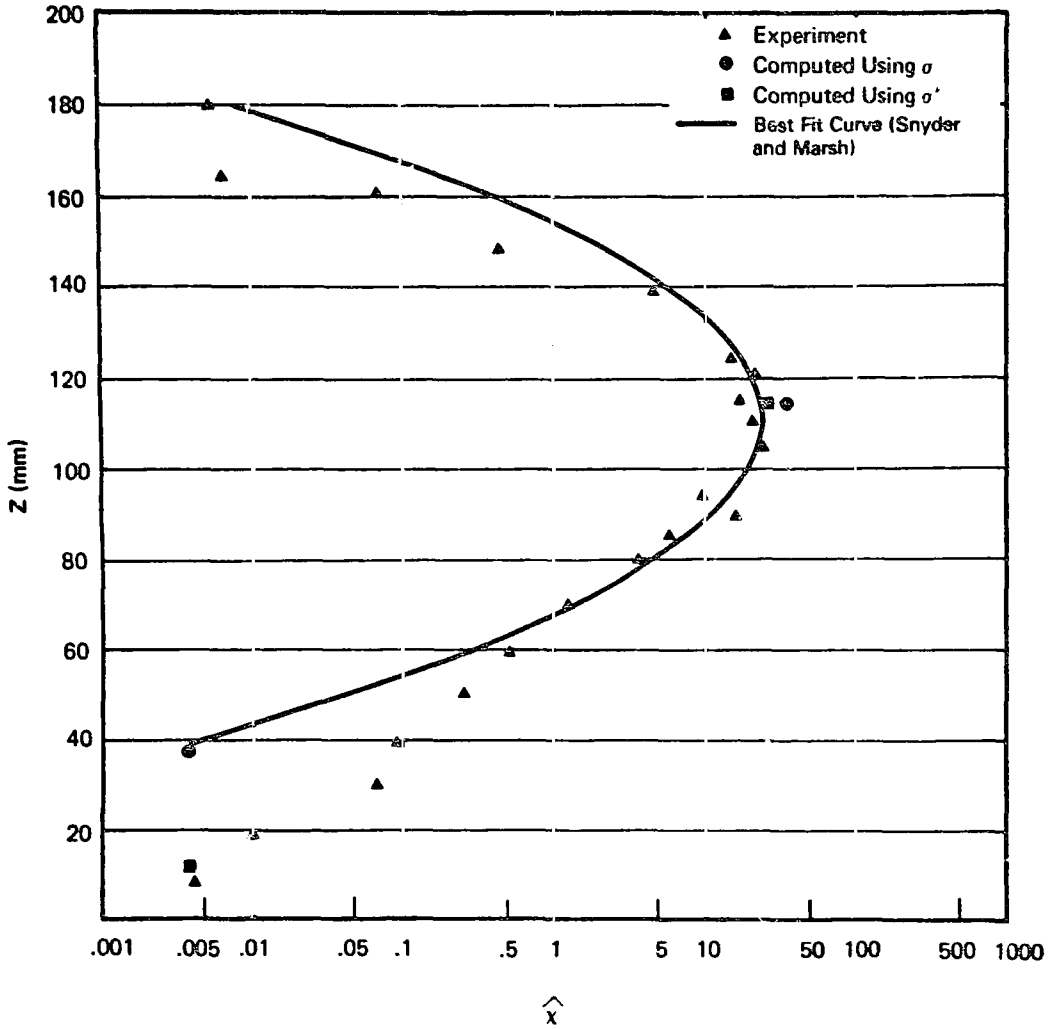

Source: Snyder and Marsh 1977

Figure 15c. Vertical concentration profile 130.2 cm downwind of a 12.5 cm stack in flat terrain.

intended (since the observed sigmas are input to the calculation, the observed concentrations must be reproduced). The crucial test of the potential flow model must come from comparison with experiments in which a terrain obstacle is present.

7.5 Comparison in Presence of Terrain Obstacle

When a 'polynomial hill' was introduced in the wind tunnel, the concentration profiles differ substantially from those measured in flat terrain. The resulting profiles at several downwind distances from the stack are shown in Figures 16a, 16b, and 16c. The three profiles were measured upstream of the hill, on the side of the hill, and at the crest of the hill, respectively. The curves drawn are given explicitly in Snyder and Marsh (1977), drawn smoothly through the experimental data points. Using the dispersion parameters derived from the flat terrain experiments, the centerline and ground-level concentrations computed with the model are indicated in Figures 16a, 16b, and 16c. The fundamental equations used include 5-20 through 5-25, 5-56, and 5-57.

Centerline values are predicted within a factor of two using either σ_z or σ_z' at all positions; the centerline concentrations predicted using σ_z lie very close to the observed values at distances 39.2 and 84.7 cm from the stack. At the most upstream position (Figure 16a) the ground-level value is not well predicted because of the boundary layer. The corresponding flat terrain measurement (Figure 15a) did not extend close enough to the ground to enter the boundary layer (height of lowest measurement was 7.5 cm).

The next measurement is part-way up the hill. Using the original values of σ_z, the model predicts an essentially zero ground-level concentration. However, using the flat terrain boundary layer-enhanced σ_z' gives a value more than double the experimental value.

At the crest of the hill (84.7 cm) where the ground-level concentration is highest, the predictions bracket the observed concentration. The observed concentration at the crest is the average of four measurements which ranged from 0.298 to 0.506, made through the sampling port at the center of the hill.

The predicted concentration using the best-fit σ_z is 1/3 of the observed value, while that computed with the enhanced σ_z' is about five times the observed value. The difference in shape between the polynomial hill used in the laboratory experiments and the hemisphere used for the computations could contribute to some of the differences in concentrations predicted and observed away from the hill crest, but the difference in shape alone cannot explain the discrepancy observed in the surface concentrations over the crest.

Further inspection of the plume profiles in the absence of the hill (Figures 15a-c) reveals that the centerline of the plume does not remain at the release height of 12.5 cm. Instead, the profiles suggest the effective plume centerline height is about 11.5 cm. Because this is evident 45.5 cm upwind of the location of the hill center, it is reasonable to assume that a similar depression also affects the plume in the presence of the hill.

Results of additional computations using σ_z (best-fit) with an assumed stack height of 11.5 cm are summarized and compared with the observations and the previous calculations in Table 3. Predictions of the centerline

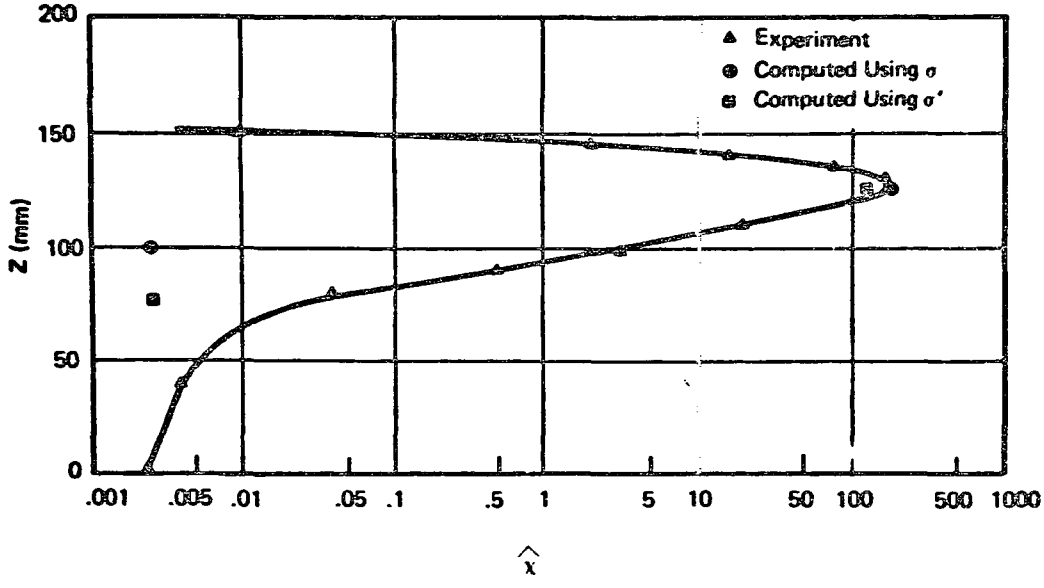

Source: Snyder and Marsh 1977

Figure 16a. Vertical concentration profile 39.2 cm downwind of a 12.5 cm stack in presence of a 23 cm hill. (Hill crest is 84.7 cm downwind of stack.)

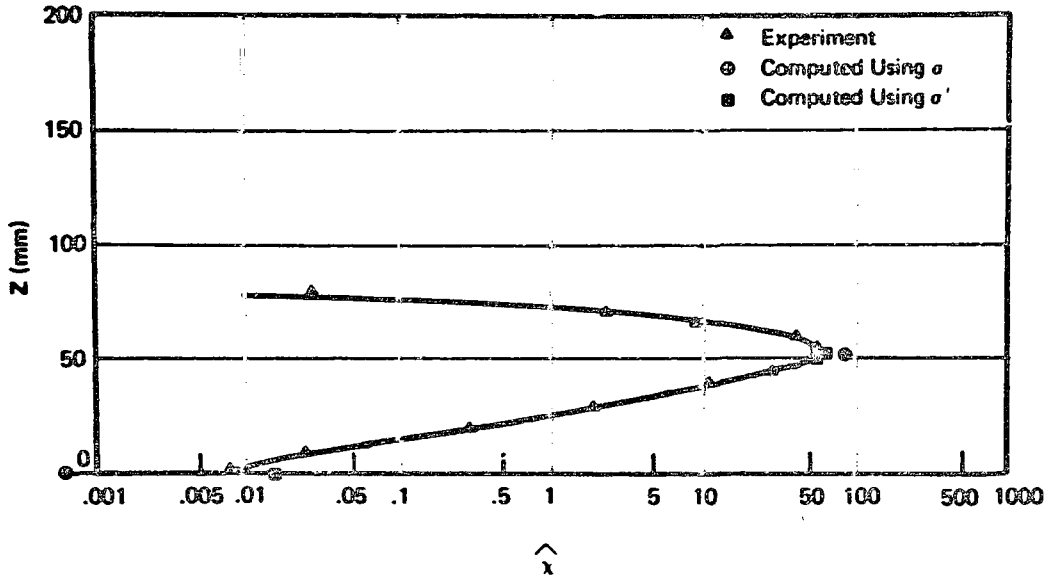

Source: Snyder and Marsh 1977

Figure 16b. Vertical concentration profile 68.2 cm downwind of a 12.5 cm stack in presence of a 23 cm hill. (Hill crest is 84.7 cm downwind of stack.)

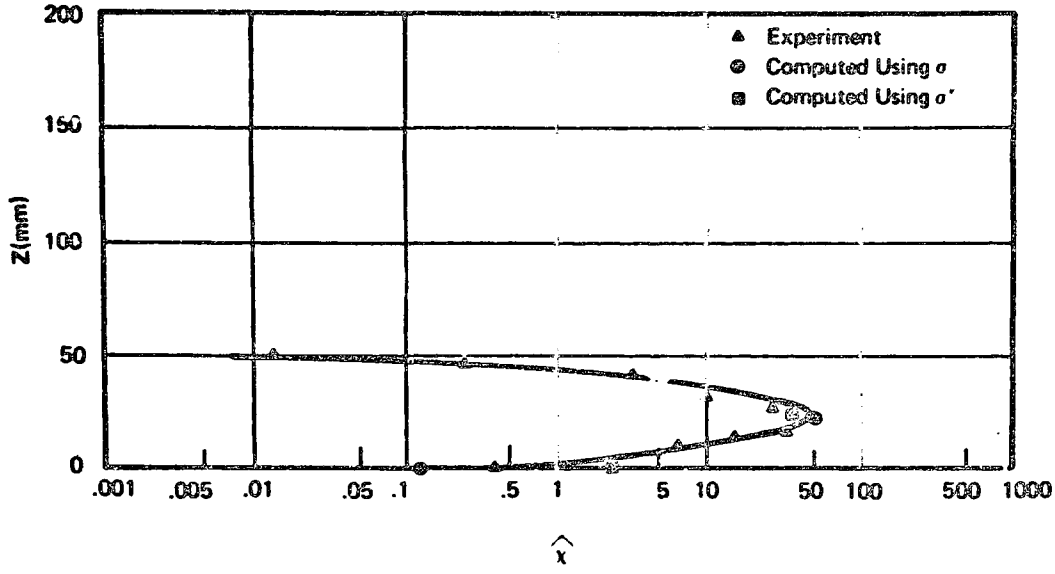

Source: Snyder and Marsh 1977

Figure 16c. Vertical concentration profile 84.7 cm downwind of a 12.5 cm stack in presence of a 23 cm hill. (Hill crest is 84.7 cm downwind of stack.)

TABLE 3. COMPARISON OF PREDICTED AND OBSERVED NORMALIZED CONCENTRATIONS AND PLUME CENTERLINE HEIGHT FOR THE 12.5 CM HIGH STACK IN THE PRESENCE OF THE 22.9 CM HIGH POLYNOMIAL HILL

Parameter	Observed Value	Predicted Value Hs=12.5	Hs=11.5
X=84.7 cm (hill crest):			
Surface Concentration	0.391	0.118	0.520
Centerline Concentration	47.9	53.2	51.4
Centerline Height (cm)	2.3	2.2	1.9
X=68.2 cm:			
Surface Concentration	<0.007*	-	-
Centerline Concentration	60.4	91.4	91.1
X=39.2 cm:			
Surface Concentration	0.003*	-	-
Centerline Concentration	181.8	187	187

*These concentrations were not measured right at the surface, but 2 to 3 mm above.

concentrations remain nearly the same, but the surface concentration at the crest has increased considerably. Now the predicted value has risen from 30% of the observed value, to 133%. Surface concentrations at the two locations upwind of the crest remain too small for a meaningful comparison.

Also included in Table 3 is the centerline height over the hill crest. When the model assumes the upwind plume height equals 12.5 cm, the predicted height over the crest agrees closely with the observation. But when the assumed height is 11.5 cm, the predicted height over the crest is 80% of that observed.

In the absence of the obstacle, the dispersion parameters for release points above the boundary layer were determined using a stack height of 12.5 cm. To determine whether these flat terrain dispersion parameters for the 12.5 cm stack can be used for other stacks, calculations were made for a 9 cm stack with the best-fit σ_z. The results are compared to experiment in Table 4. The centerline concentration is overpredicted by 50%, the surface concentration is underpredicted by 50%, and the centerline height is overpredicted by 30%. It is expected that the predicted concentrations would be closer to the observations if specific plume spread data for the 9.0 cm stack in the absence of the hill had been obtained and incorporated in the calculation.

TABLE 4. COMPARISON OF PREDICTED AND OBSERVED NORMALIZED CONCENTRATIONS AND PLUME CENTERLINE HEIGHT OVER THE HILL CREST FOR THE 9.0 CM HEIGHT STACK

Parameter	Observed Value	Predicted Value
X = 84.7 cm:		
Surface Concentration	16.6	8.0
Centerline Concentration	30.0	45.5
Centerline Height (cm)	0.9	1.2

Assessment of model performance begins by comparing predicted concentrations with observed concentrations. In comparing results from the model and laboratory experiments, sources of uncertainty are present. One measure of their effect is the change in the ratio R of ground level to centerline concentrations. From the basic Gaussian plume equation, the ratio R is:

$$R = \frac{1}{2}\frac{\chi_{g1}}{\chi_{c1}} = e^{-1/2\left[\frac{n_s}{\sigma_z}\right]^2} \qquad (7\text{-}3)$$

where n_s is the height of the streamline above the surface and σ_z is the vertical dispersion coefficient. For a typical wind tunnel experiment, (X_s, 84.7 cm; a, 23.5 cm; H_s, 12.5 cm; and aspect ratio, 1) the model calculations predict, at the crest of the hill:

$$\sigma_z = 0.58 \text{ cm}, \quad n_s = 2.16 \text{ cm}.$$

The ratio R is then computed by Equation 7-3.

Now assume, for example, that n_s and σ_z may be as much as 10% too high or too low. The new ratio R* is computed from Equation 7-3 with $\sigma_z^* = (1 \pm 0.1)\sigma_z$ and $n_s^* = (1 \pm 0.1)n_s$. More generally, if $\sigma_z^* = (1 \pm C_1)\sigma_z$ and $n_s^* = (1 \pm C_2)n_s$, then the error ratio R*/R from Equation 7-3 can be written as:

$$R^*/R = \exp\left\{\frac{1}{2}\left(\frac{n_s}{\sigma_z}\right)^2\left[1 - \left(\frac{1\pm C_2}{1\pm C_1}\right)^2\right]\right\} \qquad (7\text{-}4)$$

Note that this ratio is sensitive not only to the size of the errors represented by C_1 and C_2, but also to the value of (n_s/σ_z).

Several computations were made for the particular values of n_s and σ_z given above ($n_s^2/\sigma_z^2 \approx 14$). The effects of the errors are shown in Table 5. Note that 10% errors in σ_z and n_s can easily produce order of magnitude errors in ground-level concentrations. If a second situation is considered (the vertical plume spread is twice as large) for which n_s^2/σ_z^2 equals only 3.5, a 10% error in n_s or σ_z has less influence on the error made in predicting ground-level concentrations. Error ratios R*/R for this case are also presented in Table 5.

A source of differences among model computations and experimental results is the difference in hill shape. Because ground-level concentrations are sensitive to n_s, the difference in shape between the polynomial hill (used in these experiments) and the spherical hill (assumed in the model) can result in significant differences for points away from the crest of the hill. In addition, important differences in σ_z and n_s can develop because of boundary layer effects discussed previously.

Another way of assessing a model's performance is to compare its results with results from other modeling approaches. A useful way of comparing the potential flow model with others within a Gaussian plume framework is to compare the effective terrain correction factors. This factor relates the terrain-influenced ground-level concentration to the corresponding flat terrain value.

The definition of the terrain correction factor begins from the equation for the normalized ground-level concentration:

$$\chi_g = 2\chi_C \exp\left[-\frac{1}{2}\left(H/\sigma_z\right)^2\right] \qquad (7\text{-}5)$$

where the assumption is made in evaluating χ_C that plume reflection is negligible at plume centerline height. (This assumption requires that the plume be narrow in the sense already discussed.) When the plume is affected by terrain, flow deformations and accelerations will act to alter the height and vertical dimension of the plume (H, σ_z), as well as its centerline concentration (χ_C). The terrain correction factor (T_c) accounts for all effects of plume distortion upon ground-level concentration on the terrain feature, by modifying the exponential term in equation (7-5):

$$\chi_{gH} = 2\,\chi_{CF}\,\exp\left[-\frac{1}{2}\left(T_c H_F/\sigma_{zF}\right)^2\right] \qquad (7\text{-}6)$$

where flat-terrain values are labeled with the subscript F and complex-terrain values with the subscript H.

TABLE 5. ERROR RATIO R*/R FOR 10% ERRORS IN σ_z AND n_s

Case I: $(n_s/\sigma_z)^2 = 14$†

	$0.9\,\sigma_z$	σ_z	$1.1\,\sigma_z$
$0.9\,n_s$	1.0	3.7	9.9
n_s	0.20	1.0	3.3
$1.1\,n_s$	0.033	0.23	1.0

Case II: $(n_s/\sigma_z)^2 = 3.5$

	$0.9\,\sigma_z$	σ_z	$1.1\,\sigma_z$
$0.9\,n_s$	1.0	1.4	1.8
n_s	0.66	1.0	1.4
$1.1\,n_s$	0.42	0.69	1.0

$$R^* = e^{-1/2\left(\frac{n_s^*}{\sigma_z^*}\right)^2} \qquad R = e^{-1/2\left(\frac{n_s}{\sigma_z}\right)^2}$$

†Case I corresponds to the specific choices $n_s = 2.16$ cm, $\sigma_z = 0.58$ cm.

The terrain correction factor is all that is needed to predict the surface concentration in the presence of terrain from surface concentrations predicted in the absence of terrain. The terrain correction factors can be derived from the potential flow model results by solving Equation 7-6 for T_c in terms of the known flat terrain dispersion parameters, and the ground-level concentration calculated in the presence of the terrain (χ_{gH}):

$$T_c = \frac{\sigma_{zF}}{H_F}\sqrt{2\ln\left(\frac{2\chi_{CF}}{\chi_{gH}}\right)} \qquad (7\text{-}7)$$

Similarly, if an observed terrain-influenced surface concentration is known (as in the wind tunnel experiments), an observed terrain correction factor may be calculated using Equation 7-7. For example, Table 6 lists ground-level concentrations as observed at the hill crest; as predicted with the potential flow model (also as predicted by the "half-height assumption" to be discussed shortly); and the corresponding terrain correction factors. Note that if the source-obstacle relationship is fixed, a smaller surface concentration gives a larger terrain correction factor. The correction factors based on the observed ground concentrations vary roughly from .33 to .35, while those based on the potential flow model vary from .36 to .34. It is seen that small differences in the terrain factors are derived from much greater differences in the maximum surface concentration.

TABLE 6. COMPARISON OF NORMALIZED CONCENTRATIONS AND DERIVED TERRAIN CORRECTION FACTORS AT THE HILL CREST

	Tc	Normalized Concentration
Observed Data:		
H_s = 12.5 cm	0.325	0.391
H_s = 11.5 cm	0.353	0.391
Potential Flow Model:		
H_s = 12.5	0.357	0.118
H_s = 11.5	0.344	0.520
Half-Height Assumption:		
H_s = 12.5	0.5	0.0001
H_s = 11.5	0.5	0.0011

Two modeling approaches can be readily compared with the wind tunnel data: (1) a level trajectory, and (2) a specific partial height trajectory. In the level trajectory model the plume centerline does not rise over terrain features. When the terrain exceeds the plume height (as is the case in these wind tunnel experiments) the centerline concentration is assumed to represent the highest ground concentration (no surface reflection doubling is included).

The partial height trajectory approach assumes that the plume rises over the hill. The plume's height above the surface is described as a fraction of the initial plume height. The fraction (which may vary continuously with downwind distance--see below) depends on the initial plume height H_s; on the terrain height h_t; and on an assumed 'plume path coefficient,' C. The fractional displacement of the plume above the terrain enters into Equation (7-5) as a multiplier of the ratio H/σ_z--that is, as a terrain correction factor T_c. For plumes initially lower than the terrain ($H_s \leq h_t$):

$$T_c = C \qquad (7\text{-}8)$$

and for plume heights greater than the terrain height ($H_s > h_t$):

$$T_c = 1 - \frac{h_t}{H_s}\,(1\text{-}C) \qquad (7\text{-}9)$$

The plume path coefficient may vary between 0 (level trajectory) and 1 (terrain following trajectory). One common choice for the plume path coefficient is the "half-height" assumption: C = 0.5.

Predicted ground-level concentrations from the potential flow model are compared with those based on the half-height assumption in Table 6. The half-height assumption underpredicts the surface concentrations at the crest of the hill by two to three orders of magnitude. (If a plume path coefficient of 0.35 is used instead, the partial height approach gives a concentration of 0.153 for H_s = 12.5 cm, and 0.432 for H_s = 11.5 cm. These concentrations lie much closer to the observed concentration, and to the concentrations calculated with the potential flow model.)

These additional comparisons of surface concentration predictions using level plume and half-height assumptions emphasize the sensitivity of this particular plume configuration to the ratio (H/σ_z). (It appears the thin plume restriction (σ_z/n_s <<1) is not a serious restriction even for ratios as large as $\sigma_z/n_s \sim 0.3$, which is the case in the laboratory experiment with the 12.5 cm release height.) In light of this sensitivity, the performance of the potential flow model in reproducing the laboratory observations is acceptable, and demonstrates the usefulness of this approach to complex terrain problems where the potential flow approximation is applicable.

SECTION 8

MODIFICATIONS FOR EFFECTS OF STRATIFICATION

8.1 Qualitative Observations from Laboratory Modeling

Ambient stratification can significantly affect plume behavior and resultant atmospheric pollutant concentrations. For moderate plume heights relative to hill size, and for moderately stable stratification, laboratory experiments suggest that the plume will go over the top of the hill, but the path of the plume will be closer to the surface, and the flow over the crest will be faster than in neutral flow. For small plume heights under strong stratification, the plume will tend to go around the hill rather than over it. If the hill is a long ridge, the flow may be 'blocked' and stagnate upwind. To approximate first-order effects of moderate stratification, results of FMF experiments on plume behavior in a stratified water channel flow over a polynomial hill (Snyder 1978) have been incorporated into the complex terrain model.

8.2 Incorporating Stratification Effects

Experimental results of the FMF tow-tank experiments on plume behavior in stratified flow over a polynomial hill are reproduced in Figure 17 (Hunt et al. 1978). The height of a streamline at the hill crest (n_s) is shown as a function of stack height (H_s) for various stratifications denoted by Froude number, Fr, including the neutral flow case, Fr = ∞. For any given stack height and Froude number, the height of the streamline at the hill crest can be compared with the neutral flow case. To calculate the streamline displacement at positions upwind of the hill crest, an approximation is made.

The approximation begins from the streamlines for neutral flow over a sphere (shown in Figure 18a), and over a circular cylinder (shown in Figure 18b). Note that the effect of the sphere or the cylinder on the flow is negligible for distances greater than about two hill radii from the hill center; it is assumed that this remains true in the stratified case. Hence, the difference between the plume centerline streamline heights for neutral and for stratified flows is a maximum at the hill crest and is negligible at a distance approximately two hill radii from the center of the hill.

In the absence of additional experimental data and a more complete theory, a linear interpolation scheme is applied to compute the height of the streamline at intermediate distances from the hill. This linear approximation should be adequate; however, the interpolation scheme can easily be changed in future refinements of the model. The procedure is incorporated into the model in the following way.

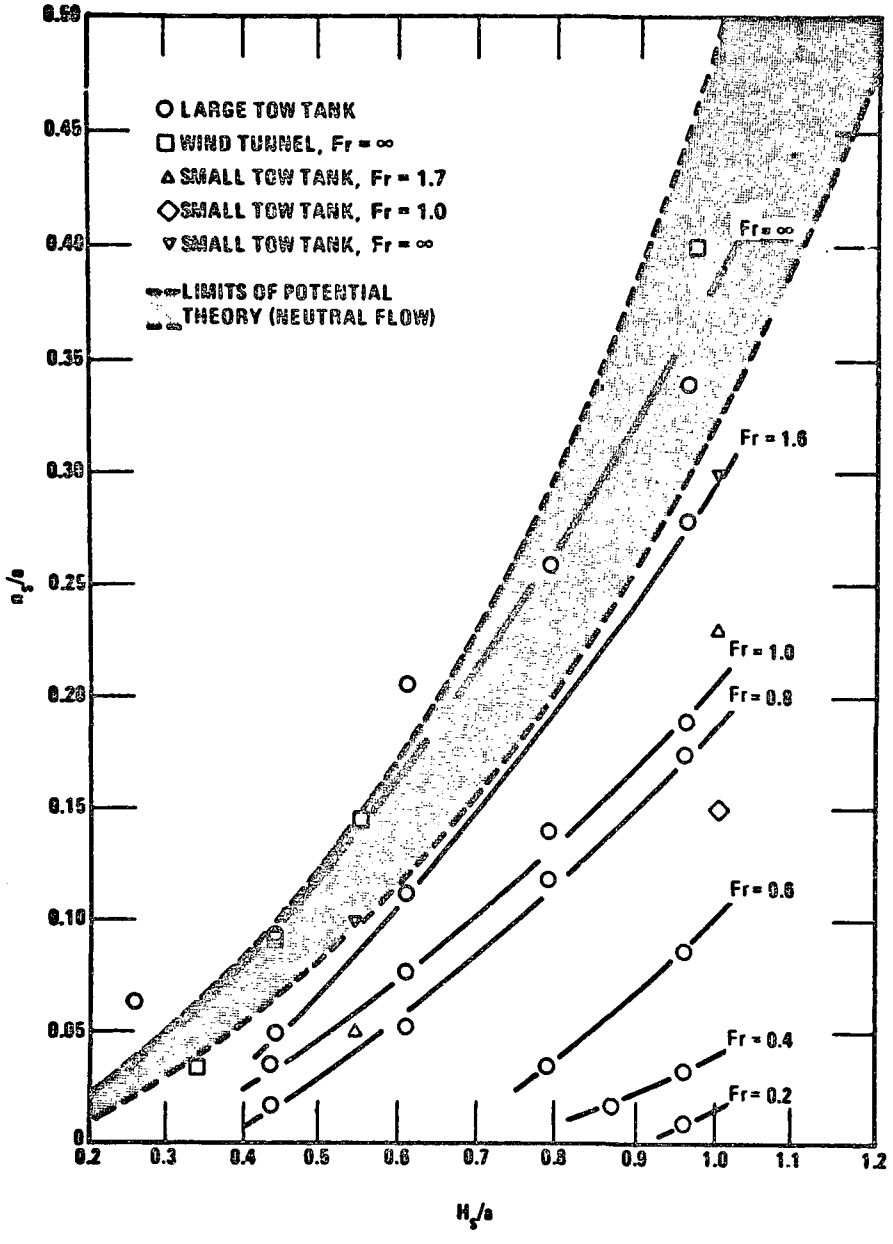

Source: Hunt et al. 1978

Figure 17. Height of the source streamline (n_s) above the hill crest (height = a) for various stack heights (H_s) and Froude numbers (F_r).

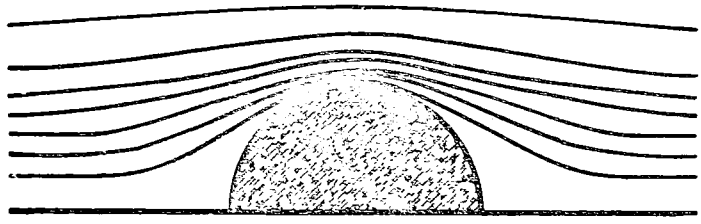

Hemispherical Hill

Figure 18a. Streamlines over a hemisphere.

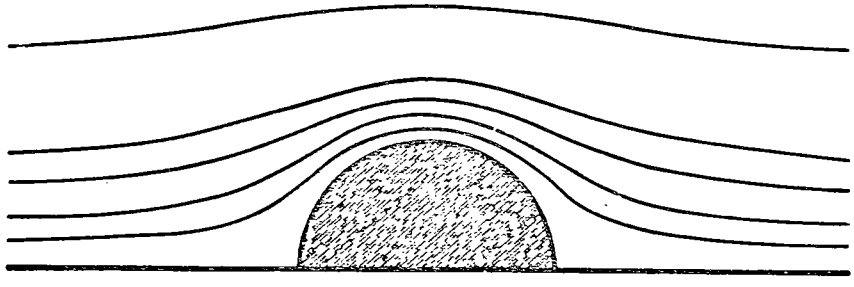

Circular Cylinder

Figure 18b. Streamlines over a half circular cylinder.

As described in Section 5.4.3, the streamline associated with the plume centerline is given by:

$$\psi(x,z) = \psi_s\ (X_s,\ H_s) \tag{8-1}$$

where ψ is the stream function for the specific hill shape investigated (refer to Equations 5-30, 5-34 for the two- and three-dimensional stream functions, respectively). At any downwind position, x, the height above the flat surface, z, can be found by solving the equation:

$$z = z\ (\psi_s, x) \tag{8-2}$$

(e.g., Equations 5-32, 5-36). In particular, the height of the streamline at the center of the terrain obstacle, z_C, (at x = 0.0) is given by

$$z_C = z\ (\psi_s, 0) \tag{8-3}$$

A similar relationship can be formed from the data in Figure 17 for the Froude number dependent height of the streamline over the terrain obstacle center, z_{CF}:

$$z_{CF} = n_s\ (Fr,\ H_s,\ a) + a \tag{8-4}$$

and fitting the data in the figure for the range of data shown ($\frac{H_s}{a} < 1$) by second-degree polynomials of the form:

$$z_{CF}/a = C_0 + C_1 \left(\frac{H_s}{a}\right) + C_2 \left(\frac{H_s}{a}\right)^2 \tag{8-5}$$

where the coefficients depend on the Froude number, Fr.

Define:

$$\Delta = z_C - z_{CF} \tag{8-6}$$

The height of the streamline, z_F, for the stable flow is then computed by

$$z_F = z - \delta \tag{8-7}$$

where z is computed for neutral flow according to Equation 8-2, and δ is given by:

$$\delta(x) = 0\ ;\ |x| \geq 2a$$

or

$$\delta(x) = \Delta\left(1 - \frac{|x|}{2a}\right);\ |x| < 2a \tag{8-8}$$

The net effect of modifying the neutral streamline is to lower the height of the plume centerline in the region within two obstacle heights

of the obstacle center. The plume centerline is depressed most at the crest of the obstacle.

This streamline depression scheme is, strictly, limited to flows similar to that investigated in Figure 17. The coefficients for Equation 8-5 have been derived for seven Froude number ranges, and for stack heights less than or equal to the height of the polynomial hill. In practice, the model uses this scheme for any stack height and any hill shape.

Where Equation 8-5 is applied to stack heights outside the range of experimental data, two physical constraints are imposed on the calculated value of z_{CF}. First, the streamline must not pass through the surface of the sphere. If it does, z_{CF}/a is set equal to 1.001. Second, the depressed streamline must not drop below its original height at the source. If it does, the streamline height is set equal to the stack height. Note that this latter condition only becomes important for stack heights much greater than the hill heights. Also, extrapolation of the curves contained in Figure 17 for stack heights above the hill height possibly introduces errors significant for the more stable applications. More observations are needed to refine the algorithm for taller stacks.

An extension of Equations 8-5 through 8-8 from flow over an isolated three-dimensional mound to flow over a two-dimensional ridge must await additional experiments to redefine the coefficients of Equation 8-5. Consequently, the model now uses the same depression for all crosswind aspect ratio hills. In practice, $\delta(x)$ (obtained from Equations 8-5, 8-6, and 8-8) for the two-dimensional hill is set equal to $\delta(x)$ for the three-dimensional hill. This depression is then subtracted from the source streamline associated with the two-dimensional hill.

In addition to the lowering of the plume centerline streamline, changes in the along streamline velocity, U(s), must be computed. It is observed that stratification speeds up the flow over the obstacle. The velocity change owing to stratification is modeled by assuming that the along streamline velocity is given by the gradient of the neutral flow stream function, ψ, (Equation 5-29) defined along the lower streamline computed by the stability modification described above. Since the gradient of the streamline function increases nearer the surface, the along streamline velocity, U(s), increases as stability lowers the plume centerline.

A final point concerns the case of direct plume impact on the obstacle. The potential flow theory approach can only be applied when the plume centerline streamline goes over the obstacle. The EPA tow tank experiments have shown that as the stratification is made stronger and the stack is made shorter relative to the obstacle height, a point is reached at which the plume no longer goes over the obstacle, but impacts and/or goes around the obstacle. Using the data in Figure 17, a minimum relative stack height, H_s/a, can be determined for a given Froude number in order that the plume go over the obstacle. This is the value of H_s/a (in Figure 17) for which a given Froude number curve intersects the ordinate (i.e., its height above the crest of the obstacle is zero). Note that as stratification increases (smaller Fr), the height of the minimum H_s/a required for passage over the obstacle increases.

Table 7 summarizes the plume impact criteria currently incorporated into the model. If H_s/a is less than the given value for a specified Froude number, it is assumed that the plume impacts the obstacle and the case is

flagged, but not otherwise treated. The plume impact criteria have been incorporated in a discrete form, not a continuous form, because the model is set up to use discrete Froude number classes in determining the streamline depression associated with the particular curves shown in Figure 17. If future refinements to the model allow a continuous depression algorithm, a continuous form of the impact criteria will be appropriate.

TABLE 7. PLUME IMPACT CRITERIA BASED ON FIGURE 17

Froude Number (Fr)	Plume impacts if H_s/a less than:
$Fr < 0.4$	0.82
$0.4 \leq Fr \leq 0.7$	0.75
$0.7 \leq Fr < 1.5$	0.375
$1.5 \leq Fr$	assumed neutral (no plume impact)

8.3 Application to the Atmosphere

To apply this approximate model of stratified flow over a hill to the atmosphere, the atmospheric stratification as described by the Froude number Fr must be known. The Froude number is defined by:

$$Fr \equiv \frac{U}{NH} \quad \text{and} \quad N \equiv \sqrt{\frac{-g}{\rho}\frac{\partial \rho}{\partial z}} \qquad (8\text{-}9)$$

Note that a length scale, H, is incorporated into Fr. Ordinarily the atmospheric stratification is specified for routine air quality modeling purposes by the Pasquill stability class, rather than by the Froude number. The classification of stratification by stability class and the application of the PGT σ_y and σ_z curves for all stack heights are approximations that ignore the variations with height of atmospheric stratification and turbulent diffusion. These approximations are not as good in the presence of a hill, because of the new length scale that is introduced into the problem. The program is written in such a way that the user must supply Fr if known, with H in Equation 8-9 corresponding to the hill height, a. If no Froude number is specified, the program assumes flow kinematics corresponding to neutral flow conditions. [Application of the model at Widows Creek (Section 12) provides an example of the use of vertical temperature and velocity profiles in defining Froude numbers.]

For routine application of the model using near-surface observations, accurate Froude numbers are not available. Under these circumstances, default potential temperature gradients may be assumed throughout the overlying layer of the atmosphere influenced by the terrain feature. The temperature gradient could be specified for each of the neutral to stable stability classes in much the same way that the gradient is specified in

current stable plume rise algorithms. Similarly, the stability-dependent wind shear algorithms used to infer stack height wind speeds could also be used to infer a mean elevated wind speed for use in calculating a Froude number. To the extent that plume rise, transport, and diffusion can be roughly characterized in this way, the Froude number-dependent streamline depression may also be characterized. But such an approach should be fully analyzed for model sensitivity to each assumption.

Additional approaches will have to be developed for cases where both the plume and terrain are above a confined surface layer. This is the problem of a true two-layer flow. Over level terrain, the importance of such a condition is reduced since ground-level impacts would obviously be small. In complex terrain, however, the model would be required to make reasonable assumptions about plume rise, transport velocities, plume spread, and Froude number in order to calculate a concentration on the elevated terrain surface.

SECTION 9

COMPARISON WITH LABORATORY EXPERIMENTS--STRATIFIED FLOW

9.1 Introduction

The approach used to test the validity of the potential flow model modified for stratification effects is the same as that used for neutral flow. In the modified potential flow model, calculations are performed using Equations 5-20 through 5-25 as in the neutral case, except that the plume centerline trajectory is specified using Equations 8-2 through 8-8 to modify the vertical displacement in neutral flow (Equation 8-1). In the absence of well documented field experiments, the model is tested by performing calculations designed to simulate the EPA tow-tank experiments.

9.2 Dispersion Coefficients, Flat Terrain

The modeling approach used to compute the concentrations over a hill in stratified flow requires knowledge of the dispersion coefficients for flat terrain in stratified flow. The EPA FMF experimental tow-tank measurements used in the comparison [catalogued as experiments SBF3-9-0, BF3-9-0, PF3-9-0 in Snyder (1977) and Snyder (1978)] are for a 9 cm stack height in a stratified flow of Froude number 0.97 (considered moderately stable). Gaussian profiles were fitted by Snyder to the plume at the two downwind distances, 50 cm and 84.7 cm. These data points and profiles as provided by Snyder are shown in Figures 19 and 20. [These graphs were changed to χ versus z, rather than z versus χ, to conform to the manner in which the experimental results were presented in Snyder (1977)]. The values of σ_z obtained by these Gaussian fits (in Figures 19 and 20) at the two downwind distances, 50 cm and 84.7 cm respectively, were used to specify a linear relationship to interpolate σ_z to other downwind distances, for use in the model calculation. The computed concentrations (shown by the circular symbols) on and off the centerline closely follow the fitted curve.

Just as was the case for neutral flow, however, the effects of the boundary layer are significant; as seen in Figures 19 and 20 the concentration measured closest to the surface is much greater than would be predicted by the Gaussian profile. Again, as a first approximation for this effect, new boundary layer enhanced sigmas (denoted by σ') were obtained by fitting a Gaussian profile only to the centerline value and to the near-surface value (in the manner described in Section 6.3). The corresponding concentrations computed with the modified sigmas are shown by the square symbols in Figures 19 and 20. Close to the ground, they represent the vertical dispersion more accurately.

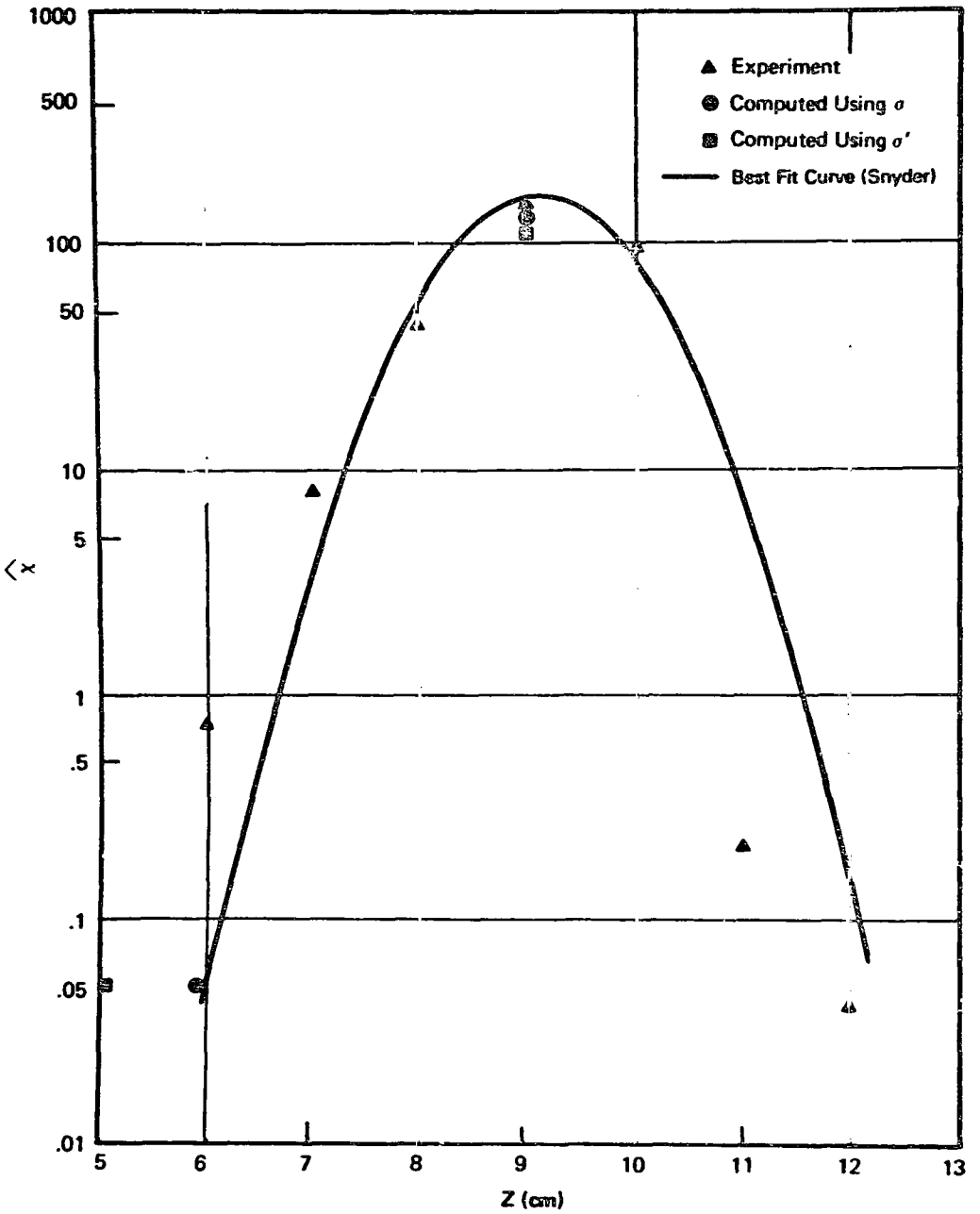

Source: Snyder 1977

Figure 19. Vertical concentration profile 50 cm downwind of a 9 cm stack for stratified flow in flat terrain.

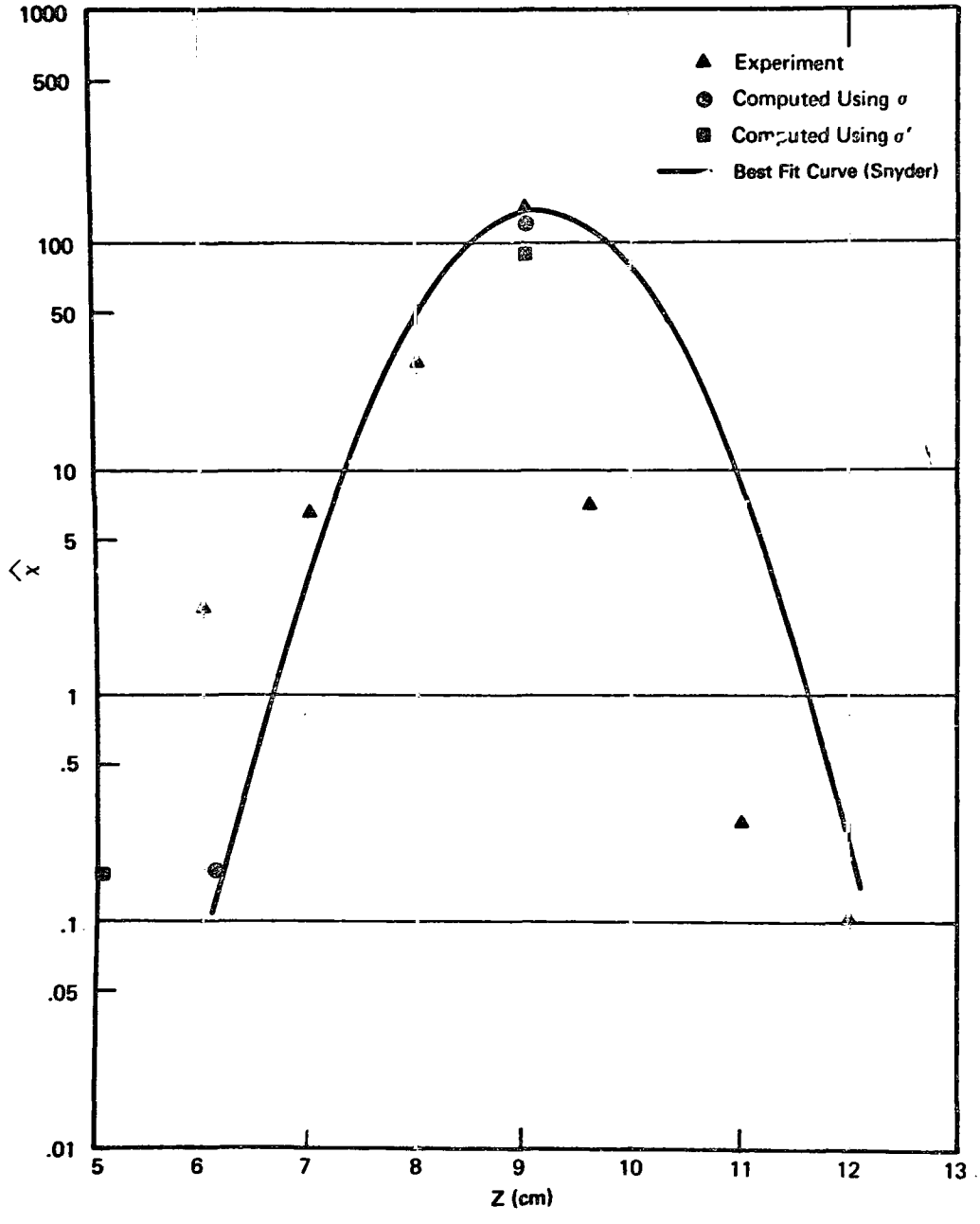

Source: Snyder 1977

Figure 20. Vertical concentration profile 84.7 cm downwind of a 9 cm stack for stratified flow in flat terrain.

9.3 Results in Presence of Terrain Obstacle

Vertical concentration profiles were not measured in the EPA experiments on stratified flow. Instead, the ground-level concentrations were measured along several lines from the crest of the hill, at various angles to the mean flow. Figure 21a shows the measured ground-level concentrations along the line on the surface going directly from the hill crest to the stack. In this coordinate system, the hill crest is located at s = 0.0 and the stack base at s = 84.7 cm. The results of the model computations using the originally derived sigmas (circular symbols) and the boundary layer-enhanced sigmas (square symbols) are also shown in Figure 21a. In the vicinity of the hill ($s \leq 20$ cm), the concentration estimates based on the boundary layer-enhanced dispersion parameter, σ', are within a factor of two of the experimental data. At the crest of the hill, the ground-level concentrations are 173% and 208% of the observed concentrations using σ_z and σ_z', respectively, while close to the upwind edge of the hemisphere, concentrations are underestimated by nearly a factor of four. In interpreting these results, it should be noted that the ground-level concentration varies exponentially with the square of the distance between plume centerline and surface, and that the model calculations are based on a hemispherical hill shape, different from the shape of the polynomial hill used in the laboratory experiments. The hemisphere, for instance, meets the flat surface at s = 23 cm, while the polynomial hill used in the experiments remains significantly above the flat surface beyond s = 30 cm. Therefore, the model underestimation with increasing distance from the crest is directly related, in part, to the differences in hill shape. Under these circumstances, the comparisons are encouraging.

The highest impacts occur at the crest. The predicted and the observed concentrations at the crest of the obstacle are shown in Table 8 for the 9 cm stack case. The terrain correction factor derived from the observations is 0.183, and that derived from the model computations using σ_z is 0.147. These are extremely low values, indicating that both the predicted and the observed surface concentrations are much larger than those that would have been predicted by a terrain-following model, or by a partial height model using terrain correction factors of 0.5 or 0.35. Concentrations predicted by each of these three approaches are also compared in Table 8. It is seen that the potential flow model offers considerable improvement in predicting the peak concentration compared to these other models. (Finally, if direct centerline impingement is assumed, the predicted concentrations are 3 to 4 times larger than the observed concentration.)

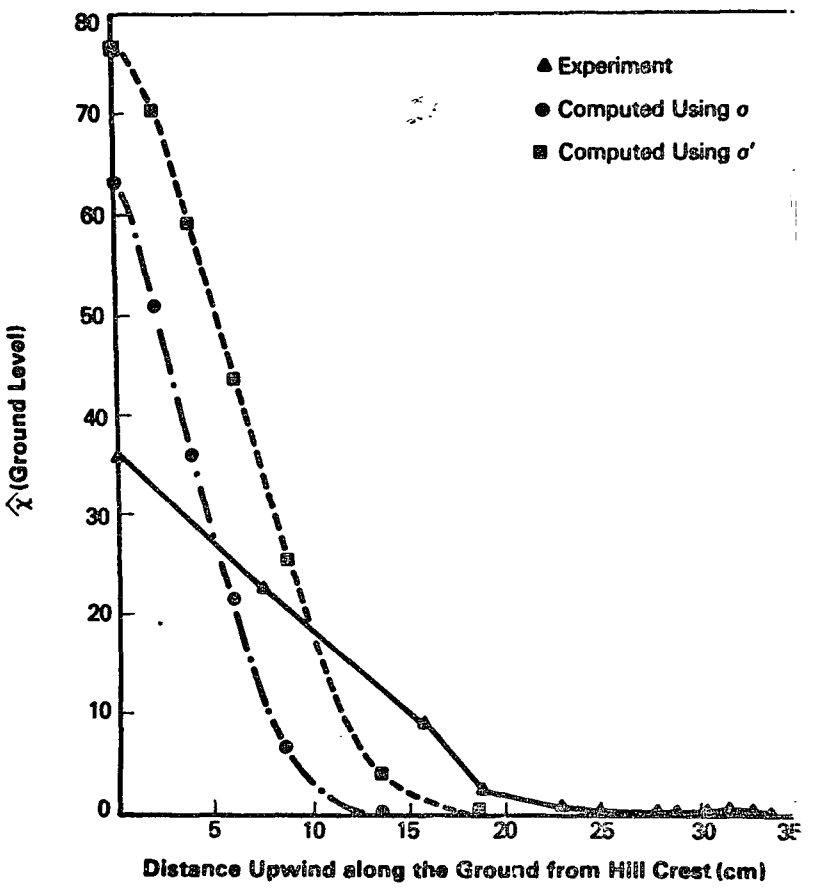

Source: Snyder 1978

Figure 21a. Ground-level concentration for stratified flow as a function of distance upwind along the ground from the hill crest for a 9 cm stack and 23cm hill.

TABLE 8. COMPARISON OF PREDICTED AND OBSERVED CONCENTRATIONS AT HILL CREST FOR THE 9 CM STACK TOW TANK EXPERIMENTS

Model	Normalized Surface Concentration at Crest	
	Predicted	Observed
Potential Flow (σ_z)	63.4	36
Potential Flow (σ_z')	76.9	36
Level Plume	125.0	36
Terrain Following	1×10^{-25}	36
Partial Height (0.5)	1×10^{-5}	36
Partial Height (0.35)	0.11	36

Measurements and computations (using both sets of sigmas) were also compared at ground level, outward from the crest at 90° to the flow. These results are shown in Figure 21b. Again, the model is seen to work best in predicting the maximum concentration close to the hill crest. Off-hill-crest concentrations, though underpredicted, are less important in regulatory applications since these concentrations are an order of magnitude smaller than those at the crest. Other phenomena are active in the experiment, perhaps producing (by recirculation?) the secondary peak beyond the margin of the experimental hill. It is not clear to what extent concentrations closer to the hill are influenced by these phenomena.

Overall, the approximations used to account for the effects of stratification in the potential flow model predict ground-level concentrations along the downwind plume trajectory within a factor of two; but the results point to the need for further consideration of surface boundary layer effects and other hill shapes. Indeed, more experiments with the same hill configuration, but a wider range of stack heights, would aid the evaluation of the model's performance.

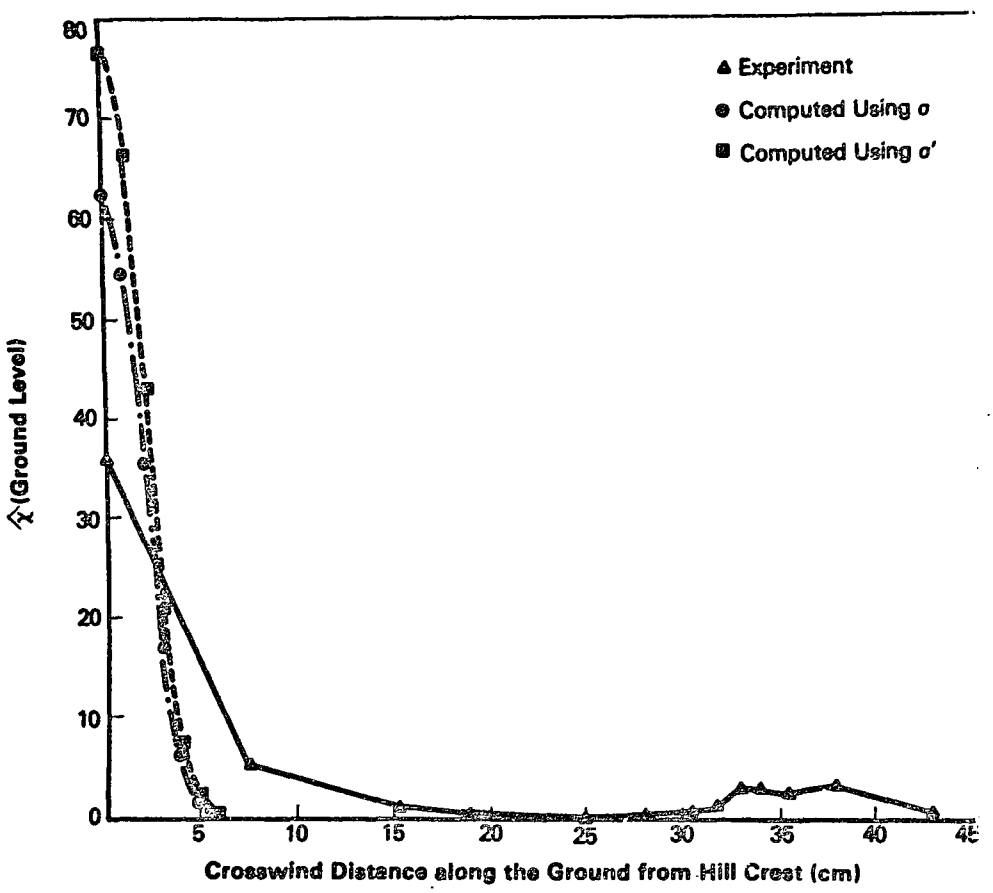

Source: Snyder 1978

Figure 21b. Ground-level concentration for stratified flow as a function of cross-wind distance along the ground from the hill crest for a 9 cm stack and 23 cm hill.

SECTION 10

MODIFICATIONS FOR ARBITRARY CROSSWIND ASPECT RATIO

10.1 Approach

The treatment of potential flow in previous chapters deals with spherical or circular ridge shaped hills. The model has been generalized to allow for intermediate shapes by using an approximation technique based on an interpolation of two-dimensional and three-dimensional flow field properties. The parameter chosen to characterize the obstacle shape is the crosswind aspect ratio, λ, defined as the ratio of half of the crosswind breadth of the obstacle, b, to the obstacle height, a. Shapes for several different values of λ, where:

$$\lambda \equiv b/a \qquad (10\text{-}1)$$

are illustrated in Figure 22.

Because streamlines are not easily defined analytically for non-axisymmetric shapes in three dimensions, an approximate procedure was developed. This procedure uses the analytical description of the streamlines for flows over a sphere and over a cylinder, as well as theoretical results (J.C.R. Hunt, personal communication to R. G. Isaacs, 20 July 1978) that describe the changes in velocity at the crest of the hill as the aspect ratio is changed, and experimental results that show the changes in the source streamline above the crest as the aspect ratio is changed.

Changes in hill shape affect the flow field in two ways. First, the shape of the plume centerline is altered and its form is found to be intermediate between the limiting two-dimensional and three-dimensional cases. Second, the velocity along the plume trajectory is changed. The approach used here to treat hill shapes intermediate between that of a circular ridge and that of a sphere is to weight the flow fields of the two extreme cases to produce an approximation for intermediate cases.

10.2 Adjustments to Plume Centerline Trajectory Streamline

As described in Section 5.4.3, the height of the streamline, z, is specified by the streamline through the source, ψ_s, such that:

$$z = z(x,\psi_s) \qquad (10\text{-}2)$$

where the particular functional dependence changes with the stream function, ψ, determined by the shape of the obstacle. Two complete analytic solutions are available: flow over a sphere and flow over a cylinder. For a cylinder ~~(as in Equation 5-32)~~

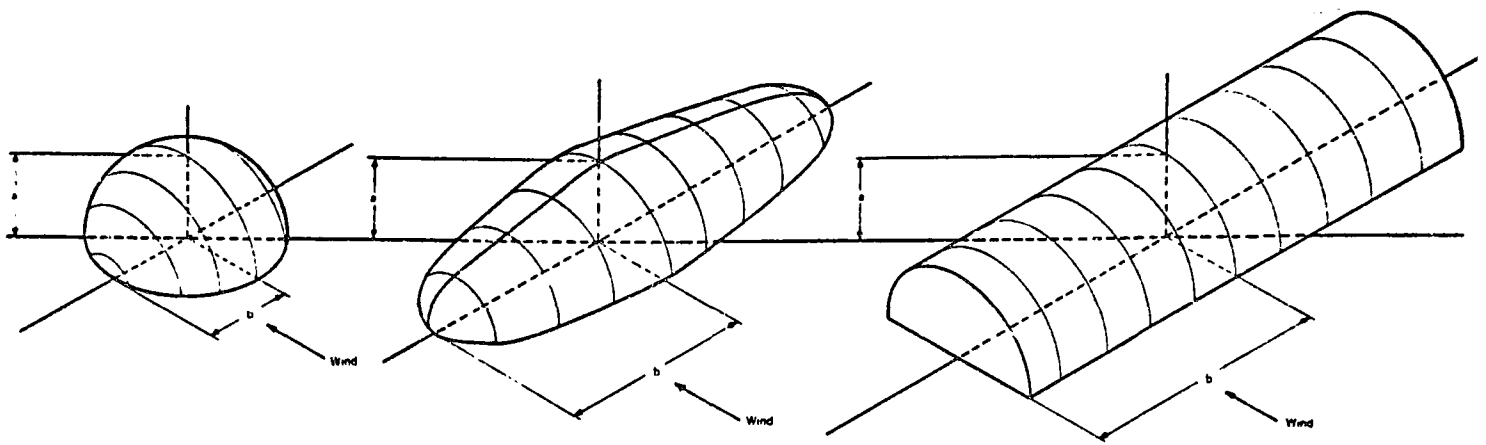

Figure 22. Definition sketch for aspect ratio λ=b/a for hills of spherical, intermediate, and cylindrical shapes.

$$z\left[1 - \frac{a^2}{x^2+z^2}\right] = H_s\left[1 - \frac{a^2}{X_s^2+H_s^2}\right] \qquad (10\text{-}3)$$

and for a sphere (as in Equation 5-35)

$$z^2\left[1 - \frac{a^3}{(x^2+z^2)^{3/2}}\right] = H_s^2\left[1 - \frac{a^3}{(X_s^2+H_s^2)^{3/2}}\right] \qquad (10\text{-}4)$$

where z is the height of the streamline at position x.

As defined above, the sphere corresponds to an aspect ratio of unity, $\lambda = 1$, and the cylinder (circular ridge) corresponds to an infinite aspect ratio, $\lambda = \infty$. For a general aspect ratio the height will be a function of λ and may be written as:

$$z = z(\psi_s, x, \lambda) \qquad (10\text{-}5)$$

Experimental data (Snyder et al. 1979b) suggests that the streamline height, z, is some weighted average of the heights of the streamline appropriate to flow over a cylinder, and to flow over a sphere.

The plume centerline height, evaluated from experiments with stack heights equal to the obstacle height and to one half the obstacle height, is a strong function of the aspect ratio for $\lambda \lesssim 4$, and is a weak function for larger aspect ratios. This behavior is described by a simple power law form for the aspect ratio weighting function (λ^{-d});

$$z = \left[Z_{SPH}(\psi,x) - Z_{CYL}(\psi,x)\right]\lambda^{-d} + Z_{CYL}(\psi,x) \qquad (10\text{-}6)$$

where Z_{SPH} is the streamline height over the sphere, and Z_{CYL} is the streamline height over the cylinder. For large aspect ratios the third term dominates, and the twodimensional flow over the cylinder is recovered. When $\lambda=1$, the threedimensional flow over the sphere is recovered.

Data from the wind tunnel experiments are used to determine the value of the exponent in Equation 10-6. Streamline heights above the tunnel floor at a downwind distance of 84.7 cm (at the location of the hill crest) are nondimensionalized with the hill height, 23.4 cm, and introduced into Equation 10-6 to solve for "d". The mean values obtained lie between 1 and 1.2, fitting the observed data to within 0.25 cm.

The value currently used in the model algorithm for the aspect ratio exponent is -1.1, so the equation for the source streamline height for an obstacle with a crosswind aspect ratio λ is:

$$z = \left[Z_{SPH}(\psi,x) - Z_{CYL}(\psi,x)\right]\lambda^{-1.1} + Z_{CYL}(\psi,x) \qquad (10\text{-}7)$$

A description of the wind tunnel experiments used to define the neutral flow streamlines over obstacles of arbitrary aspect ratio is contained in Section 11.

10.3 Adjustments to Velocity Field

Changes in the aspect ratio of the hill also affect the speed of flow along the streamline. An approximate scheme, which incorporates theoretical results of Hunt, has been developed to account for this effect. One way to characterize the flow is by the so-called "speed-up factor," S, defined as the ratio of the velocity at the crest of the hill, U_c, to the velocity far upstream, U_∞:

$$S \equiv U_c/U_\infty \tag{10-8}$$

The speed-up factor (Hunt et al. 1978) S will depend on the shape of the hill. In particular, for $\lambda = \lambda_1 = 1$, (the spherical hill), potential flow theory shows that

$$S_{SPH} = S(\lambda_1) = 1.5 \tag{10-9}$$

and for $\lambda = \lambda_2 \to \infty$ (the circular ridge):

$$S_{CYL} = S(\lambda_2) \to 2 \tag{10-10}$$

For intermediate shapes, the theory (Hunt et al. 1978) shows that:

$$S(\lambda) = 2/[\quad - \beta(\lambda)] \tag{10-11}$$

where

$$\beta(\lambda) = 1 + \frac{1}{\lambda^2-1} - \frac{\lambda}{(\lambda^2-1)^{3/2}} \ln\left[\lambda+\sqrt{\lambda^2-1}\right] \tag{10-12}$$

Some representative values of $\beta(\lambda)$ and $S(\lambda)$ are tabulated in Table 9; note the asymptotic behavior as $\lambda \to 1$. These results apply only to the surface velocity at the crest of the hill. To use this result in approximating the velocity field at other points, let the velocity at any point be considered as an appropriately weighted average of the velocity corresponding to the flow over a hill and that over a sphere:

$$U(x,z) = G_{CYL}(\lambda)\, U_{CYL}(x,z) + G_{SPH}(\lambda)\, U_{SPH}(x,z) \tag{10-13}$$

where the weighting functions G_{CYL} and G_{SPH} are yet to be determined. These functions are found by using the theoretical expression for the speed-up factor to find the weighting functions at the crest of the hill, and by assuming that the weights determined are applicable everywhere in the flow field. In addition, the proper limiting forms for flow over a sphere and over a cylinder are again required. Thus:

TABLE 9. REPRESENTATIVE VALUES OF SPEED-UP FACTOR S

λ	$\beta(\lambda)$	$S(\lambda)$
1.000	0.666...*	1.500*
1.0001	0.66675	1.50009
1.001	0.6669	1.5003
1.01	0.669	1.502
1.05	0.680	1.515
1.1	0.692	1.529
1.2	0.714	1.555
1.5	0.767	1.622
2.0	0.826	1.703
3.0	0.891	1.803
5.0	0.944	1.894
10.0	0.980	1.961
20.0	0.993	1.986
100.0	0.99957	1.99914

*Asymptotic value as $\lambda \to 1$; when $\lambda \to 1$, $\beta \to 2/3\ (1+O(\lambda-1))$

$$U = U(x,z,\lambda) = \left[\frac{S(\lambda) - S_{SPH}}{S_{CYL} - S_{SPH}}\right] U_{CYL} + \left[\frac{S_{CYL} - S(\lambda)}{S_{CYL} - S_{SPH}}\right] U_{SPH} \qquad (10\text{-}14)$$

Substituting $S_{SPH} = 1.5$ and $S_{CYL} = 2.0$ results in

~~$U(x,z,\lambda) = 2.0\,[S(\lambda) - 1.5]\,U_{CYL}(x,z) + 2.0\,[2.0 - S(\lambda)]\,U_{SPH}(x,z)$~~

Therefore

$$G_{CYL} = 2\,(S(\lambda) - 1.5)$$

$$G_{SPH} = 2\,(2\text{-}S(\lambda)) \qquad (10\text{-}15)$$

where $S(\lambda)$ is determined from Equations 10-11 and 10-12. This correction is applied to each component of the velocity separately. Thus having modified both the velocity field and the plume trajectory (streamline shape), the ~~program proceeds as previously for spherical and cylindrical hills. Note~~ that because the speed-up factor for λ=10 is within 2% of its value at $\lambda=\infty$, the interpolation algorithm, for convenience, equates two dimensional flow with all aspect ratios greater than or equal to 10.

9-1/8"

SECTION 11

COMPARISON WITH LABORATORY EXPERIMENTS—NEUTRAL FLOW OVER HILLS OF INTERMEDIATE ASPECT RATIO

11.1 Background

Potential flow model calculations for hills of aspect ratios 1, 2, 3, and 10 (effectively infinity) are compared to observed laboratory concentrations under neutral flow wind tunnel conditions.

The wind tunnel experiments were conducted at the FMF (by W. H. Snyder and R. E. Britter). Results of that study were made available to ERT in the form of an internal data report (Snyder et al. 1979b).

Model computations retain the dimensions employed in the data report, except for the definition of the aspect ratio. As in the earlier comparisons for the polynomial hill, linear vertical and horizontal spread statistics near the hill location are developed from the wind tunnel data obtained for the no-terrain case (Snyder et al. 1979a). This amounts to specifying dispersion rates present on the laboratory scale rather than attempting to scale down dispersion rates observed in the atmosphere.

11.2 Comparison of Hill Shapes

Four idealized hill models are used in the wind tunnel experiments. All have a triangular longitudinal cross-section. Hill 'C2' is a circular cone, with surface slope of one half. Hills 'C4' and 'C6' are fabricated by inserting triangular ridge pieces between the original cone halves, and hill 'CX' is a simple triangular ridge that spans the width of the tunnel. Dimensions of these hills are summarized in Figure 23.

Snyder and Britter (1979b) define aspect ratios for these hill shapes to be the crosswind length of the hill between the two half-height points, divided by the hill height. In this report, however, the definition of the aspect ratio uses one half the full crosswind hill dimension divided by the hill height (see Figure 22). For the two limiting hill shapes contained in the model, the full crosswind dimension of the hill is either well defined and sharp (sphere), or effectively infinity (cylinder).

In the case of the sphere, the surface slope varies from zero at the crest to infinity at the base, and so the crosswind dimension has distinct and abrupt end points. When this idealized hill form is used to represent hill shapes with considerably smaller slope discontinuities at their bases, some smaller crosswind dimension should be selected that would increase the similarity of the physical hill to the spherical hill. For the wind tunnel experiments of Snyder and Britter, the half hill height crosswind dimension of the cone coincides identically with the base of a spherical hill of equal

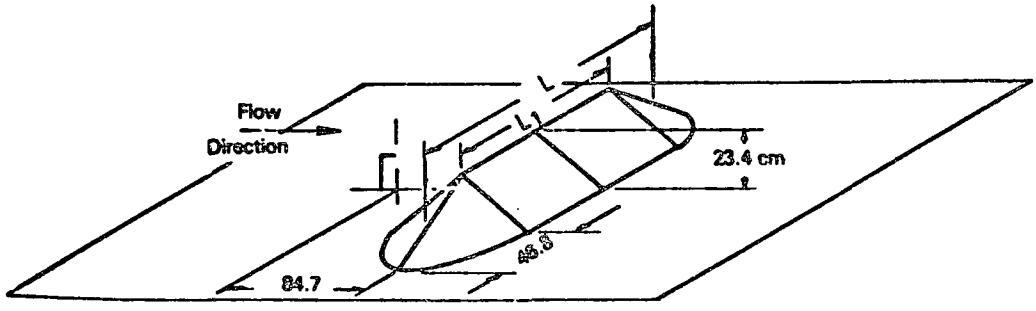

HILL	C2	C4	C6	CX
L_1 (cm)	0	45	90	∞
L (cm)	46	91	136	∞
Aspect Ratio	1	2	3	∞

Source: Snyder et al. 1979b

Figure 23. Details of hills used in EPA wind tunnel experiments.

height. Therefore, aspect ratios for the hills studied by Snyder and Britter are defined in this report to be one-half the values defined by Snyder and Britter. This definition takes the longitudinal base of the experimental hills to be the distance between the half hill height points, and the aspect ratio to be the hill height divided by one half this base dimension. Consequently, the hill shapes used in the wind tunnel experiments correspond to model aspect ratios of 1, 2, 3, and 10 (effectively infinity).

Differences between the circular cross-sections employed in the model and the triangular sections used in the wind tunnel will undoubtedly produce discrepancies between predicted and observed concentrations. The sharp slope discontinuity at the crest of hills C2, C4, C6, and CK will certainly lead to flow separation and increased turbulence downwind of the crest. However, more subtle effects of slope differences upwind of the crest are not intuitively apparent. Comparisons between predicted and observed concentrations are therefore confined to laboratory data obtained at the crest of the obstacles.

11.3 Dispersion Coefficients, Flat Terrain

Wind tunnel experiments for release heights equal to 11.7 cm and 23.4 cm are compared with model calculations. Because all of the obstacle heights equal 23.4 cm, these two release heights represent final plume elevations equal to 0.5 and 1.0 hill heights. Separate dispersion coefficients (σ_y,σ_z) are derived for each release height, based on experiments with no hill present.

Vertical concentration profiles in the absence of hills were taken at downwind distances of 33, 84.7, and 293 cm from the release point. The hill crests in later experiments were positioned at the second distance, 84.7 cm. Snyder and Britter (1979a) fit a Gaussian curve to each concentration profile to produce a best fit to all of the data points. In the case of 11.7 cm release height, the plume intercepts the ground before the 84.7 cm downwind distance is reached, so a reflected Gaussian is fit to the data. The effective stack height in each case is assumed to be equal to the release height.

Although Gaussian parameters are used to describe the vertical profiles, it is evident that the observed profiles are not Gaussian. Snyder and Britter point out that the observed profiles are not symmetric, and that the concentrations decrease much too slowly in the "tails". In addition, their observations of maximum ground concentrations indicate that the plume from the lowest release (0 cm) is subject to reduced transport velocities, and that the plume from the highest release (23.4 cm) apparently experiences lower turbulence intensities, compared to the plume from the 11.7 cm release height. Both flow retardation and gradients in turbulence intensity throughout the surface boundary layer would tend to distort a vertical Gaussian plume profile.

Lateral plume concentration profiles are also obtained at 33, 84.7, and 293 cm distances from the source. These observations are generally taken at the height above the surface corresponding to the maximum concentration in the vertical profile. Because the lateral dispersion is measured in the horizontal plane, factors that tend to produce a non-Gaussian concentration

profile are not present, and so the crosswind distributions are nearly Gaussian.

Analysis of vertical plume spread (σ_z) with downwind distance from 33 cm to 293 cm suggests that its linear variation with x for the region near x = 84.7 cm can be adequately represented by the trend from x = 33.0 cm to x = 84.7 cm. Curvature in $\sigma_z(x)$ is very small over the range of observations. The best fit Gaussian sigmas derived by Snyder et al. (1979a) are obtained by using data from the entire vertical profile.

A second approach useful in this comparison study is the calculation of Gaussian sigmas which describe concentrations adequately at the surface and at plume centerline height, but not necessarily above the centerline height. These sigmas use only two data points: the surface concentration, and the centerline maximum concentration. Such sigmas (as in Sections 7 and 9) are used to reduce discrepancies between modeled and observed concentrations resulting from the non-Gaussian shape of the observed vertical distribution, especially near the surface.

Comparisons are made between calculated concentrations and observed concentrations along the center of the tunnel floor in the region near x = 84.7 cm using plume spread values derived by Snyder et al. (1979a) and the 2-point values based on the centerline maximum and the near-surface plume concentration. It was found that an average of the two σ_z values provided the best match to the observed concentrations near x = 84.7 cm. Consequently, the linear function of x used to describe $\sigma_z(x)$ (for the 11.7 cm release height) is based on the average σ_z from the two methods at 84.7 cm, and on Snyder and Britter's value at 33 cm (because the two sigmas differed only by 2 mm at this distance). The expression for the 23.4 cm release height also uses the average σ_z at 84.7 cm because the 2-point sigma is very close to the reported sigma. At x = 33 cm, the trailing edge of the plume is well above the surface (10 cm), so only the reported sigma is used.

Review of the horizontal plume spread (σ_y) values derived by Snyder et al. (1979a) also indicates that its linear variation with x near x = 84.7 cm can be adequately represented by the trend from x = 33 cm to 84.7 cm. No additional sigma computations are needed for horizontal spread because the observed standard deviation in the concentration distributions is nearly Gaussian.

The final specification of the dispersion parameters is as follows:

$$\text{(a) HS} = 11.7 \text{ cm} \qquad \sigma_y = 0.409 + 0.097X \text{ cm}, \quad \sigma_z = 0.738 + 0.048X \text{ cm} \tag{11-1}$$

$$\text{(b) HS} = 23.4 \text{ cm} \qquad \sigma_y = 0.119 + 0.081X \text{ cm}, \quad \sigma_z = 0.82 + 0.039X \text{ cm} \tag{11-2}$$

Note that increased dispersion of the lower plume relative to the upper is evident in the σ_y relations. This is not as apparent in the σ_z relations. The sigma of release height (b) at x = 0 is quickly compensated by a smaller distance coefficient. By x = 33 cm, the sigma for (a) is slightly greater than the sigma for (b).

11.4 Comparisons for Plume Height Equal to the Obstacle Height

Wind tunnel experiments for stack height equal to hill height (23.4 cm) are analyzed first because the no-hill observations suggested that the plume released at 23.4 cm is less affected by the surface boundary layer than is the plume released at 11.7 cm (see Section 11.3). Surface boundary layer effects are not considered in the model, so their presence may reduce the quality of the predicted versus observed comparisons.

11.4.1 Observed and Predicted Concentrations

Concentrations are measured at the hill crest (x = 84.7 cm) several times for each obstacle form. A longitudinal section is taken at the local surface under the plume axis, producing one observation of the surface concentration at the crest; the second observation is taken from a vertical concentration profile at the crest; and the third observation is taken in conjunction with a lateral profile at crest height. All of these values are normalized by the factor Uz^2/Q where U is the freestream velocity in the tunnel [400 centimeters per second (cm/s)], z is the hill height, and Q is the emission rate of the tracer substance.

These overlapping observations show considerable scatter in surface concentrations at the hill crests. For example, multiple observations at the crest of hill C6 during a vertical profile measurement sequence produced observations ranging from 0.013 to 0.079. When the complete series of vertical profile points is plotted, an average value of 0.03 is obtained from the observed trend. Similar scatter is observed in the lateral and longitudinal profiles. In some cases, the scatter exceeds 50% of the average value derived from the profile trends. Table 10 summarizes the average observed ground concentrations obtained at the hill crests for aspect ratios of 1, 2, 3, and 10.

TABLE 10. OBSERVED NORMALIZED CONCENTRATIONS AT HILL CREST FOR STACK HEIGHT EQUAL TO HILL HEIGHT

Hill		Normalized Ground Concentration Observation* 1	Observation 2	Observation 3	Average
C2	1	0.161	0.16**	0.159	0.160
C4	2	0.031	0.042	0.060	0.038
C6	3	0.03**	0.02**	0.013	0.021
C8	10	0.015	0.016	0.021	0.017

*Observation 1 is taken in conjunction with a vertical section; observation 2 is taken in conjunction with a longitudinal section; and observation 3 is taken in conjunction with a lateral section.

**Values reported to fewer significant digits are interpolated from a number of data points obtained near the crest.

One correction must be made to these concentrations before they can be compared to the predicted concentrations. In both systems, a normalized concentration is used, based on the scale $\bar{u}a^2/Q$. The normalized concentrations reported by Snyder and Britter, and listed in Table 10, use 400 cm/s for the scaling velocity. This is the free stream velocity in the wind tunnel. The model computations assume the scaling velocity is equal to the free streamline velocity at source height, consistent with the usual application of the Gaussian plume equations. Therefore, the scaling factor for the wind tunnel observations has been changed so that the scaling velocit is that observed at source height with no obstacle in the tunnel, 356 cm/s. The new normalized concentrations are listed in Table 11.

TABLE 11. COMPARISON OF PREDICTED AND OBSERVED NORMALIZED SURFACE CONCENTRATIONS FOR STACK HEIGHT EQUAL TO HILL HEIGHT*

	Predicted Concentration		
	Hill Crest	Hill Maximum	Observed Concentration
1	0.199	0.284	0.142
2	0.0103	0.037	0.034
3	0.0035	0.015	0.019
5	0.0015	0.008	-
10	0.0005	0.003	0.015

*The observed values are normalized using the source height velocity.

Normalized concentrations predicted by the complex terrain model incorporate vertical and horizontal plume spread parameters derived in Section 11.3, and the aspect ratio weighting function derived in Section 10. Computations are made for aspect ratios of 1, 2, 3, 5, and 10. The results are also listed in Table 11.

Comparing predicted and observed values shows that the hill crest computation overpredicts by 40% at aspect ratio equal to 1, and quickly underpredicts for aspect ratio equal to or greater than 2. Over the ridge, the model prediction is only 3.4% of the observed value. When the maximum predicted concentration for any position on the hill is compared with the observed concentration at the crest in the wind tunnel, better agreement is found at most aspect ratios. Overpredictions of 100% and 9% are found for aspect ratios 1 and 2; underpredictions of 25% and 80% at aspect ratios of 3 and 10. Still the trend is evident: predicted ground-level concentrations fall off much more rapidly with aspect ratio than do the observed ground-level concentrations. This trend is visually apparent in Figure 24.

The potential flow model concentrations may also be compared with observations and other modeling methods using the terrain correction factor (as in Section 7). Table 12 summarizes surface concentrations and implied terrain correction factors for: the wind tunnel observations; the potential flow model; and the surface concentrations resulting from the half-height assumption model; the flat terrain assumption model (i.e., terrain-following plume); and the level plume assumption model (no surface reflection doubling). The comparison illustrates the sensitivity of maximum surface

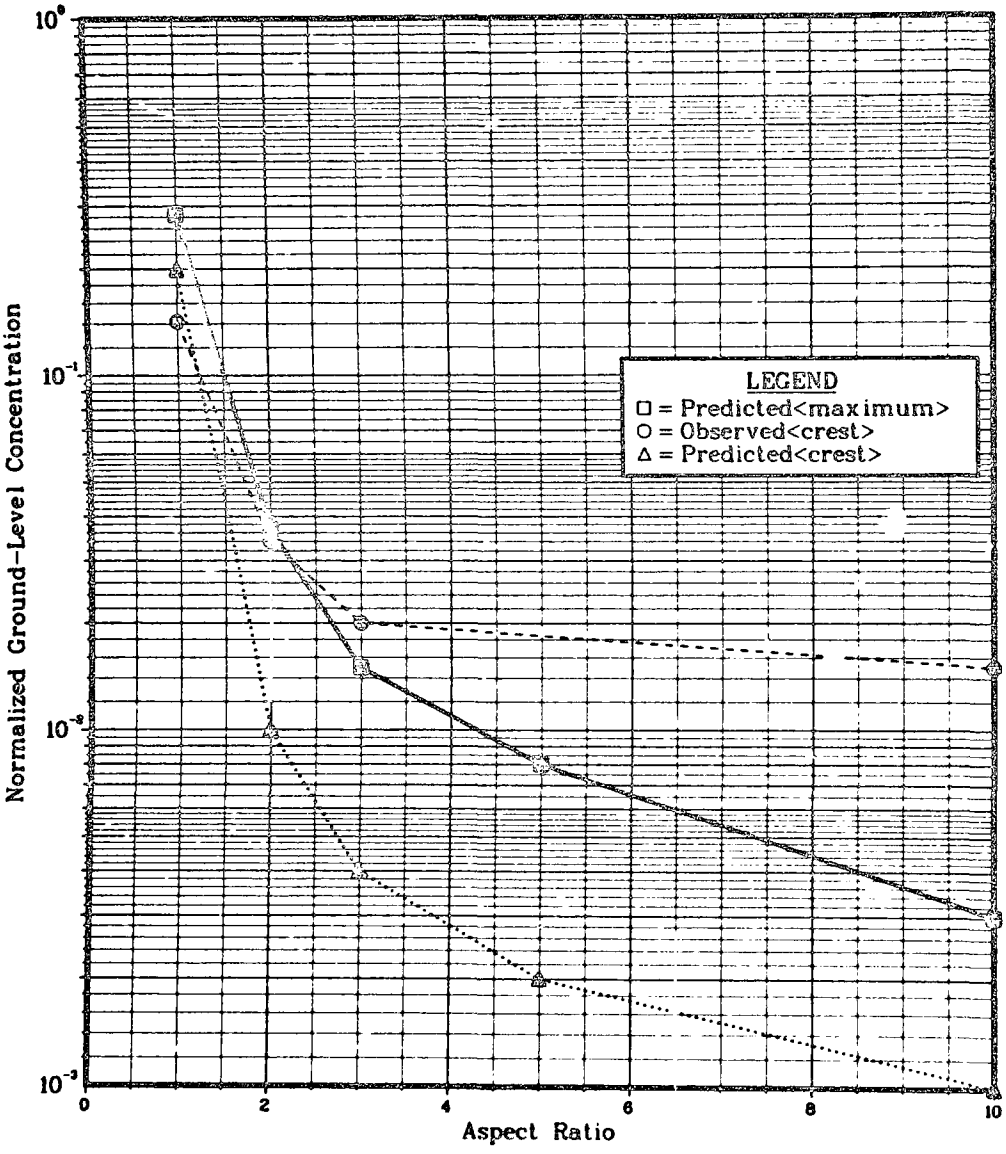

Figure 24. Predicted and observed concentrations for stack height equal to hill height (23.4 cm).

TABLE 12. COMPARISON OF SURFACE CONCENTRATIONS AT HILL CREST BETWEEN THE POTENTIAL FLOW MODEL, THE WIND TUNNEL OBSERVATIONS, THE HALF-HEIGHT ASSUMPTION, THE TERRAIN-FOLLOWING PLUME ASSUMPTION, AND THE LEVEL PLUME ASSUMPTION FOR A STACK HEIGHT EQUAL TO HILL HEIGHT*

Aspect Ratio	Surface Concentration at Hill Crest					Terrain Correction Factors				
	Model	Observed	1/2-Height	No Hill	Level	Model	Observed	1/2-Height	No Hill	Level
1	0.199	0.142	0.108	10^{-6}	3.03	0.460	0.483	0.5	1.0	0.0
2	0.0103	0.034	0.108	10^{-6}	3.03	0.629	0.567	0.5	1.0	0.0
3	0.0035	0.019	0.108	10^{-6}	3.03	0.680	0.598	0.5	1.0	0.0
	0.0005	0.015	0.108	10^{-6}	3.03	0.764	0.610	0.5	1.0	0.0

*The terrain correction factors associated with the potential flow model and the observations are derived from the concentrations that are predicted by the model and observed in the tunnel (see Equation 7-7). Those correction factors for the other approaches are assumed values, and the corresponding surface concentrations are calculated from Equation 7-6.

concentrations to the terrain correction factor. Terrain correction factors derived from the observations vary between 0.48 and 0.61 depending on the crosswind aspect ratio.

11.4.2 Other Plume Characteristics

The algorithm used to predict plume centerline height at the hill crest has been designed to reproduce the observed variations of the centerline height with aspect ratio. However, the limiting cases, in which the aspect ratio equals either 1 or 10, are completely specified by the theoretical solution to potential flow over a sphere and over a cylinder. Therefore, the overall magnitude of the predicted centerline height for these cases must be compared to the observations because only relative variations with aspect ratio has been fixed. Note that plume spread statistics are completely determined by the spreading equations, by the theoretical streamline solutions for sphere and cylinder, and by the weighting for streamline position and velocities as functions of aspect ratio.

Figures 25 and 26 compare predicted with observed values of vertical plume spread, σ_z, and plume centerline height, z_c, over the crest. Two observed z_c measures are plotted, and three observed σ_z measures are shown. Each of these represents a different interpretation of the vertical profiles.

The plume centerline height may be defined either as the height at which the maximum concentration occurs, or as the height associated with the centroid of the observed vertical concentration distribution. These two heights are shown in Figure 27 for the triangular ridge. The results of these two possibilities yield the two illustrated curves marked "centroid" and "maximum" in the comparison figures.

Similarly, σ_z is sensitive to the centerline definition used. The first choice (labeled as "Snyder et al." on Figure 25) is derived by fitting a reflected Gaussian curve to the vertical profile. The other two σ_z curves (labeled by "centroid" and "maximum") are calculated using a 2-point reflected plume equation similar to that used in Section 11-3. The surface concentration is taken to be the average of the surface observations, and the elevated concentration is taken either near the centroid height, or at the height of maximum concentration. In the case of the centroid calculation, the concentration used is the average of the concentration at the centroid height, and the maximum concentration.

The resulting curves show that the predicted behavior of the plume centerline at the hill crest is bounded by the interpretations of the experimental data and, for aspect ratios larger than 2, the predicted vertical spread tends to fall below all of the values derived from the observations. The shape of the predicted z_c curve begins to level off quickly at aspect ratio 3 but, overall, the predictions of plume centerline height above the crest are within 15% of the observed heights. The shape of the predicted σ_z curve only weakly echoes that of the observed curves. For aspect ratios less than 3, the model overpredicts σ_z by as much as 50% in the case of σ_z (maximum), and overpredicts the corresponding centerline height by 50% as well.

However, if the "centroid" version of the observed σ_z is adopted for aspect ratios less than or equal to 2, the predicted vertical plume spread and the centerline height agree with those observed to within 20%.

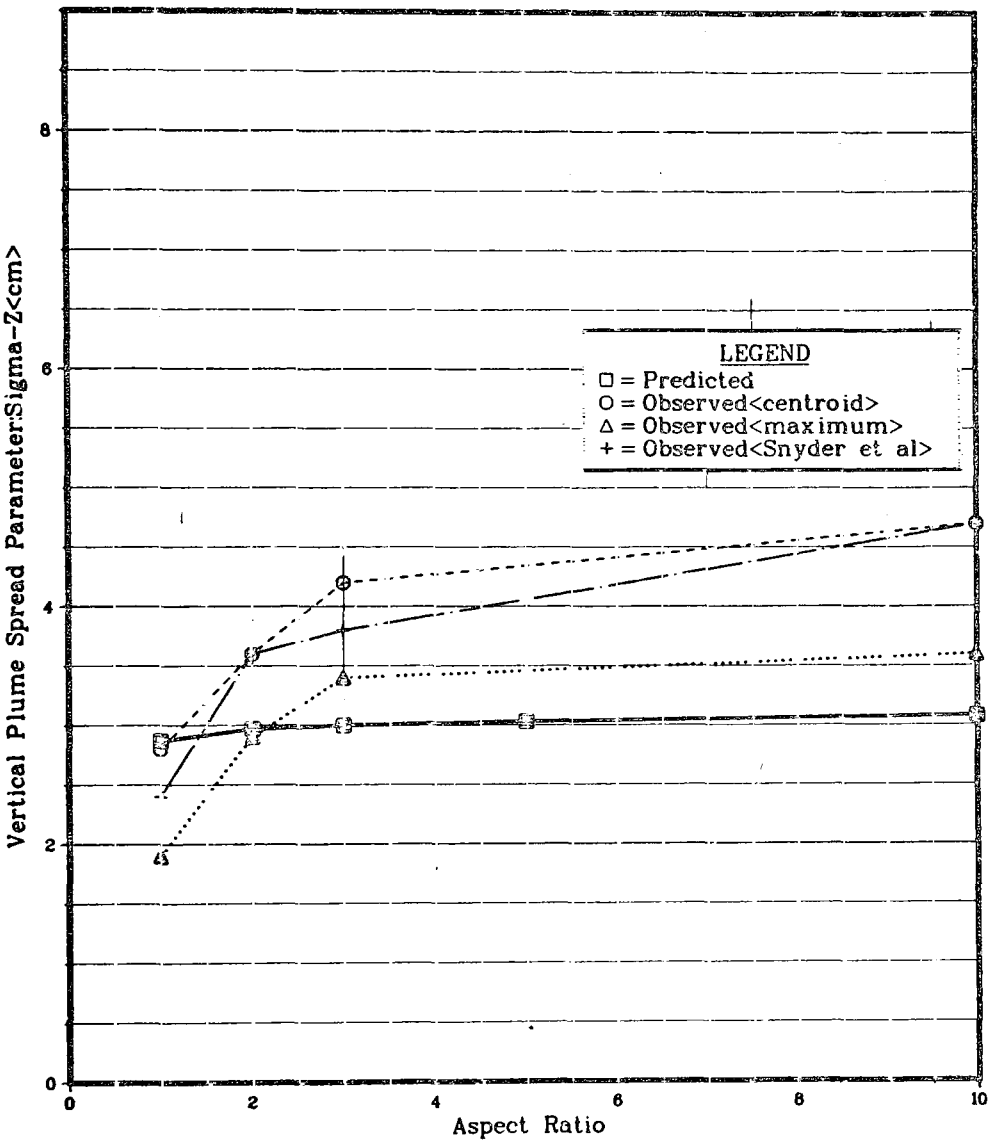

Figure 25. Vertical plume spread at hill crest for stack height equal to hill height (23.4 cm).

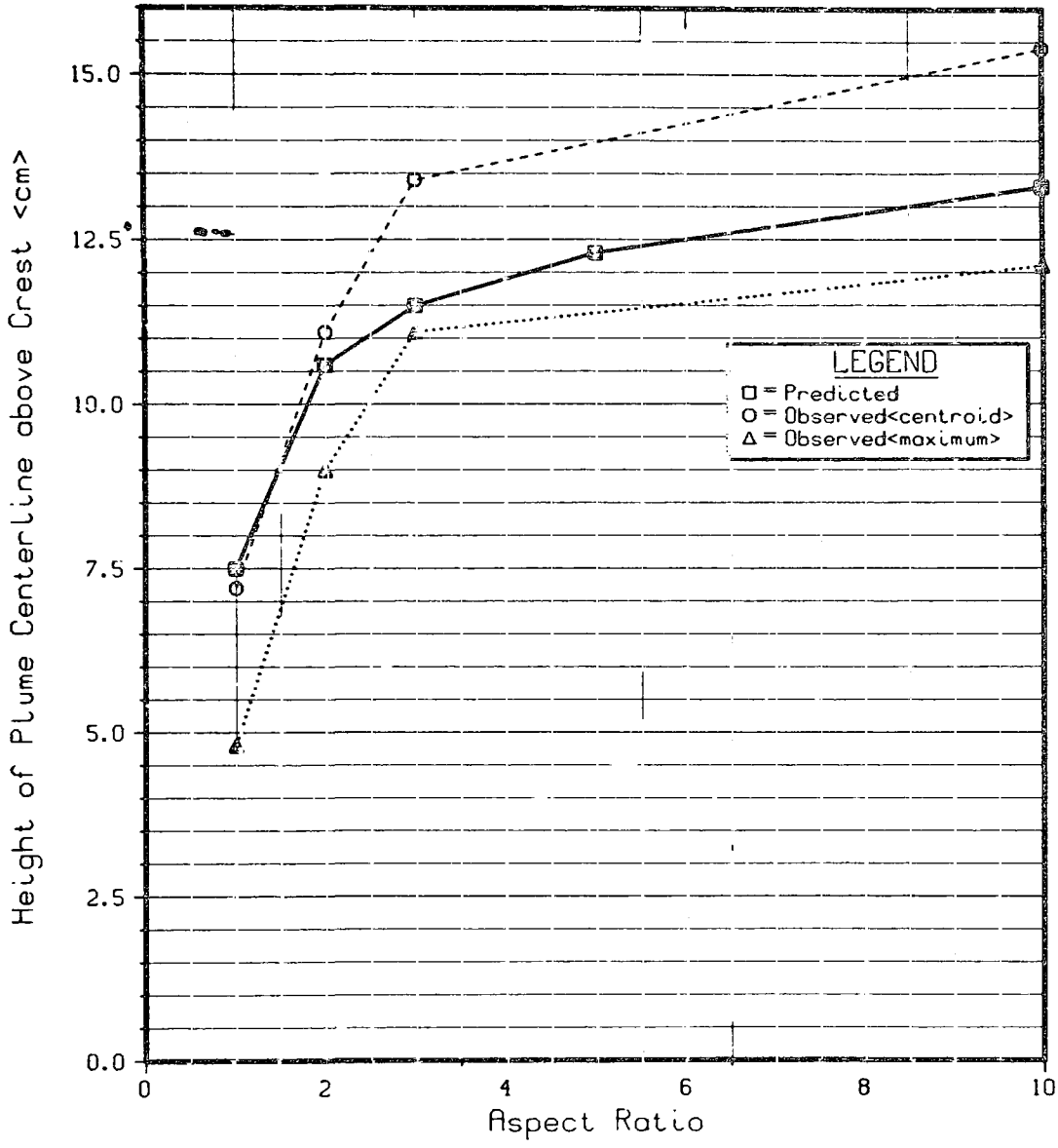

Figure 26. Predicted and observed plume height at hill crest for stack height equal to hill height (23.4 cm).

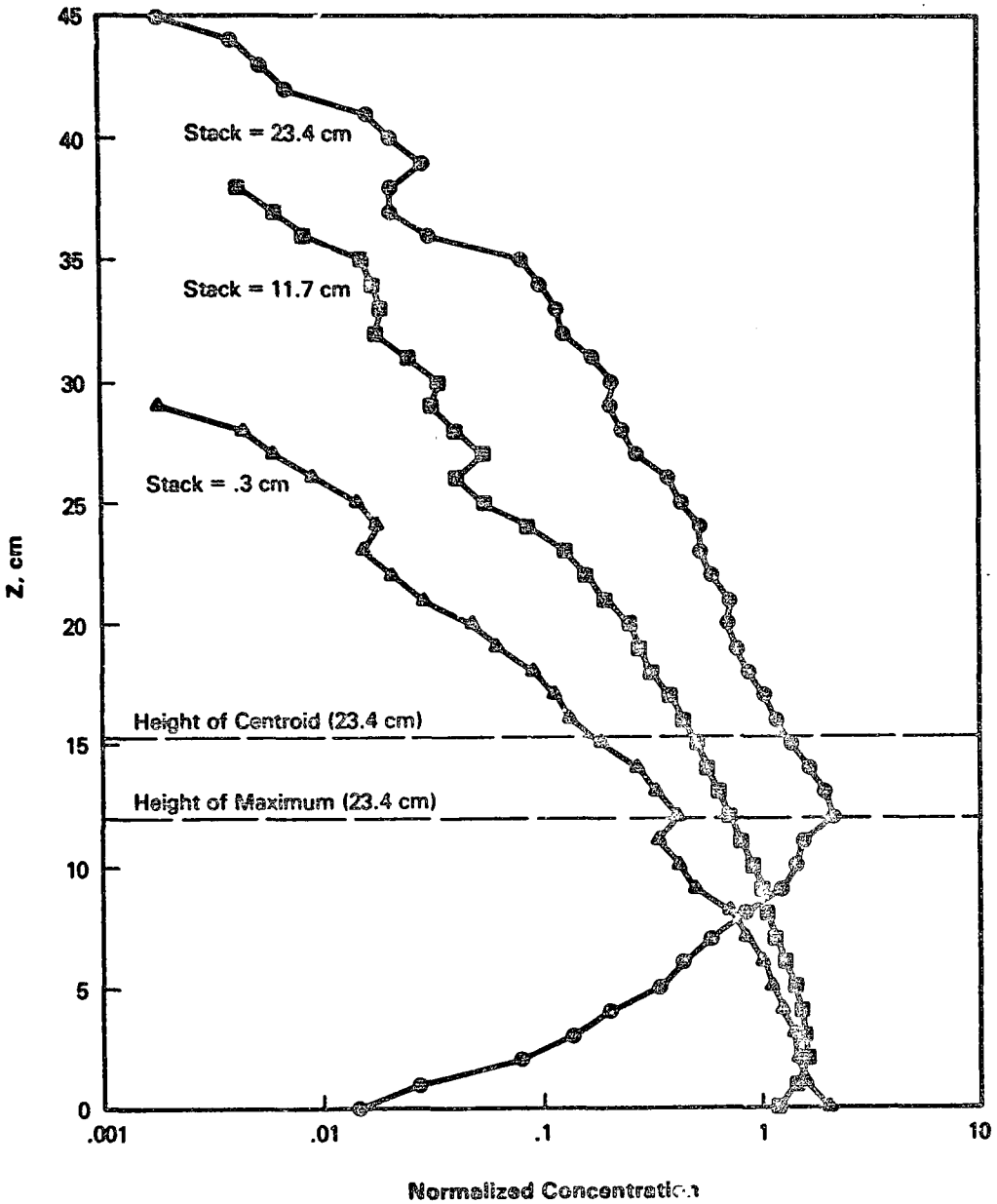

Figure 27. Vertical concentration profiles over CX, the triangular ridge.

For aspect ratios of 3 and larger, the model predictions of σ_z are too small. Values of vertical spread are underpredicted by 27% at aspect ratio 3, and by 57% at aspect ratio 10. Therefore, some of the concentration underpredictions with increasing aspect ratio may be directly related to qualitative and quantitative differences in σ_z. Note, for example, that the observed vertical spread over the ridge (4.7 cm) exceeds that measured at the same downwind distance over flat terrain (4.0 cm) according to the most recent data report (Snyder et al. 1979b). Because potential flow over a two-dimensional ridge acts to compress streamlines in the vertical, this enhanced σ_z must result from increased dispersion in the presence of the terrain feature.

A similar conclusion may be drawn from the horizontal spread, σ_y. Figure 28 shows that the shapes of the predicted and observed curves are dissimilar. The overlap at aspect ratio 1 is virtually exact, but the sharp rise at aspect ratio 2 is missing from the model results. Beyond aspect ratio 3, the trends again agree, but the predicted curve lies about 25% below the observed. Over the two-dimensional ridge the observed value exceeds the flat terrain value by 40%. Note that the observed σ_y values are taken from the lateral profile in a horizontal plane through the concentration maximum over the crest.

11.4.3 Mass Flux

A measure of how well the observed plume conforms to a Gaussian description is the value of its normalized mass flux. The ideal Gaussian plume has unit mass flux defined by the relation:

$$\hat{M} = \frac{2\pi \sigma_y \sigma_z}{Q} U \chi_{CL} \qquad (11\text{-}3)$$

where both the velocity U and concentration X are centerline values.

How well the wind tunnel experiments preserve a mass flux of 1.0 suggests how well the model predictions may agree with the observations. Three curves of the observed normalized mass flux are plotted in Figure 29. The observed "Snyder et al." curve uses the σ_z and centerline concentration values derived by Snyder and Britter (1979b), while the other two curves are based on the σ_z and concentration maximums derived for the centroid height and the height of maximum concentration. Overall, the centroid interpretation of the observed profiles yields the mass flux closest to unity. All three give much the same result for aspect ratio greater than or equal to 3. Figures 25 and 26 indicate that the centroid interpretation of the observations matches the predicted values of plume depth and height better than the other interpretations for small aspect ratio.

11.5 Comparison for Plume Height Equal to Half the Obstacle Height

The complex terrain model is now compared to observations with the half hill height stack. Predicted normalized concentrations incorporate the vertical and horizontal plume spread parameters derived in Section 11.3 and the aspect ratio weighting function derived in Section 10. Computations are

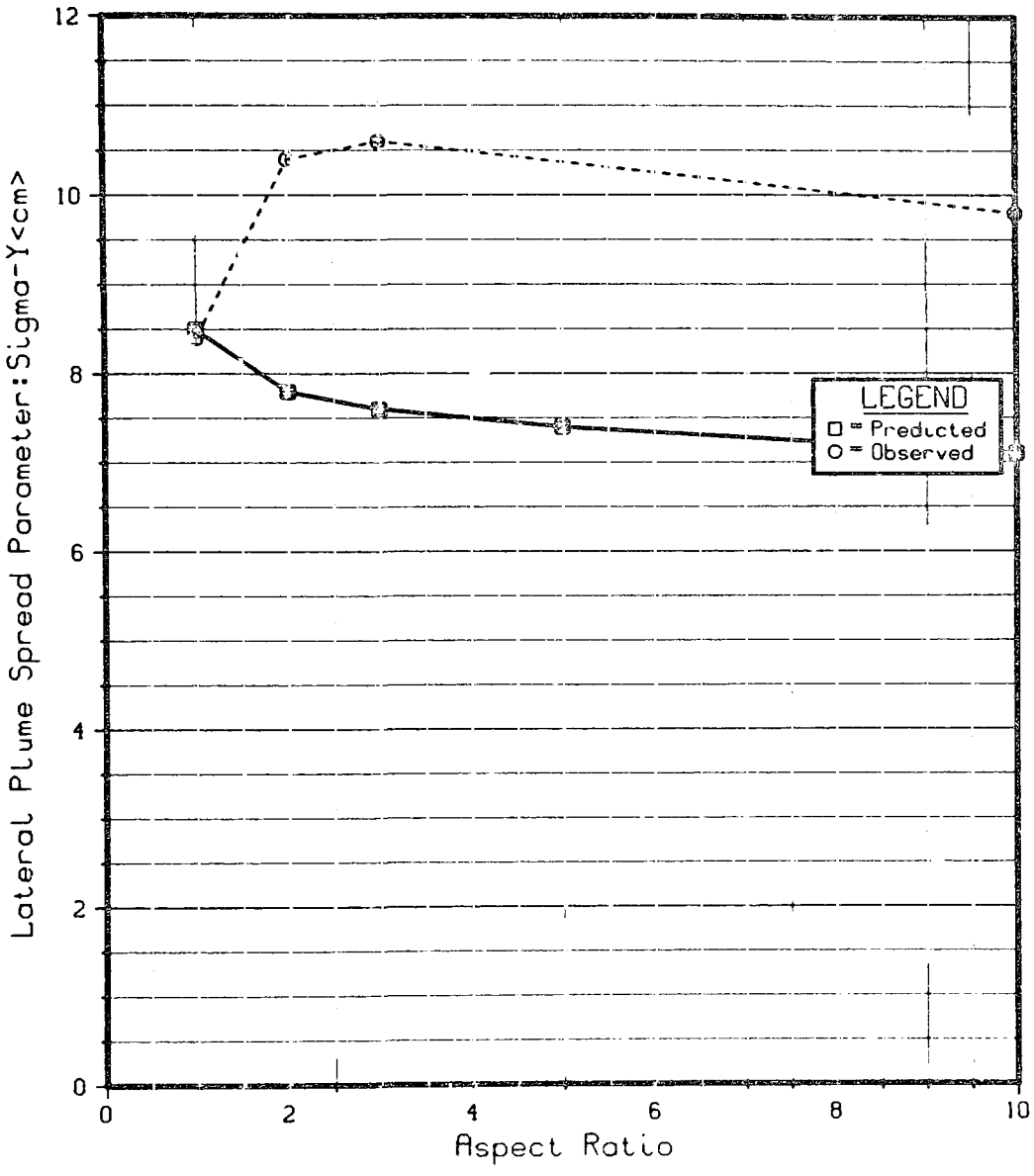

Figure 28. **Lateral plume spread at hill crest for stack height equal to hill height (23.4 cm).**

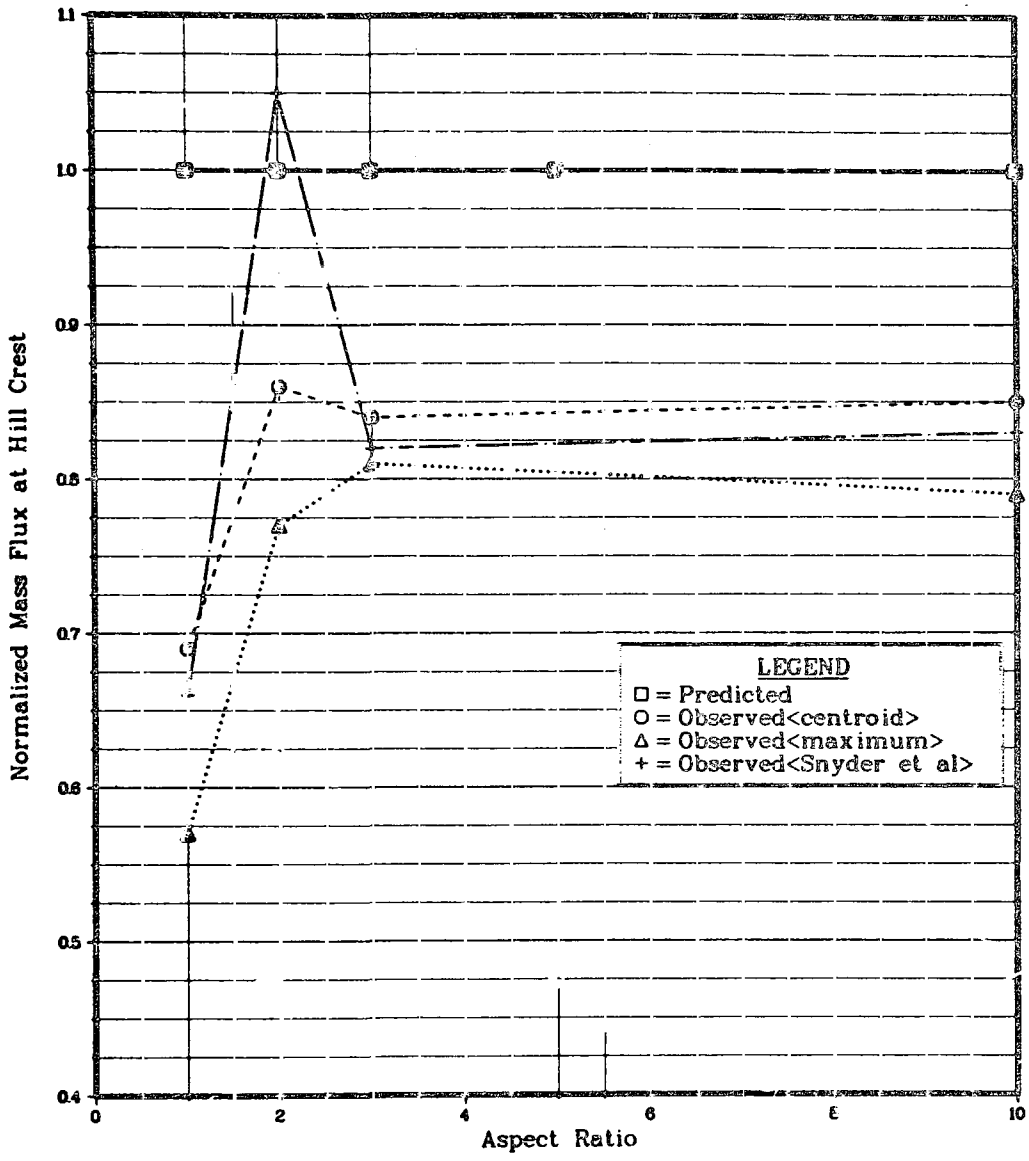

Figure 29. Predicted and observed Gaussian mass flux for stack height equal to hill height (23.4 cm).

made for aspect ratios of 1, 2, 3, 5, and 10. The results, listed in Table 13, represent the maximum predicted concentrations near the crest as well as those predicted right at the hill crest.

TABLE 13. PREDICTED AND OBSERVED NORMALIZED SURFACE CONCENTRATIONS FOR A STACK HEIGHT EQUAL TO HALF HILL HEIGHT

Hill	λ	Predicted Concentration Hill Crest	Hill Maximum	Observed Concentration
C2	1	2.50	2.61	2.09
C4	2	1.30	1.43	1.25
C6	3	0.99	1.18	1.18
-	5	0.76	0.97	—
CX	10	0.57	0.73	0.98

Observed concentrations measured at the hill crests, and corrected for source streamline velocity, are also listed in Table 13. These values represent the average of the observations taken from vertical, lateral, and longitudinal profiles through the hill crest. These surface observations agree very well (within 5%). The observed concentrations are compared directly to the predicted concentrations in Figure 30. The complex terrain model overpredicts the observed concentrations by as much as 25% for aspect ratios between 1 and 2, and underpredicts by as much as 42% at aspect ratio 10.

Unlike the previous experiment in which the stack height was equal to the hill height (Section 11.3), vertical profiles of the plume over the hill crests showed virtually no elevated concentration maximums. Apparently the plume is so greatly influenced by the boundary layer that the plume centerline cannot be readily identified over the crest. This is especially the case for the profile over the cone. At larger aspect ratios, a weak drop in concentration does become discernable in a shallow layer near the surface (Figure 27).

Although the predicted and observed plume spread statistics cannot be compared directly (because the model is not designed to simulate the physics of the experiment) it is instructive to highlight the differences between the observations and the predicted values.

The disparity between model predictions and observed plume characteristics is shown by comparing the plume spread parameters and centerline height evaluated at the crest. These are plotted in Figures 31 through 33. Figure 31 compares the predicted centerline height above the hill crests against the height of the centroid of the observed vertical concentration distribution. This comparison only illustrates that the predicted height lies between an absolute upper bound and the hill surface. Presumably, the true source streamline in the wind tunnel lies somewhere below the predicted values. The greatest qualitative disagreement between predicted and observed quantities is found in the σ_y comparison. The most

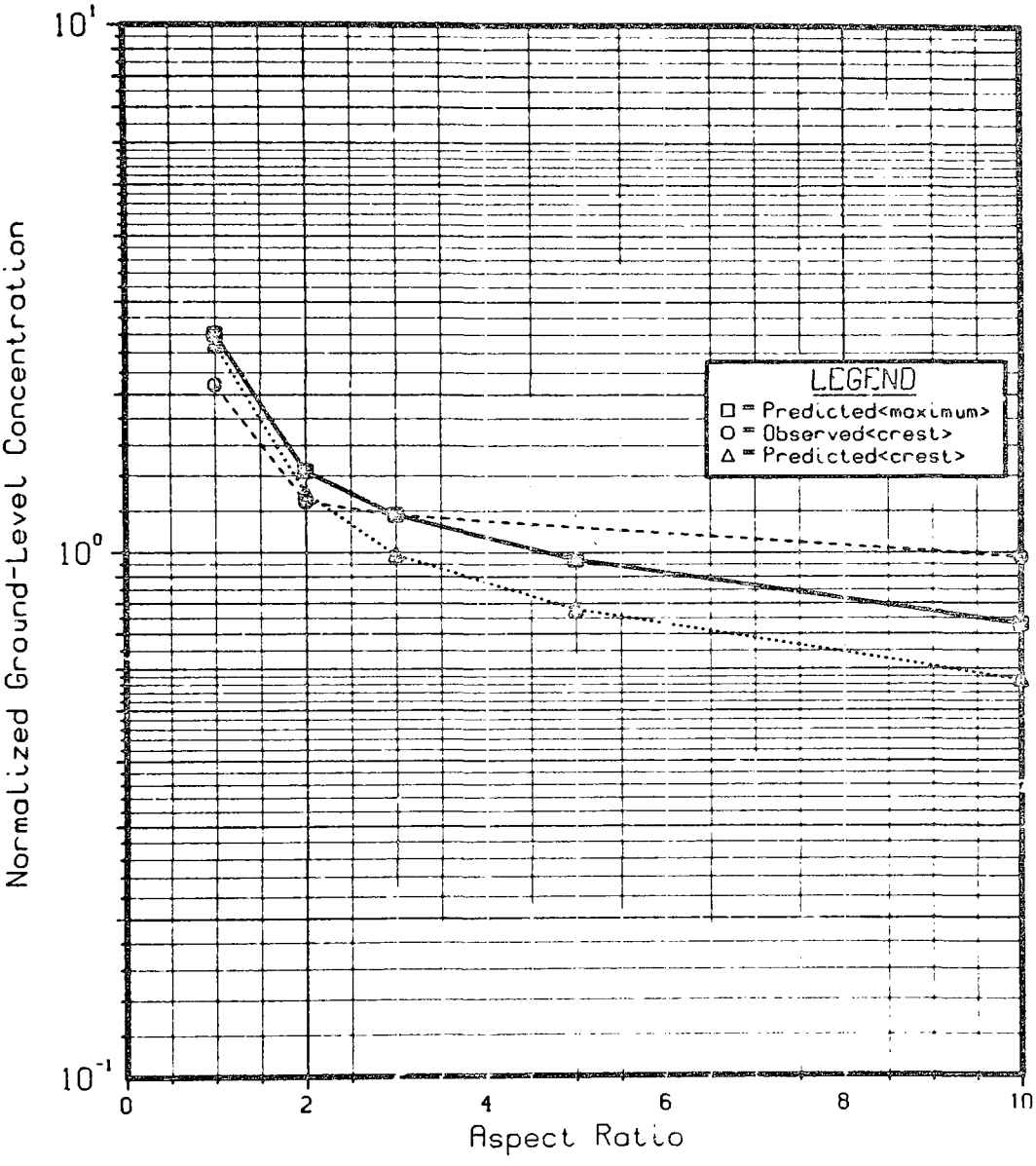

Figure 30. **Predicted and observed concentrations for stack height equal to half the hill height (11.7 cm).**

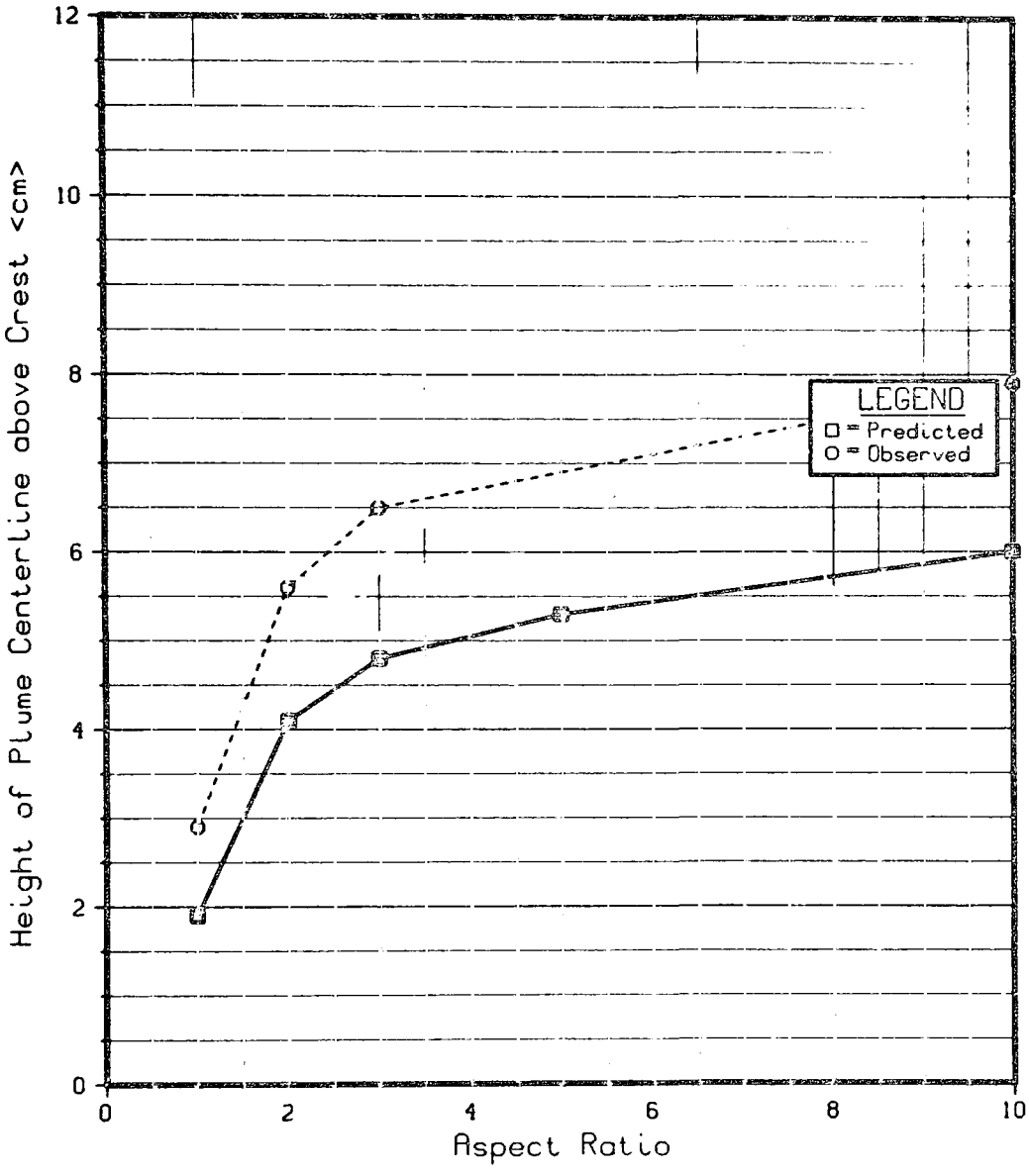

Figure 31. Predicted and observed plume height at hill crest for stack height equal to half the hill height (11.7 cm).

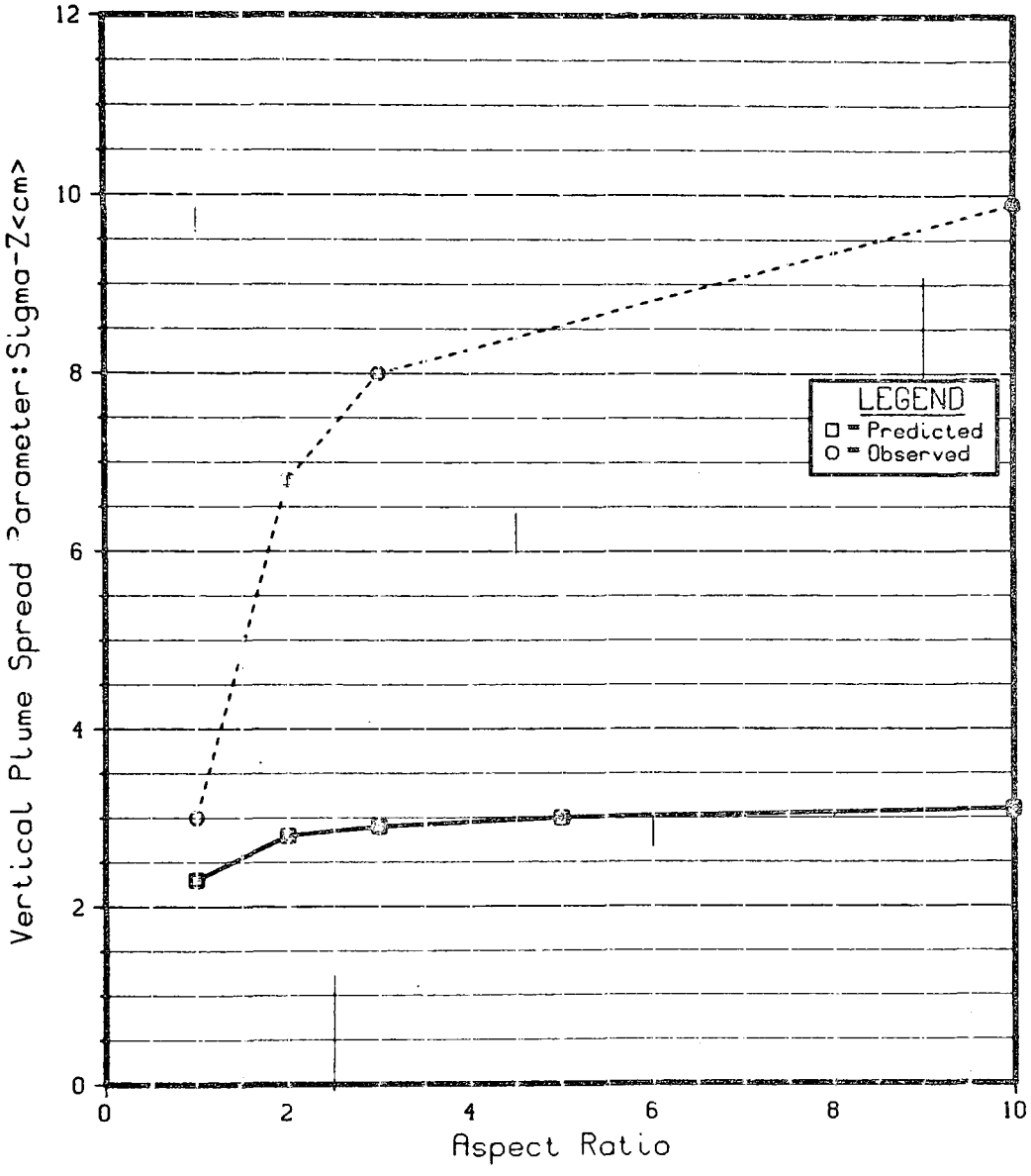

Figure 32. Vertical plume spread at hill crest for stack height equal to half the hill height (11.7 cm).

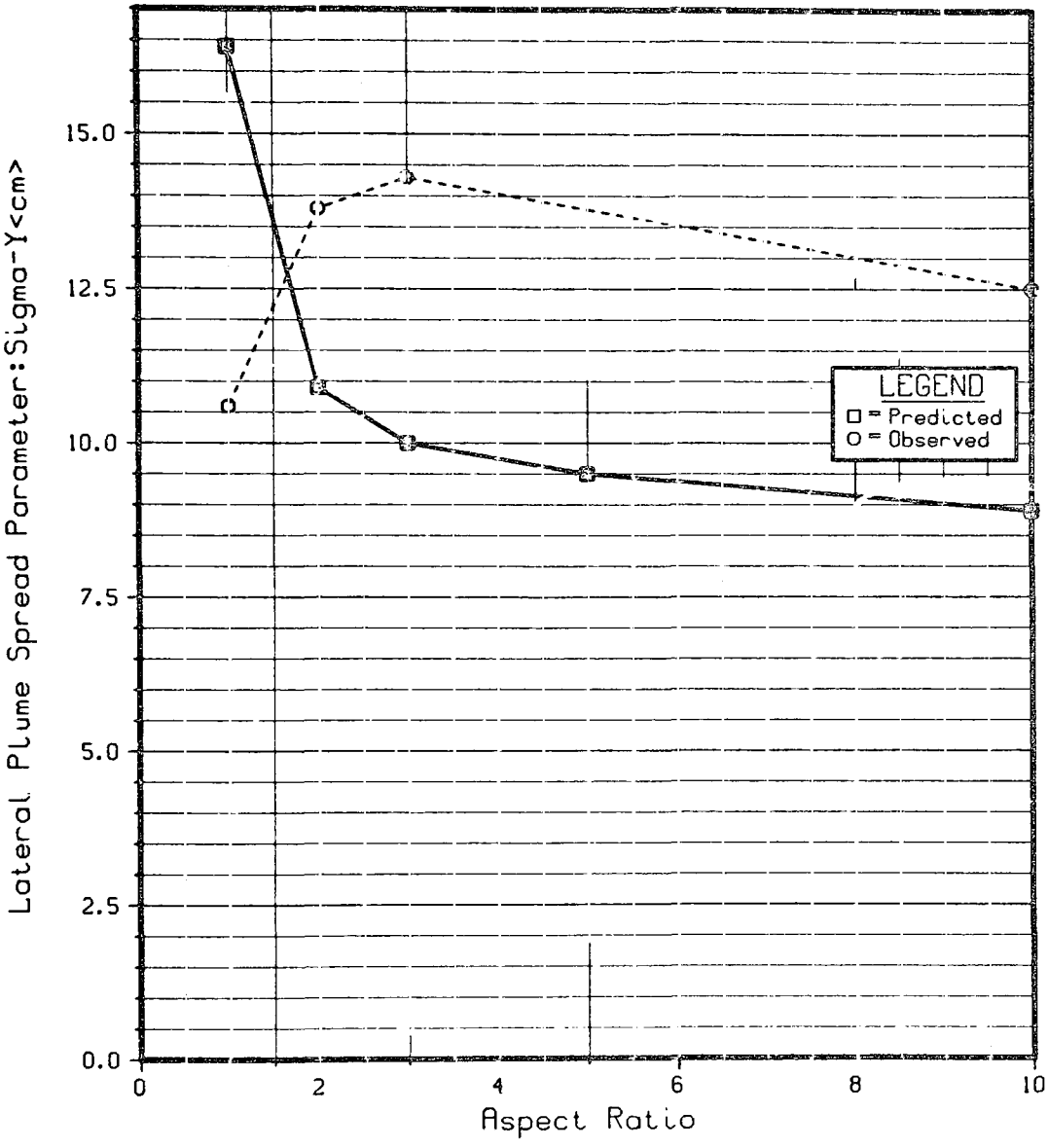

Figure 33. Lateral plume spread at hill crest for stack height equal to half the hill height (11.7 cm).

notable quantitative disagreement is found in the vertical plume spread, σ_z.

This trend is similar to the σ_z results in Section 11.5, although more pronounced. Apparently, increased turbulence levels in the wind tunnel boundary layer strongly affect plume dispersion near the obstacles. This is borne out by the turbulence measurements conducted in the wind tunnel.

In conjunction with their tracer experiments, Snyder and Britter measured velocity fields above the upwind bases of hills C2 through CR (Snyder et al. 1979b) and observed that:

1) Mean velocities systematically decrease at all elevations with increasing aspect ratio. Very close to the surface the mean velocity is independent of the hill's aspect ratio and is about 1/4 of that in the undisturbed boundary layer. The larger the aspect ratio, the greater is the height to which the hill's influence extends.
2) Because of the hills, longitudinal turbulence is decreased and vertical turbulence is (considerably) increased very close to the surface. Surface turbulence increases systematically with increasing aspect ratio. Increased turbulence, especially longitudinal, is observed to 3 to 4 hill heights above the surface, the increase being larger for the larger-aspect-ratio hills.
3) Negative Reynolds stresses, quite large in magnitude, are observed below half the hill height. Although the scatter of the data is quite large, it is apparent that the magnitude of the negative Reynolds stress increases with aspect ratio.

Measurements over the crests of the hills show:

1) In very crude terms, hills with aspect ratio of 2 and above show similar flow behavior, whereas the cone (C2) shows distinctly different behavior. For example, the speed-up factors are 1.15 for the cone and 0.95 to 1.0 for the other hills. Yet the changes are not monotonic with aspect ratio.
2) Changes in turbulence relative to the unobstructed boundary layer increased with elevation and (in this case, systematically) with increasing aspect ratio.
3) Very large negative Reynolds stresses are observed; negative values are observed to one-half hill heights above the crests.

In summary, the observations indicate that vertical turbulence near the surface upwind of the hills increases considerably over the unobstructed flow, increasing systematically with aspect ratio. Large negative Reynolds stresses associated with the increased turbulence are active up to one-half the hill height and, consequently, have a profound effect on the development of vertical plume spread over the hill. Because the turbulence increases with aspect ratio, σ_z rises graphically as shown in Figure 32. This aspect ratio dependence of turbulence intensity is not accounted for in the model.

11.6 Summary and Conclusions

The potential flow complex terrain model has been compared with laboratory observations of flow over four hill shapes with aspect ratio varying from 1 to 10 (effectively to infinity). All hills are the same height with the same downwind cross-section: a triangle with a slope of 0.5. Stack heights used in the comparison correspond to full hill height, and to one-half the full hill height.

At small aspect ratios and for either stack height, the model overpredicts concentrations at the crest: by 40% for the higher stack, and by 20% for the lower stack. The maximum predicted concentration near the crest is 100% larger than the observed value at the crest for the higher stack and 25% larger for the lower stack. At large aspect ratios the model underpredicts in both cases. Comparisons with surface concentrations using the level plume and terrain-following plume assumptions show that the level plume approach overpredicts observed concentrations by two orders of magnitude, and the terrain-following plume approach underpredicts by four orders of magnitude.

For aspect ratios greater than 1, σ_z is consistently underpredicted. In the presence of the hills σ_y and σ_z both show marked enhancement over their flat-terrain values. For example, the ratio of σ_y over the ridge ($\lambda = 10$) to σ_y over flat terrain is 1.45 for the half-hill-height stack, and 1.40 for the full-hill-height stack. The respective σ_z ratios are 2.06 and 1.18. These enhancements are not observed to result from flow deformations. Such changes certainly cannot be reproduced by potential flow deformations alone.

Table 14 compares observed to predicted σ_y and σ_z ratios for all four aspect ratios and for both stack heights. Also included in the table are ratios of observed to predicted speed-up factors. These factors are based on velocities along the source streamline. The ratios obtained appear to be roughly inverse to the horizontal spread ratios. If the model is to compare favorably with these wind tunnel results, the mechanisms controlling the observed plume shape must be better understood.

TABLE 14. COMPARISON OF OBSERVED TO PREDICTED RATIOS OF PLUME SIZE PARAMETERS AND SPEED-UP FACTORS(S) AS A FUNCTION OF ASPECT RATIO

Parameter	Aspect Ratio 1	2	3	10
Stack = 0.5 Hill:				
$\frac{\sigma_y \text{ (obs.)}}{\sigma_y \text{ (pred.)}}$	0.65	1.27	1.43	1.40
$\frac{\sigma_z \text{ (Snyder et al.)}}{\sigma_z \text{ (pred.)}}$	1.3	2.43	2.76	3.19
$\frac{S \text{ (obs.)}}{S \text{ (pred.)}}$	0.89	0.76	0.70	0.69
Stack = Hill:				
$\frac{\sigma_y \text{ (obs.)}}{\sigma_y \text{ (pred.)}}$	0.99	1.33	1.39	1.39
$\frac{\sigma_z \text{ (Snyder et al.)}}{\sigma_z \text{ (pred.)}}$	0.84	1.21	1.27	1.53
$\frac{\sigma'_z \text{ (centroid)}}{\sigma_z \text{ (pred.)}}$	0.98	1.21	1.40	1.53
$\frac{S \text{ (obs.)}}{S \text{ (pred.)}}$	0.94	0.78	0.74	0.73

SECTION 12

MODEL COMPARISON WITH FIELD OBSERVATIONS (WIDOWS CREEK DATA)

12.1 Background

Measured sulfur dioxide (SO_2) concentrations near the Tennessee Valley Authority (TVA) Widows Creek Steam Electric Power Plant in Alabama are compared with concentrations predicted by the potential flow complex terrain model. The routine meteorological data from two towers, the occasional temperature and velocity profiles, and the continuous SO_2 measurements at five monitors on a nearby ridge and one monitor on a nearby mound make the Widows Creek data base a promising testing ground for the complex terrain model. Comparison of the model predictions with the observations at Widows Creek tests the model's ability to predict concentrations on real terrain features under complex, uncontrolled atmospheric flow conditions.

12.2 The Widows Creek Steam Electric Power Plant

The 2,600 megawatt (Mw) coal-fired power plant operated by the TVA at Widows Creek, Alabama, is currently composed of eight individual boilers and three main stacks. Boilers 1 though 6 feed a single 304.8-meter (m) stack; boilers 7 and 8 each feed a 152.4-m stack. The 304.8-m stack has been in use for all six boilers since early 1978. Prior to this time, boilers 1 through 6 fed separate 82-m stacks that were subject to frequent downwash events. To avoid the complicating effects of downwash and multiple plume interactions, only data commencing in January 1978 is used.

Figure 34 displays the topography of the area. The terrain feature of greatest interest is the bluff located to the southeast of the plant. Its face rises 840 feet (255 m) in a distance of 0.9 kilometers (km), yielding a nearly uniform slope of about 1:4 ($\sim 16^{o}$). At the top of the rise, roughly 2.6 km from the plant, the terrain levels at the plateau called Sand Mountain, 275 m above the power plant elevation. Atop this plateau, five SO_2 monitors are positioned in an arc with a mean distance of 3.5 km from the plant. The two monitors closest to the crest are 3.2 km from the plant, and that at the center of the arc is 4 km away. Two meteorological towers are identified in Figure 34. One is near power plant elevation on the valley floor, and the other is near the central monitor of the plateau sampling arc.

Other terrain features are located to the northwest of the power plant. Two of these--Summerhouse Mountain and Cumberland Plateau--have single SO_2 monitors at their crests. Only Summerhouse Mountain (275 m) is isolated enough to be considered a second suitable terrain feature for comparing predicted and observed concentrations.

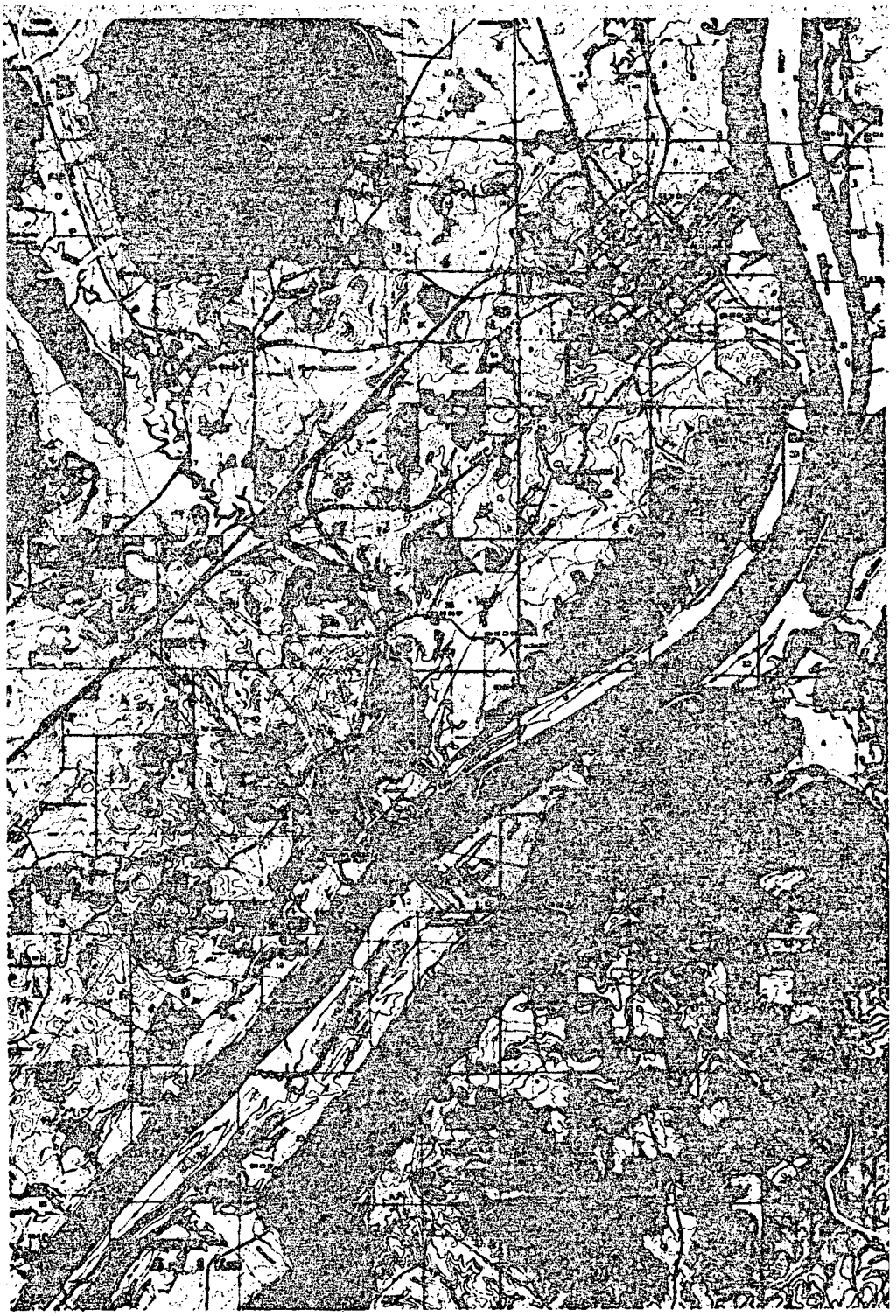

Figure 34. The Widows Creek steam electric power plant and surrounding features.

The Sand Mountain ridge is shown in cross-section in Figure 35. Application of the complex terrain model to this feature requires selecting an appropriate circular cylinder and placing it at an appropriate distance from the source. The selection made in this report is compared to the actual terrain in Figure 35. The height, or radius, of the circular cylinder is taken to be 275 m, and its center is placed 3.2 km from the source. This source-to-crest distance places the model crest receptor at the approximate average downwind distance of the monitors in the observing arc, although the actual ridge crest lies as close to the source as 2.6 km. In effect, the ridge is modeled as if it curved through the sampling arc. If the actual geometry had been preserved, the model crest would coincide with the true crest, and the monitors would lie on the downwind side of the circular cylinder.

Application of the model to Summerhouse Mountain follows in similar fashion. For this comparison, the hill crest is set a distance of 8.7 km from the Widows Creek facility. The height is the same as that used at Sand Mountain, 275 m. However, the crosswind shape lies between that of a simple sphere and cylinder. The approximate crosswind distance through the monitor from one 0.5 hill-height point to the other is 2.2 km. The aspect ratio defined in the complex terrain model is one-half this length divided by the height of the hill. Therefore the crosswind aspect ratio for the model hill is set at 4.

12.3 Case Selection for Model Comparisons

9-1/8"

12.3.1 Analysis of the Tennessee Valley Authority Sulfur Dioxide Monitor Data

Digitized SO_2 concentrations and meteorological data (temperature and winds at 10 m and 61 m) collected at the TVA Widows Creek Steam Electric Power Plant were supplied by the TVA Air Quality Branch, Muscle Shoals, Alabama. The computer tape contained, in part, hourly SO_2 concentrations from the five monitors on Sand Mountain and the single monitor on Summerhouse Mountain for the period January 1, 1978, to September 30, 1978. This is the period of most interest as the last of boilers 1-6 was tied into the new 304.8-m stack in late December, 1977.

The first step in selecting the hours best suited for model comparisons was to search for those hours with at least one monitor reporting an SO_2 concentration greater than or equal to 0.10 parts per million (ppm) or 570 $\mu g/m^3$. A total of 73 hours was identified for ridge impacts (Sand Mountain), and 48 hours for mound impacts (Summerhouse Mountain).

Next, hours with unstable stability classifications were ruled out. The stability was assessed primarily from the temperature gradients between 10 m and 61 m at the tower atop the ridge. Because the layer between 61 and 10 m may not be entirely representative of conditions at stack heights of 150 and 300 m, the cut-off value for temperature differences was set at 1.5 times the dry adiabatic lapse rate, or -0.75°C/51 m (-1.35°F/51 m). This criterion reduced the number of comparison cases to 27 hours of ridge impact, and 15 hours of mound impact. For almost all of these hours, the source-receptor trajectory corresponded readily with the wind direction recorded by the 61-m sensor on the ridge. Table 15 and 16 list the selected hours and corresponding SO_2 concentrations for Sand Mountain and Summerhouse Mountain.

TABLE 15. HOURS SELECTED FOR MODEL COMPARISONS AT SAND MOUNTAIN (RIDGE)

			SO_2 Concentrations (10^{-3} ppm) at Ridge Monitors				
Year	Day	Hour	M 11	M 6	M 3	M 9	M 10
78	3	1300	50	140	150	90	50
78	3	1400	0	0	330	310	210
78	3	1500	0	120	140	200	170
78	11	1300	130	310	0	0	99999
78	11	1400	270	400	20	0	0
78	11	1500	150	310	300	0	0
78	22	1400	150	90	60	110	100
78	22	1500	220	270	200	270	240
78	22	1600	170	220	240	260	280
78	22	1700	110	200	210	220	190
78	22	1800	80	120	150	170	130
78	22	1900	140	120	100	100	0
78	40	1300	0	0	160	210	160
78	126	1600	110	170	100	90	30
78	190	900	0	220	180	90	20
78	214	1800	20	160	130	20	0
78	226	1000	0	200	850	600	200
78	226	1100	150	220	180	150	0
78	226	1200	200	160	120	120	80
78	230	1000	0	230	140	10	0
78	230	1300	0	0	30	160	220
78	232	200	200	100	70	110	20
78	232	1400	60	170	80	120	10
78	232	1500	10	150	150	170	0
78	238	1300	50	190	80	140	120
78	263	1400	0	240	150	420	370
78	263	1500	40	200	150	290	270

TABLE 16. HOURS SELECTED FOR MODEL COMPARISONS AT SUGARHOUSE MOUNTAIN (ISOLATED HILL)

			SO_2 Concentration (10^{-3} ppm) at Monitor 15
Year	Day	Hour	M 15
78	4	2000	100
78	4	2100	450
78	24	1000	130
78	143	600	140
78	143	700	120
78	166	2300	120
78	166	2400	140
78	167	100	140
78	220	600	190
78	222	2400	150
78	223	100	130
78	258	900	170
78	260	2300	240
78	260	2400	260
78	262	200	100

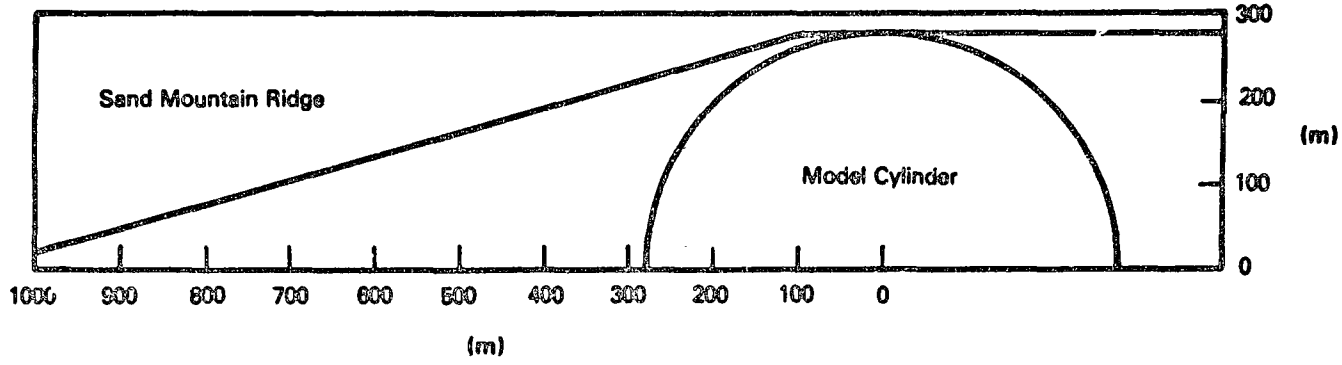

Figure 35. Comparison of the idealized cross-section of Sand Mountain to the southeast of Widows Creek power plant with the circular cylinder assumed in the complex terrain model.

For each of these hours the TVA Air Quality Branch furnished all available temperature, and velocity profiles, and hourly emissions data.

12.3.2 Analysis of Selected Emissions and Atmospheric Data

Upon receipt of the available temperature and wind profiles for the days identified, the hours of significant impact were compared against the times of profile observations. Case hours were considered for further analysis if they could be matched to temperature profiles taken within one hour. Table 17 lists all hours that satisfied this criterion.

The vertical temperature and velocity profiles are essential to compute final plume rise and the Froude number, so that the model may use the best available information in determining the plume centerline height over the hill crest. The cases likely to produce the largest predicted concentrations have the plume centerline closest to the hill height. Therefore the cases selected in Table 17 are analyzed first for final plume rise height.

Final plume rise is calculated using the revised Briggs plume rise equations (Briggs 1975). Nearly all cases are associated with stable stratification in the layer through which the plume travels. Final rise under these conditions follows the relations:

$$\Delta h = 2.6\,(F/us)^{1/3}$$

$$F = g\,R_s^2\,V_s\,\frac{T_s - T_a}{T_s} \qquad (12\text{-}1)$$

$$s = \frac{g}{T_a}\,\frac{\partial\theta}{\partial z}$$

where

T_a = ambient average temperature (^oK),

T_s = stack exhaust temperature (^oK),

V_s = stack exhaust velocity (m/s),

R_s = stack top radius (m),

g = acceleration due to gravity = 9.8 m/s,

$\frac{\partial\theta}{\partial z}$ = vertical potential temperature gradient (^oK/m), and

u = average wind speed in the layer (m/s).

Temperature and velocity profiles, supplemented where necessary by the tower data, provide values for T_a, $\partial\theta/\partial z$, and u. Most other quantities are

TABLE 17. CASES OF SIGNIFICANT IMPACT THAT HAVE ASSOCIATED VERTICAL PROFILES OF TEMPERATURE

Ridge Impact Hours

				Profile Observation Time	
Julian Day	Month	Day	Hour	Temperature	Velocity
3	1	3	1300	1227	1332
40	2	9	1300	1228	1312
190	7	9	0900	0841	0700
226	8	14	1200	1247	1140
230	8	18	1000	0920	0925
230	8	18	1300	1223	1305
232	8	20	14-1500	1225+1638	1430

Mound Impact Hours

				Profile Observation Time	
Julian Day	Month	Day	Hour	Temperature	Velocity
4	1	4	20-2100	2030	2355
166	6	15	2400	0005	2340
222	8	10	2400	0004	2322

determined for each stack and, with the exception of the stack radius, depend on the individual boiler loads for each hour. Boiler loads for each unit and hour under study are listed in Table 18.

TABLE 18. HOURLY GROSS LOAD MW

Julian Date	Month	Day	Hour	Unit 1	2	3	4	5	6	7	8
3	01	03	1300	100	73	114	103	104	106	Off	311
40	02	09	1300	46	60	47	55	51	53	Off	344
190	07	09	0900	123	123	130	125	129	128	Off	456
226	08	14	1200	111	Off	129	131	128	123	524	Off
230	08	18	1000	112	59	Off	130	122	128	271	281
230	08	18	1300	112	61	Off	133	132	130	290	281
232	08	20	1400	Off	59	129	133	132	127	480	Off
232	08	20	1500	Off	60	130	130	130	127	480	Off
4	01	04	2000	94	90	110	90	98	101	398	Off
4	01	04	2100	96	88	110	90	108	104	413	Off
166	06	15	2400	101	57	90	89	59	69	Off	241
222	08	10	2400	82	Off	88	64	84	51	244	297

Preliminary calculations for the tall stack indicate that the impact of emissions from this stack during the hours under study are very small on the ridge. Consequently, only plume rise from units 7 and 8 is discussed in detail. Equations for exit temperature and velocity for boiler units 7 and 8 were provided by the TVA Air Quality Branch. Those for unit 7 are:

No Scrubber	Scrubber
$T = 399\ (^{\circ}K)$	$T = 365\ (^{\circ}K)$
$V = 0.047G + 1.04\ (m/s)$	$V = 0.042G\ (m/s)$

and those for unit 8 are:

No Scrubber	Scrubber
$T = 389\ (^{\circ}K)$	$T = 367\ (^{\circ}K)$
$V = 0.034G + 0.494\ (m/s)$	$V = 0.030G + 0.624\ (m/s)$

In Table 18 the quantity "G" is the gross load of the boiler in Mw. Results of the plume rise calculations are given in Table 19 as final plume height. The final plume height is the sum of the stack height and the final plume rise, Δh.

TABLE 19. FINAL PLUME HEIGHTS OF EMISSIONS FROM BOILERS 7 AND 8 BOTH WITH AND WITHOUT FULL SO_2 SCRUBBING

				Plume Height (m)		Scrubbed Plume Height (m)	
Julian Day	Month	Day	Hour	Unit 7	Unit 8	Unit 7	Unit 8
3	1	3	1300	-	445	-	422
40	2	9	1300	-	432	-	409
190	7	9	0900	-	325	-	307
226	8	14	1200	1,085	-	855	-
~~230~~	~~8~~	~~18~~	~~1000~~	~~350~~	~~345~~	~~319~~	~~326~~
230	8	18	1300	833	802	736	733
232	8	20	14-1500	600	-	533	-
4	1	4	20-2100	309	-	289	-
166	6	15	2400	-	335	-	317
222	8	10	2400	368	374	335	352

Of the seven hours identified for impact on the ridge (Sand Mountain) only four were selected for comparison with the model: day 3 hour 1300, day 40 hour 1300, day 190 hour 0900, and day 230 hour 1000. Plume heights during these hours varied from 325 meters to 445 m. For the other three hours, plume heights varied between 600 m and 1,085 m, which exceed twice the height of the ridge.

The three hours identified for impact on the isolated mound (Summerhouse Mountain) saw similar final plume heights (309 to 375 m).

Temperature profiles for each of the seven case hours remaining (after screening for plume rise) are presented in Figures 36 through 42. The dashed lines identify the mean temperature gradient used in the plume rise calculation, and the horizontal line is the resultant final plume height from the 152.4-m stacks. In all cases plume rise is seen to take place entirely within the layers described by the indicated mean temperature gradients.

The SO_2 emission rates from each boiler unit were calculated from hourly boiler loads, weekly sulfur content and heat value of the coal for each unit, and monthly averages of the gross energy output of the facility per heat input as fuel. The sulfur content had been adjusted by TVA to reflect 90% conversion of the sulfur content to SO_2. To compute

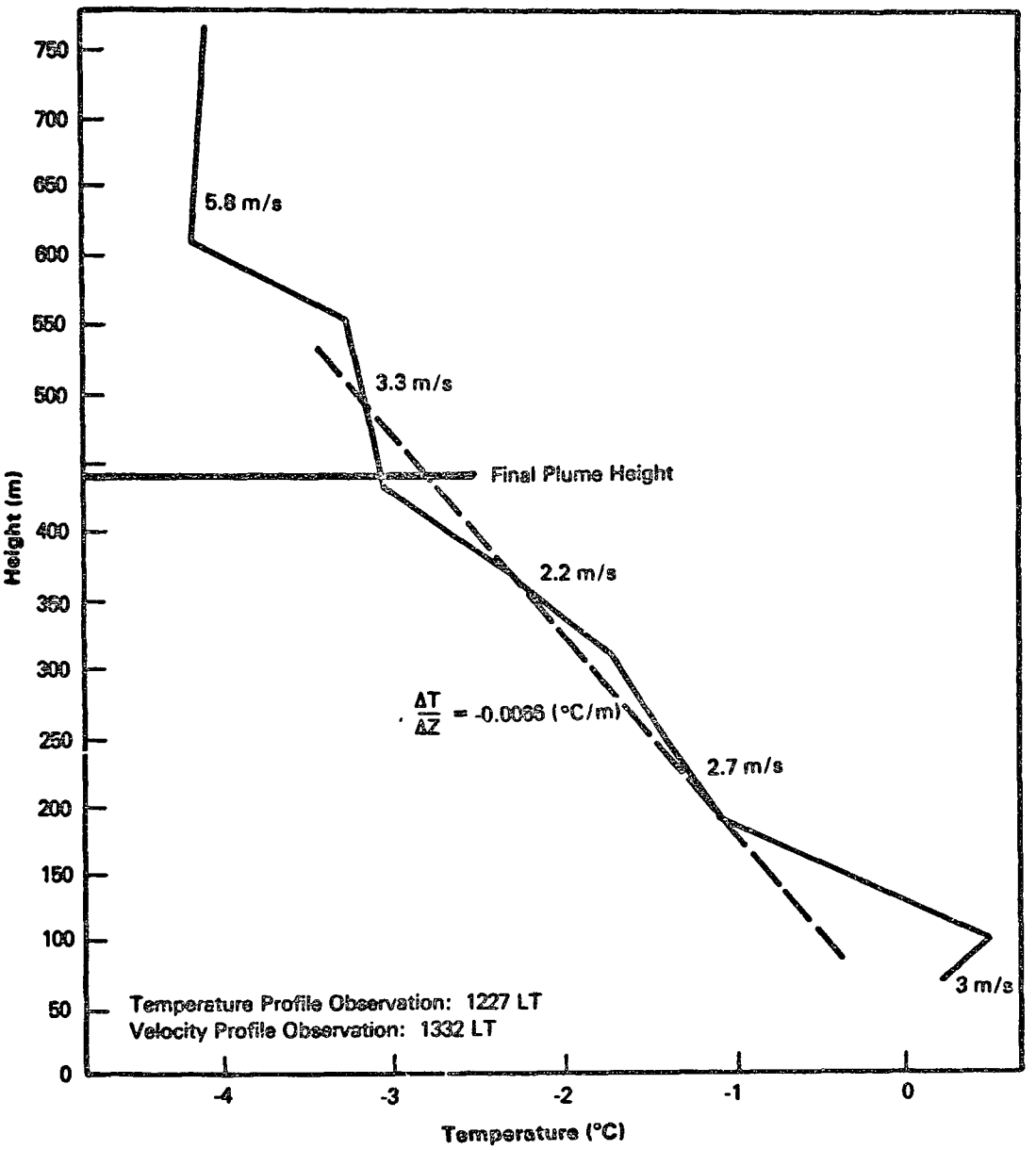

Figure 36. Temperature profile used to calculate plume rise and Froude number on day 3, hour 1300, 1978.

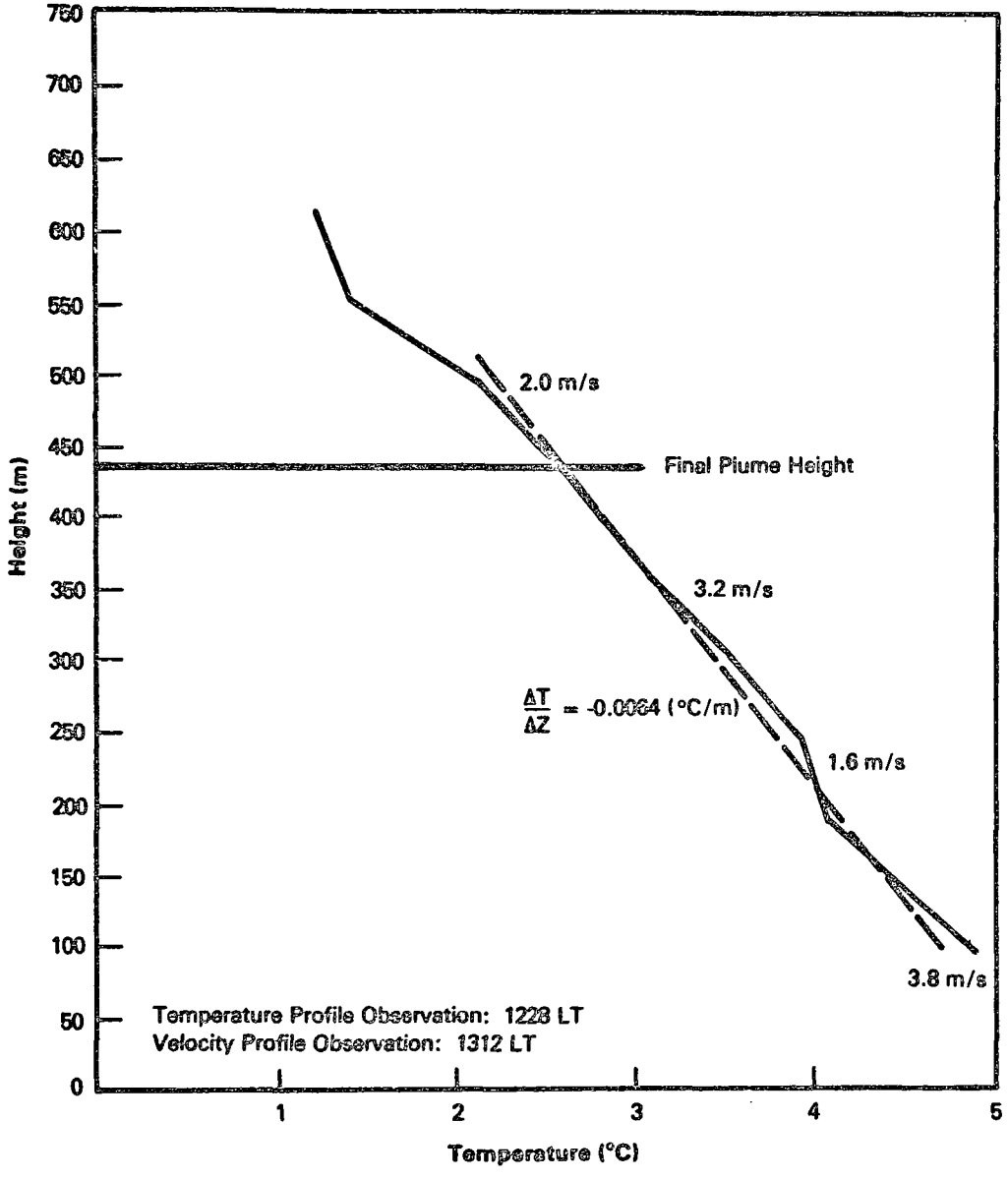

Figure 37. Temperature profile used to calculate plume rise and Froude number on day 40, hour 1300, 1978.

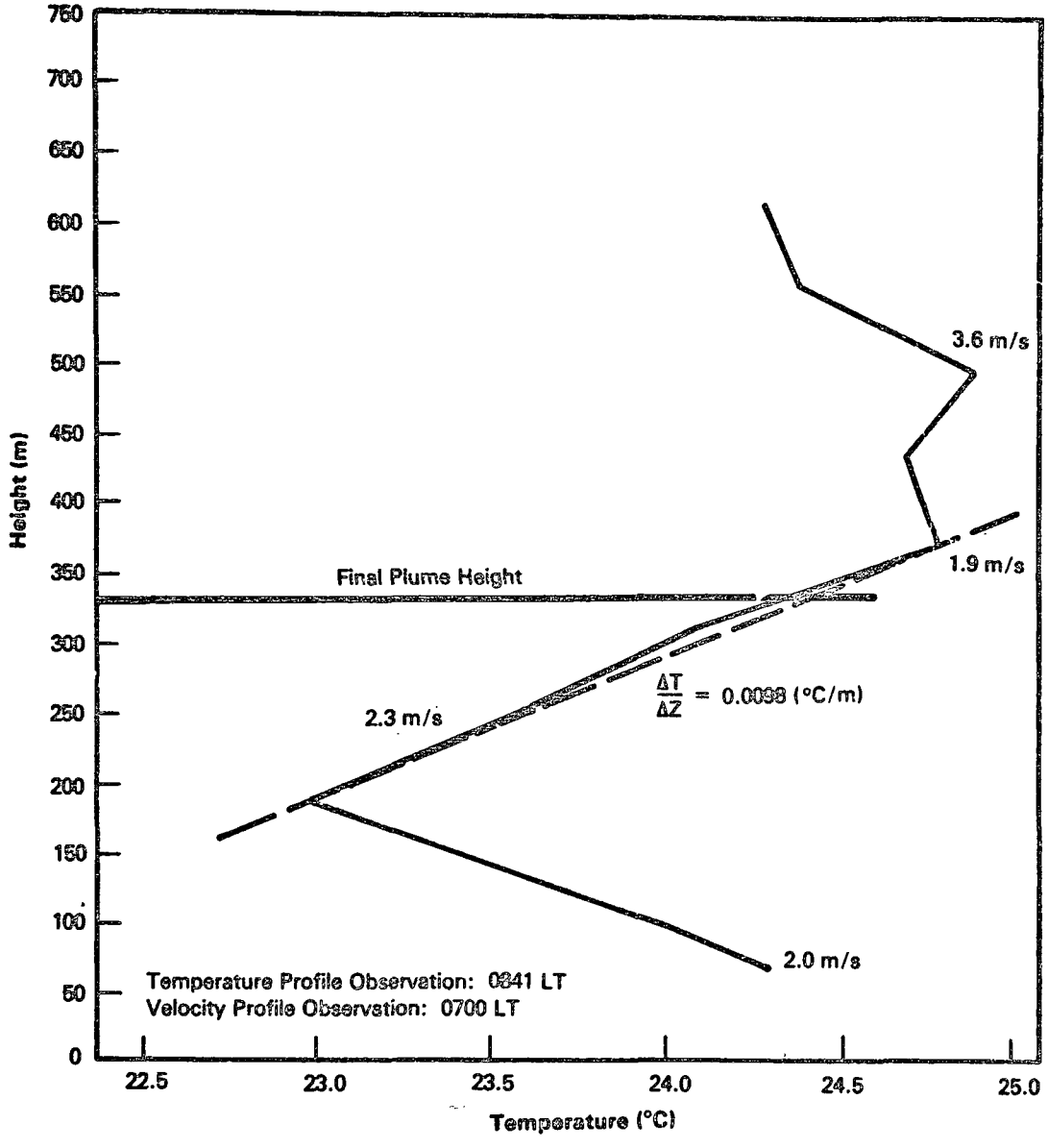

Figure 38. Temperature profile used to calculate plume rise and Froude number on day 190, hour 0900, 1978.

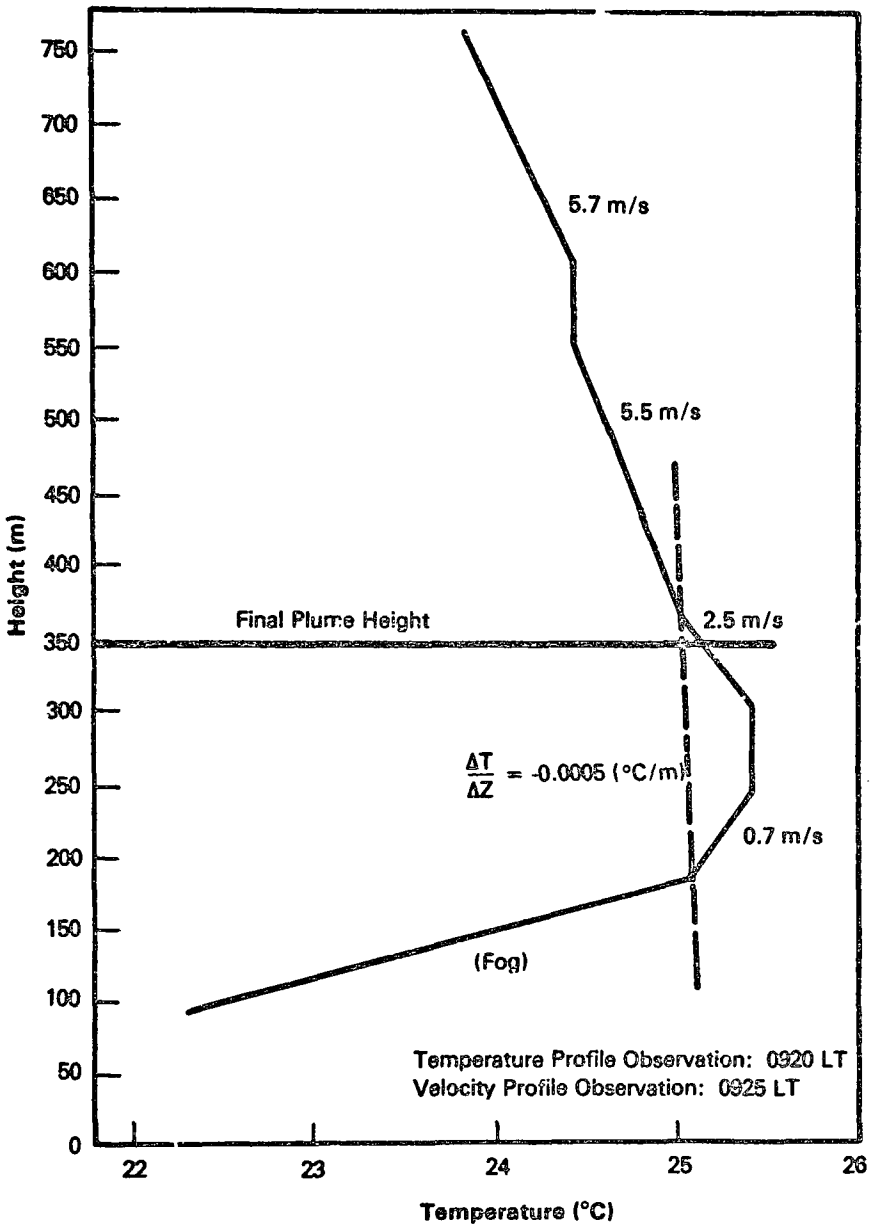

Figure 39. Temperature profile used to calculate plume rise and Froude number on day 230, hour 1000, 1978.

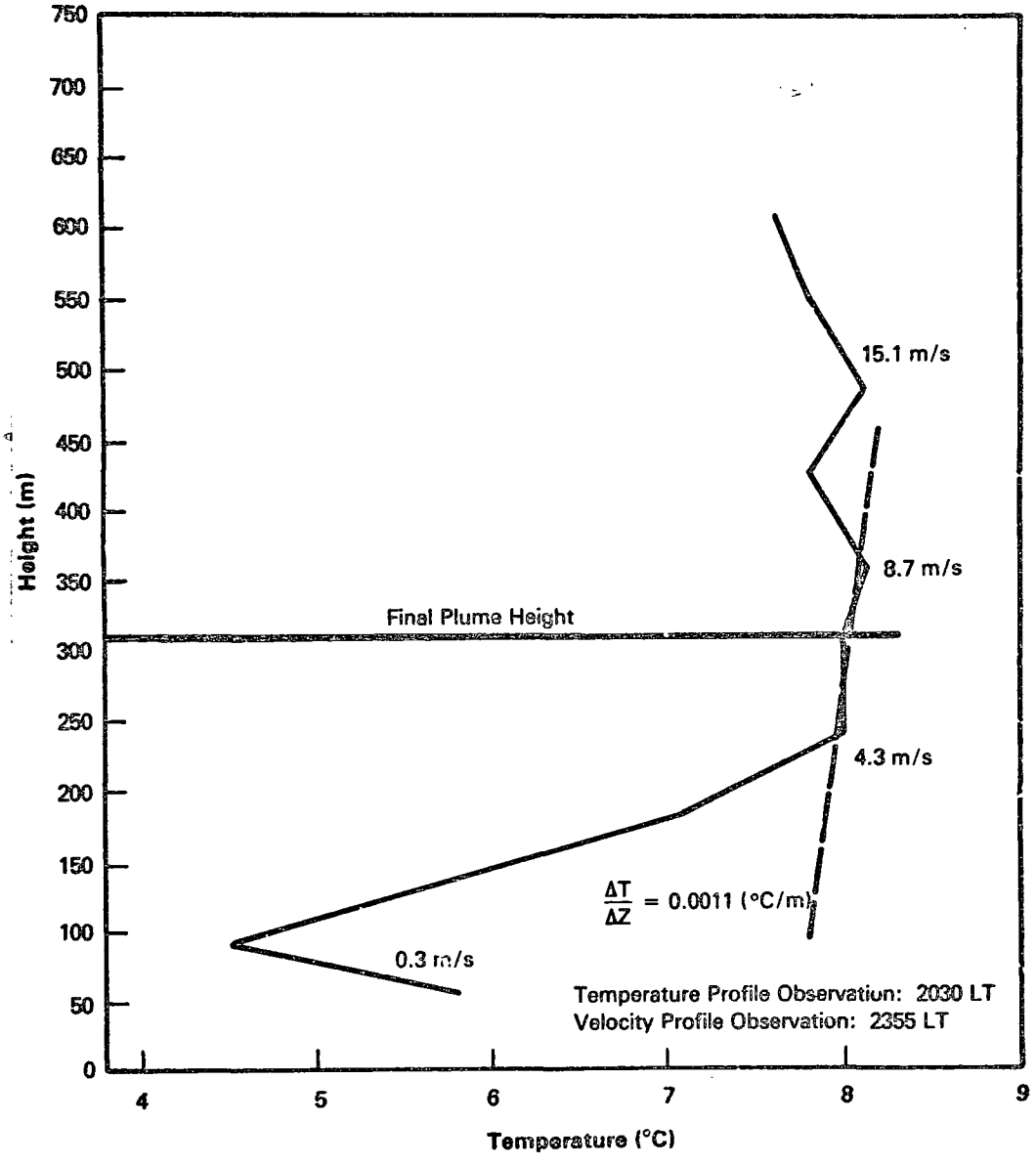

Figure 40. Temperature profile used to calculate plume rise and Froude number on day 4, hour 2100, 1978.

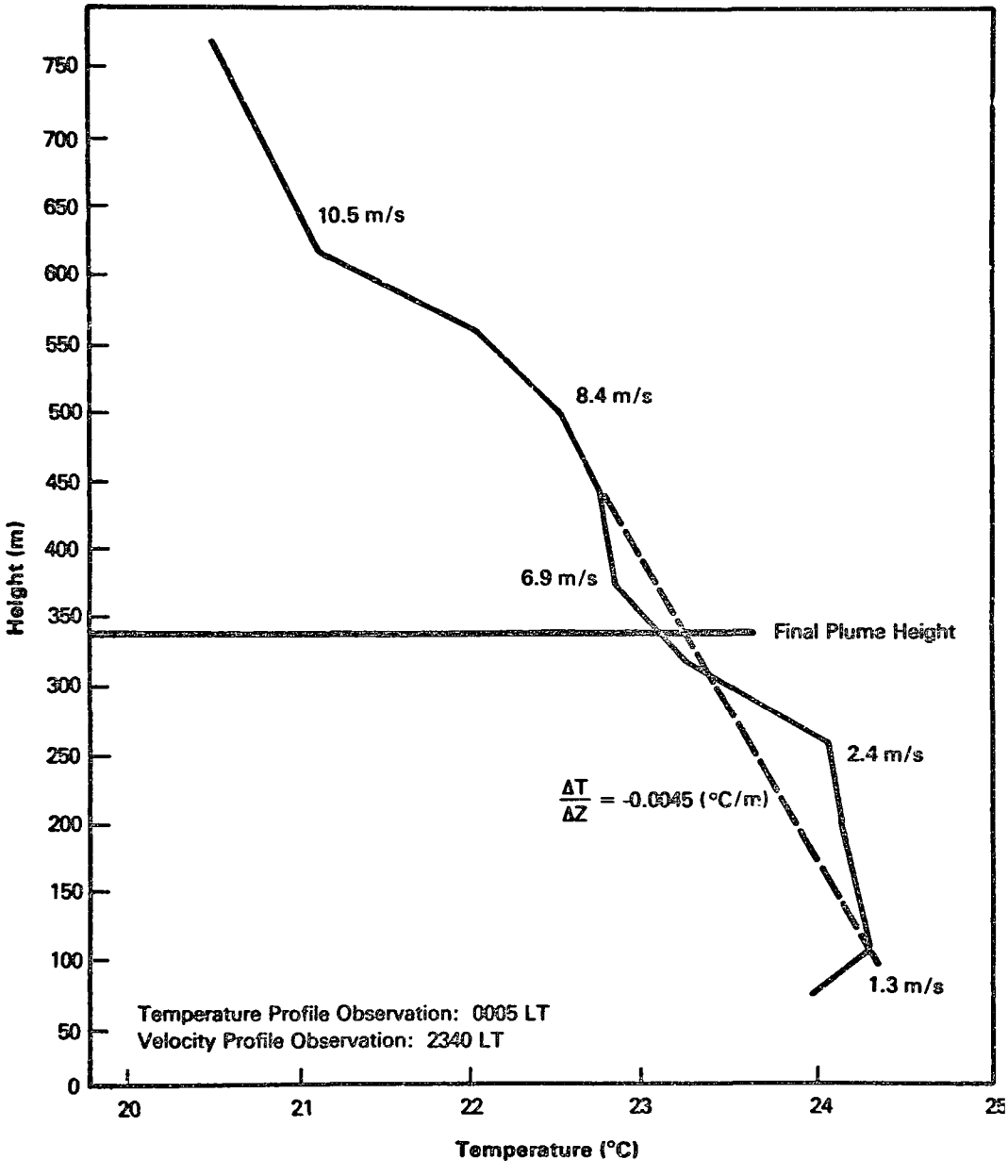

Figure 41. Temperature profile used to calculate plume rise and Froude number on day 166, hour 2400, 1978.

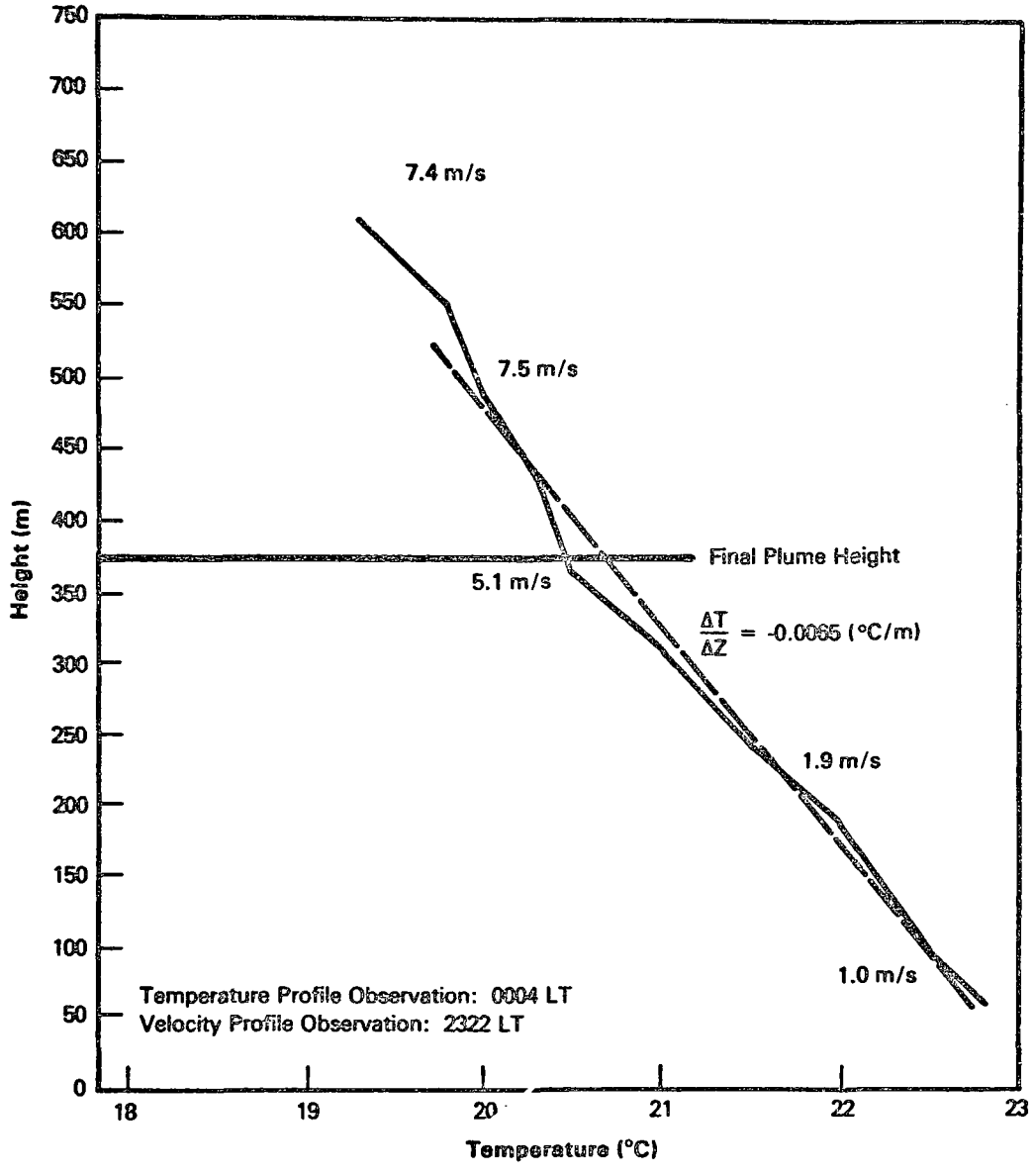

Figure 42. Temperature profile used to calculate plume rise and Froude number on day 222, hour 2400, 1978.

the hourly emission rate, the sulfur and heat content measurements made on samples taken once a week at each boiler were averaged (over units 1-6, and over units 7-8 separately) for each week to minimize the variability found among individual samples. In addition, the weekly averaged sulfur content of the coal used in units 7 and 8 were plotted in time and smoothed to reduce the variability observed in the small number of samples. Resulting emission rates for all units are summarized in Table 20 for the seven case hours.

TABLE 20. HOURLY UNCONTROLLED SO_2 EMISSIONS FROM EACH BOILER UNIT DURING HOURS SELECTED FOR MODEL ANALYSIS

Julian Day	Month	Day	Hour	SO_2 Emissions (g/s) from Each Boiler							
				1	2	3	4	5	6	7	8
3	1	3	1300	529	386	603	545	550	561	0	1,984
40	2	9	1300	221	288	225	264	245	254	0	1,756
190	7	9	0900	217	217	229	220	227	225	0	3,442
230	8	18	1000	204	108	0	237	222	233	2,094	2,171
4	1	4	2100	508	466	582	476	572	550	2,536	0
166	6	15	2400	208	117	185	183	121	142	0	1,672
222	8	10	2400	166	0	178	130	170	103	1,842	2,242

These emissions represent uncontrolled conditions. Operation of scrubbers on units 7 and 8 with a maximum efficiency of 80% was intermittent during this period.

12.4 Predicted and Observed Concentrations

12.4.1 Application of the Complex Terrain Model

Six physical quantities must be specified before the model can be run: X_s, the distance from the source to the hill crest; H_s, the height of final plume rise; a, the height of the hill; , the crosswind aspect ratio of the hill; SC, the atmospheric stability class; and Fr, the Froude number based on the hill height. The first four quantities have already been addressed for impacts on both the nearby ridge (Sand Mountain) and the isolated mound (Summerhouse Mountain). The remaining two are derived here.

The Froude number is defined as:

$$Fr = \frac{U}{aN}, \qquad (12\text{-}2)$$

where

$$N = \sqrt{\frac{g}{T}\frac{\partial\theta}{\partial z}} \qquad (12\text{-}3)$$

U is the mean velocity of the free stream (m/s),

a is the height of the hill (m),
T is the average temperature (°K),
$\partial\theta/\partial z$ is the potential temperature lapse rate (°K/m), and
g is the acceleration due to gravity, 9.8 m/s^2.

Knowledge of the temperature profile alone allows the calculation of N, the Brunt-Vaisala frequency, and the free-stream velocity may be determined from the velocity profile or extrapolated from the meteorological tower wind data if the available wind profiles are not representative of the case hour. The particular velocities chosen were subjectively selected within the height range of 300 to 400 m. Table 21 presents the Froude number results for those seven hours selected for model comparison. For all three hours showing significant impacts on Summerhouse Mountain (mound), flow conditions are closest to neutral flow; two of the four hours showing significant impacts on Sand Mountain (ridge) are tending to stable stratification.

TABLE 21. SUMMARY OF RESULTS OF FROUDE NUMBER CALCULATIONS

Julian Day	Hour	U(m/s)	$\partial\theta/\partial z$ (°K/m)	Fr
6-1/2"				
3	1300	2.7	0.0032	0.91
40	1300	3.1	0.0034	1.02
190	0900	2.6*	0.0196	0.37
230	1000	2.5	0.0093	0.52
9-1/8"				
4	2100	7.0	0.0109	1.30
166	2400	4.5	0.0053	1.24
222	2400	5.0	0.0033	1.73

*Extrapolated from tower data.

Dispersion stability classes for these hours are not directly measured. The tower data give stability class estimates for the layer below the stacks based on the temperature gradient (Table 22). Data more appropriate to the elevation of the plumes can be taken from the temperature profiles, and stability class can be determined again from the temperature gradient. Neither of these methods, however, takes account of the wind speed, or the influence of upwind terrain features.

TABLE 22. STABILITY CLASSIFICATION SYSTEM

Stability Description	Stability Class	Temperature Change with Height (°C/100 m)
Extremely Unstable	1 or A	< -1.9
Moderately Unstable	2 or B	-1.9 to -1.7
Slightly Unstable	3 or C	-1.7 to -1.5
Neutral	4 or D	-1.5 to -0.5
Slightly Stable	5 or E	-0.5 to +1.5
Moderately Stable	6 or F	+1.5 to +4.0
Extremely Stable	7 or G	> +4.0

For the ridge impact cases, the model was run with both the inferred stability class and the next 'less stable' class. The case period on days 3 and 40 are both hour 1300 with low wind speeds. Under these conditions, the dispersion class may fall between the inferred class (D) and the next less stable class (C). The other two periods, hour 0900 on day 190 and hour 1000 on day 230, have much more stable temperature gradients and slightly lower wind speeds, so the inferred stability class (E) may be representative; Stability class D calculations were also performed for comparison.

All three mound impact cases have moderate wind speeds and temperature gradients that correspond to stabilities between class D and E at night (hour 2100 or 2400). Because of the wind speeds and terrain roughness, stability class D may be more appropriate; both class E and class D calculations were made. Table 23 summarizes these choices for the seven case hours.

TABLE 23. RANGES OF DISPERSION STABILITY CLASS DESIGNATIONS APPROPRIATE TO THE CASE HOURS BASED ON TEMPERATURE PROFILES, WINDS, AND TIME OF DAY

Julian Day	Hour	Stability Class Profile ΔT	Range Modeled
3	1300	D	C-D
40	1300	D	C-D
190	0900	E	D-E
230	1000	E	D-E
4	2100	E	D-E
166	2400	E	D-E
222	2400	D	D-E

The complex terrain model was run for 28 cases, four runs for each of the seven case hours. The four runs per case hour arise from the four possible combinations of two plume heights and two stability classes. (The "scrubbed" and "unscrubbed" stack parameters give different plume rises.) Predicted concentrations are normalized by the quantity Q/Ua^2, where Q is the emission rate, U the stack top velocity, and a the hill height. Table 24 lists the results of the model computations for the four ridge impact cases; and Table 25 the results for the three mound impact cases.

In the two cases characterized by very low Froude numbers (days 190 and 230), ground-level concentrations increase with plume height. This effect is spurious; it results from using the empirically-derived streamline depression algorithm for cases not supported by the experimental data (see Section 8). It emphasizes that the potential flow model may not apply to stable conditions.

Tables 24 and 25 also list the terrain correction factors calculated from Equation 7-7 and the plume path coefficients calculated from Equation 7-9. These factors are highly sensitive to Froude number: for Froude numbers significantly greater than 1.0 the plume path coefficient is approximately 0.6, for Froude numbers less than or equal to 1.0, the coefficient varies from approximately 0.2 to 0.4. (The plume lowers with increasing stratification.)

TABLE 24. RESULTS OF MODEL CALCULATIONS FOR HOURS SHOWING IMPACT ON THE NEARBY RIDGE (SAND MOUNTAIN)

Julian Day	Plume Height (m)	Stability Class	Froude Number	Normalised Concentration	Inferred Terrain Correction Factor	Inferred Plume Path Coefficient
3	445	4(D)	0.91	0.0008	0.597	0.349
3	445	3(C)	0.91	0.1497	0.598	0.349
3	422	4	0.91	0.0017	0.598	0.383
3	422	3	0.91	0.1656	0.599	0.383
40	432	4	1.02	0.0009	0.611	0.390
40	432	3	1.02	0.1514	0.613	0.390
40	409	4	1.02	0.0018	0.617	0.430
40	409	3	1.02	0.1671	0.618	0.430
190	325	4	0.37	0.4663	0.344	0.225
190	325	5(E)	0.37	0.1459	0.344	0.225
190	307	4	0.37	0.4371	0.372	0.299
190	307	5	0.37	0.1248	0.372	0.299
230	347	4	0.52	0.1951	0.412	0.258
230	347	5	0.52	0.0182	0.412	0.258
230	322	4	0.52	0.1814	0.452	0.358
230	322	5	0.52	0.0153	0.452	0.358

TABLE 25. RESULTS OF MODEL CALCULATIONS FOR HOURS SHOWING IMPACT ON THE ISOLATED MOUND (SUMMERHOUSE MOUNTAIN)

Julian Day	Plume Height (m)	Stability Class	Froude Number	Normalized Concentration	Inferred Terrain Correction Factor	Inferred Plume Path Coefficient
4	309	4(D)	1.30	0.1040	0.658	0.616
4	309	5(E)	1.30	0.0200	0.658	0.616
4	289	4	1.30	0.1195	0.668	0.651
4	289	5	1.30	0.0296	0.666	0.651
166	335	4	1.24	0.0896	0.648	0.571
166	335	5	1.24	0.0116	0.649	0.571
166	317	4	1.24	0.0982	0.655	0.602
166	317	5	1.24	0.0170	0.655	0.602
222	370	4	1.73	0.0429	0.708	0.607
222	370	5	1.73	0.0016	0.708	0.607
222	344	4	1.73	0.0558	0.715	0.643
222	344	5	1.73	0.0034	0.715	0.643

12.4.2 Comparison with Observed Concentrations

The concentrations predicted at hill crest beneath the plume centerline are compared to the maximum observed concentrations. Stack-top wind speeds are estimated from velocities measured at 61 m on both the valley and mountain meteorological towers, and compared against speeds obtained from the vertical profiles. In most cases, the average of the speeds from the towers compared favorably with wind speeds in the lower portion of the vertical wind profiles; this average wind speed is used in the concentration normalization factor.

Derived emission rates and wind speeds, and the resultant normalization factors for each of the seven test case hours are summarized in Table 26. The normalization factors convert model concentrations to units of $\mu g/m^3$. Only the two 152-m stacks (boiler units 7 and 8) are included because the impact from the 304-m stack is small. Note that normalization factors are given for uncontrolled emissions only. The TVA Air Quality Branch reports that no scrubbing occurred on unit 7 during these hours, and either three quarters or full scrubbing (80% removal efficiency) occurred on Unit 8. In addition, slightly different gross load values (GW) were reported for both units during these hours. This information has been integrated with the previous data, and revised emissions for units 7 and 8 are presented in Table 27 along with the new normalization factors.

Additional plume rise computations have been made for the seven case hours using a multiple-layer plume rise extension of the stable Briggs plume rise equations (Holzworth 1978). For hours when unit 7 does not operate, the scrubbed plume rise height is calculated; for all other hours, unscrubbed plume height is calculated. When both units 7 and 8 are operating, the higher plume elevation corresponding to unit 7 is used because SO_2 concentrations of the unscrubbed unit 7 plume are more than twice those of the scrubbed unit 8 plume. The multilayer plume heights are compared with the single layer plume heights in Tables 28a and 28b. Both give nearly the same values for days 3, 4, and 40. The greatest difference occurs for day 166, where the new plume rise exceeds the previous value by 56 m. Concentrations predicted using the multilayer plume heights are also compared with the observed values.

For the hours of impact on the ridge (Sand Mountain) the model can overpredict in all cases. On day 3, a dispersion rate somewhere between class C and class D is required to match the observed concentration. The class D computation overpredicts by 118%. On day 40, however, the class C result overpredicts by less than 20%, and may therefore be considered a match. On day 190, the model overpredicts by 80% under class E, the best the model can do on that hour. On day 230, a dispersion class slightly more stable than Class E is required to reproduce the observation. (The class E value overpredicts by only 18%.)

The three cases of impact on Summerhouse Mountain produce one hour of virtual agreement, one hour of underprediction, and one hour of agreement for a stability class between stabilities D and E.

Plume size enhancement due to increased turbulence and mixing associated with the rise of buoyant plumes should improve the results for the more stable dispersion classes. Calculations with plume enhancement are presented in Table 29. As expected, results for the more stable dispersion

TABLE 26. UNCONTROLLED SO_2 CONCENTRATION NORMALIZATION FACTORS FOR TEST COMPARISON HOURS

Julian Day	Terrain Height a(m)	SO_2 Emissions Unit 7 & 8 Q (g/s)	Stack Top Velocity U (m/s)	Normalization Factor = Q/UH^2 ($\mu g/m^3$)
3	275	1984	2.0	13,117
40	275	1756	2.5	9,288
190	275	3442	1.2	37,928
230	275	4265	1.5	37,598
4	275	2536	3.0	11,178
166	275	1672	4.5	4,913
222	275	4084	1.4	38,574

TABLE 27. REVISED SO_2 EMISSION RATES FOR UNITS 7 AND 8 AND COMBINED CONCENTRATION NORMALIZATION FACTORS THAT INCLUDE SCRUBBER OPERATIONS

Julian Day	Old Emissions (g/s) Unit 7	Old Emissions (g/s) Unit 8	New Load/Old Load Unit 7	New Load/Old Load Unit 8	Unit 8 Scrubbing Factor*	New Emissions (g/s) Unit 7	New Emissions (g/s) Unit 8	Normalization Factor ($\mu g/m^3$)
3	0	1,984	-	0.987	0.4	0	783	5,177
40	0	1,756	-	1.027	0.4	0	721	3,814
190	0	3,442	-	0.991	0.2	0	682	7,515
230	2,094	2,171	1.036	1.041	0.4	2169	904	27,090
4	2,536	0	0.995	-	-	2,523	0	11,121
166	0	1,672	-	1.048	0.2	0	350	1,028
222	1,842	2,242	1.220	0.990	.4	2,247	888	29,611

*Scrubbing factor = 1 - scrubber utilization x scrubber efficiency.

TABLE 28a. COMPARISON OF PREDICTED AND OBSERVED SO_2 CONCENTRATIONS ($\mu g/m^3$) AT WIDOWS CREEK

Julian Day	Single-layer Plume Height (m)	Multilayer Plume Height (m)	Model T-Factor	Complex Terrain Model Predictions			Observed Concentration
				Stability C	Stability D	Stability E	
			Ridge Impact				
3	422	422	0.599	857	9	-	393
40	409	402	0.618	656	8	-	550
190	307	320	0.352	-	3427	1039	576
230	347	370	0.373	-	6158	711	603
			Mound Impact				
4	309	301	0.663	-	1234	260	1179
166	317	373	0.640	-	65	5	367
222	370	392	0.705	-	999	24	393

TABLE 28b. COMPARISON OF PREDICTED AND OBSERVED SO_2 CONCENTRATIONS ($\mu g/m^3$) AT WIDOWS CREEK

Julian Day	Froude Number	Plume Height (m)	Observed Concentration	Half-Height Assumption Predictions			Level Plume Model Predictions		
				Stability C	Stability D	Stability E	Stability C	Stability D	Stability E
				Ridge Impact					
3	0.91	422	393	654	1	-	1,648	890	-
40	1.02	402	550	574	3	-	1,354	1,192	-
190	0.37	320	576	-	362	5	-	10,941	16,633
230	0.52	370	603	-	136	0	-	18,386	9,672
				Mound Impact					
4	1.30	301	1,179	-	1,887	864	-	4,400	9,496
166	1.24	373	367	-	67	6	-	304	386
222	1.73	392	393	-	1,459	70	-	7,672	7,632

TABLE 29. COMPARISON OF OBSERVED CONCENTRATIONS ($\mu g/m^3$) AT WIDOWS CREEK AND PREDICTED CONCENTRATIONS BASED ON THE POTENTIAL FLOW MODEL WITH BUOYANT PLUME ENHANCEMENT

Julian Day	Multilayer Plume Height (m)	Observed Concentration	Complex Terrain Model Predictions Stability C	Stability D	Stability E
		Ridge Impact			
3	422	393	982	270	-
40	402	550	729	157	-
190	320	576	-	4,599	3,354
230	[illegible]	603	-	12,038	7,711
		Mound Impact			
4	301	1,179	-	1,529	531
166	373	367	-	99	16
222	392	393	-	2,123	246

stability class lie closer to the observed concentrations, and the cases overpredicted before are now even further off.

Additional perspective on the model's performance is gained by comparing it with a level plume model and with the half-height model under the same conditions. Predictions by the level plume model and half-height model are presented in Table 28b parallel to those by the potential flow complex terrain model.

For the half-height model, the impact on days 3, 40, 4, 166, and 222 are generally similar to those of the potential flow model. On days 3 and 40, the half-height concentrations are smaller, and overpredict the observed concentrations by a smaller margin under stability class C(3); on days 4 and 222, the half-height predictions are larger. In all four cases, both models bracket the observations.

On days 190 and 230 (very low Froude numbers), the behavior of the half-height model is markedly different from the potential flow model. Instead of a tendency to overpredict, the model significantly underpredicts. If the plume is assumed to approach closer to the terrain crest (i.e., a plume path coefficient of 0.35 instead of 0.5), the partial height model gives results similar to the potential flow model.

The level plume model predictions differ sharply from the other two models in all cases, and from the observations in six out of the seven cases. On day 166 the level plume model predictions are 83% and 105% of the observations for stability classes D and E. Day 166 is significantly underpredicted by the potential flow and half-height models. In the other six cases the level plume model overpredicts by factors from 2 to 30.

Table 30 summarizes these comparisons as a function of the magnitude of the observed concentration. For the largest observed concentration, only the level plume approach is clearly inappropriate. For the remaining cases, the level plume result is usually very high; the half-height approach generally brackets or underpredicts the observations; and the potential flow model (with and without buoyancy enhancement) brackets or overpredicts the observed concentrations. The complex terrain model seems a distinct improvement over the level plume model, especially if some shift in stability class is used.

TABLE 30. SUMMARY OF COMPARISONS OF THE POTENTIAL FLOW MODEL WITH HALF-HEIGHT AND LEVEL PLUME ASSUMPTIONS.*

Observed	Level Plume	Half-Height	Model	Model with Buoyancy
1,176	9,496-4,400	1,887-864	1,234-260	1,529-531
603	18,386-9,672	136-0	6,158-711	12,038-7,711
576	16,633-10,941	362-5	3,427-1,039	4,599-3,354
550	1,354-1,192	574-3	656-8	729-157
393	1,648-890	654-1	857-9	982-270
393	7,672-7,632	1,459-70	999-24	2,123-246
367	386-304	67-6	65-5	99-16

*Observed concentrations ($\mu g/m^3$) ranked according to size.

Given the irreducible uncertainties in the emissions and the atmospheric data at plume height, more detailed comparisons of the predicted and observed concentrations for these seven cases are not warranted.

12.5 Summary and Conclusions

Plume interactions with two terrain features near the Widows Creek Steam Electric Power Plant have been modeled with the potential flow complex terrain model. Meteorological conditions used in the model correspond to seven hours selected from nine months of hourly SO_2 and meteorological data collected by the TVA Air Quality Branch. The hours selected for comparison were derived by matching hours of high measured SO_2 concentrations on the two terrain features with neutral-to-stable atmospheric conditions. In addition, only those hours with nearly coincident vertical temperature and velocity profiles were considered. Of the seven hours finally selected, four are associated with impacts on the ridge, and three are associated with impacts on the isolated mound. The highest measured SO_2 concentration on the ridge during the 9-month period was 0.850 ppm (2,227 $\mu g/m^3$) observed on day 226, and that on the mound was 0.450 ppm (1,179 $\mu g/m^3$) observed on day 4.

The hour associated with the greatest ridge impact was not selected for model analysis because no suitable velocity and temperature profiles exist for that period. Consequently, the model's ability to simulate the greatest observed impact on the ridge is not known. The case hour of greatest impact on the mound (day 4, hour 2100) was simulated; one choice of predicted concentration was nearly equal to that observed.

A partial height model using a plume path coefficient of 0.5 performed about as well as the potential flow model for all Froude numbers greater than 0.6. For lower Froude numbers a path coefficient of 0.35 produced results similar to potential flow model. The level plume model greatly overpredicted most of the time, and matched observed concentrations for the one hour in which the other models markedly underpredicted.

Uncertainties in the meteorological conditions at plume height, and in the emissions from the facility, cloud the comparison of model predictions with observations. Given the range of data, reasonable combinations of assumptions can produce good correspondence between the concentrations in six of the seven cases. This does not, however, constitute an adequate evaluation of the model because of the uncertainties underlying these assumptions. The three greatest uncertainties lie in the specification of the dispersion parameters, the final plume height, and the actual emission rate. Data are not available for more accurate estimates of diffusion rates and plume elevation.

Nonetheless, the preliminary comparison for the hour of greatest impact on Summerhouse Mountain is encouraging and the bracketing of observed concentrations (in many of the other cases) suggests that better observations may well improve model performance.

REFERENCES

ASME. 1968. Recommended Guide for the Prediction of the Dispersion of Airborne Effluents. M. Smith, ed. New York, NY.

Briggs, G. A. 1975. Plume Rise Prediction. Lectures on Air Pollution and Environmental Impact Analysis, American Meteorological Society, pp. 80-84.

Briggs, G. A. 1973. Diffusion Estimation for Small Emissions, NOAA Atmospheric Turbulence and Diffusion Laboratory Contribution File No. 79.

Briggs, G. A. 1969. Plume Rise, Critical Review (TID-25075). Atomic Energy Commission, Division of Technical Information, Oak Ridge, TN.

Britter, R. E., J. C. R. Hunt, and J. S. Puttock. 1976. Predicting Pollution Concentrations Near Buildings and Hills. Proceedings of Conference on Systems and Models in Air and Water Pollution. Inst. Meas. and Control, London, England.

Cabe, D. B. et al. 1977. Application of the Gaussian Dispersion Model to Predicting Maximum Plume Concentrations in Abruptly Rising Terrain. Air Pollution Control Association (APCA) Paper No. 77-58.2.

Cramer, H. E., H. V. Geary, and J. F. Bowers. 1975. Diffusion-Model Calculations of Long-Term and Short-Term Ground-Level SO_2 Concentrations in Allegheny County, Pennsylvania. EPA 903/9-75-018. Prepared for U.S. Environmental Protection Agency, Region III, Philadelphia, PA.

Csanady, G. T. 1973. Turbulent Diffusion in the Environment. Boston: D. Reidel.

Egan, B. A. 1975. Turbulent Diffusion in Complex Terrain. Proceedings of Workshop on Air Pollution Meteorology and Environmental Assessment. American Meteorological Society, Boston, MA, September 30-October 3.

Egan, B. A. and A. Bass. 1976. Air Quality Modeling of Effluent Plumes in Rough Terrain. Proceedings of Third Symposium on Atmospheric Turbulence, Diffusion and Air Quality. American Meteorological Society, Raleigh, NC, October, 19-22.

Egan, B. A., R. D'Errico, and C. Vaudo. 1979. Assessing Air Quality Levels in Regions of Mountainous Terrain. Proceedings of Fourth Symposium on Turbulence, Diffusion and Air Pollution. American Meteorological Society, Reno, NV, January 15-18.

EPA 1978. Guideline on Air Quality Models. EPA-450/2-78-027. U.S. Environmental Protection Agency, Office of Air Quality Planning and Standards, Research Triangle Park, NC.

Hinds, W. T. 1970. Diffusion Over Coastal Mountains of Southern California. Atmospheric Environment 4:107-124.

Hoffnagle, G. W., B. A. Egan, and B. H. Greene. 1977. Application of Models in Complex Terrain. Proceedings of Joint Conference on Applications on Air Pollution Meteorology. November 25-December 2. American Meteorological Society, Boston, MA.

Holzworth, G. C. 1978. Estimated Effective Chimney Heights Based on Rawinsonde Observations at Selected Sites in the United States. Journal of Applied Meteorology 17(2): 153-160.

Hunt, J. C. R. and R. J. Mulhearn. 1973. Turbulence Dispersion from Sources Near Two-Dimensional Obstacles. Journal of Fluid Mechanics 61:245-274.

Hunt, J. C. R., J. S. Puttock, and W. H. Snyder. 1979. Turbulent Diffusion from a Point Source in Stratified and Neutral Flows Around a Three-Dimensional Hill. Part I - Diffusion Equation Analysis. Atmospheric Environment 13:1227-1239.

Hunt, J. C. R. and W. H. Snyder. 1978. Flow Structure and Turbulent Diffusion Around a Three-Dimensional Hill. Part II - Surface Concentrations due to Upstream Sources (unpublished manuscript).

Hunt, J. C. R., W. H. Snyder, and R. E. Lawson, Jr. 1978. Flow Structure and Turbulent Diffusion Around a Three-Dimensional Hill. Fluid Modeling Study on Effects of Stratification; Part 1, Flow Structure. EPA-600/4-78-041. U.S. Environmental Protection Agency, Research Triangle Park, NC.

Irwin, J. S. 1979. Scheme for Estimating Dispersion Parameters as a Function of Release Height. EPA-600/4-79-062. U.S. Environmental Protection Agency, Research Triangle Park, NC.

Leahey, D. M. 1974. Observational Studies of Atmospheric Diffusion Processes over Irregular Terrain. Proceedings of the 67th Meeting of the Air Pollution Control Association, Denver, CO, June 9-13.

Leahey, D. M. and J. Halitsky. 1973. Low Wind Turbulence Statistics and Related Diffusion Estimates from a Site Located in the Hudson River Valley. Atmospheric Environment 7:49-61.

MacCready, P. B., L. B. Baboolal, and P. B. Lissaman. 1974. Diffusion and Turbulence Aloft over Complex Terrain. Proceedings of the Symposium on Atmospheric Diffusion and Air Pollution. American Meteorological Society, Santa Barbara, CA, September. pp. 216-225.

Miller, C. W. 1978. An Examination of Gaussian Plume Dispersion Parameters for Rough Terrain. Atmospheric Environment 12:1359-1364.

Milne-Thomson, L. M. 1960. Theoretical Hydrodynamics. New York: Macmillan.

Pasquill, F. 1978. Atmospheric Dispersion Parameters in Plume Modeling. EPA-600/4-78-021. U.S. Environmental Protection Agency, Research Triangle Park, NC.

Schiermeier, F. A. and L. E. Niemeyer. 1970. Large Power Plant Effluent Study (LAPPES). Volumes 1-4. National Air Pollution Control Administration Publication Nos. APTD 70-2, 0589.

Shearer, D. L., D. H. Minott, and G. R. Hilst. 1977. Development of Vertical Dispersion Coefficients for Rolling Terrain Environments. Prepared for the U.S. Energy Research and Development Administration. EY-76-C-02-4026.

Snyder, W. H. 1977. Data Report. Project: Hunt Hill Study. Part: No Hill. EPA Fluid Modeling Facility (unpublished manuscript).

Snyder, W. H. 1978. Data Report. Project: Hunt Hill Study. Part: Water Channel - Polynomial Hill. EPA Fluid Modeling Facility (unpublished manuscript).

Snyder, W. H. and R. E. Britter. 1979a. Sandspray Boundary Layer Characterization (SSBL4). Unpublished EPA data report.

Snyder, W. H. and R. E. Britter. 1979b. Aspect Ratio Study (ASRAT). Unpublished EPA data report.

Snyder, W. H. and G. L. Marsh. 1977. Data Report. Project: Hunt Hill Study. Part: Wind Tunnel - Polynomial Hill. U.S. Environmental Protection Agency Fluid Modeling Facility (unpublished manuscript).

Start, G. E., R. R. Ricks, and C. R. Dickson. 1976. Effluent Dilutions over Mountainous Terrain. Proceedings of the Third Symposium on Atmospheric Turbulence Diffusion and Air Quality. American Meteorological Society, Raleigh, NC, October 19-22.

Start, G. E., C. R. Dickson, and L. L. Wendell. 1975. Diffusion in a Canyon within Rough Mountainous Terrain. J. Appl. Meteor. 14:3, 333-346.

Sutton, O. G. 1970. Micrometeorology. New York: McGraw-Hill.

Turner, D. B. 1970. Workshop of Atmospheric Dispersion Estimates. U.S. Department of Health, Education and Welfare. Public Health Service Publication 999-AP-26, 88 pp.

Williams, M. D. 1977. Comments in Report to the U.S. EPA of the Specialists' Conference on the EPA Modeling Guideline, p. 210.

Wilson, R. B. et al. 1976. Diffusion Under Low Windspeed Conditions Near Oak Ridge, Tennessee. U.S. Department of Commerce, National Oceanic and Atmospheric Administration, Environmental Research Laboratories, NOAA Technical Memorandum ERL ARL-61, August.

APPENDIX A

PROGRAM DESCRIPTION - CMPLX MODEL

APPENDIX A

PROGRAM DESCRIPTION - CMPLX MODEL

A1. Introduction

This section summarizes the essential operating features of the computer model CMPLX developed during the initial phase of this work. Because of the research nature of this computer code, it is expected that significant revisions may evolve based on subsequent experimental and theoretical developments. Therefore, no attempt has been made to produce comprehensive program documentation at this time, particularly with respect to the specified input/output format chosen. However, the overview presented here will enable the potential user to become thoroughly familiar with the fundamental programming aspects of the code and orient him to its use.

The CMPLX program is a Gaussian point-source diffusion model applicable to isolated terrain obstacles of arbitrary crosswind aspect ratio in the flow field downwind from the source. The plume is assumed to be embedded in a potential flow field determined by the specific source/obstacle configuration involved. This geometry determines: (1) the plume trajectory above the surface, and (2) the kinematic constraints on plume dispersion imposed by the spatial dependence of the velocity field. The theoretical aspects incorporated within the code have been previously described (Section 5) and will be referenced by equation number. Since the formalism adopted has been pursued rigorously only for neutral flows and the limiting aspect ratio cases of a three-dimensional axisymmetric hill and a two-dimensional circular ridge, certain approximations have been incorporated to extend the model to a broader class of potential field situations, including the effects of stratification and intermediate aspect ratios. These features are discussed in Sections 8 and 10, respectively, and will not be repeated here.

The code in its present form consists of a main program, four subroutines, and two function subroutines. In the course of the discussion to follow, reference will be made to the program flowchart (Appendix B) by FORTRAN statement numbers in parentheses and flowchart page number and to the computer program listing (Appendix C) by compiler line number (at the far right of each printed record). Comment cards have been used extensively in the listing, and essential data presented there will not be repeated. Variable and subroutine names are capitalized by convention. A sample output listing is illustrated in Appendix D.

A2. Main Program

A flowchart of the main program (Appendix B, p. 148) illustrates the following features of the calculations performed for each case.

- read input values for a particular situation (XS, HS, HA, XL, ALAM, DELINT, RKST, FROUDE),
- specify necessary constants,
- define relevant nondimensional parameters,
- compute streamline and velocity field aspect ratio weighting factors for neutral flow (A),
- specify two- and three-dimensional streamline for neutral flow and weight for given aspect ratio (B),
- compute empirical streamline lowering for stable stratification effects (C),
- perform along-streamline line integrals (D), and
- compute dispersion coefficients, centerline and ground-level concentrations; print out results (E)

(Program elements followed by capital letters are explained in the following sections.)

A2.1 Aspect Ratio Weighting Factors (A)

As described in Section 10, the effects on a flow field of a hill with intermediate aspect ratio ALAM, falling between the two- and three-dimensional limits, ALAM = 10.0, ALAM = 1.0, are defined by streamline (WZ) and velocity field (WV2, WV3) weighting factors. If the specified value of ALAM is less than or equal to unity (601) a three-dimensional computation is made (WV2 = 0.0; WZ, WV3 = 1.0). Conversely, all aspect ratios greater than or equal to 10.0 are assumed to characterize two-dimensional situations (602), and the values (WV2 = 1.0; WZ, WV3 = 0.0) are assigned. If neither condition is satisfied, a general weighting of streamline height based on one set of wind tunnel experiments is adopted:

```
WZ  =  1.0/ALAM**1.1
```

while velocity fields are defined based on the speed-up factor SUP (Equation 10-13), and weights are given by (Equation 10-17):

```
WV2  =  2.0 * (SUP - 1.5)
WV3  =  2.0 * (2.0 - SUP)
```

A2.2 Neutral Streamline Evaluation (B)

Beginning with statement 603 (Appendix B, p. 150), two- and three-dimensional streamlines are evaluated through the source as (XX,ZZ) pairs assuming the obstacle to be one of these limiting cases. The code sequence to statement 605 is performed twice: once for ND = 2 and once for ND = 3. The value of the stream function through the source PSIP, determined by parameters XS, HS, HA, is first computed by calling function subroutines PSIP2D or PSIP3D. Since this value must remain constant along the trajectory, the streamline Equation 5-28 is solved for each ZZ value to yield a unique

XX value defining the streamline (see discussion in Section 5.4.3). Only positive XX values are computed, since the streamline is symmetric about the origin at the obstacle center.

The upper and lower limits to possible ZZ values are given by the height of the streamline H1 above the crest ZC (at XX=0.0) and that at XX = 100.0 (taken as infinity), respectively. Appropriate ZZ values are selected within this range at two resolutions. A total of NINC values are computed with INC2 values in the range:

$$H1 \leq ZZ \leq (ZC+HS)/2.0$$

and NINCMI (=NINC-INC2) values such that:

$$(ZC+HS)/2.0 < ZZ \leq ZC$$

Dual resolution is adopted since the streamline becomes relatively flat in the region determined by INC2. Nominal values of NINC = 550 and INC2 = 150 have been selected to provide adequate resolution in each region. Thus a total of 550 (XX,ZZ) pairs are computed.

Computed (XX,ZZ) pairs are stored (line 8, Appendix B, 151) and indexed by an integer value from 1 to NINC in arrays (FITX(ND,II), FITZ(ND, II)), respectively. They are placed in common with subroutine ZITRPL (Appendix B, p. 163), which provides a z-value for any given x-value by linear interpolation. Once the two- and three-dimensional streamlines are evaluated, the aspect ratio streamline weighting factor (WZ) is used to compute a weighted neutral streamline stored as (FITX(1, II), FITZ(1, II)). The x-resolution chosen is that of the three-dimensional streamline (i.e., FITX(1, II) = FITX(3, II)) necessitating a call to ZITRPL to find the height of the two-dimensional streamline ZEE2, corresponding to each new x-value (two- and three-dimensional streamlines have different (x,z) resolutions). The weighted z-value is given by:

$$FITZ(1, II) = (1.0 - WZ)*ZEE2+WZ*FITZ(3, II)$$

This sequence terminates on statement 605.

A2.3 Streamline Lowering Because of Stable Stratification Effects (C)

As previously discussed (Section 8), the predominant effect of stable stratification is assumed to be a lowering of the streamline below the value it would attain at the crest of the obstacle in neutral flow. The magnitude of the effect is based on experiment for the three-dimensional case and assumed to extend proportionally to the general case. This aspect of the calculation (statements 605 to 610) is illustrated in the flowchart in Appendix B, p. 152.

If PGT stability class (KST) of 4 or less (A = 1, B = 2, C = 3, D = 4) is specified, no stability effect is computed. For stably stratified cases, a correction is applied to the neutral streamline with a maximum depression at the crest (XX = 0.0), decreasing linearly with increasing |XX| to no depression for all |XX| $\geq$ 2.0*HA. For each KST, a value of the streamline height above the crest ZCF is computed as a function of HS and Froude number Equations, 8-1 to 8-8. For other XX within two hill heights,

the streamline depression DELTA3 and fractional streamline depression FRAC3 are evaluated with respect to the neutral three-dimensional streamline. Although data is available only for the three-dimensional effect, it is assumed that a similar depression is applicable to two-dimensional and aspect ratio weighted streamlines. For the two-dimensional case, a fractional weighting FRAC2 appropriate to each two-dimensional XX value (=FITX(2, II)) is evaluated. Finally, each streamline value is multiplied by the appropriate fractional depression:

```
FITZ(1, II)  =  FITZ(1, II) * FRAC3
FITZ(2, II)  =  FITZ(2, II) * FRAC2
FITZ(3, II)  =  FITZ(3, II) * FRAC3
```

(Note: it is necessary to retain and weight the two- and three-dimensional streamlines at this point since they are used in TKER to compute the final velocity fields.)

A2.4 Along Streamline Line Integrals (D)

The line integrals ϕ and Γ (see Section 5; Equations 5-11, 5-12, and 5-23, 5-24) determining the magnitude of crosswind and normal dispersion are evaluated by the coding between statements 610 and 101 (See Appendix B, pp. 153 to 155 for flowchart.)

The values of these integrals PHID and TEED, respectively, are stored in arrays indexed by integer values JJ corresponding to a given position along the x-axis, S2(JJ), and downwind distance from the source, DDW(JJ). These are related by DDW (JJ) = S2(JJ) - XS. Since these integrals are continuous functions of along streamline distance, s, it was decided to sample their values at a discrete number of points determined by a user-specific dimensional resolution, DELINT (nondimensionally, DEL). The total number of values sampled, JF, is restricted only by the total array size (dimension) of the affected variables within the region of interest along the x-axis:

```
JF = AINT((XL-XS)/DEL)
```

where XS is the stack position from obstacle center and XL is an arbitrary point chosen downwind of the obstacle. (These arrays are currently subscripted for 50 values.)

The integration is performed by Simpson's rule along streamline segments with upper limit BB and lower limit AA corresponding to one DEL interval. The fine resolution within each segment is selected by specifying NN. The integration mesh size is then:

```
H = (BB-AA)/FN = DEL/FN
```

(FN is the floating point value of NN.)

When JJ = 1, the lower limit is set as XS; the source position and the upper limit is taken as:

```
BB = SS = AINT(XS) + DEL
```

On subsequent iterations, the upper limit is chosen as:

$$BB = SS = AINT(XS) + JJ * DEL$$

and lower limit

$$AA = SS - DEL$$

For each JJ, the values of the ϕ and T integrals for the specified DEL interval are computed as follows:

$$PINT = \int_{AA}^{BB} P \, dx$$

$$TINT = \int_{AA}^{BB} T \, dx$$

The respective kernels P, T are evaluated at each grid point x by calling a sequence of two subroutines TKER and D1D2 (see Appendix B, pp. 158, 159, 161). Returned values from those subroutines include the P and T kernels along streamline velocity UUU and slope M and the diffusivities in each direction D1, D2. (Subroutines will be described in more detail in the following section.) The segment of the integrals for each JJ value are summed iteratively in arrays PHI(JJ), TEE(JJ):

```
PHI(JJ) = PINT + PHI(JJ-1)
TEE(JJ) = TINT + TEE(JJ-1)
```

These arrays are the line integral values along the streamline from the source XS to the position S2(JJ) along the x-axis without multiplication by the diffusivities D1, D2. As described earlier (Section 5.5, Equations 5-6 and 5-17), effective diffusivities are defined at each downwind distance (or constant values are prescribed, C1, C2). The ϕ and T integrals at distance S2(JJ) along the x-axis are given by:

```
PHID(JJ) = PHI(JJ) * D1
TEED(JJ) = TEE(JJ) * D2
```

This procedure continues for JF iterations and proceeds along the x-axis to a position of S2(JF) = AINT(XS) + JF*DEL. By choosing an appropriate value of XL (say, one hill height along the positive x-axis), calculations are performed along the windward trajectory and terminate after passing the obstacle crest to the leeward side.

A3.5 Compute Sigmas, Centerline and Ground-Level Concentrations (E)

Beginning on line 101, parallel calculations are begun to compute dispersion coefficient estimates and centerline and ground-level concentrations as a function of downwind distance from the source for two cases:

1) a flat terrain situation, with the given stack parameters and stability class (left branch in flowchart, Appendix B, p. 156 and 157); and

2) the analogous situation with the obstacle centered at downwind distance DDW(JJ) = -XS (right branch).

For the first case, the dispersion coefficients used are the conventional PGT "flat" terrain values evaluated as SIGZNH(JJ) and SIGYNH(JJ), respectively, while centerline and ground-level concentrations are computed using the Gaussian solution (Equations 5-7 and 5-20) with height above the surface taken as a constant value given by the effective stack height HS.

To evaluate the functions in the presence of the obstacle, Equations 5-20 through 5-25 are used with the dispersion coefficients SIGZH(JJ) and SIGYH(JJ) given in terms of the ϕ and T integrals and along streamline velocity, US(JJ). Centerline concentrations, CCLH(JJ), are the coefficients of the exponential term in the Gaussian solution and ground-level values are computed by multiplying the centerline values by a factor equal to 2.0 times the exponential term using the appropriate SIGZH(JJ) and height of plume centerline above surface, ANS(JJ). This height is determined by subroutine SURF, which computes the distance from the surface along the normal to the streamline at a given x-value. This subroutine will be described further in the next section.

After printing out the required tables of the values described above, (see test case, Appendix D), the program computes off-axis, ground-level concentrations CGL(JJ,K) by multiplying centerline concentrations by a crosswind exponential expressed in fractional increments of SIGYH(JJ) up to two standard deviations off-axis. An integer flag, IY, is set to facilitate this additional calculation if required.

If new data is encountered by the read statement 555, the entire sequence is repeated commencing at start. Otherwise, the program proceeds to line 999 where the job ends (EOJ means end of job).

A3. Subroutines

This section briefly describes subroutines D1D2, PSI2D, PSI3D, TKER, SURF, and ZITRPL.

A3.1 Subroutine D1D2

This subroutine computes the required values of along-streamline diffusivities in the vertical (D1) and crosswind (D2) directions. Basic features of D1D2 are schematically presented in the flowchart on pp. 158 and 159 of Appendix B. It consists of a number of branches that perform the following functions:

- If the branching parameter IFLAG = 0, the calculations are performed for constant diffusivity values (statement 80) specified as C1 and C2, for the normal and crosswind diffusivities, respectively.

- If a diffusivity is sought for the "flat" case, such as in Section E of the main program (see Section A.2.5 above), the value of the parameter H is set:

$$H = 0.0$$

and dispersion coefficients are read directly from the PGT curves as a function of stability class KST for a given downwind distance (XX-XS) (statement 99).

- If IFLAG $\neq$ 0 and H $\neq$ 0.0, the calculation continues, and the distance along the streamline PS and the advection time PT are computed by D1D2 using a Taylor series of the form:

$$s_{i+1} = s_i + \left(\frac{\partial s}{\partial x}\right) \Delta x$$

$$t_{i+1} = t_i + \left(\frac{\partial t}{\partial x}\right) \Delta x$$

each time D1D2 is called during the Simpson's rule integration scheme (Section A.2.4). For each JJ interval, it is necessary to keep count of the integration loop counter I. When both JJ and I are zero (at point -XS), diffusivities are set identically equal to zero (statement 75). For each subsequent I = 0, the initial values of PS,PT are set equal to the values PSA(JJ-1), PTA(JJ-1) from the previous DEL interval integration. Note that calls to D1D2 are arranged to increase the x-argument linearly from -XS to BB (the upper limit for any integration segment.) Therefore, when XX = BB (statement 97), i.e., the upper limit for a particular DEL integration limit is reached, the value of PS and PT are, respectively, the along-streamline distance and time. The PS value is dimensionalized and used at the downwind distance x (statement 98) to evaluate dimensional vertical and horizontal dispersion coefficients for the flat case using the PGT prescription for a specified KST. Dimensional diffusivities are then computed (beginning at statement 71) using the dimensional advection time P1. These are non-dimensionalized for return to the main program (statement 90).

In this manner the diffusivities from D1D2 are returned as functions of downwind distance at a resolution equivalent to DEL, scaled with respect to the "flat" PGT values.

A3.2 Statement Functions: PSI2D, PSI3D

For given dimensionless x- and z-arguments, the statement functions PSI2D and PSI3D (see Appendix B, p. 160) return the dimensionless values of the two- and three-dimensional stream functions for flow over a half cylinder and an axisymmetric hemisphere, respectively.

A3.3 Subroutine TKER

This subroutine computes the aspect ratio weighted velocity field (UU,VV), which is used to evaluate slope (M), along streamline velocity (UUU), and the P and T kernels for a given x-value. It is called repeatedly during the Simpson's rule integration scheme described in the previous section. The following steps are followed (see Appendix B, p. 161 and 162) for each x-value:

- Velocity components for two-dimensional flow (U2,V2) are computed from an analytical expression derived from the two-dimensional stream function for given x and z. (Subroutine ZITRPL is called by setting argument ND = 2 to obtain the appropriate z-value along the two-dimensional streamline).
- An analogous computation is performed for the components of the corresponding three-dimensional velocity field, first calling ZITRPL (X, NINC, 3, Z) to provide the height along the three-dimensional streamline.
- The aspect ratio weighted velocity field is computed from weighting factors WV2, WV3 (see Section 5.2.1):

  UU = WV2 * U2 + WV3 * U3
  VV = WV2 * V2 + WV3 * V3

- Slope M:

  M = VV/UU

- Finally, the kernels P and T are computed for each x within the integration, in addition to along-streamline velocity.

A3.4 Subroutine SURF

SURF is called during evaluation of ground-level concentrations to compute the distance between the plume centerline given by the streamline equation for a given x-value and the surface. This distance is defined as the length of the line segment normal to the streamline at point (S3, ZEE) and intersecting the surface. The point of intersection with the surface may fall into one of two regions:

(1) before the windward and after the leeward edge of the obstacle (AXINT $\geq$ 1.0); i.e., in the flat part of the topography; or

(2) on the obstacle AXINT < 1.0

In the first case, the intersection point XINT obeys the equation of the line normal to the streamline at point (S3, ZEE) (i.e., has the negative reciprocal slope SLO) and has a zero z-value. For the second case, the intersection point XT,ZT obeys the equation of the same line and also the equation of the circle defining the surface in the x,z plane. For both cases, the value ZNS is calculated from the basic geometric relationship for the distance between two points.

A3.5 Subroutine ZITRPL

This is a simple linear interpolation routine that returns the z-value (ZEE) for any given x-value (SX) within the range defined by arrays FITX(ND, II), FITZ(ND, II) of NINC discrete, x- and z-values, respectively, defining the ND-dimensional streamline (ND equals 1 is the aspect ratio weighted streamline). Since only positive definite values are stored in these arrays and symmetry about the x = 0-axis is assumed, the absolute value XX = ABS(SX) of the argument is taken. A DO loop searches down the FITX(ND,II) array in order of descending x-magnitude by incrementing the argument until the condition:

$$FITX(ND, KP1) \leq XX \leq FITX(ND,K)$$

is met at which point control passes to statement 2 and the DO loop is terminated. At this point, a linear interpolation for the appropriate z-value ZEE is performed, and ZEE is returned to the calling program.

APPENDIX B

PROGRAM FLOW CHART

Main Program

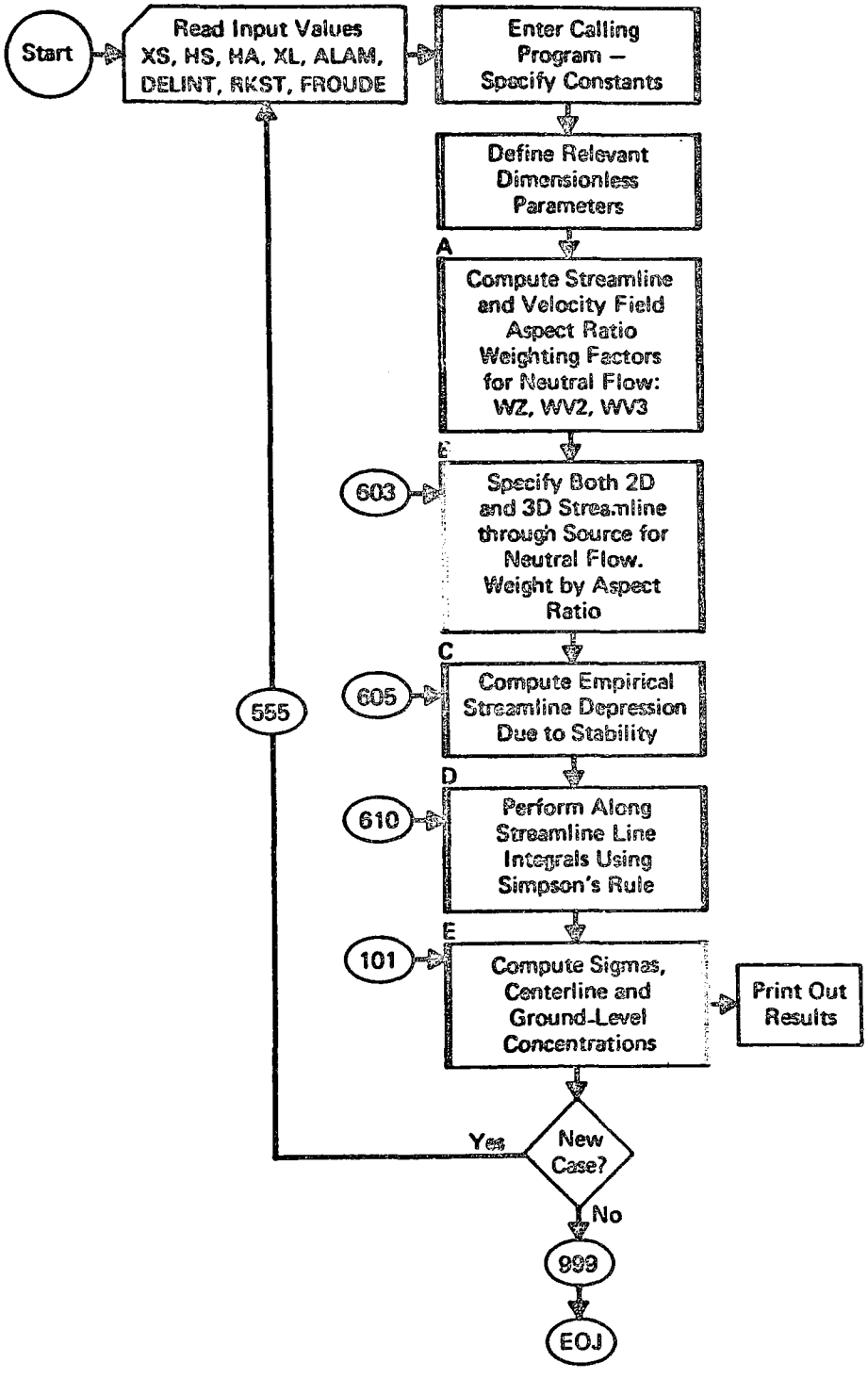

A. Compute Streamline and Velocity Field Aspect Ratio Weighting Factors for Neutral Flow.

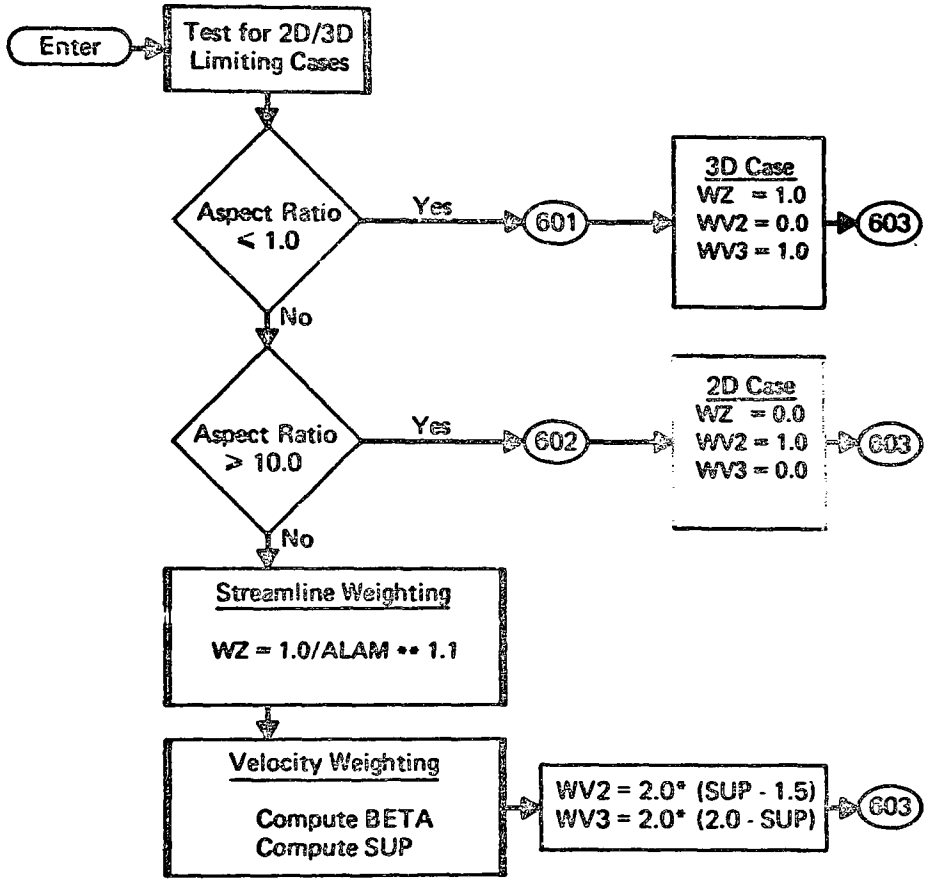

B1. Specify Both 2D & 3D Streamline through Source for Neutral Flow; Weight by Aspect Ratio

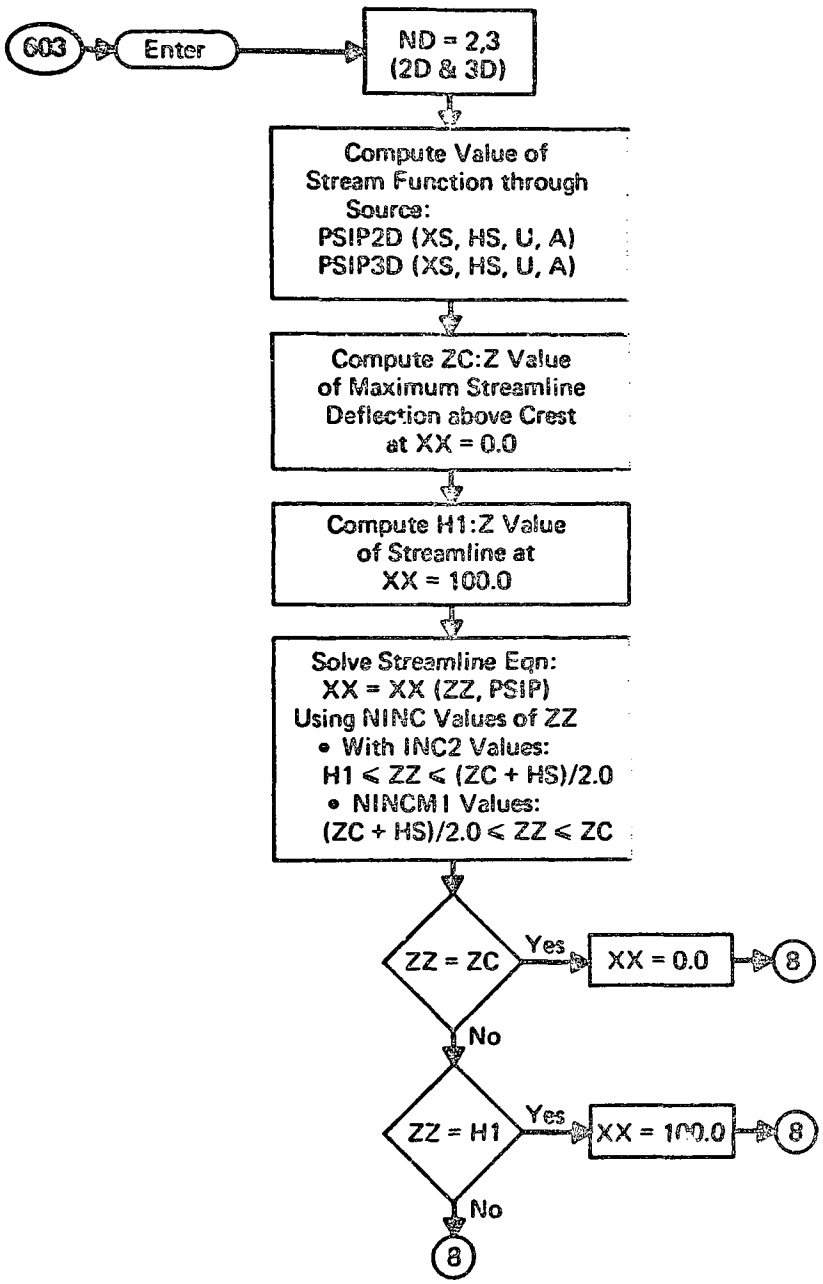

B2. (Continued)

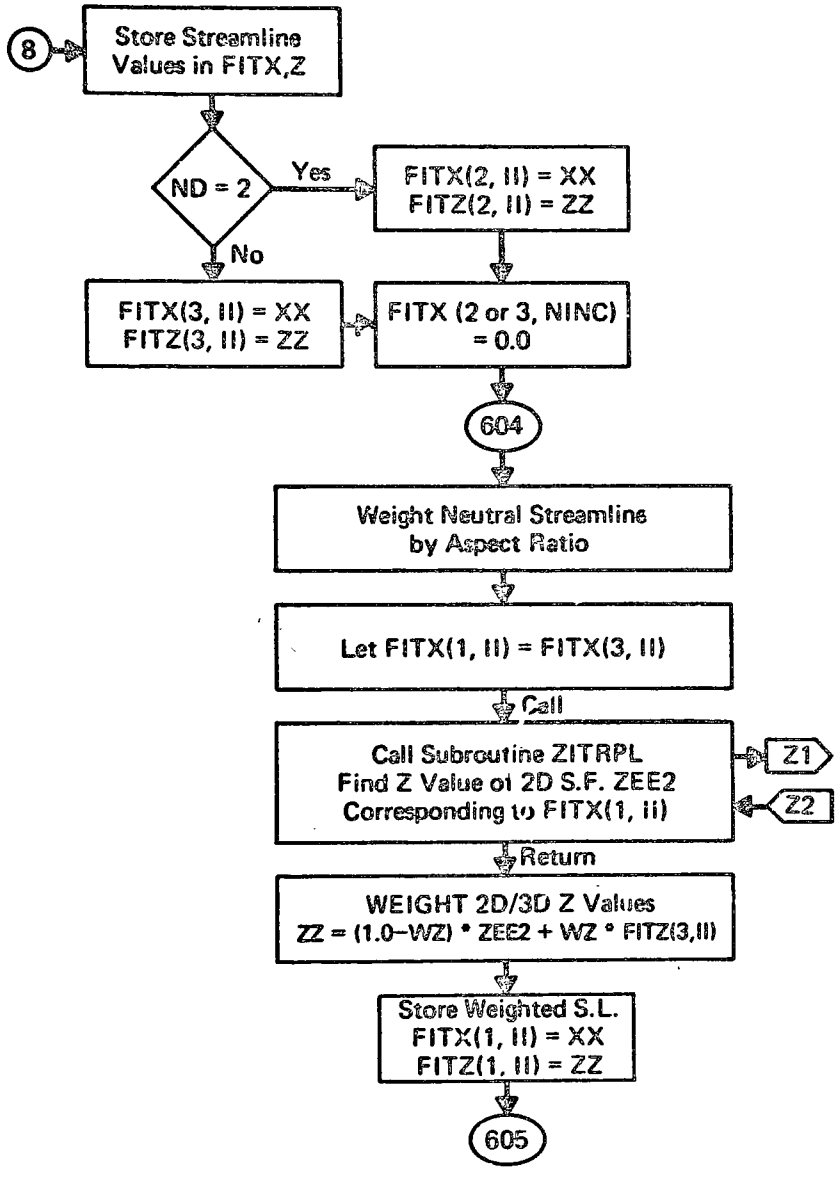

C. Compute Empirical Streamline Depression Due to Stability

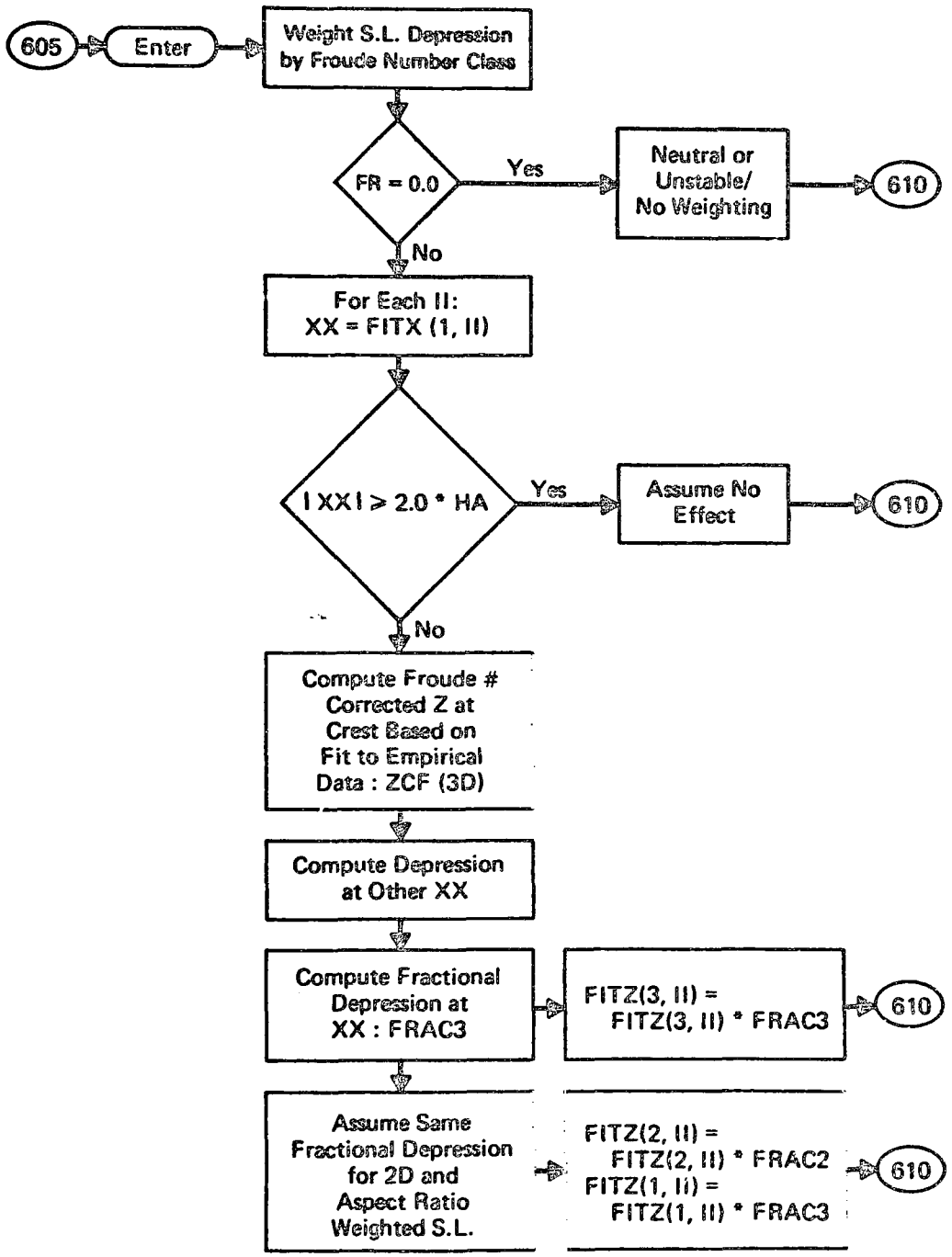

D1. Perform along Streamline Line Integrals

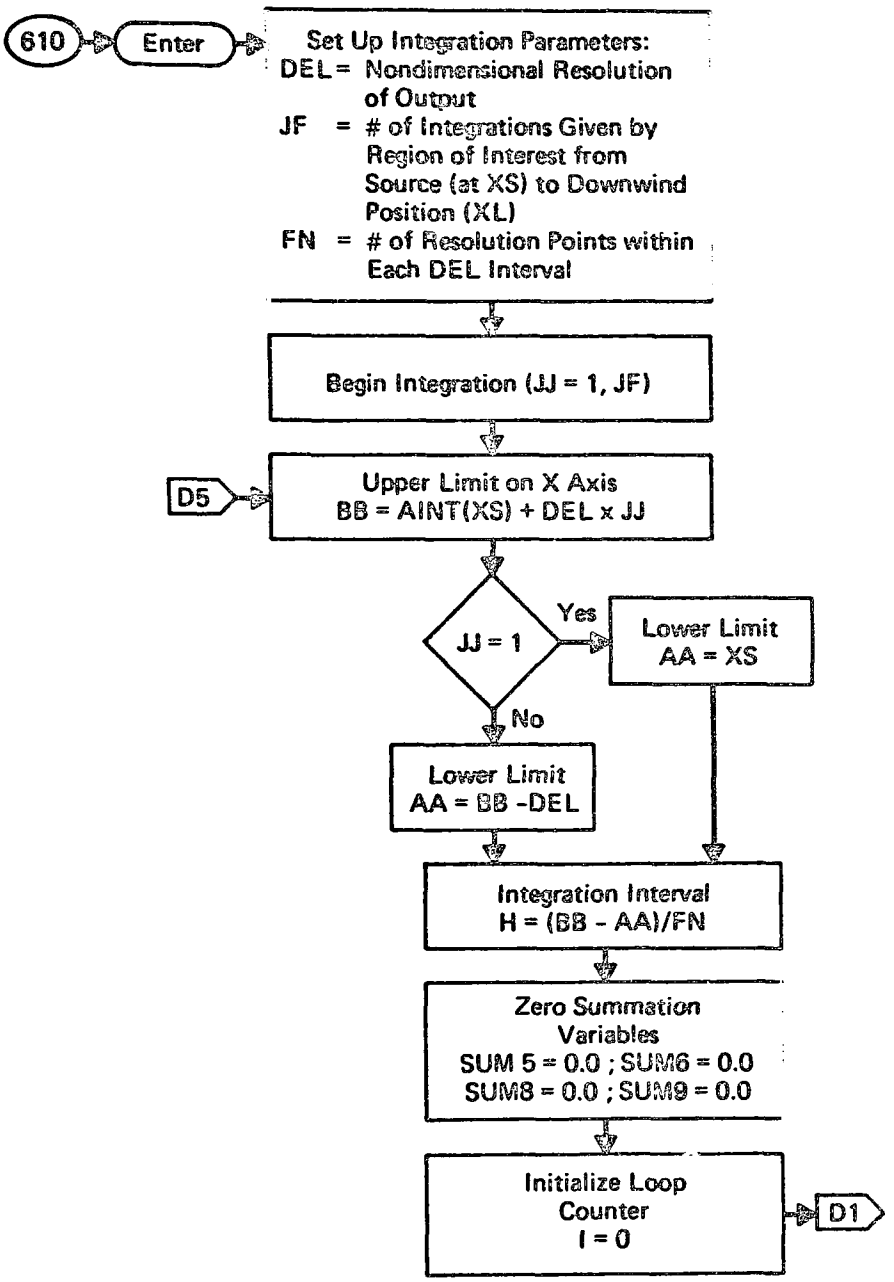

D2. (Continued)

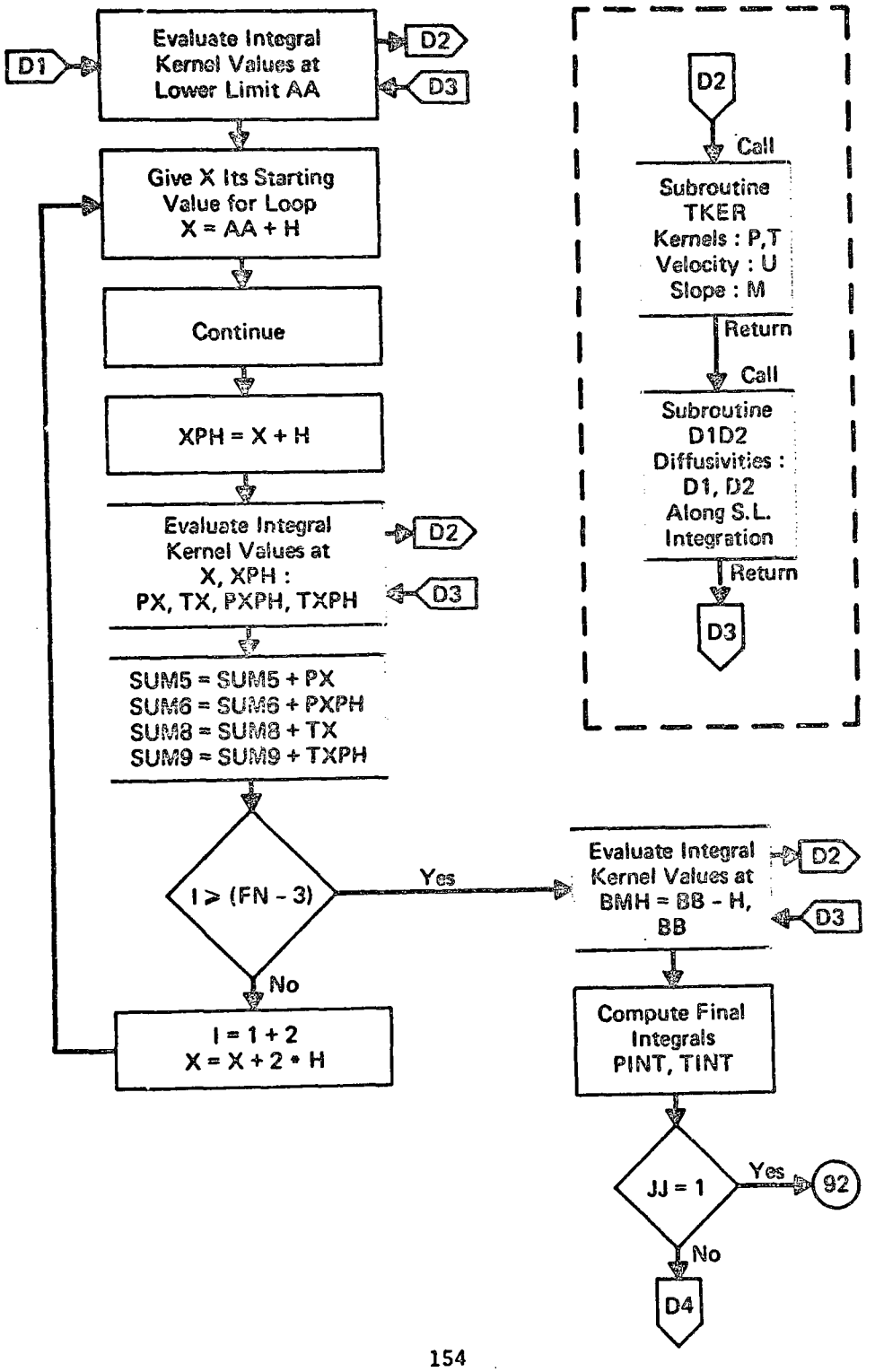

D3. (Continued)

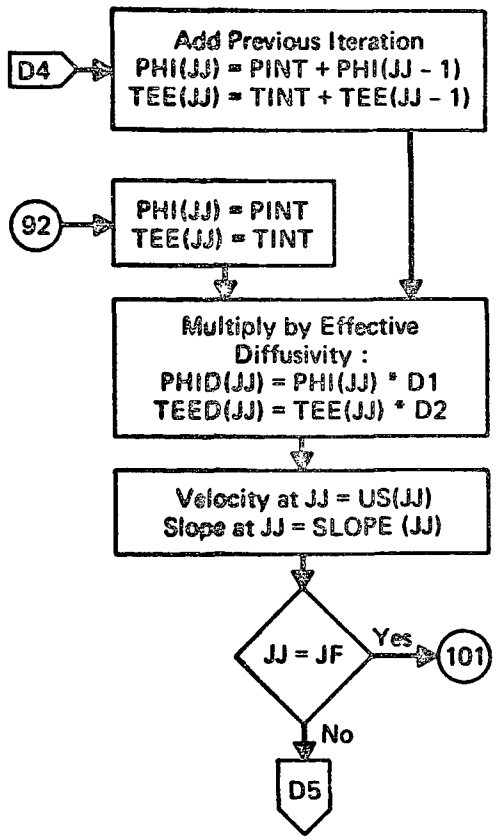

p. D1

E1. Compute Sigmas, Centerline, and Ground-Level Concentrations

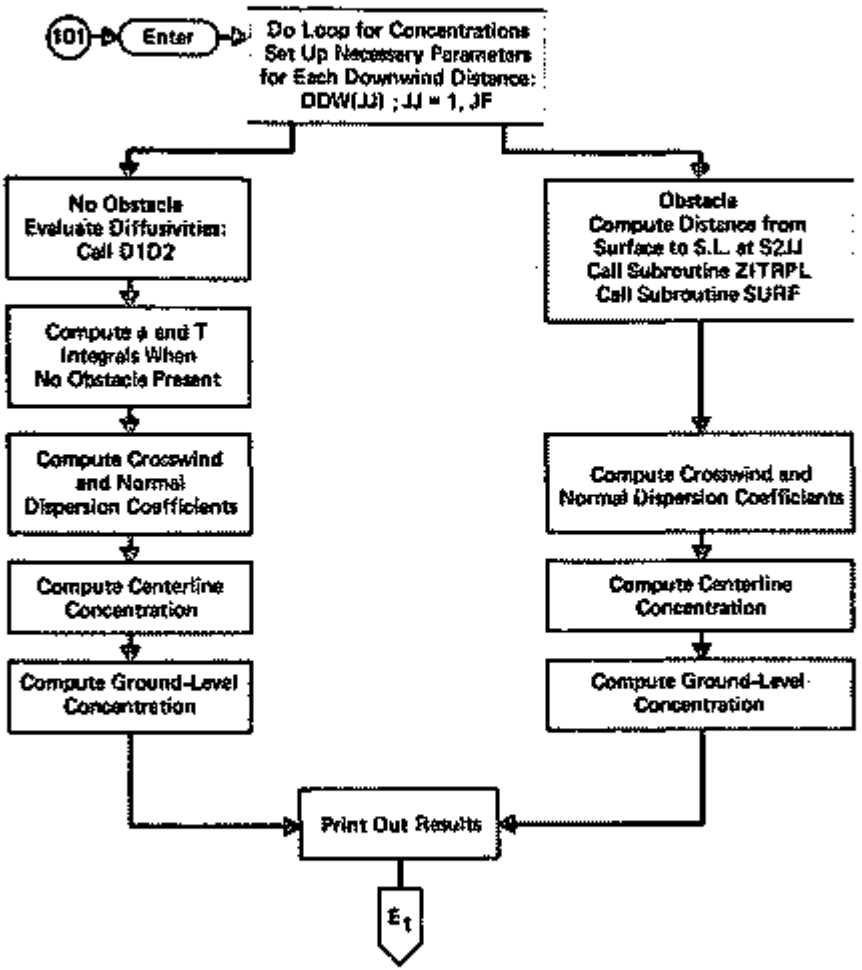

Compute Sigmas, Centerline, and Ground-Level Concentrations (Continued)

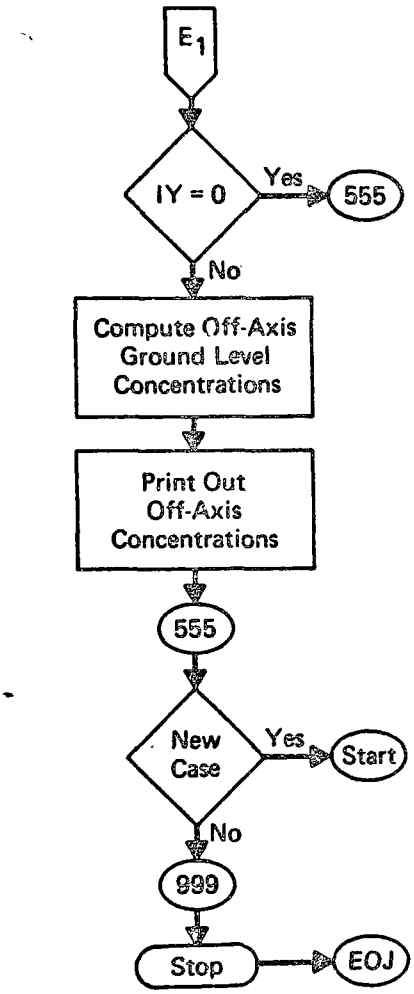

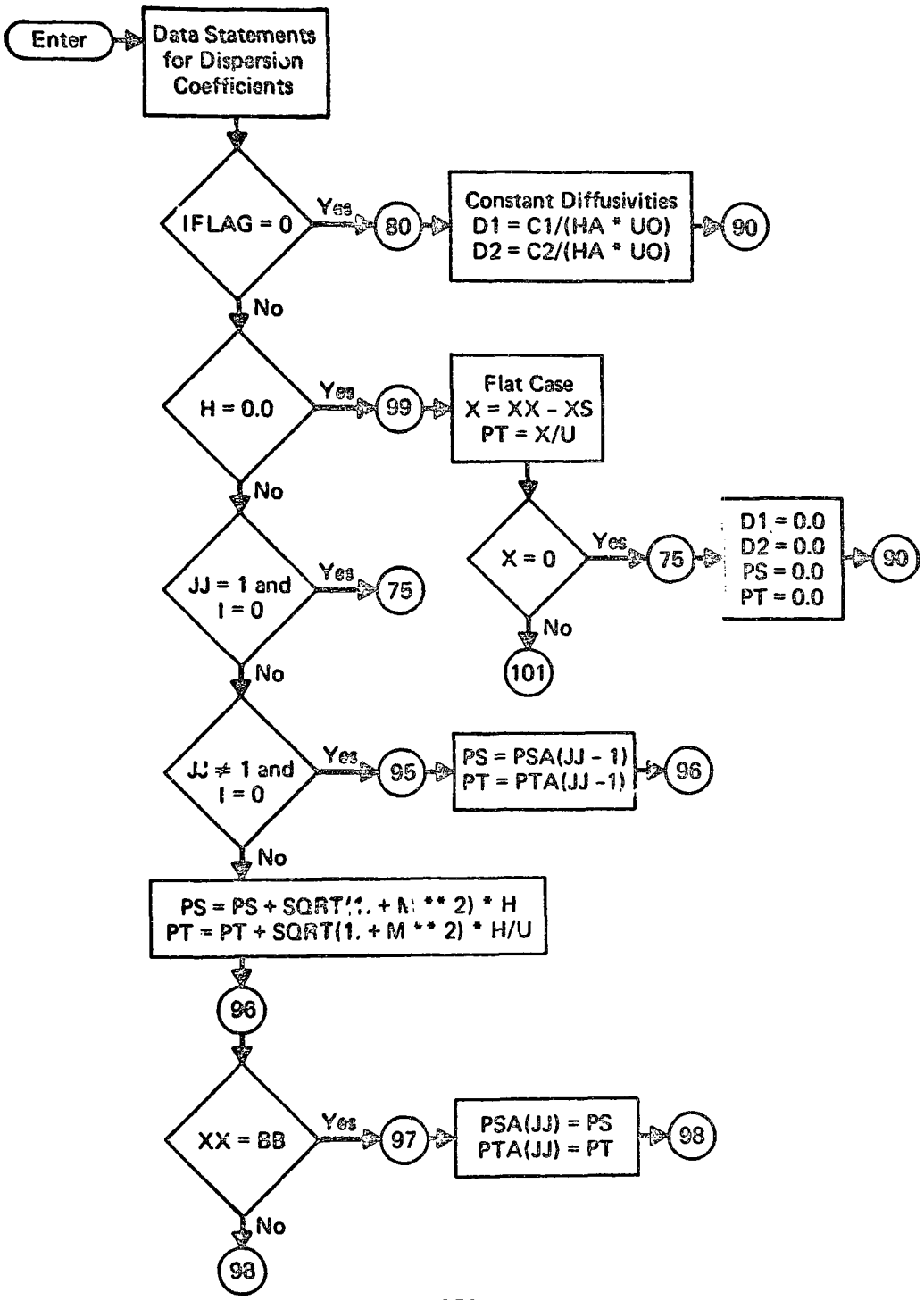
Enter
Data Statements for Dispersion Coefficients
IFLAG = 0
Yes
80
Constant Diffusivities
D1 = C1/(HA * UO)
D2 = C2/(HA * UO)
90
No
H = 0.0
Yes
99
Flat Case
X = XX - XS
PT = X/U
No
X = 0
Yes
75
D1 = 0.0
D2 = 0.0
PS = 0.0
PT = 0.0
90
No
101
JJ = 1 and I = 0
Yes
75
No
JJ ≠ 1 and I = 0
Yes
95
PS = PSA(JJ - 1)
PT = PTA(JJ -1)
96
No
PS = PS + SQRT(1. + M ** 2) * H
PT = PT + SQRT(1. + M ** 2) * H/U
96
XX = BB
Yes
97
PSA(JJ) = PS
PTA(JJ) = PT
98
No
98

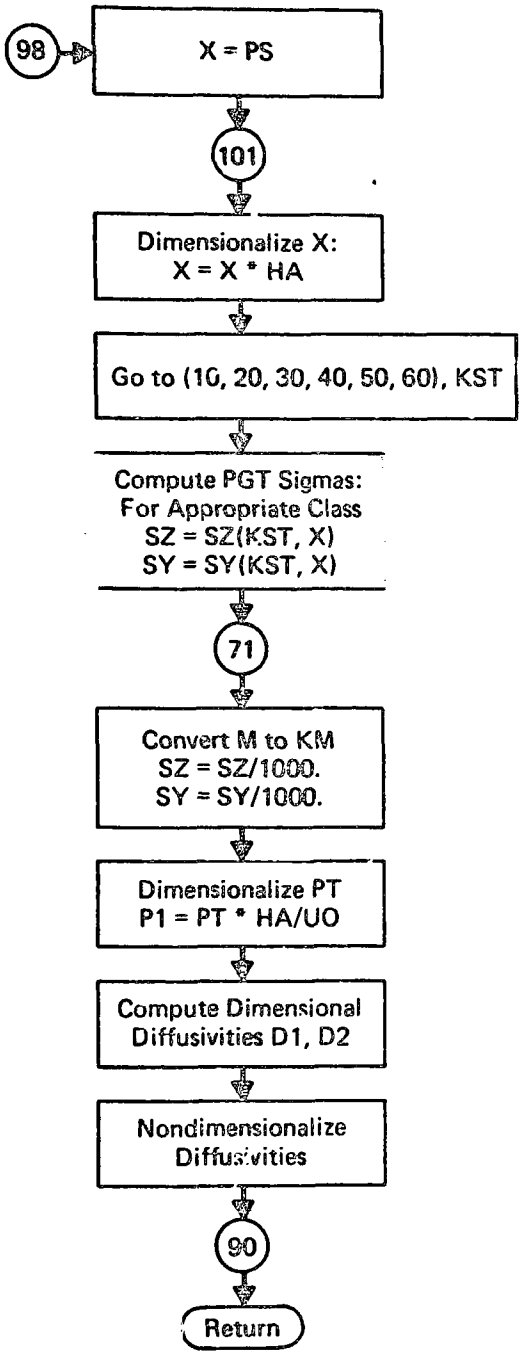
98
X = PS
101
Dimensionalize X:
X = X * HA
Go to (10, 20, 30, 40, 50, 60), KST
Compute PGT Sigmas:
For Appropriate Class
SZ = SZ(KST, X)
SY = SY(KST, X)
71
Convert M to KM
SZ = SZ/1000.
SY = SY/1000.
Dimensionalize PT
P1 = PT * HA/UO
Compute Dimensional
Diffusivities D1, D2
Nondimensionalize
Diffusivities
90
Return

Statement Function PSI2D (X, Z, U, A)

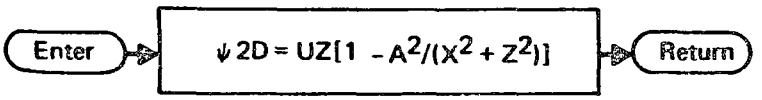

Statement Function PSI3D (X, Z, U, A)

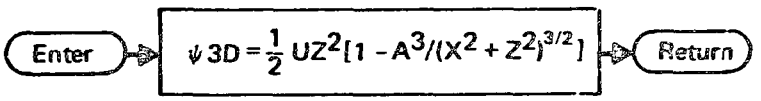

Subroutine TKER (X, Z, A, Y, P, T, RX2, UUU, M, WZ2, WZ3, WV2, WV3)

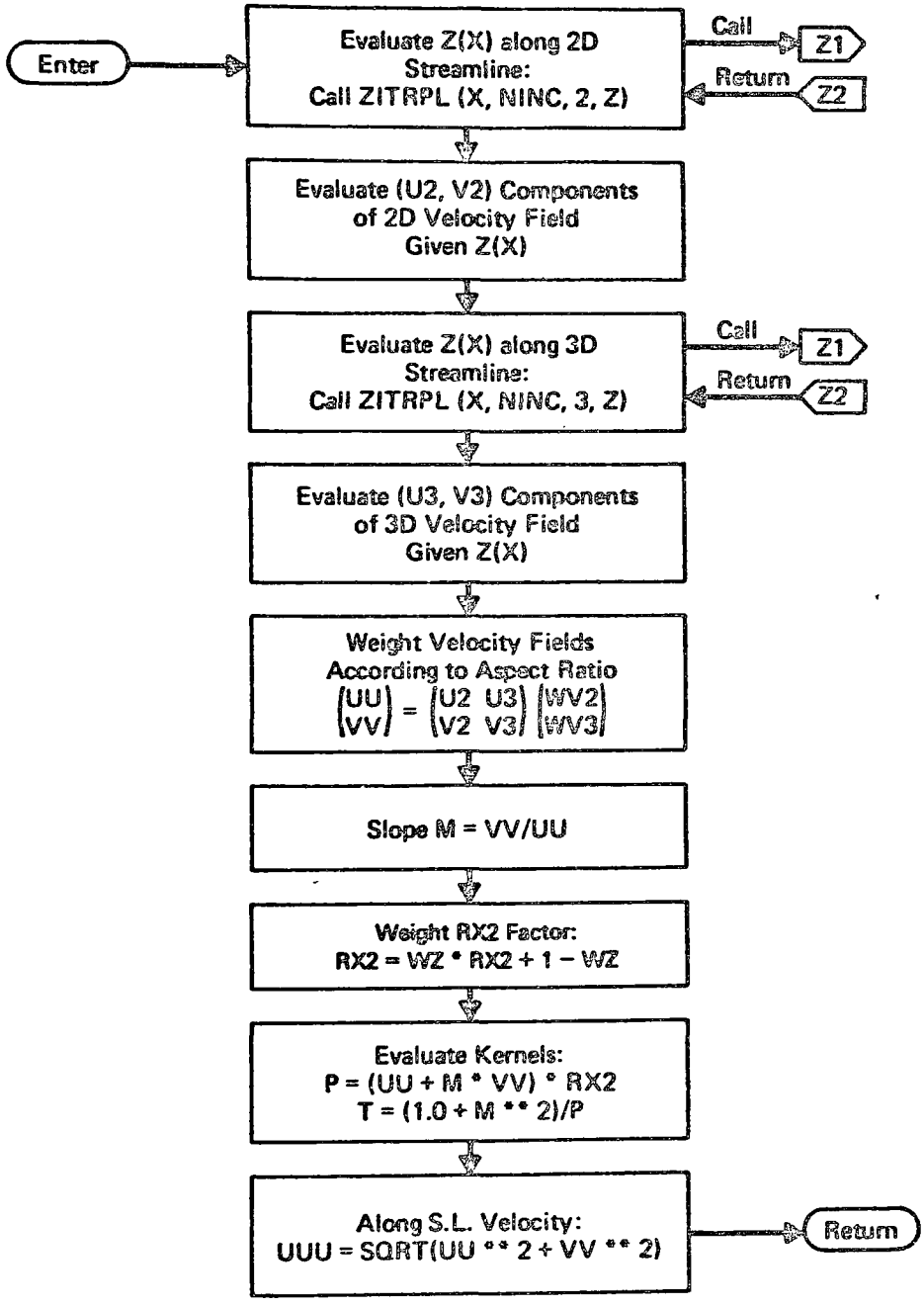

Subroutine SURF (S3, ZEE, SLD, A, ZNS)

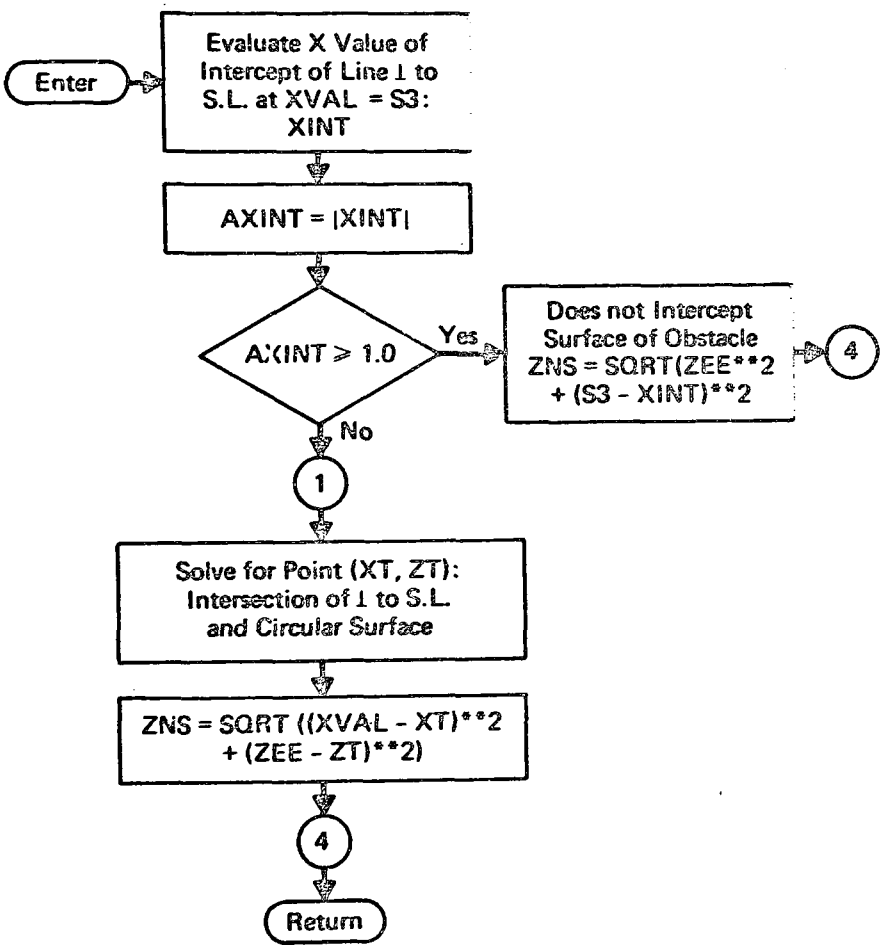

Subroutine ZITRPL (SX, NINC, ND, ZEE)

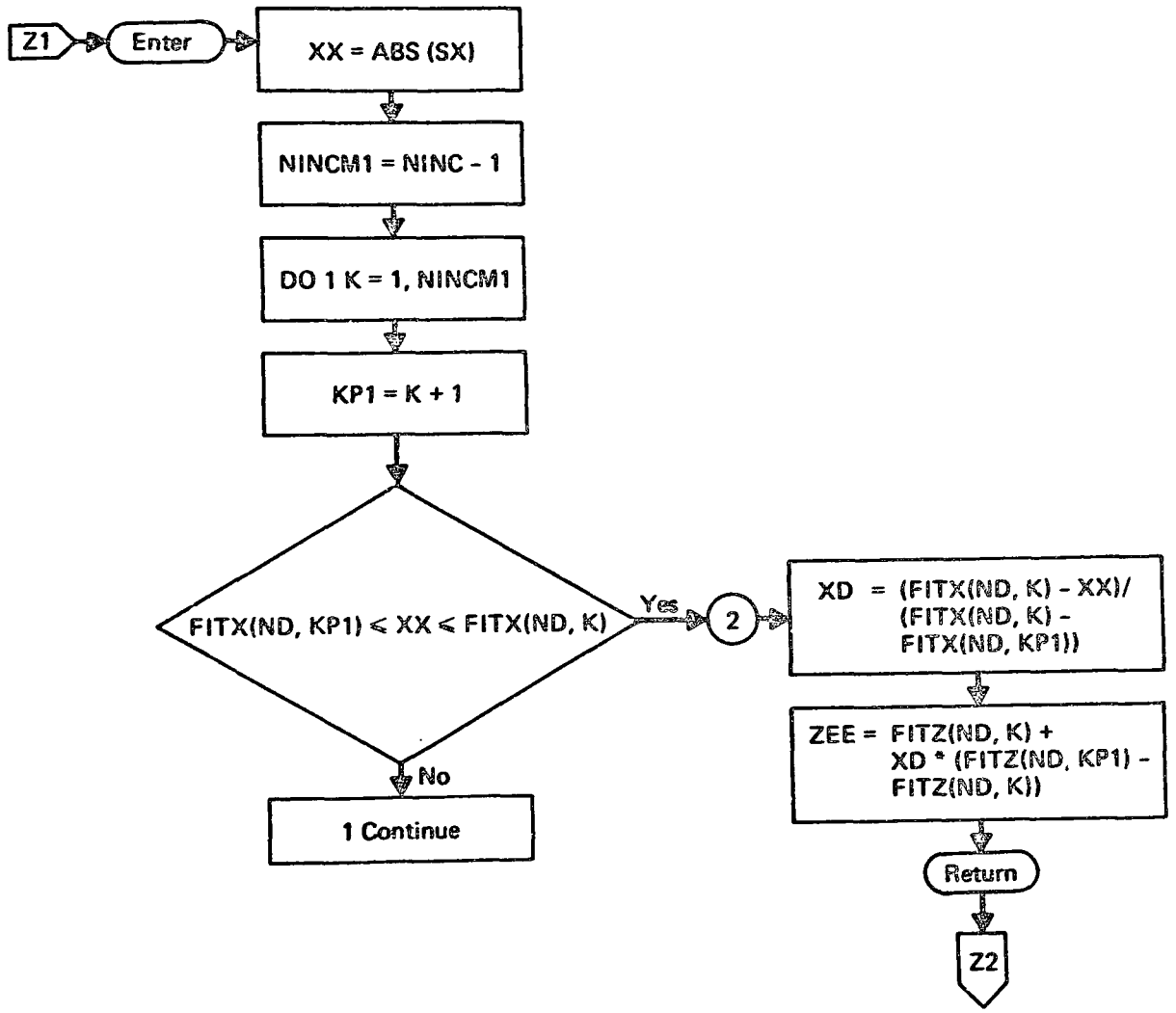

APPENDIX C
SOURCE PROGRAM LISTING

```
//  MSGLEVEL=1,CLASS=B,TIME=20
/*ROUTE  PRINT RMT22
//  EXEC FTG1CLG,REGION.GO=100K,TIME.GO=20,PARM='NOSOURCE,NOMAP'
//FORT.SYSIN DD *
C      ***** ERT MODEL  "CMPLX"  : GAUSSIAN DIFFUSION MODEL, COMPLEX****
C      *****                       TERRAIN.                          ****
C      VERSION UPDATE 2.1 JANUARY 1980
C      ********************************************************************
C      THIS PROGRAM COMPUTES THE POTENTIAL FLOW PARAMETERS OF AN OBSTACL
C      OF ARBITRARY ASPECT RATIO IMBEDDED IN A MEAN FLOW OF VELOCITY UO
C      WITH GIVEN STABILITY CLASS; KST.
C      A TURBULENT PLUME IS IMBEDDED IN THE POTENTIAL FLOW (HUNT AND
C      MULHERN, 1973)
C      ------------------------------------------------------------------
C      R. G. ISAACS, ERT, INC.    1978
C      ------------------------------------------------------------------
C      MODIFICATIONS ACCOUNT FOR WIND TUNNEL DATA FOR INTERMEDIATE
C      ASPECT RATIOS BETWEEN SPHERE(CONE) AND CYLINDER(TRIANGULAR
C      RIDGE).
C      ------------------------------------------------------------------
C      D.G.STRIMAITIS, ERT INC.   1979
C      ------------------------------------------------------------------
C      INPUT PARAMETERS REQUIRED
C      XS     = DISTANCE OF SOURCE UPWIND OF THE CENTER OF THE OBSTACLE (KM)
C      HS     = PLUME HEIGHT (KM)
C      HA     = HEIGHT OF OBSTACLE (KM)
C      XL     = UPWIND DISTANCE OF RECEPTOR FROM CENTER OF OBSTACLE (KM)
C      ALAM   = OBSTACLE ASPECT RATIO
C      DELINT= DOWNWIND RESOLUTION (KM)
C            NOTE: [(XL-XS)/DELINT].LE.50
C      RKST   = PGT STABILITY CLASS (REAL)
C      FROUDE= FROUDE NUMBER (U/NH)
C      ------------------------------------------------------------------
C      OTHER DEFINITIONS
C      UO     = FREE STREAM VELOCITY
C      ND     = DIMENSION (2 OR 3)
C      YS     = DISTANCE OF SOURCE DISPLACEMENT FROM AXIS OF SYMMETRY
C      PSIP   = VALUE OF STREAM FUNCTION AT SOURCE
C      PSI    = STREAM FUNCTION FOR OBSTACLE (PSI2D OR PSI3D)
C      IFLAG = SWITCH CONTROLLING DIFFUSIVITY CALCULATION
C               IFLAG = 1 : DIFFUSIVITY VARIES W/ X; = 0 : CONSTANT
C      D1     = DIFFUSION COEFFICIENT IN 'N' DIRECTION (COMPUTED)
C      D2     = DIFFUSION COEFFICIENT IN 'GAMMA' DIRECTION (COMPUTED)
C      C1     = DIFFUSION COEFFICIENT IN 'N' DIRECTION (CONSTANT)
C      C2     = DIFFUSION COEFFICIENT IN 'GAMMA' DIRECTION (CONSTANT)
C      IY     = SWITCH FOR OFF AXIS CALCULATION;=0(NOT COMPUTED);=1(COMPU
C      ********************************************************************
C
       CALL ERRSET(208,400,-1,1)
C      SPECIFICATION STATEMENTS
       COMMON FITX(3,600),FITZ(3,600)
       COMMON NINC
       COMMON ZC,XS
       DIMENSION PHI(50),TEE(50),US(50),R2S(50)
       DIMENSION PHID(50),TEED(50)
       DIMENSION S2(50),DDW(50),ANS(50),SIGZNH(50),SIGYNH(50),CCLNH(50),
      1CGLNH(50),SIGZH(50),SIGYH(50),CCLH(50),CGLH(50),FNH(50),FH(50)
       DIMENSION FLUXNH(50),FLUXH(50),TFACNH(50),TFACH(50)
       DIMENSION R(20)
       DIMENSION SLOPE(50)
       DIMENSION YD(11),CGL(50,11),YYD(11)
       DIMENSION A0(7),A1(7),A2(7),ZCF(7)
```

```
      REAL MX,MXPH,MA,MB,MBMH
      DATA A0/-0.070,-0.040,-0.042,-0.052,-0.040,-0.533,-0.476/
      DATA A1/0.189,0.105,0.105,0.103,0.052,1.047,0.924/
      DATA A2/0.174,0.185,0.142,0.141,0.173,-0.418,-0.409/
C     ------------------------------------------------------------------
C     FORMAT STATEMENTS
200   FORMAT(8F10.3)
201   FORMAT(10X,8(1PE12.3))
202   FORMAT(10X,I3,4(1PE12.3,5X))
203   FORMAT(2(1PE12.5))
204   FORMAT (1H0,3X,'COEFFS.  = ',1P10E11.4,/,13X,1P10E11.4,/)
205   FORMAT(10X,2(1PE12.5))
206   FORMAT(I1)
207   FORMAT(10X,1PE12.5)
208   FORMAT(30X,I2)
209   FORMAT('1')
210   FORMAT(45X,'DIFFUSION EQUATION SOLUTIONS',/,15X,'SIGMA Z, SIGMA Y
     1PLUME CENTERLINE AND GROUND LEVEL CONCENTRATIONS',/,15X,
     2'FOR AN OBSTACLE OF ARBITRARY ASPECT RATIO',////)
211   FORMAT(10X,'FLOW PARAMETERS ',//,T15,'OBSTACLE HEIGHT =',F5.1,T38,
     1'WIND SPEED = ',F3.1,T60,'SOURCE HEIGHT = ',F4.2,T97,'CROSSWIND DI
     2SP=',F3.1,//,T15,'DIST.  SOURCE FROM OBSTACLE CENTER=',F6.1,T60,
     3'DIST.  OF FINAL RECPTR= ',F5.1,T97,'ASPECT RATIO','=',F4.1,//T15,
     4'VERTICAL DIFFUSIVITY = ',1PE10.3,T60,'CROSSWIND DIFFUSIVITY = ',
     51PE10.3,T97,'KST = ',I3,///)
212   FORMAT(T10,'DISTANCE',T25,'DISTANCE',T40,'DISPLACEMENT',T55,
     1'SIGMA Z',T70,'SIGMA Z',T85,'SIGMA Y',T100,'SIGMA Y',T115,'WIND SP
     2EED',/,
     3T10,'FROM OBSTACLE',T25,'FROM SOURCE',T40,'ABOVE SURF.',T55,'(NO O
     4BSTACLE)',T70,'(OBSTACLE)',T85,'(NO OBSTACLE)',T100,
     5'(OBSTACLE)',/)
213   FORMAT(1X,1P08E15.3)
214   FORMAT(//,T10,'DISTANCE',T25,'DISTANCE',T40,'DISPLACEMENT',T55,
     1'CENTERLINE',T70,'CENTERLINE',T85,'GROUNDLEVEL',T100,'GROUNDLEVEL
     2',/,
     3T10,'FROM OBSTACLE',T25,'FROM SOURCE',T40,'ABOVE SURF.',T55,
     4'CONCENTRATION',T70,'CONCENTRATION',T85,'CONCENTRATION',T100,
     5'CONCENTRATION',/,T55,'(NO OBSTACLE)',T70,'(OBSTACLE)',
     6T85,'(NO OBSTACLE)',T100,'(OBSTACLE)',/)
215   FORMAT(//,T10,'DISTANCE',T25,'MASS FLUX',T40,'MASS FLUX',T55,
     1'RATIO GL/CL',T70,'RATIO GL/CL',T85,'T FACTOR',T100,'T FACTOR',/
     2T10,'FROM OBSTACLE',T25,'(NO OBSTACLE)',T40,'(OBSTACLE)',T55,
     3'(NO OBSTACLE)',T70,'(OBSTACLE)',T85,'(NO OBSTACLE)',
     4T100,'(OBSTACLE)',/)
216   FORMAT(1X,1P07E15.3)
217   FORMAT(45X,'DIFFUSION EQUATION SOLUTIONS',/,15X,'SIGMA Z, SIGMA Y
     1PLUME CENTERLINE AND GROUND LEVEL CONCENTRATIONS',/,15X,
     2'FOR AN OBSTACLE OF ARBITRARY ASPECT RATIO',////)
218   FORMAT(/,T2,'PRINT OUT FITX AND FITZ BEFORE CONSIDERING THE PGT C
     1ASS',//)
219   FORMAT(//,T2,'PRINT OUT FITX AND FITZ AFTER CONSIDERING THE PGT C
     1ASS',//)
220   FORMAT(/,T2,'DOWNWIND',T60,'OFF AXIS DISTANCE',/,
     1T2,'DISTANCE',T12,1P11E10.2,/)
221   FORMAT(2X,1P12E10.2)
222   FORMAT(//,3X,'XS=',F8.1,3X,'HS=',F8.1,3X,'HA=',F8.1,3X,
     1'KST=',I2,//,3X,'ALAM=',F5.1,3X,'FROUDE=',F6.2,3X,'IFLAG=',
     2I2,3X,'IY=',I2,//)
223   FORMAT(//,3X,'PLUME IMPACTS HILL AND DOES NOT GO OVER TOP',/)
224   FORMAT(//,3X,'FROUDE NUMBER CLASS=IFR=',I5,/)
230   FORMAT(15X,'INPUT STREAM CONSTANTS',/)
231   FORMAT(6X,'XS',8X,'HS',8X,'HA',8X,'XL',7X,'ALAM',6X,'DLINT',
     16X,'RKST',6X,'FR')
```

```
C     ------------------------------------------------------------------
C     SPECIFY CONSTANTS
      PI=3.14159
      C1=2.0E-3
      C2=2.0E-3
      YS=0.0
      ROOT=0.0
      AA=0.0
      BB=0.0
      A=1.0
      IFLAG=1
      IY=1
C     ASSUME DIMENSIONLESS VALUE FOR BOTH FREE STREAM VELOCITY UO
C     AND HORIZONTAL WIND SPEED U
      UO=1.0
      U=1.0
555   READ(5,200,END=999) XS,HS,HA,XL,ALAM,DELINT,RKST,FROUDE
      WRITE(6,230)
      WRITE(6,231)
      WRITE(6,200) XS,HS,HA,XL,ALAM,DELINT,RKST,FROUDE
      KST=RKST
      IF(FROUDE.EQ.0.0) KST=4
      IF(FROUDE.EQ.0.0) FROUDE=999.
      WRITE(6,222) XS,HS,HA,KST ALAM,FROUDE,IFLAG,IY
C     ------------------------------------------------------------------
C     DEFINE RELEVANT DIMENSIONLESS RATIOS
      HS=HS/HA
      XS=XS/HA
      XL=XL/HA
C     ------------------------------------------------------------------
C     ******************************************************************
C     COMPUTE STREAMLINE AND VELOCITY FIELD WEIGHTING FACTORS FOR
C     NEUTRAL FLOW BASED ON ASPECT RATIO,ALAM
C     WZ    = COMBINED STREAMLINE WEIGHTING
C     SUP   = SPEED UP FACTOR
C     WV2   = 2D VELOCITY WEIGHTING
C     WV3   = 3D VELOCITY WEIGHTING
C     IF(ALAM.EQ.1.0) FLOW IS 3D AXIALLY SYMMETRIC HILL
C     IF(ALAM.GE.10.0) FLOW IS 2D CIRCULAR RIDGE
      IF(ALAM.LE.1.0) GO TO 601
      IF (ALAM.GE.10.0) GO TO 602
C     HEIGHT
      WZ=1.0/ALAM**1.1
C     VELOCITIES
      BETA= 1.0+ 1.0/(ALAM**2-1.0) -ALAM*ALOG(ALAM+SQRT(ALAM**2-1.0))/
     1(ALAM**2-1.0)**1.5
      SUP=2.0/(2.0-BETA)
      WV2=2.0*(SUP-1.5)
      WV3=2.0*(2.0-SUP)
      GO TO 603
601   WZ=1.0
      WV2=0.0
      WV3=1.0
      GO TO 603
602   WZ=0.0
      WV2=1.0
      WV3=0.0
603   CONTINUE
      WRITE(6,200) WZ,WV2,WV3
C     ******************************************************************
C     THIS SECTION CALCULATES BOTH 2D AND 3D STREAMLINE THROUGH
C     SOURCE GIVEN XS,HS,AND HA
C     PSIP2D= VALUE OF STREAMFUNCTION ALONG STREAMLINE IN 2D FLOW
```

```
C     PSIP3D= VALUE OF STREAMFUNCTION ALONG STREAMLINE IN 3D FLOW
C     STREAMLINE EQUATION IN EACH CASE EVALUATED BY SOLVING:
C     PSI2D(X,Z) = PSIP2D OR
C     PSI3D(X,Z) = PSIP3D
C     ------------------------------------------------------------------
C     NEUTRAL STREAMLINE STORED AS:
C     X      = FITX(ND,II)
C     Z      = FITZ(ND,II)
C     ND     = 2 OR 3 (2D OR 3D)
C     ------------------------------------------------------------------
      DO 604 ND=2,3
C     ------------------------------------------------------------------
C     DEFINE STREAM FUNCTION,VALUE THROUGH SOURCE,  AND B
      IF(ND.GT.2) GO TO 1
      PSIP=PSI2D(XS,HS,U,A)
      B=PSIP/U
      GO TO 2
1     PSIP=PSI3D(XS,HS,U,A)
      B=2.0*PSIP/U
2     WRITE(6,203) B,PSIP
C     ------------------------------------------------------------------
C     COMPUTE ZC = Z DISPLACEMENT OF SOURCE STREAMLINE OVER CREST OF HI
      IF(ND.GT.2) GO TO 3
      ZC=.5*(B+SQRT(B**2+4.0*A**2))
      GO TO 4
C       SOLVE CUBIC EQN FOR 3D ZC
3     RADCL=(A**6/4. )-(B**3/27. )
      IF(RADCL)  310,320,330
310   THTA=(ARCOS((.5*A**3)/(B/3. )**1.5))/3.
      EM=2. *SQRT(B/3. )
      ZC=EM*COS(THTA)
C     SECOND AND THIRD SOLNS LESS THAN ZERO
      ROOT=-1.
      GO TO 4
320   ZC=1.5874*A
      ROOT=0.
      GO TO 4
330   AA=(.5*A**3+SQRT(RADCL))**(1./3. )
      BB=(.5*A**3-SQRT(RADCL))**(1./3. )
      ZC=AA+BB
      ROOT=1.
4     BETA=(ZC-A)/A
C     ------------------------------------------------------------------
C     DEFINE X IN TERMS OF Z FOR CURVE FIT Z(X)
C     NINC IS THE TOTAL NUMBER OF POINTS TAKEN FOR THE FIT
C     INC2 IS THE NUMBER OF THESE POINTS IN THE REGION AWAY FROM THE HI
C     WHERE THE SLOPE IS DECREASING.
C     THESE CARDS CONTROL THE GOODNESS OF THE FIT
C     H1 IS THE VALUE OF THE STREAMLINE DISPLACEMENT AT INFINITY
C     B IS TWICE THE VALUE OF THE STREAM FUNCTION AT ANY X VALUE
C     ------------------------------------------------------------------
      NINC=550
      INC2=150
      H1=SQRT(B)
      IF(ND EQ.2) H1=H1*H1
      NINCMI=NINC-INC2
      HLFPT=0.5*(ZC+HS)
      ZINC2=(HLFPT-H1)/INC2
      ZINC1=(ZC-HLFPT)/NINCMI
      WRITE(6,201) PSIP,B,ROOT,AA,BB,ZC,BETA,H1
      NINC=NINC+1
      DO 100 I=1,NINC
      IF(I.GT.INC2) GO TO 9
```

```
      J=I-1
      ZZ=H1+J*ZINC2
      GO TO 10
9     J=I-INC2-1
      ZZ=HLFPT+J*ZINC1
10    CONTINUE
      IF(ND.GT.2) GO TO 5
      IF(ZZ.EQ.H1) GO TO 61
      ARG=   ((ZZ*(ZZ*(B-ZZ)+A**2))/(ZZ-B))
      GO TO 6
5     IF(ZZ.EQ.H1) GO TO 61
      ARG=   ((A**3/(1.0-B/ZZ**2))**(2.0/3.0)-ZZ**2)
6     IF(ARG.LT.0.0) GO TO 7
      XX=SQRT(ARG)
      GO TO 8
C     XX    = 100.  TAKEN AS EFFECTIVE INFINITY
61    XX=100.
      GO TO 8
7     XX=0.0
      ZZ=ZC
8     CONTINUE
      II=I
      FITZ(ND,II)=ZZ
      FITX(ND,II)=XX
      FITX(ND,NINC)=0.00
100   CONTINUE
604   CONTINUE
C     ***************************************************************************
C     WRITE(6,218)
C     THIS LOOP (DO 605) WEIGHTS THE NEUTRAL STREAMLINE WITH
C     ASPECT RATIO USING WZ
      DO 605 II=1,NINC
      XX=FITX(3,II)
      FITX(1,II)=XX
C     ZITRPL= SUBROUTINE PROVIDES Z INTERPOLATION FOR ANY X VALUE
C             GIVEN STREAMLINE IN FITX(ND,II),FITZ(ND,II) ARRAYS
      CALL ZITRPL(XX,NINC,2,ZEE2)
      FITZ(1,II)=ZEE2*(1.0-WZ)+FITZ(3,II)*WZ
C     WRITE(6,200)  FITX(1,II),FITZ(1,II),FITX(2,II),FITZ(2,II),FITX(3,
C    1I),FITZ(3,II)
605   CONTINUE
C     ***************************************************************************
C     FIRST ORDER EFFECT OF STABILITY TAKEN AS DEPRESSION OF STREAMLINE
C     BELOW THAT EXPECTED IN NEUTRAL FLOW
C     SCALING OF NEUTRAL STREAMLINE DETERMINED BY EXPERIMENT
C     ---------------------------------------------------------------------------
      IF(FROUDE.GE.900.) GO TO 610
      IF(FROUDE.GE.1.50.AND.FROUDE.LT.900.) IFR=1
      IF(FROUDE.GE.1.10.AND.FROUDE.LT.1.50) IFR=2
      IF(FROUDE.GE.0.92.AND.FROUDE.LT.1.10) IFR=3
      IF(FROUDE.GE.0.83.AND.FROUDE.LT.0.92) IFR=4
      IF(FROUDE.GE.0.70.AND.FROUDE.LT.0.83) IFR=5
      IF(FROUDE.GE.0.40.AND.FROUDE.LT.0.70) IFR=6
      IF(FROUDE.LT.0.40                   ) IFR=7
      IF(IFR.LE.5.AND.HS.LT.0.375         ) WRITE(6,223)
      IF(IFR.EQ.6.AND.HS.LT.0.75          ) WRITE(6,223)
      IF(IFR.EQ.7.AND.HS.LT.0.82          ) WRITE(6,223)
      WRITE(6,224) IFR
C     CALCULATE THE TOW-TANK ZC AND CHECK THAT IT EXCEEDS THE HILL HEIGHT
      ZCF(IFR)=1.+(A0(IFR)+A1(IFR)*HS+A2(IFR)*HS**2)
      IF(ZCF(IFR).LT.1.) ZCF(IFR)=1.001
      DELMAX=FITZ(3,NINC)-ZCF(IFR)
      DO 606 II=1,NINC
```

```
      XX=FITX(3,II)
      IF(ABS(XX).GE.2.) GO TO 606
      DELTA3=DELMAX*(2.-ABS(XX))/2.
      FRAC3=(FITZ(3,II)-DELTA3)/FITZ(3,II)
      FITZ(1,II)=FITZ(1,II)*FRAC3
      XX=FITX(2,II)
      IF(ABS(XX).GE.2.) GO TO 608
      DELTA2=DELMAX*(2.-ABS(XX))/2.
      FRAC2=(FITZ(2,II)-DELTA2)/FITZ(2,II)
      FITZ(2,II)=FITZ(2,II)*FRAC2
608   FITZ(3,II)=FITZ(3,II)-DELTA3
606   CONTINUE
610   CONTINUE
C     WRITE(6,219)
C     DO 609 II=1,NINC
C     WRITE(6,200)  FITX(1,II),FITZ(1,II),FITX(2,II),FITZ(2,II),FITX(3,
C    1I),FITZ(3,II)
609   CONTINUE
C     ***************************************************************
C     PERFORM ALONG STREAMLINE LINE INTEGRAL
C     ---------------------------------------------------------------
C     BEGIN CALCULATIONS AS A FUNCTION OF DISTANCE FROM SOURCE
C     DELINT= DIMENSIONAL DOWNWIND RESOLUTION
C     DEL   = DOWNWIND RESOLUTION OF OUTPUT IN FRACTIONAL OBSTACLE HEIG
C     NN    = NUMBER OF RESOLUTION ELEMENTS ALONG STREAMLINE
C     TKER  = SUBROUTINE RETURING VELOCITY FIELD AND INTEGRAL KERNEL AT
C               GIVEN X
C     D1D2  = SUBROUTINE RETURNING EITHER CONSTANT DIFFUSIVITIES OR
C               PGT SCALED DIFFUSIVITIES AT GIVEN X
C     PHID  = LINE INTEGRAL DETERMINING DISPERSION NORMAL TO STREAMLINE
C     TEED  = LINE INTEGRAL DETERMINING DISPERSION IN CROSSWIND DIRECTI
C     US    = ALONG STREAMLINE VELOCITY
C     SLOPE = ALONG STREAMLINE SLOPE
C     ---------------------------------------------------------------
      DEL=DELINT/HA
      JF=AINT((XL-XS)/DEL)
      DO 101 JJ=1,JF
      SS=AINT(XS)+JJ*DEL
      IF(ABS(SS).LT.(DEL/2.0)) SS=0.0
      S2(JJ)=SS
C     ---------------------------------------------------------------
C     INTEGRATE FOR EFFECTIVE SIGMA Y AND Z SQUARED
C     NUMERICAL INTEGRATION BY SIMPSONS RULE
C     ADAPTED FROM DORN AND MCCRACKEN 1972
C     SET UP INTEGRATION PARAMETERS
C     ---------------------------------------------------------------
      NN=100
      FN=NN
      AA=SS-DEL
      IF(JJ EQ.1) AA=XS
      BB=SS
      H=(BB-AA)/FN
      TWOH=2.0*H
      Y=YS/HS
      SUM5=0.0
      SUM6=0.0
      SUM8=0.0
      SUM9=0.0
      I=0
      CALL TKER(AA,ZA,A,Y,PA,TA,RA,UA,MA,WZ,WV2,WV3)
      CALL D1D2(KST,UA,AA,D1,D2,XS,IFLAG,C1,C2,MA,H,JJ,I,BB,HA,UG)
C     GIVE X ITS STARTING VALUE FOR LOOP
      X=AA+H
```

```
C       INITIALIZE LOOP COUNTER
        I=1
C       BEGIN INTEGRATION
25      CONTINUE
        XPH=X+H
        CALL TKER(X,ZX,A,Y,PX,TX,RX,UX,MX,WZ,WV2,WV3)
        CALL TKER(XPH,ZXPH,A,Y,PXPH,TXPH,RXPH,UXPH,MXPH,WZ,WV2,WV3)
        CALL D1D2(KST,UX,  X,D1,D2,XS,IFLAG,C1,C2,MX,H,JJ,I,BB,HA,UO)
        CALL D1D2(KST,UXPH,XPH,D1,D2,XS,IFLAG,C1,C2,MXPH,H,JJ,I,BB,HA,UO)
        SUM5=SUM5+PX
        SUM6=SUM6+PXPH
        SUM8=SUM8+TX
        SUM9=SUM9+TXPH
        IF(I.GE.(NN-3)) GO TO 28
        I=I+2
        X=X+TWOH
        GO TO 25
C       EVALUATE INTEGRALS
28      BMH=BB-H
        CALL TKER(BB,ZB,A,Y,PB,TB,RB,UB,MB,WZ,WV2,WV3)
        CALL TKER(BMH,ZBMH,A,Y,PBMH,TBMH,RBMH,UBMH,MBMH,WZ,WV2,WV3)
        CALL D1D2(KST,UBMH,BMH,D1,D2,XS,IFLAG,C1,C2,MBMH,H,JJ,I,BB,HA,UO)
        CALL D1D2(KST,UB,BB,D1,D2,XS,IFLAG,C1,C2,MB,H,JJ,I,BB,HA,UO)
        PINT=H/3.0*(4.0*SUM5+2.0*SUM6+PA+PBMH*4.0+PB)*U
        TINT=H/3.0*(4.0*SUM8+2.0*SUM9+TA+4.0*TBMH+TB)/U
C       WRITE(6,205) PINT,TINT
        IF(JJ.EQ.1) GO TO 92
        PHI(JJ)=PINT+PHI(JJ-1)
        TEE(JJ)=TINT+TEE(JJ-1)
        TEED(JJ)=TEE(JJ)*D2
        PHID(JJ)=PHI(JJ)*D1
        GO TO 93
92      TEE(JJ)=TINT
        PHI(JJ)=PINT
        PHID(JJ)=PHI(JJ)*D1
        TEED(JJ)=TEE(JJ)*D2
93      CONTINUE
        US(JJ)=UB*U
        R2S(JJ)=RB
        SLOPE(JJ)=MB
21      CONTINUE
101     CONTINUE
C       ***********************************************************************
C       COMPUTE SIGMAS, CENTERLINE AND GROUND LEVEL CONCENTRATIONS
C       WITH THE OBSTACLE AND WITHOUT THE OBSTACLE AS A FUNCTION OF
C       DOWNWIND DISTANCE
C       -----------------------------------------------------------------------
C       FLAT TERRAIN VALUES
C       DDW    = DOWNWIND DISTANCE FROM SOURCE
C       SIGZNH= NORMAL DISPERSION COEFFICIENT (NO OBSTACLE)
C       SIGYNH= CROSSWIND DISPERSION COEFFICIENT (NO OBSTACLE)
C       CCLNH = CONCENTRATION , CENTERLINE (NO OBSTACLE)
C       CGLNH = CONCENTRATION , GROUNDLEVEL (NO OBSTACLE)
C       TFACNH= T FACTOR (NO OBSTACLE)
C               ((IDENTICALLY UNITY))
C       -----------------------------------------------------------------------
C       VALUES WITH OBSTACLE PRESENT
C       SIGZH = NORMAL DISPERSION COEFFICIENT (OBSTACLE)
C       SIGYH = CROSSWIND DISPERSION COEFFICIENT (OBSTACLE)
C       CCLH  = CONCENTRATION, CENTERLINE (OBSTACLE)
C       CGLH  = CONCENTRATION, GROUNDLEVEL (OBSTACLE)
C       TFACH = T FACTOR (OBSTACLE)
C       -----------------------------------------------------------------------
```

```
      DO 102 JJ=1,JF
      DDW(JJ)=S2(JJ)-XS
C     EVALUATION : NO OBSTACLE (NH)
      P=PHID(JJ)
      T=TEED(JJ)
      U1=US(JJ)
      R2=R2S(JJ)
      U2R2=R2*U1*U1
      S2JJ=S2(JJ)
      CALL D1D2(KST,U,S2JJ,D1,D2,XS,IFLAG,C1,C2,0.0,0.0,0.0,0.0,0.0,HA,U0)
      PHINH=D1*HS**2*U*DDW(JJ)
      TEENH=D2*DDW(JJ)/(U*HS**2)
      SIGZNH(JJ)=SQRT(2.0*PHINH/(U**2*HS**2))
      SIGYNH(JJ)= SQRT(2.0*HS**2*TEENH)
      CCLNH(JJ)=(1.0/(4.0*PI*SQRT(PHINH*TEENH)))
      ARG3=HS**2/(2.0*(SIGZNH(JJ))**2)
      IF(ARG3.GE.179.5 ) GO TO 70
      CGLNH(JJ)=CCLNH(JJ)*EXP(-ARG3)
      CGLNH(JJ)=2.0*CGLNH(JJ)
      GO TO 71
70    CGLNH(JJ)=1.1E-78
71    CONTINUE
C     ------------------------------------------------------------------
C     EVALUATION : OBSTACLE (H)
      SIGZH(JJ)=SQRT(2.0*P/U2R2)
      SIGYH(JJ)=SQRT(2.0*R2*T)
C     COMPUTE DISTANCE FROM SPHERE SURFACE ANS
      S3=S2(JJ)
      IF(S3.EQ.0.0) GO TO 17
C     CORRECTION FOR FIT MADE OVER HILL BY INTERPOLATING FROM EXACT S.F
      IF(ABS(S3).GT.(2.0*A)) GO TO 75
      CALL ZITRPL(S3,NINC,1,ZEE)
      GO TO 76
75    CALL ZITRPL(S3,NINC,1,ZEE)
76    SLO=SLOPE(JJ)
C     SURF  = SUBROUTINE RETURNS DISTANCE ALONG NORMAL TO STREAMLINE
C             FROM SURFACE
      CALL SURF(S3,ZEE,SLO,A,ZNS)
      ANS(JJ)=ZNS
      GO TO 18
17    ANS(JJ)=FITZ(1,NINC)-A
 18   CONTINUE
      ARG2=(U2R2*(ANS(JJ))**2/P)
      IF((2.0*ARG2).GE.179.5) GO TO 72
      IF(ALAM.GE.10.) GO TO 72
      CCLH(JJ)=(1.0+EXP(-ARG2          ))/(4.0*PI*SQRT(P*T))
      CGLH(JJ)=(1.0+EXP(-2.0*ARG2 ))*(EXP(-ARG2/4.0          ))/(4.0*
     1PI*SQRT(P*T))
      CGLH(JJ)=2.0*CGLH(JJ)
      GO TO 73
72    CCLH(JJ)=1.0/(4.0*PI*SQRT(P*T))
      IF((ARG2/4.).GT.179.5) GO TO 77
      CGLH(JJ)=(EXP(-ARG2/4.0))/(4.0*PI*SQRT(P*T))
      CGLH(JJ)=2.0*CGLH(JJ)
      GO TO 73
77    CGLH(JJ)=1.1E-78
73    CONTINUE
      FNH(JJ)=CGLNH(JJ)/CCLNH(JJ)
      FH(JJ)=CGLH(JJ)/CCLNH(JJ)
      IF(FH(JJ).LT.3.0E-76) FH(JJ)=3.0E-76
      IF(FNH(JJ).LT.3.0E-76) FNH(JJ)=3.0E-76
      FLUXNH(JJ)=U*SIGZNH(JJ)*SIGYNH(JJ)*CCLNH(JJ)
      FLUXH(JJ)=US(JJ)*SIGZH(JJ)*SIGYH(JJ)*CCLH(JJ)
```

```
      TFACNH(JJ)=SIGZNH(JJ)*SQRT(2.0*ALOG(2.0/FNH(JJ)))/HS
      TFACH(JJ)=SIGZNH(JJ)*SQRT(2.0*ALOG(2.0/FH(JJ)))/HS
102   CONTINUE
C     ------------------------------------------------------------------
C     PRINT OUT RESULTANT ARRAYS OF SIGMAS AND CONCENTRATIONS
      WRITE(6,209)
      WRITE(6,210)
      WRITE(6,211) HA,UO,HS,YS,XS,XL,ALAM,D1,D2,KST
      WRITE(6,212)
      WRITE(6,213) (S2(JJ),DDW(JJ),ANS(JJ),SIGZNH(JJ),SIGZH(JJ),
     1SIGYNH(JJ),SIGYH(JJ),US(JJ),JJ=1,JF)
      WRITE(6,214)
      WRITE(6,216) (S2(JJ),DDW(JJ),ANS(JJ),CCLNH(JJ),CCLH(JJ),
     1CGLNH(JJ),CGLH(JJ), JJ=1,JF )
      WRITE(6,215)
      WRITE(6,216) (S2(JJ),FLUXNH(JJ),FLUXH(JJ),FNH(JJ),FH(JJ),TFACNH(J
     1),TFACH(JJ),JJ=1,JF)
      IF(IY.EQ. 0) GO TO 555
      WRITE(6,209)
      DO 903 JJ=1,JF
      DO 904 K=1,11
      YYD(K)=K*.1
      YD(K)=YYD(K)/SIGYH(JJ)
      CGL(JJ,K)=CGLH(JJ)*EXP(-0.5*YD(K)**2)
904   CONTINUE
903   CONTINUE
      WRITE(6,220)(YYD(K),K=1,11)
      DO 906 JJ=1,JF
      WRITE(6,221)(DDW(JJ),(CGL(JJ,K),K=1,11))
906   CONTINUE
      GO TO 555
999   STOP
      END
      SUBROUTINE D1D2(KST,U,XX,D1,D2,XS,IFLAG,C1,C2,M,H,JJ,I,BB,HA,UO)
C     THIS SUBROUTINE EVALUATES THE DIMENSIONLESS DIFFUSIVITIES D1 AND
C     D2 IN THE Z AND Y DIRECTIONS ,RESPECTIVELY
      REAL M
      DIMENSION PSA(50),PTA(50)
      DIMENSION XD(5),AD(6),BD(6)
      DIMENSION XA(7),XB(2),XE(8),XF(9),AA(8),BA(8),AB(3),B1(3),
     1AE(9),BE(9),AF(10),BF(10)
      DATA XA/.5,.4,.3, 25,.2,.15, 1/
      DATA XB/.4,.2/
      DATA XD/30.,10.,3.,1.,.3/
      DATA XE/40.,20.,10.,4.,2.,1.,.3,.1/
      DATA XF/60.,30.,15.,7.,3.,2 ,1.,.7,.2/
      DATA AA/ 453.85,346.75,258.89,217.41,179 52,170.22,158.08,122.8/
      DATA BA/2.1166,1.7283,1.4094,1.2644,1.1262,1.0932,1.0542,.9447/
      DATA AB/109.30,98.483,90.673/
      DATA B1/1.0971,0.98332,0.93198/
      DATA AD/44.053,36.650,33.504,32.093,32.093,34.459/
      DATA BD/0.51179,0.56589,0.60486,0.64403,0.81066,0.86974/
      DATA AE/47.618,35.420,26.970,24.703,22.534,21 628,21.628,23.331,
     1 24.26/
      DATA BE/0.29592,0.37615,0.46713,0.50527,0 57154,0.63077,0 75660,
     1 0.81956,0.8366/
      DATA AF/34 219,27.074,22.651,17.836,16.187,14 823,13.953,13 953,
     1 14.457,15.209/
      DATA BF/0.21716,0.27436,0.32681,0.41507,0 46490,0 54503,0 63227
     1 0.68465,0.78407,0.81558/
      IF(IFLAG.EQ.0) GO TO 80
      IF(H.EQ.0.0) GO TO  99
      IF(JJ.EQ.1.AND.I.EQ 0) GO TO 75
```

```
      IF(JJ.NE.1.AND.I.EQ.0) GO TO 95
      PS=PS+SQRT(1.0+M**2)*H
      PT=PT+SQRT(1.0+M**2)*H/U
      GO TO 96
95    PS=PSA(JJ-1)
      PT=PTA(JJ-1)
96    CONTINUE
      IF(XX.EQ.BB) GO TO 97
      GO TO 98
97    PSA(JJ)=PS
      PTA(JJ)=PT
98    CONTINUE
      X=PS
      GO TO 101
99    X=XX-XS
      PT=X/U
      IF(X.EQ.0.0) GO TO 75
101   CONTINUE
      X=X*HA
      GO TO (10,20,30,40,50,60),KST
C     STABILITY A
10    TH=(24.167-2.5334*ALOG(X))/57.2958
      IF(X.GT.3.11) GO TO 69
      DO 11 ID=1,7
      IF(X.GE.XA(ID)) GO TO 12
11    CONTINUE
      ID=8
12    SZ=AA(ID)*X**BA(ID)
      GO TO 71
C     STABILITY B
20    TH=(18.333-1.8096*ALOG(X))/57.2958
      IF(X.GT.35.) GO TO 69
      DO 21 ID=1,2
      IF(X.GE.XB(ID)) GO TO 22
21    CONTINUE
      ID=3
22    SZ=AB(ID)*X**B1(ID)
      GO TO 70
C     STABILITY C
30    TH=(12.5-1.0857*ALOG(X))/57.2958
      SZ=61.141*X**0.91465
      GO TO 70
C     STABILITY D (NEUTRAL)
40    TH=(8.3333-0.72382*ALOG(X))/57.2958
      DO 41 ID=1,5
      IF(X.GE.XD(ID)) GO TO 42
41    CONTINUE
      ID=6
42    SZ=AD(ID)*X**BD(ID)
      GO TO 70
C     STABILITY E
50    TH=(6.25-0.54287*ALOG(X))/57.2958
      DO 51 ID=1,8
      IF(X.GE.XE(ID)) GO TO 52
51    CONTINUE
      ID=9
52    SZ=AE(ID)*X**BE(ID)
      GO TO 70
C     STABILITY F
60    TH=(4.1667-0.36191*ALOG(X))/57.2958
      DO 61 ID=1,9
      IF(X.GE.XF(ID)) GO TO 62
61    CONTINUE
```

```
      ID=10
62    SZ=AF(ID)*X**BF(ID)
      GO TO 70
69    SZ=5000.
      GO TO 71
70    IF(SZ.GT.5000.) SZ=5000.
71    SY=1000.*X*SIN(TH)/(2.15*COS(TH))
      SZ=SZ/1000.
      SY=SY/1000.
      P1=PT*HA/U0
      D1=SZ**2/(2.0*P1)
      D2=SY**2/(2.0*P1)
      D1=D1/(HA*U0)
      D2=D2/(HA*U0)
      GO TO 90
75    D1=0.0
      D2=0.0
      PS=0.0
      PT=0.0
      GO TO 90
80    D1=C1/(HA*U0)
      D2=C2/(HA*U0)
C     WRITE(6,102) C1,C2,D1,D2,HA,U0
102   FORMAT(20X,6E10.3)
90    CONTINUE
      RETURN
      END
      FUNCTION PSI2D(X,Z,U,A)
C     2D STREAM FUNCTION FOR FLOW OVER CIRCULAR RIDGE
      PSI2D        =U*Z*(1.0-(A**2/(Z**2+X**2)))
      RETURN
      END
      FUNCTION PSI3D(X,Z,U,A)
C     3D STREAM FUNCTION FOR FLOW OVER AXIALLY SYMMETRIC HILL
      PSI3D    =.500*U*Z**2*(1.0-A**3/(X**2+Z**2)**1.5)
      RETURN
      END
      SUBROUTINE TKER( X,Z,A,Y,P,T,RX2,UUU,M,WZ,WV2,WV3)
      REAL M
      COMMON NINC
C     SUBROUTINE WEIGHTS VELOCITY FIELD BY ASPECT RATIO
C     ------------------------------------------------------------------
C     2D VELOCITY FIELD
C     U2     = VELOCITY IN X DIRECTION
C     V2     = VELOCITY IN Z DIRECTION
      CALL ZITRPL(X,NINC,2,Z)
      X2=X*X
      Z2=Z*Z
      R2=X2+Z2
      A2=A*A
      R4=R2*R2
      U2=(1.0-2.0*A2*X2/R4+A2/R2)
      V2=-2.0*A2*X*Z R4
C     ------------------------------------------------------------------
C     3D VELOCITY FIELD
C     U3     = VELOCITY IN X DIRECTION
C     V3     = VELOCITY IN Z DIRECTION
      CALL ZITRPL(X,NINC,3,Z)
      YY=Z*Y
      Z2=Z*Z
      X3=X*X2
      RX2=Z2*(1.0+Y**2)
      R=(X2+Z2)**.50
```

```
      R2=R*R
      R3=R*R2
      R5=R3*R2
      A3=A*A*A
      U3=(1.0+A3/(2.0*R3)-3.0*A3*X2/(2.0*R5))
      V3=-3.0*X*Z*A3/(2.0*R5)
C     ------------------------------------------------------------------
C     WEIGHTED VELOCITIES
C     UU     = VELOCITY IN X DIRECTION
C     VV     = VELOCITY IN Y DIRECTION
C     M      = SLOPE
C     RX2    = DISTANCE FROM AXIS OF SYMMETRY TO STREAMLINE
C     UUU    = ALONG STREAMLINE VELOCITY
C     P      = KERNEL OF PHI LINE INTEGRAL
C     T      = KERNEL OF T LINE INTEGRAL
      UU=WV2*U2+WV3*U3
      VV=WV2*V2+WV3*V3
      M=VV/UU
      RX2=WZ*RX2+1-WZ
      P=(UU+M*VV)*RX2
      T=(1.0+M**2)/P
      UUU=(UU+M*VV)/SQRT(1.0+M**2)
      RETURN
      END
      SUBROUTINE SURF(S3,ZEE,SLO,A,ZNS)
C     THIS SUBROUTINE COMPUTES THE DISTANCE OF THE STREAMLINE FROM
C     THE SURFACE OF THE SPHERE (OR PLANE)
      XVAL=S3
      XINT=XVAL+SLO*ZEE
      AXINT=ABS(XINT)
      IF(AXINT.LT.A) GO TO 1
      DSQ=ZEE**2+(XVAL-XINT)**2
      ZNS=SQRT(DSQ)
      GO TO 4
1     BEE=XINT/SLO
      BDM=BEE/SLO
      BDMSQ=BDM*BDM
      OPOM2=1.0+1.0/(SLO**2)
      B2MA2=BEE**2-A**2
      ROOT=BDMSQ-OPOM2*B2MA2
      XPL=(BDM+SQRT(ROOT))/OPOM2
      XMI=(BDM-SQRT(ROOT))/OPOM2
      ZXPL=BEE-XPL/SLO
      ZXMI=BEE-XMI/SLO
      IF(ZXPL.GT.0.0) GO TO 2
      XT=XMI
      ZT=ZXMI
      GO TO 3
2     XT=XPL
      ZT=ZXPL
3     CONTINUE
      DSQ=(XVAL-XT)**2+(ZEE-ZT)**2
      ZNS=SQRT(DSQ)
4     RETURN
      END
      SUBROUTINE ZITRPL(SX,NINC,   ND      ,ZEE)
      COMMON FITX(3,600),FITZ(3,600)
      XX=ABS(SX)
      NINCM1=NINC-1
      DO 1 K=1,NINCM1
      KP1=K+1
      IF(XX.LE.FITX(ND,K).AND.XX.GE.FITX(ND,KP1)) GO TO 2
1     CONTINUE
```

```
2       XD=(FITX(ND,K)-XX)/(FITX(ND,K)-FITX(ND,KP1))
        ZEE=FITZ(ND,K)+XD*(FITZ(ND,KP1)-FITZ(ND,K))
        RETURN
        END
/*
//GO.FT05F001 DD *
-3.2        402        .275        .5          10.         .15         4.          1.02
/*
/*EOF
```

APPENDIX D

SAMPLE OUTPUT LISTING

TEST CASE

Hill Height	=	.275 km
Plume Height	=	.402 km
Distance Hill to Stack	=	3.2 km
Stability Class	=	4 (PGT "D")
Froude Number	=	1.02
Aspect Ratio	=	10

INPUT STAGE CONSTANTS

XB	WB	dB	XL	ALAM	ALPHT	BURST	FD
-3.200	0.602	0.074	0.300	10.000	0.150	0.000	1.020

XBO -3.2 WBO 0.0 WAM 0.3 KSTG 4

ALAMO 10.0 FDOUBF= 1.02 IFLAG= 1 IT= 1

0.0	1.000	2.0						
1.6511E+00	1.6511E+00							
	1.6511E+00	1.6511E+00	0.0	2.0	0.0	1.0012E+00	0.6112E-01	1.6512E+00
0.1333E+00	1.0677E+00							
	1.0677E+00	0.1302E+00	-1.0012E+00	2.0	0.0	1.0322E+00	0.3322E-01	1.6612E+00

PERIODIC NUMBER CLASSIFIED 1

DIFFRACTION FORMATION SOLUTIONS
SIGMA P, SIGMA V PLANE CENTERLINE AND GROUND LEVEL CONCENTRATIONS
FOR AN OBSTACLE OF ARBITRARY ASPECT RATIO

PLUM PARAMETERS:

OBSTACLE HEIGHT = 0.0 WIND SPEED = 1.0	SOURCE HEIGHT = 1.00	CROSSWIND DIS=0.0
DIST. SOURCE FROM OBSTACLE CENTER= -11.0	DIST. OF FINAL RECEPTOR= 1.0	ASPECT RATIO=10.0
VERTICAL DIFFUSIVITY = 2.000E-05	CONSERVATION DIFFUSIVITY = 2.400E-02	KST = 4

DISTANCE FROM OBSTACLE	DISTANCE FROM SOURCE	DISPLACEMENT ABOVE GROUND	SIGMA Z (NO OBSTACLE)	SIGMA Z (OBSTACLE)	SIGMA Y (NO OBSTACLE)	SIGMA Y (OBSTACLE)	WIND SPEED
-1.000E+01	1.100E+01	1.000E+00	0.000E+00	0.000E+00	0.000E+00	0.000E+00	0.000E+00
-9.000E+00	1.200E+01	1.000E+00	0.000E+00	0.000E+00	0.000E+00	0.000E+00	0.000E+00
-8.000E+00	2.000E+01	1.000E+00	0.000E+00	0.000E+00	0.000E+00	0.000E+00	0.000E+00
-7.000E+00	3.000E+01	1.000E+00	0.000E+00	0.000E+00	0.000E+00	0.000E+00	0.000E+00
-6.000E+00	4.000E+01	1.000E+00	0.000E+00	0.000E+00	0.000E+00	0.000E+00	0.000E+00
-5.000E+00	5.000E+01	1.000E+00	0.000E+00	0.000E+00	0.000E+00	0.000E+00	0.000E+00
-4.000E+00	6.000E+01	1.000E+00	0.000E+00	0.000E+00	0.000E+00	0.000E+00	0.000E+00
-3.000E+00	7.000E+01	1.000E+00	0.000E+00	0.000E+00	0.000E+00	0.000E+00	0.000E+00
-2.000E+00	8.000E+01	1.000E+00	0.000E+00	0.000E+00	0.000E+00	0.000E+00	0.000E+00
-1.000E+00	9.000E+01	1.000E+00	0.000E+00	0.000E+00	0.000E+00	0.000E+00	0.000E+00
0.0	1.000E+02	1.000E+00	0.000E+00	0.000E+00	0.000E+00	0.000E+00	0.000E+00
1.000E+00	1.100E+02	1.000E+00	0.000E+00	0.000E+00	0.000E+00	0.000E+00	0.000E+00
2.000E+00	1.200E+02	1.000E+00	0.000E+00	0.000E+00	0.000E+00	0.000E+00	0.000E+00
3.000E+00	1.300E+02	1.000E+00	0.000E+00	0.000E+00	0.000E+00	0.000E+00	0.000E+00
4.000E+00	1.400E+02	1.000E+00	0.000E+00	0.000E+00	0.000E+00	0.000E+00	0.000E+00

DISTANCE FROM OBSTACLE	DISTANCE FROM SOURCE	DISPLACEMENT ABOVE GROUND	CONCENTRATION (NO OBSTACLE)	CONCENTRATION (OBSTACLE)	GROUND LEVEL CONCENTRATION (NO OBSTACLE)	GROUND LEVEL CONCENTRATION (OBSTACLE)
-1.000E+01	1.100E+01	1.000E+00	0.000E+00	0.000E+00	1.100E+00	1.100E+00
-9.000E+00	1.200E+01	1.000E+00	0.000E+00	0.000E+00	1.100E+00	1.100E+00
-8.000E+00	2.000E+01	1.000E+00	0.000E+00	0.000E+00	2.000E+00	1.000E+00
-7.000E+00	3.000E+01	1.000E+00	0.000E+00	0.000E+00	3.000E+00	1.000E+00
-6.000E+00	4.000E+01	1.000E+00	0.000E+00	0.000E+00	4.000E+00	1.000E+00
-5.000E+00	5.000E+01	1.000E+00	0.000E+00	0.000E+00	5.000E+00	1.000E+00
-4.000E+00	6.000E+01	1.000E+00	0.000E+00	0.000E+00	6.000E+00	1.000E+00
-3.000E+00	7.000E+01	1.000E+00	0.000E+00	0.000E+00	7.000E+00	1.000E+00
-2.000E+00	8.000E+01	1.000E+00	0.000E+00	0.000E+00	8.000E+00	1.000E+00
-1.000E+00	9.000E+01	1.000E+00	0.000E+00	0.000E+00	9.000E+00	1.000E+00
0.0	1.000E+02	1.000E+00	0.000E+00	0.000E+00	1.000E+01	1.000E+00
1.000E+00	1.100E+02	1.000E+00	0.000E+00	0.000E+00	1.100E+01	1.000E+00
2.000E+00	1.200E+02	1.000E+00	0.000E+00	0.000E+00	1.200E+01	1.000E+00
3.000E+00	1.300E+02	1.000E+00	0.000E+00	0.000E+00	1.300E+01	1.000E+00
4.000E+00	1.400E+02	1.000E+00	0.000E+00	0.000E+00	1.400E+01	1.000E+00

-3.000E+00	1.000E+00	1.000E+00	1.000E+00	1.000E+00	0.000E+00	0.000E+00
-2.000E+00	1.000E+00	1.000E+00	1.000E+00	1.000E+00	0.000E+00	0.000E+00
-1.000E+00	1.000E+00	1.000E+00	1.000E+00	1.000E+00	0.000E+00	0.000E+00
0.000E+00	1.000E+00	1.000E+00	1.000E+00	1.000E+00	0.000E+00	0.000E+00
1.000E+00	1.000E+00	1.000E+00	1.000E+00	1.000E+00	0.000E+00	0.000E+00
2.000E+00	1.000E+00	1.000E+00	1.000E+00	1.000E+00	0.000E+00	0.000E+00
3.000E+00	1.000E+00	1.000E+00	1.000E+00	1.000E+00	0.000E+00	0.000E+00

RIGHT-HAND SIDE FROM FACTOR	BASIS SOLUTION (-1 INDICATES ZERO)	BASIS SOLUTION (INDICATES ZERO)	RATIO OF/FC (NO INDICATES ZERO)	RATIO OF/FC (INDICATES ZERO)	T FACTOR (-1 INDICATES ZERO)	T FACTOR (INDICATES ZERO)
-1.000E+01	1.000E+01	1.000E+01	0.000E+00	0.000E+00	0.0	0.000E+00
-9.000E+00	1.000E+01	1.000E+01	0.000E+00	0.000E+00	0.0	0.000E+00
-8.000E+00	1.000E+01	1.000E+01	0.000E+00	0.000E+00	0.0	0.000E+00
-7.000E+00	1.000E+01	1.000E+01	0.000E+00	0.000E+00	0.0	0.000E+00
-6.000E+00	1.000E+01	1.000E+01	0.000E+00	0.000E+00	0.0	0.000E+00
-5.000E+00	1.000E+01	1.000E+01	0.000E+00	0.000E+00	0.0	0.000E+00
-4.000E+00	1.000E+01	1.000E+01	0.000E+00	0.000E+00	0.0	0.000E+00
-3.000E+00	1.000E+01	1.000E+01	0.000E+00	0.000E+00	0.0	0.000E+00
-2.000E+00	1.000E+01	1.000E+01	0.000E+00	0.000E+00	0.0	0.000E+00
-1.000E+00	1.000E+01	1.000E+01	0.000E+00	0.000E+00	0.0	0.000E+00
0.000E+00	1.000E+01	1.000E+01	0.000E+00	0.000E+00	0.0	0.000E+00
1.000E+00	1.000E+01	1.000E+01	0.000E+00	0.000E+00	0.0	0.000E+00
2.000E+00	1.000E+01	1.000E+01	0.000E+00	0.000E+00	0.0	0.000E+00